CITY SCALE APPROACHES TO ASSESS THE ROLE OF REALISTIC ROOF GREENING IN IMPROVING URBAN CLIMATE & HABITAT

MITALI Y. JOSHI

LIÈGE université

LEMA

CITY-SCALE APPROACHES TO ASSESS THE ROLE OF A REALISTIC ROOF GREENING IN IMPROVING URBAN CLIMATE AND HABITAT

Mitali Yeshwant Joshi

This dissertation has been approved by:

Supervisor
Prof. Dr. Jacques Teller

The work in this thesis was carried out at the Local environment and management analysis (LEMA) research group of the Urban and Environmental Engineering department (UEE) in Faculty of applied sciences of the University of Liège. This PhD was funded through the ARC grant for Concerted Research Actions for project number 19/23–28 "CityRoof" financed by the French Community of Belgium (Wallonia- Brussels Federation).

Publisher:
Mitali Yeshwant Joshi
LEMA research group, UEE Department,
Faculty of Applied Sciences, University of Liège
B52, allée de la Découverte, 9, B52, 4000 Liège, Belgium
mjoshi@uliege.be

CITY-SCALE APPROACHES TO ASSESS THE ROLE OF A REALISTIC ROOF GREENING IN IMPROVING URBAN CLIMATE AND HABITAT

DISSERTATION

Thesis submitted in partial fulfilment
of the requirements for the degree of
Doctor in Architecture and Urban planning

by
Mitali Yeshwant Joshi

born on the 4th November 1993
in Latur, India

Jury Members:

Chair/secretary	Prof. Dr. Luc Courard	University of Liège
Supervisor	Prof. Dr. Jacques Teller	University of Liège
Committee member	Prof. Dr. Grégory Mahy	University of Liège
Committee member	Prof. Dr. Shady Attia	University of Liège
Committee member	Dr. Marjorie Musy	CEREMA
Committee member	Dr. Marjolein van Esch	TU Delft

Acknowledgements

Academic research caught my attention during my master's education at the University of Twente as I knew it would allow me to be a student forever. Haha. Then, one thing led to another, and here I am, ready to finish my PhD. This, of course, wouldn't have been possible without the support of many people. I thank everyone who has been a part of this journey and played a part in the completion of this PhD.

First, I would like to thank my Supervisor *Prof. Jacques Teller*, who gave me an opportunity to start my PhD journey. Thank you for trusting and allowing me to be independent in my work while being available when I needed advice. I also want to thank you for involving me in other projects, which again provided me with opportunities to learn more about flood risk assessments and the beautiful Wallonia region. I hope we continue our collaboration in the future.

I would also like to thank my committee members *Prof. Grégory Mahy, Prof. Luc Courard and Prof. Shady Attia*. Your critical feedback and constructive criticism have helped me to refine my work and to produce a better-quality thesis. A special thanks to external jury members *Dr. Marjolein van Esch* and *Dr. Marjorie Musy* for your valuable comments on my work.

A special thanks to *Grégory Mahy*, who ignited my interest in plants and biodiversity. Thanks to you, Grégory, I know the difference between greenwashing and the actual introduction of meaningful green spaces in the cities. Thank you for your guidance and support throughout the biodiversity aspect of this PhD. I hope to work more on this subject and collaborate with you in the future.

I would like to thank *Dr. Marjorie Musy*, who gave me an opportunity to intern at CEREMA to learn my first ever urban microclimate analysis model *Solene-microclimat*. *Marjorie*, Thank you for hosting me and giving me a chance to learn directly from you, even amidst the COVID-19 pandemic. Also, a special mention for giving me an introduction to French cuisine and culture.

I also want to thank *Dr. Auline Rolder* for teaching me all the technical know-how of Solene-microclimat. I also want to thank *Dr. Sihem Guernouti* for providing valuable feedback during the discussion on work involving Solene-microclimat.

I want to express my gratitude to *Prof. Mario Cools*, who never said no to providing

guidance on the statistics part of my work. *Mario*, thank you for making me understand the basics of clustering and principal component analysis, without which I couldn't publish my work in a reputed journal. Thank you for all the fruitful discussions.

I want also to thank *Marc Binard* and *Gilles-Antoine Nys*. Marc, thank you for supporting me with the LiDAR point cloud data acquisition in the initial stages of my PhD. And thank you, Gilles-Antoine, for familiarising me with the FME workbench and 3D modelling of roofs. Without your unwavering support in identifying flat roofs in Liège, my work wouldn't even proceed. Thank you for everything.

I also want to thank my fellow city-roof project PhDs: *Lucie Rivière and Mostafa Kazemi*. I learned the basic elements of green roofs because of your work on this project. I loved working as a group on this project with you two. Thank you for being with me on this journey together.

My research at LEMA has been fun and interesting, thanks to my fellow LEMA labmates: *Suxia Gong, Louis Durrant, Constance Uyttebrouck, Anasua Chakraborty, Negarsadat Medani, Wissal Selmi, Iris Reuter, Ngoc Nguyen Bich, Antoinette Marie Reine Nishimwe, Jules Muvana, Mohamed Elhadi, Lucia Sagaineti, and Kahina Labadoui* and neighbouring SBD labmates: *Waqas Ahmed, Ramin Rahif, Muriel Diaz and Deepak Amaripadath*.

Suxia, since we started the journey on the same day, you have always understood the pains and gains of my journey. Our discussions related to work or personal lives in research made me feel that I am not alone and that I have a friend who is going through similar challenges as me. Louis, I remember how you made me feel at ease in the initial days when I couldn't speak a word in French. You were my labmate with whom I could communicate easily in English.

I also want to especially thank Constance for being there to help me with every small administrative issue. You were my go-to person for every small thing in the lab in my initial days. Thank you for helping me with everything and also with French translations. Thanks also to Wissal, Muriel, Ramin, Waqas, Lucia, Elhadi and Kahina for being my after-work lab buddies. I really had a fun time in Liège because of all of you.

Thank you, Anasua and Deepak, my fellow Indians. Anasua, I have always loved to chat with you about work and life. Moreover, you were my support for all administrative work, which I dreaded when I broke my ankle in an unfortunate accident. Thank you, Deepak, for involving me in your work during my PhD. I could learn about indoor climates and building-level studies, thanks to you.

Staying in touch with family and friends became difficult during my PhD, but I was lucky that my close ones stayed beside me, even when I was busy. I want to thank my friends and family who understood and supported my journey. A special thanks

to my extended family and my in-laws (*Amma, Appa and Akka*) for their support and well wishes for me.

This PhD would still not be finished if it wasn't for Srinidhi, my *husband*. I was so scared to look at Python codes or understand physics equations, but today, I can proudly say that I am not scared of it anymore. This is all because of you. Thank you for being my friend, guide, and work buddy during this PhD. Thank you for tolerating my emotional outbreaks and keeping me motivated, especially in my final Ph.D. days. *Love you*.

Lastly, I would like to thank my parents, who are doctorates themselves and may also have contributed to my decision to pursue a PhD. My parents gave their unwavering support in all my endeavours and strived to give me the best education, even when it meant that their only child had to be away from them. Thank you, *Mummy* and *Pappa*, for being my cheerleaders always.

Abstract

Green roofs (GRs) are a sustainable alternative to conventional roofs that provide multiple ecosystem services, especially when the urban ecosystems primarily consist of massive proportions of built infrastructures. Most existing studies analyse the ecosystem services green roofs provide at the building or prototype levels. Some studies examine the ecosystem services at the block or neighbourhood scale. However, city-scale studies of ecosystem services provided by green roofs are limited. Moreover, there are no studies using realistic proportions of potential roofs while analysing their impact on ecosystem services at city-scale. Therefore, this dissertation aims to assess the impact of realistic roof greening on ecosystem services of urban heat island (UHI) mitigation and contribution to ecological connectivity at a city scale. For this PhD, we use the city of Liège in Belgium as the case study.

Three main steps are involved to accomplish the objective of this thesis. Firstly, we identify the realistic potential roofs for greening employing geoinformation science (GIS) and remote sensing and using parameters such as the area and slope of the roof along with the structure of buildings. Secondly, we analyse the role of potential green roofs on the UHI effect using three approaches to estimate city-scale impacts. The first approach utilises a highly resolved weather research and forecasting (WRF) model using urban physics parametrised with the BEP+BEM model using the local climate zones (LCZ) as the land use classification. The second approach involves classifying the urban blocks in the city of Liège into unique and realistic urban morphological archetypes using a systematic PCA-based k-means clustering approach. With this approach, we obtained nine unique urban morphological archetypes for Liege. Thereafter, we analysed the microclimate of these unique morphological archetypes using the Solene-microclimat model. The third approach employed random forest (RF) regression to predict the impact of green roofs on the surface UHI (SUHI).

Lastly, we analysed the role of green roofs in Liege's ecological network of dry grasslands. Creating analogous habitats on potential green roofs can restore the urban dry grasslands that are crucial for pollinator species in temperate Europe. Therefore, we model the ecological connectivity of existing dry grassland patches and the potential green roofs using graph theory with Graphab 2.8 software.

The results suggest that around 20% (350 hectares) of the existing total buildings in the city have the potential for developing green roofs in Liege. Moreover, most of the potential area comes from large buildings in the city, which could be a suitable target for initial implementation in the city. Regarding the approaches explored for green roofs' role in UHI mitigation, results show that green roofs generally reduce air and surface temperatures. Realistic roof greening may not be sufficient at city or regional scale. Only, it is effective in some parts of the study area. Realistic roof greening reduces air and surface temperature in large, low-rise LCZs/archetypes. It can be extremely beneficial in reducing the surface temperature at block scale. For a significant reduction in air temperature, the building height must be smaller, and the building area must be larger. Our research mainly provided insight into the interplay between urban morphology, realistic roof greening potential, and the reduction in temperatures, improving our understanding of UHI mitigation with green roofs at the city scale. The remote sensing approach needs further analysis to improve the accuracy of the results.

Apart from this, results based on the role of green roofs in ecological connectivity indicated that urban dry grassland connectivity with analogous green roofs, particularly benefits the high and moderate mobility pollinator species, with limited impact on low mobility species. Introduced green roofs mainly create a compact network of dry grasslands in the center, with limited improvement in connectivity of the existing dry grasslands. Local connectivity analysis reveals that retrofitting 30-50% of the potential green roofs will improve connectivity for high and moderate mobility species. For improving the connectivity for lower mobility species, however, almost all the potential roofs need to be greened. Additionally, the study shows that building heights and configurations can strongly influence the role of green roofs in ecological connectivity.

This PhD effectively provides an overview of the impact of green roofs on the UHI effect and ecological connectivity. It also broadly suggests policy recommendations where the green roof implementation could benefit dense urban areas. Apart from this, the study stresses the importance of urban morphology for improving the ecosystem services provided by green roofs.

Contents

List of Figures

List of Tables

1 Introduction

Unprecedented urbanisation in the world has given rise to enormous challenges associated with energy consumption, social inequality, air and water pollution, and resource depletion, resulting in a massive strain on urban systems [7]. The United Nations (UN) has estimated that around one-third of the world's population will live in cities by 2050 [8]. Thus, it is essential to transform significantly the way urban spaces are built and managed to ensure the sustainable development of cities [9].

At present, urban ecosystems consist of a large proportion of built infrastructure along with high population densities [10, 11]. Urban ecosystems experience the urban heat island (UHI) effect, air and water pollution, and frequent flooding owing to the lack of green spaces [12–14]. In this context, the concept of Nature-Based Solutions (NBS) is gaining popularity to resort to nature to address urban challenges in a sustainable way [15].

1.1 Why green roofs?

NBSs are often considered an alternative to or combined with grey infrastructure. The rationale for NBS implementation is that they provide multi-fold benefits while generating limited negative impacts, thus proving cost-effective on a medium-to-long term perspective [16, 17]. NBS can aid cities in adapting to climate change, one of the main challenges urban areas will continue to face in the coming decades [18].

Some examples of NBS are green roofs, green walls, previous pavements, street trees and vegetation, and urban parks.

One of the critical factors in implementing NBS in cities is the availability of space [19]. While new development projects can easily accommodate several NBS at the planning stage, the integration in existing built-up areas is constrained by already existing urban forms and land uses. This constraint is extremely relevant in high-density urban areas [20]. Now, urban sustainability is often connected to urban forms; for instance, a dense and compact urban form is usually considered as more sustainable than sprawled development [21, 22]. Impervious surfaces such as building roofs and walls are abundant within urban ecosystems. These are located on buildings that consume significant energy and are responsible for substantial greenhouse gas (GHG) emissions [23]. Given this background, nature-based solutions (NBS) such as green roofs and green walls are highly relevant, especially in dense urban areas [24–26]. In this study, we mainly focus on analysing the impact of green roofs on urban ecosystem services.

1.2 What are green roofs?

Green roofs are defined as living vegetation planted on the roofs of buildings [27, 28]. Green roofs can improve the energy performance of the buildings and aid in combating the UHI effect by reducing the atmospheric temperature and providing human thermal comfort [29]. Green roofs also manage stormwater due to their high water retention capacity [30]. Apart from the environmental benefits, green roofs are also observed to enhance urban residents' quality of life [31] (See Figure 1.1).

Green roofs can be broadly classified into intensive and extensive green roofs [32] based on differences in substrate thickness, benefits, costs, maintenance levels, and vegetation type [33–35]. Intensive ones have a thick layer of substrate, which is the growing medium, wherein many varieties of plants can be cultivated [36]. Additional structural support is required for this type of roof due to the heavy weight of the substrate [37]. For example, urban rooftop agriculture and rooftop gardening are often categorized as intensive green roofs [33, 36]. In contrast, extensive green roofs have a relatively thin layer of lightweight substrate, which needs little or no additional structural support. This type of green roof requires lower maintenance, resulting in more widespread application potential compared to intensive green roofs [37]. Extensive green roofs are upheld for being cost-effective in terms of installation, making the benefits affordable [31]. Researchers have recently designed a new type of green roof, semi-intensive green roofs, combining the advantages of both intensive- and extensive green roofs [38]. Despite the differences in typologies and benefits,

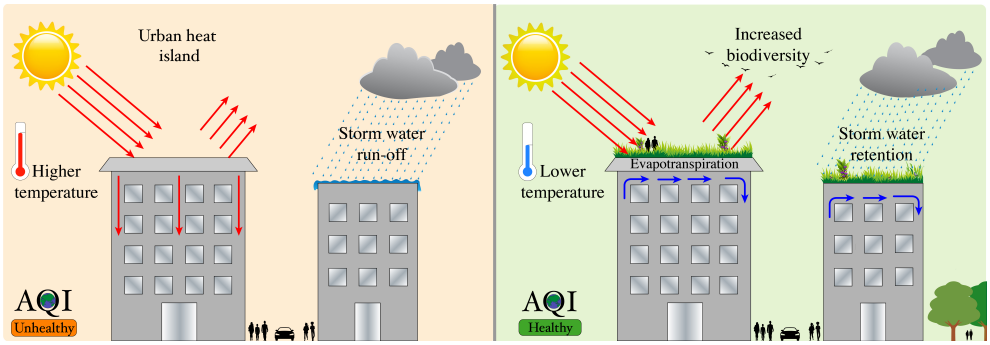

Figure 1.1: Schematic representing the diverse processes involved in conventional roofs and green roofs (AQI—Air Quality Index)

these types of green roofs are usually considered sustainable and environmentally friendly [39].

Since green roofs are sustainable with multiple benefits, private and public sectors are promoting their installation [40]. Many municipalities in North America, Europe, and Asia actively encourage green roof installation through policy instruments such as construction regulations and economic incentives [38, 41, 42]. Moreover, academic research on the subject of green roofs has increased exponentially in recent years [25].

1.3 Literature review and research gaps

1.3.1 Realistic roof greening

Several studies simulate 100% green roof scenarios, which are unrealistic, especially in European cities where many buildings may have sloped roofs. It is possible to install green roofs on sloped roofs; however, the installation and maintenance costs for this are extremely high [43–45]. Therefore, installing them on flat roofs is more feasible. Another assumption in most studies analysing green roofs' impact on ecosystem services is the use of the arbitrary green roof fraction in the study area. If it is a residential area, the buildings mainly have sloped roofs in European cities [46–48] and since they are privately owned, implementing green roofs on them could be challenging [49, 50]. However, installing green roofs on commercial buildings such as malls, industrial buildings, or public buildings like schools or hospitals can be relatively easier since the buildings are often maintained by municipalities [51].

Since the benefits of green roofs are highly dependent on their proportions in a city, assuming the fractions arbitrarily or considering 100% roof greening may lead

to overestimating the benefits of green roofs. Therefore, analysing a more realistic potential of green roofs in an area is crucial.

1.3.2 Green roofs' impact on ecosystem services

Methodology for literature review

The review intended to identify the research gaps in the field of ecosystem services provided by green roofs. The review included four main ecosystem services: biodiversity enhancement, stormwater management, urban heat island mitigation, and air quality. The review also had aspects of social acceptance and feasibility to understand possible challenges faced for the implementation of green roofs. The review is based on peer-reviewed journal articles found by searching the SCOPUS database. The search comprised relevant synonymous terms to identify relevant literature regarding the six aspects mentioned above. The literature search constituted a combination of terms such as green roofs, city, and one of the mentioned aspects to ensure that the selection of publications was relevant to the individual aspects. To ensure a reasonable number of publications, we added proxies of the key terms in our query (Table 1.1). Moreover, the key terms were searched only in the paper's title, abstract, and keywords to obtain the literature specific to the subject. The review focused only on research articles to obtain an overview of the original research done in the field of green roofs.

We conducted this search in April 2020, restricting it to research articles written in English and published from January 2011 to December 2019. Subsequently, we filtered the papers by screening the titles and abstracts and eliminated those articles that did not focus on understanding the impact of green roofs on the selected aspects. Additionally, we only focused on papers that compare green roofs with bare, impervious, and conventional roofs. Papers including other kinds of green urban infrastructure were not reviewed.

Quantity and scale of existing studies

The search strategy resulted in a total of 739 papers. We read the abstracts of all 739 papers and, based on the filtering process outlined in the previous section, selected the 158 most relevant studies for a full-text review. Figure 1.2 provides the details of the papers obtained initially regarding each aspect and the number of papers selected for the review based on the selection criteria. It is evident from Figure 1.2 that there is a significant amount of literature available on the contribution of green roofs to water management and UHI mitigation as compared to the other aspects, based on our

Table 1.1: Search terms and their combinations.

Search terms	**Synonyms**
Green Roofs	Green Roof * OR Roof * garden OR Vegetat * roof OR Roof * greening AND
City	City OR Urban AND
Aspects:	
Biodiversity	Biodiversity
Water Management	Flood OR "stormwater management" OR "water quality" OR "quality of water" OR "rainwater harvesting" OR "stormwater retention" OR "water pollution"
UHI	"Urban heat island" OR UHI OR "microclimate regulation" OR "climate regulation "OR "human thermal comfort" OR "pedestrian thermal comfort" OR "energy efficiency" OR "building energy"
Air Quality	"air quality" OR "quality of air" OR "air pollution"
Societal acceptance	"acceptance" OR "perception" OR "preference" OR "adoption" OR "attitude" OR "reaction" OR "willingness"
Feasibility	Feasibility" OR "cost-benefit analys *" OR "economic analys *" OR "social analys *" OR "life cycle cost" OR "economic benefits" OR "economic impact"

search strategy. Additionally, we classified the studies based on their scale: at a city, neighbourhood, or building/prototype level (Figure 1.3). Most studies were observed to have been carried out at a prototype or single-building scale. However, aspects such as water management, UHI, and feasibility consist of a few studies which were carried out at city and neighbourhood scales. Most air quality and biodiversity studies were experimental and carried out on specific buildings or prototypes. In the case of social acceptance, the studies discuss the opinions of various stakeholders; therefore, the study's scale was irrelevant.

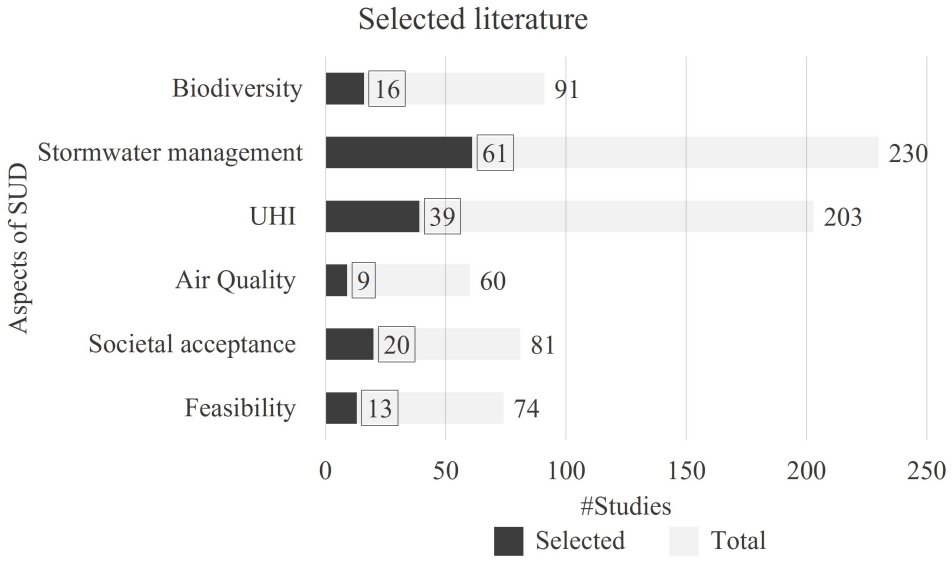

Figure 1.2: Schematic representing total search results and the number of studies selected for full-text review

Main findings on green roofs' impact on various ecosystem services

The detailed literature review can be found in Joshi et al. [52]. Here, we present the main findings of the green roofs' impact on various ecosystem services along with their social acceptance and feasibility.

1. Regarding the impact on biodiversity, the review suggests that green roofs on buildings with lower heights have been observed to support species in a better way [53]. Given that urban areas are densifying and becoming more compact, cities are predicted to grow vertically. Thus, the height of buildings is an essential parameter for analyzing the impact of green roofs on biodiversity. In the review, we did not find enough studies in the literature on the effect of height on green roofs' impact on biodiversity. We found only two studies where Braaker et al. [53] considered buildings of 15 m or less, and Wang et al. [54] considered a 50 m tall roof garden. We need more studies analyzing the impact of building height on the contribution of green roof in urban biodiversity. Similarly, there is a paucity in the literature on green roofs' role in ecological connectivity. We found that only Braaker et al. [53] and Joimel et al. [55] consid-

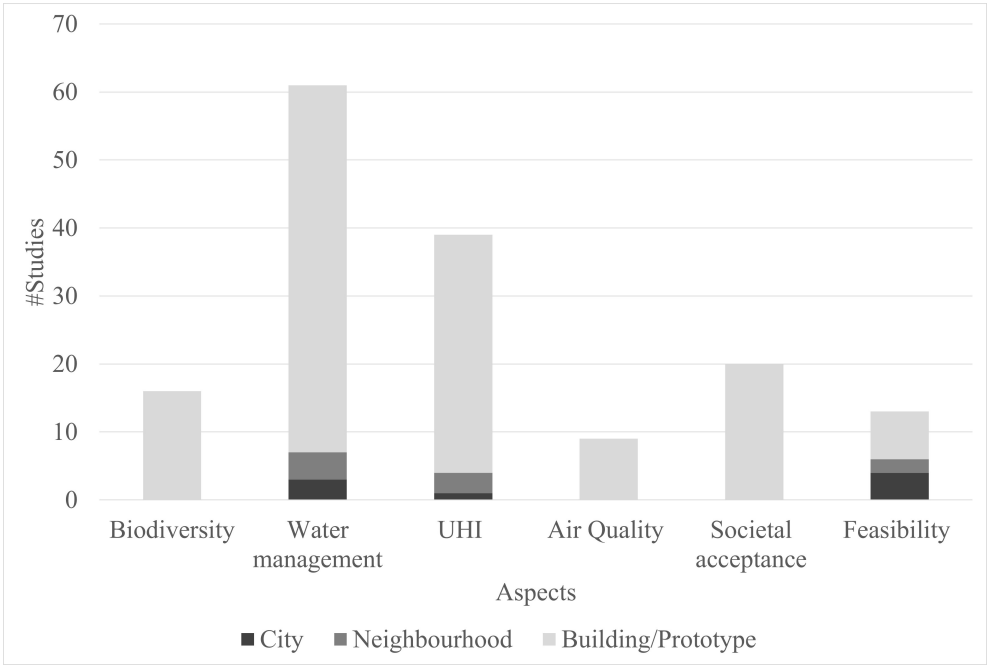

Figure 1.3: Classification of studies based on the scale at which they were carried out

ered this aspect to an extent. As green roofs' are considered to be a substitute for green areas on the ground, they are supposed to facilitate the movement of organisms through urban landscapes [56]. Therefore, more evidence is needed to understand the role of green roofs' in strengthening ecological networks at an agglomeration scale. Apart from this, our review also pointed out a concern regarding mosquito abundance on green roofs [57], which can affect people's health, especially in dense urban areas.

2. Our review suggests that green roofs aid in water management owing to their high water retention potential. However, the retention is high only for low- to moderate-intensity rainfall. Furthermore, green roofs can be one of the factors in preventing flood hazards. Still, other solutions are needed in case of extreme rainfall. The review also suggested that the runoff from green roofs also acts as a source of phosphorus in the case of most commercial substrates, which can pollute water resources. The concentration of pollutants in extensive green roofs is lower than in intensive green roofs due to the presence of fertilisers in intensive green roofs. Alternative substrates and vegetation types were also observed to reduce the concentrations of nutrients or metals.

3. Regarding UHI mitigation, our review suggests that green roofs have a limited impact on pedestrian thermal comfort. A significant impact can only be found with low-rise buildings. Building height has an influence on the impact of green roofs on the temperature at street level. Besides, urban morphology is observed to play an important role in temperature regulation [58]. The performance of green roofs may also vary depending upon the urban morphology of a block and its surroundings. This should be further analysed in future studies.
   Apart from this, our review suggests that green roofs substantially reduce roof surface temperatures compared to bare roofs. Additionally, most studies reported significant reductions in energy demand and consumption due to a decrease in cooling loads. Heating load reductions were also observed in cases where appropriate substrates, thermal insulation, and plant species were used. However, these effects are prominent only on the top floors. Green roofs also decrease the indoor temperature of a building. Even if, slight warming can be experienced during the night. It should be noted that the maintenance of green roofs is important for the desired benefits, especially in extreme weather.
4. Regarding the impact on air quality, our review suggests that green roofs reduce the concentrations of pollutants in the air near the green roof. The literature on the improvement in the air quality near the street also shows a positive impact on air quality [59–61]. However, the urban morphology used in the models for air quality was quite simplified, and the results might vary in reality due to more complex morphologies.
5. In terms of social preference and acceptance, our review suggests that green roofs with low-cost and high aesthetic value are in demand. Moreover, our review suggests that hindrances such as high costs and maintenance and lack of knowledge often affect green roofs' acceptability in urban areas. In the feasibility studies, high installation costs were considered as a barrier at the private level, suggesting the need for subsidies. Apart from this, the adoption of green roofs also depends on the type of housing. For instance, the UHI benefits such as energy savings are mainly reported to be significant at top floors and negligible elsewhere. Ergo, it can be challenging to get the approval of all residents of a multi-story building, given that the benefits are unevenly distributed.
   Concerning social preference, most studies considered well-maintained green roofs, which are effectively green, for understanding users' perspectives. However, due to extreme weather conditions in some regions, the vegetation during the months of winter or summer can be brown and dry, resulting in a different opinion of users. More extensive studies are required to study the social acceptability of green roofs during the dry months when vegetation is dried.

In the review, we observed that the social benefits in the feasibility analyses were only considered in terms of public health, but the impact of green roofs on social cohesion/inclusion was not considered. Greening strategies, at times, tend to increase property prices and result in gentrification and the marginalisation of the poor [62]. More studies are needed to understand the social impact of green roofs at the neighbourhood scale.

1.3.3 Research gaps and questions

Based on the comprehensive review of green roofs and ecosystem services, we chose two ecosystem services for this work: Urban heat island mitigation and contribution to urban biodiversity. Following are the four main research gaps identified based on the comprehensive literature review:

1. In terms of the chosen ecosystem services, there are no studies using realistic fractions of green roofs in the study area.
2. There are limited studies analysing the impact of green roofs on the UHI effect and urban biodiversity at a city- or regional-scale.
3. While there are studies showing the importance of urban morphology in urban microclimate and the UHI effect, the interplay of urban morphology, UHI effect and mitigation solutions like green roofs has never been studied.
4. The role of green roofs in the urban ecological network at the city-scale has not been studied previously.

Based on the research gaps, this work aims to assess the role of realistic roof greening in improving urban climate and habitat, with Liège city in the Walloon region of Belgium as a case study. The main focus is on extensive type of green roofs, given our focus on greening existing roofs at city scale, they are more cost-effective. This dissertation answers the following broad research questions in the context of Liège and also the applicability of the methods used for other parts of the world.

Q1: What is the existing potential of green roofs in the city?
Q2: How will realistic roof greening influence the Urban heat island effect in different morphologies at city-scale?
Q3: What is the role of green roofs in urban ecological connectivity?

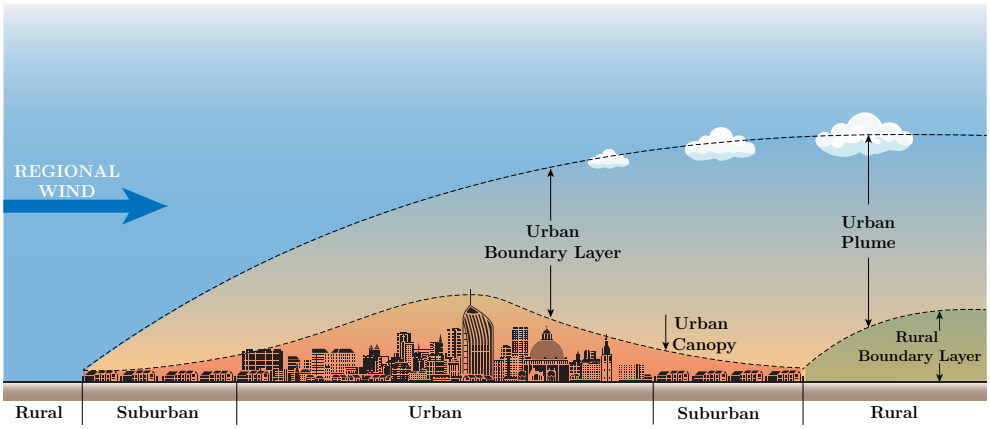

Figure 1.4: Schematic representation of the urban atmosphere [1, 2]

1.4 Ecosystem services in focus

1.4.1 Urban Climate Regulation

Urbanisation has led to drastic changes in the nature of surface and atmospheric properties of a region, which involves the transformation of radiative, thermal, moisture and aerodynamic characteristics, thereby dislocating the natural solar and hydrologic balances [2]. Particularly, urban construction materials reduce the water permeability and store the heat. Similarly, the dense urban morphology creates the possibility of radiation trapping and air stagnation. This causes the inadvertent climate modifications in the form of urban boundary layer.

The urban boundary layer is a local to mesoscale phenomenon, with its attributes shaped by the characteristics of the general urban surface. Beneath the building roof level is the urban canopy layer, which is produced by micro-scale processes operating in the street canyons between the buildings 1.4. The climate in the urban canopy layer is dominated by the characteristics of immediate surroundings. For instance, green roofs can significantly impact the thermal environment in the urban canopy layer by modifying land surface energy and water transport processes, which in turn affects the thermal environment in the urban boundary layer [1, 63]. In this dissertation, the impact of roof greening is primarily analysed on the urban canopy layer.

1.4.2 Biodiversity and Ecological Connectivity

Dry grasslands are important environmentally as they support a diverse range of flora and fauna with genetic diversity that can withstand harsh conditions, including

high temperatures and water stress [64, 65]. However, dry grasslands are highly fragmented due to intensive agriculture, pasture grazing and urbanisation [66]. Although urbanisation is one of the causes of fragmentation, the urban environment presents an opportunity to create analogous habitats on hard surfaces like pavements, roofs and walls, which can boost the ecosystem services in dense urban areas. Creating analogous habitats on these surfaces, which are the sites hosting indigenous biodiversity due to their structural or functional resemblance to natural habitats [67], can help restore species-rich dry grassland networks in urban areas of temperate Europe [64, 68].

Dry grasslands can create suitable habitats for diverse and endangered insect species [69, 70]. The alarming decline in insect population is affecting pollination and decomposition and increasing pests in urban areas [71, 72]. However, dry grasslands have become rare due to anthropogenic activities in temperate Europe [73, 74]. The fragmentation and the consequent isolation of dry grasslands reduce the insect diversity and richness [75] and decrease their functional dispersal [76]. This further lowers the ability of species to respond effectively to environmental changes, reducing their ecological resilience [77]. Creating analogous habitats on impervious roofs can be one of the suitable options for improving the connectivity for insects, as it can restore the dry grassland network in the city [78].

Extensive green roofs are targeted to increase biodiversity support in urban areas due to their lower constraint on building as compared to intensive green roofs. However, Extensive green roofs face constraints like shallow substrate depth, low water retention, high sensitivity to climate variations and limited space for root and aboveground biomass development [79]. Extensive green roofs, planted with native flora, are proposed as habitats analogous to dry grasslands and rocky environments in temperate regions, given their shared environmental constraints [65, 80]. This hypothesis of green roofs being analogous habitats of dry grasslands is also proven in recent studies like Rivière et al. [65], Schröder and Kiehl [81], and Thuring and Dunnett [82]. Hence, existing suitable building roofs can be retrofitted with extensive analogous green roofs to generate micro-habitats of dry grasslands within the city. In this dissertation, we assess the contribution of green roofs to ecological connectivity of urban dry grasslands in the city.

1.5 Study Area: Liège City, Belgium

Liège is situated in the Wallonia region of Belgium, with 195,965 inhabitants in 2020 [83]. The urban area of Liège is the third most highly populated in the country after Brussels and Antwerp. The total area of Liege municipality is around 69 km2.

There are 136,170 buildings in the city, with a total area of building roofs about 10 km2, which represents around 14% of the city area. Additionally, Liège city has a dense built-up area which lacks green space, particularly in the city centre, which makes green roofs a suitable solution to increase urban green spaces (Figure 1.5).

During the 19th century, Wallonia underwent substantial industrial development based on the exploitation of mineral resources (coal) and the emergence of an important steel industry [84]. The period also profoundly altered the Walloon industrial belt, including Liège. Liège expanded rapidly, contributing to an early form of urban sprawl reinforced by a dense network of public transport [84].

Liège has a unique combination of historical architecture shaped by modernist urbanism and traditional industrial identity. However, the decline of the steel industry in Europe has greatly impacted Liège's economy, resulting in significant job losses and the need for redevelopment of industrial sites [84, 85]. The simultaneous increase in car mobility, the presence of the waterway (Meuse River) and the central location of Liège in Europe have opened new avenues of economic development in the city. Considering the potential for development, Liège presents an ideal case study to assess the effects of innovative green infrastructure, such as green roofs, to enhance and revitalise the city [84, 86].

In addition to that, due to the dense built-up in the city, the occurrence of heatwaves in the city of Liège will be more frequent with higher air and surface temperatures [87, 88]. Placing green roofs can potentially reduce the subsequent UHI effect caused by the dense built-up (Figure 1.6).

Additionally, Liège, located in the Mosane valley of Wallonia region in Belgium, is an interesting case study as one of the key habitats for biodiversity in the Mosan Valley is dry calcareous grasslands [89–91]. The urbanized area of Liège creates a strong gap in the connectivity of specialist species of dry grasslands. Consequently, dry grasslands have been identified as high priority for development in the ecological network of the city of Liège by local authorities [89]. However, developing ground dry grasslands in the heart of Liège is difficult given the dense built-up.

1.6 Overview of research strategy and methods

The dissertation is divided into three parts for three research questions. It is mainly based on assessing the impact of realistic roof greening obtained from Part I of the dissertation on urban climate and biodiversity.

1.6.1 Part I: Identifying existing potential buildings for roof greening

In *chapter 2*, potential buildings that can be retrofitted with green roofs in the city of Liège are identified. The potential buildings are identified based on the slope of the roofs, structure of the building and area of the roofs. The slope of the roofs is analysed by processing the LiDAR point cloud dataset using the RANSAC algorithm. The structure of the buildings is identified using Belgium's cadastral data. Along with this, we also compute the potential of identified roofs in different priority zones which are based on socio-economic level of the region, availability of green spaces and high land surface temperature regions in the city.

As a realistic potential of roof greening, we consider all flat roofs to have potential irrespective of their structural capacity, to ensure a wider applicability of this approach.

Differences in consideration of potential roofs for greening

In *chapter 3 and 5*, all the flat roofs greater than 10 m^2 are considered to have green roof potential, given the possibility to include this size because of resolution (2m) in *chapter 5*, and because of aggregation in each LCZs in *chapter 3*. In *chapter 6*, flat roofs with size 100 m^2 are assumed to have potential for greening as the resolution of the study is 30m, making one raster cell to be 90 m^2.

For ecological connectivity analysis, flat roofs with greater than 100 m^2 area are considered to have potential for greening as smaller habitat areas do not support significant biodiversity [64].

1.6.2 Part II: Exploring UHI mitigation potential of realistic roof greening

The impact of green roofs on urban climate is analysed at the regional scale (*chapter 3*), microscale (*chapter 4 and 5*) and city scale (*chapter 6*), with three spatial resolutions, 333m, 2m and 30m and three different approaches: using weather research and forecasting (WRF) model, Solene-microclimat model and statistical model with remote-sensing, respectively.

In *chapter 3*, the impact of the realistic fraction of green roofs on the UHI effect during a heatwave in Liège, Belgium is analysed at a regional scale, employing a high-resolution WRF study using the BEP-BEM parameterisation with local climate zone (LCZ) land use classification. In *chapter 4*, since the LCZs developed by WUDAPT are generic and not specific to the context, context-specific urban morphological archetypes for the city Liège were identified. We did this using a systematic clustering approach. The obtained archetypes can be directly used for analysing urban microcli-

mate using object-resolving models. The microclimate of these urban morphological archetypes is studied using Solene-microclimat software in *chapter 5*. The impact of green roofs on the microclimate of each archetype was analysed. Additionally, the possible reasons for differences in the impact of green roofs on the microclimate in the archetypes were investigated.

Unlike the highly sophisticated physics-based climate models, in *chapter 6*, the impact of green roofs on surface temperature is analysed using the random forest regression, where land surface temperature (LST) is the dependent variable and morphological variables are the independent variables, influencing the LST. We simulated green roofs by substituting the NDVI value of built-up pixels with the NDVI suitable for green roofs.

The models used to analyse the impact of green roofs on urban climate are briefly described below:

WRF model

With the WRF model, the impact of realistic roof greening at a regional scale is analysed. The WRF model is an NWP and atmospheric simulation model intended for both research and operational applications. WRF model has a dynamic solver that incorporates compressible and non-hydrostatic Euler equations with several physical and dynamic options designed for regional scale. However, as there is an increasing interest in simulating the urban atmosphere, urban canopy schemes are developed and integrated into WRF due to the complex dynamics of urban climate. Urban canopy schemes such as BEP-BEM (Building energy parameterization and building energy modelling) are included in WRF as physics options to represent better urban morphology, such as building and street geometry and the surface characteristics such as albedo, emissivity, and urban/vegetation fraction [92]. The BEP-BEM scheme is a multi-layered urban canopy model which divides the urban canopy into several vertical layers at various heights. It independently solves fluxes and meteorological variables in each layer, enabling the characterisation of building height distribution in high-density built areas. The BEP-BEM model computes the surface momentum, heat exchanges, humidity, and turbulent kinetic energy fluxes to the atmospheric dynamics governing equations. Details of this model are explained in *chapter 3*

Solene-microclimat model

Solene-microclimat model [93] is employed for assessing the impact of green roofs on outdoor air and surface temperature in realistic urban morphological archetypes.

With Solene-microclimat, a researcher can investigate the model in depth and propose changes relevant to its study area as it is editable [94]. It also has the advantage of describing an urban block realistically (for instance, buildings with sloped roofs) due to tetrahedral meshing. Solene-microclimat can simulate the microclimate at the district scale with a high resolution (up to 1 m). It has been previously used to assess the impact of adaptation strategies such as green roofs and walls on outdoor and indoor thermal comforts and building energy consumption [95, 96].

The modelling approach of Solene-microclimat is based on the coupling of radiative, thermal and CFD (Computational Fluid Dynamics) models. The model can simulate an extensive range of mitigation solutions. The model generates several outputs, such as hourly air and surface temperature, along with all the energy budget components of the surfaces in $\mathrm{W/m^2}$. More details can be found in *chapter 5*.

Random Forest-based statistical model

We generate a statistical model using Random Forest (RF) regression algorithm to predict the changes in Land surface temperature (LST) after employing green roofs. RF is a supervised machine-learning algorithm proposed by [97]. The RF regression algorithm combines a large set of regression trees, where the dataset is broken down into smaller subsets to predict a response variable by learning decision rules [98]. The trees are combined using bootstrap aggregation or bagging, such that each set is run independently, and the outputs are merged to achieve an accurate prediction [99]. RF regression is a supervised and straightforward method, which is fast and robust to the noise in the data [100, 101], which is why we employ this algorithm for the analysis.

The RF regression includes LST as a dependent variable and eight morphological variables such as building density, sky view factor and solar radiation as independent variables. The details can be found in *chapter 6*.

1.6.3 Part III: Identifying the role of green roofs in the urban ecological network

In this part, the role of green roofs in the urban ecological connectivity of dry grasslands is analysed. *Chapter 7* highlights preliminary results on the usefulness of green roofs in strengthening the ecological network of dry grasslands in Liège with a particular focus on large and small bees. The analysis is largely dependent on the distance between the potential green roofs and existing dry grassland sites within the municipal boundary of Liège. The green roofs located within the foraging distance of bees are identified using Euclidean distance.

As green roofs are in the near proximity of the existing dry grasslands, in *chapter 8*, we perform a detailed study on the role of potential green roofs in the ecological connectivity of dry grasslands in Liège by modelling ecological networks using spatial landscape graphs. We utilised the software Graphab 2.8 [102, 103] to model the ecological networks. A spatial graph is a network of nodes connected by links. In ecological network applications, nodes correspond to habitat patches, and links indicate flows of individual species between habitat patches. Spatial graphs have the advantage of being mathematic objects with network properties. It is, therefore, possible to calculate multiple metrics that help evaluate the network's connectivity and the importance of the different components of the network (nodes and links) for the overall connectivity [102, 104]. In *chapter 8*, we model networks with different percentages of potential green roofs in Liège city, to identify the optimum percentage of potential green roofs needed to impact the ecological connectivity of dry grasslands significantly.

Finally, in the *chapter 9*, conclusions and possible directions for future studies are presented.

The dissertation is made up of a series of articles that have been published/submitted to peer-reviewed journals. For this reason some overlap may occur between the various chapters.

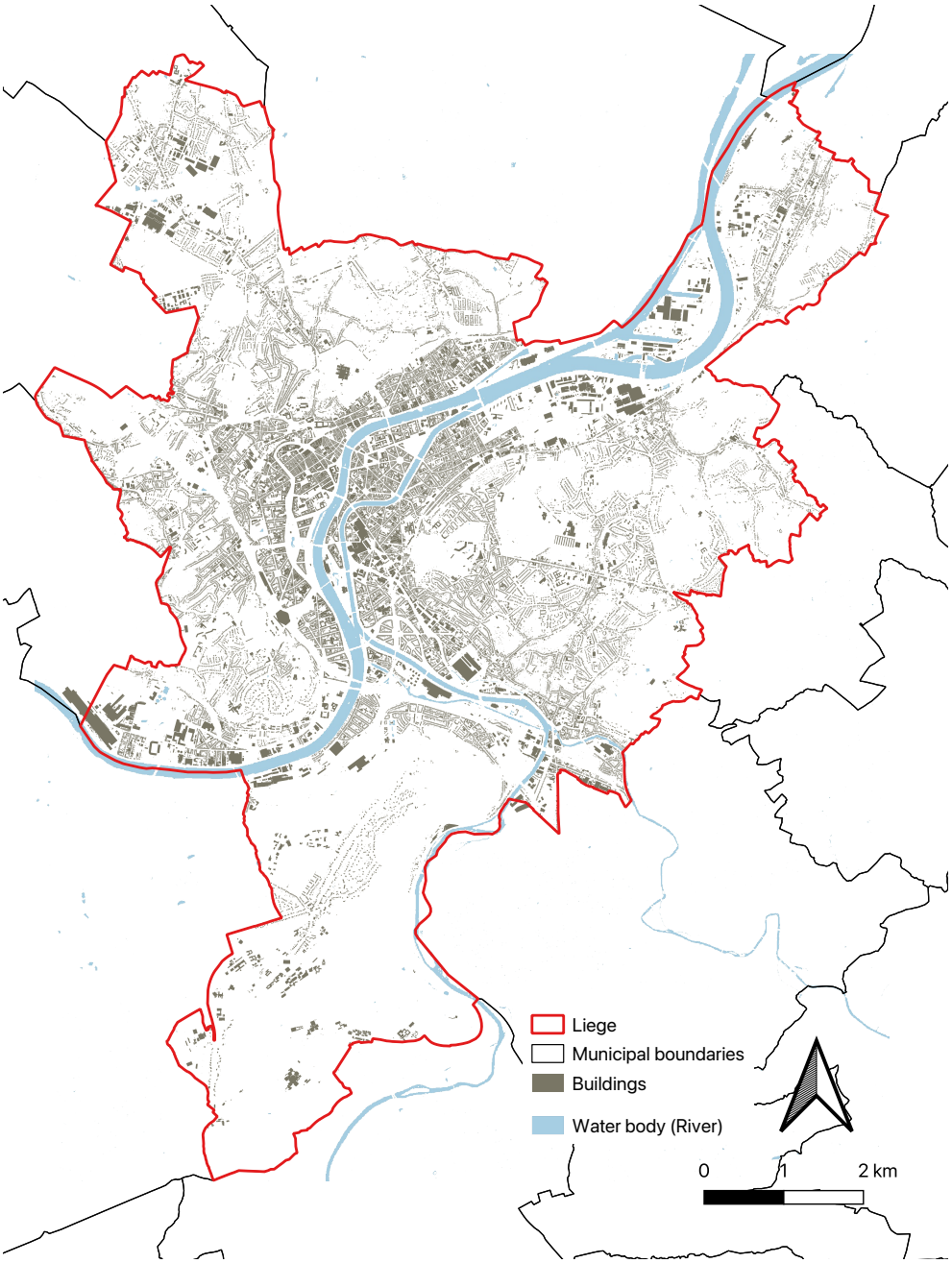

Figure 1.5: Liège City

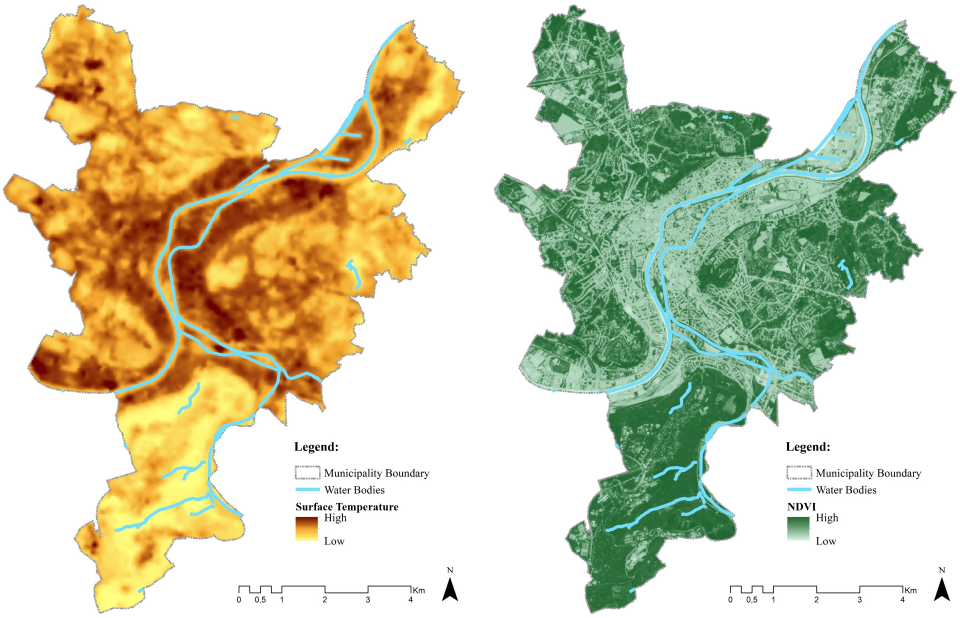

Figure 1.6: spatial variation of LST and NDVI in Liège

Part I

Identifying existing potential buildings for roof greening

2

Identifying the potential of green roofs on existing buildings in Liège city[1]

Cities are experiencing increased pressure on social, economic, and environmental sectors due to the rapid urbanisation and increasing risk owing to climate change affecting the urban environment. Solutions such as green roofs are often discussed in the context of smart and sustainable cities as they present a multi-functional and solution-oriented approach to address these challenges. Green roofs become extremely relevant in the context of highly urbanised and compact cities where impervious surfaces are abundant. Therefore, in this paper, we analyse the potential of green roofs at a city scale with the help of parameters such as area and slope of the roof and structure of the building. We also identify the priority zones based on environmental and socio-economic parameters. The study is carried out in the city of Liège, Belgium. The results suggest that around 20% (350 hectares) of the total buildings in the city have the potential for developing green roofs. Moreover, the potential of green roofs is quite significant in terms of roof area in the priority zone. Due to significant socio-economic deprivation in high-priority zones, implementation of green roofs might not be affordable. Buildings with larger roof sizes are mostly owned by companies or commercial establishments, thus, making larger roofs more relevant for retrofitting green roof. Thus, our approach can act as a preliminary decision-making tool for urban planners to analyse the potential of green roofs and prioritize them in deprived

[1] Published as: **M.Y.Joshi**, and J.Teller, *Potential for urban greening with green roofs: a way towards smart cities* (2021). ISPRS Annals of the Photogrammetry, Remote Sensing and Spatial Information Sciences. **6**, 87-94 doi: 110.5194/isprs-annals-VI-4-W2-2020-87-2020

areas.

2.1 Introduction

Unprecedented urbanisation along with the increasing climate change has led to increased pressure on social, economic and environmental sectors impacting the human life and the natural environment in the cities [105, 106]. Urban and environmental issues induced by the rapid growth of population and their consumption-driven lifestyles prove to be a challenge for urban planners [107, 108]. In such a situation, urban planners are redirected towards the frontier of sustainable cities [109]. The rapid advancements in the information and communication technologies (ICTs) have also placed the concept of smart cities in the urban planning domain [110]. Smart city concept has been promoted as an instrument to manage various urban and environmental challenges such as environmental pollution, urban heat island, biodiversity loss and socio-economic inequalities [111]. Many researchers have indicated that the smart and sustainable cities should be intertwined to achieve the desired outcome [112, 113]. As a result, it is argued that cities could not be smart without being sustainable. Therefore, in this paper, we combine the smart and sustainable city approach with a view to addressing the aforementioned urban and environmental problems.

Nature-based solutions (NBS) are often put forward in the context of sustainable urban development. These solutions present a multi-functional and solution-oriented approach by addressing social, economic and environmental sustainability issues simultaneously [114]. Urban Green Infrastructure (UGI) such as green roofs are one of the NBS which are highly relevant in urban areas that are abundant in impervious surfaces such as building roofs [25]. Moreover, high urban densities and compact nature of the cities make it difficult to implement other UGIs such as planting trees and developing urban green spaces. Furthermore, green roofs provide multiple urban ecosystem services such as energy efficiency, urban heat island mitigation, regulation of microclimate and provision of a better quality of life [42, 115]. Thus, green roofs with their multi-dimensional benefits aid in sustainable urban development.

Green roofs are a sustainable alternative to conventional roofs and are defined as the living vegetation installed on the building roofs [27, 116]. There are mainly of two types of green roofs, intensive and extensive [34]. Intensive roofs are characterized by a thick layer of substrate with a diverse variety of plants whereas extensive roofs have a thinner layer of substrate which are light weight and require low level of maintenance as compared to intensive green roofs [27, 37]. Most of the studies are concentrating on implementation of extensive type of green roofs as they incur lower installation

and maintenance cost.

Having a potential for social acceptance [117, 118], green roofs can be incorporated at a city scale with the help of municipalities. However, due to different types of roofs and type of construction of respective buildings, not all the buildings are able to accommodate green roof strategy. Thus, identifying the potential for mobilizing the green roofs at a city scale is an essential prelude to its implementation. Apart from this, cities often witness an unequal distribution of green spaces. This not only affects the quality of life of citizens but also results in a discontinuity in green spaces affecting the biodiversity [55, 119]. Moreover, there is a spatial variation of built-up densities which also results in different temperature in different parts of the city [120]. Additionally, socio-economic inequalities are evident in cities worldwide [8, 121]. Socio-economically deprived regions also experience a lower quality of life owing to the existing social, economic and environmental problems [122]. As UGIs such as green roofs are argued to have multiple benefits, it is important to prioritize their implementation accordingly.

Many studies have identified the potential of green roofs at various scales for different cities in the world. Building characteristics, for instance, building slope, area, orientation, and strength are mainly used for identifying the potential for developing green roofs [44, 45, 123–125], focused on identifying priority areas for implementing green roofs based on optimizing their ecosystem service provision. They include ecosystem services such as thermal regulation, runoff control, biodiversity, food production, social cohesion and recreation. A study by Herrera-Gomez et al. [13], particularly identifies the areas where green roofs can be retrofitted in order to reduce urban heat island effect. As combining the identification of potential of green roofs with their prioritization is important, studies such as Silva et al. [126] integrate the building characteristics with existing greens and population density to ensure urban greening in the areas where it is needed the most. A similar approach is used by Grunwald et al. [43], where ecosystem services such as improvement of urban air quality, climate regulation, water retention and biodiversity enhancement are used to identify priority areas for developing green roofs. In this paper, we employ a similar approach of integrating the identification of potential of green roof with prioritization along with socio-economic development as an added parameter. We identify the potential of green roofs along with a prioritization based on i) lack of existing greens, ii) high temperature zones and iii) socio-economic deprivation. Altogether, we investigate whether the achieved potential of green roofs is beneficial in terms of society and environment suggesting their contribution to the sustainable smart cities.

2.2 Materials and methods

2.2.1 Study area and available datasets

Liège, situated in the Wallonia region of Belgium, is the third most populous city of Belgium with a total of 195,965 inhabitants. The total area of Liège municipality is around 69 km^2. There are 136,170 buildings in the city, with a total area of building roofs about 10 km^2, which represents around 14% of the city area. There is a variety of roof and building structures in Liège, which makes the detection of the potential of green roofs challenging and crucial. This study is performed using different types of data sources (LiDAR, PICC (Projet Informatique de Cartographie Continue) data from Public Service of Wallonia (SPW)) which were analysed with the help of GIS environment (ArcMap Version 10.7.1, ESRI) and FME workbench.

2.2.2 Mapping potential of green roofs

In this study, we mainly consider the building characteristics such as roof slope, area of the roof and structure of the building (Figure 2.1). Although any roof, irrespective of the slope, can be greened, high slope roofs may require additional support to avoid slipping of vegetation materials. Moreover, maintenance of high sloped roof can be difficult. Additionally, flat rooftops require lower initial investment for retrofitting a green roof [45]. Thus, we consider flat roofs to have potential for implementing green roofs.

To identify flat roofs, we used the LiDAR point cloud data obtained from SPW with a point density of 0.8 point/m^2. At first, we clipped the point cloud with existing building footprints of Liège obtained from the PICC data. We then analysed the point cloud within each building footprint to obtain the information on flat roofs as follows:

Confronting the sparse nature of LiDAR data, the unsupervised interpolation of planes from point cloud could be a challenge [127]. Several methods such as RANdom SAmple Consensus (RANSAC) [128] and the Hough transform [129], allow to ignore the outliers statistically. In this methodology, we used the former as it is computationally more efficient than the Hough transform. RANSAC is currently running quicker and is better tailored for shape detection of roof planes [130].

One disadvantage of unsupervised shape detection algorithms is the definition of initial parameters. Due to the sparse point density, the non-deterministic nature of RANSAC might detect inconsistent shapes. Depending on the starting points, which are randomly determinate, the results might differ between concurrent interpolations. Given that the junctions between clusters are more detailed, this problem is less encountered in high-density point clouds. Planes detection could thus lead to

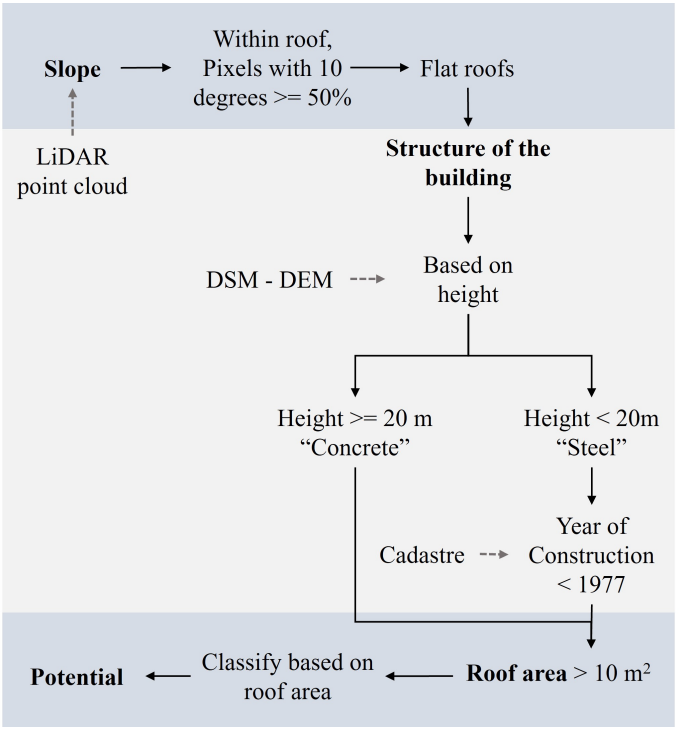

Figure 2.1: Methodology for identifying the potential of green roofs

false positives and/or false negatives or spurious planes [131]. To avoid misdetections, tuning parameters is often the responsibility of the expert. For this study, we need roofs that can be mobilized for greening. As building roofs/planes have obstructions such as chimneys, elevator shafts and staircases, retrofitting small-sized roofs with green roof can be challenging. Therefore, we only consider planes with minimum area of 10 m^2 and slope between 0- 10° [132]. Other planes are not considered as relevant. Two other limits have been set to prevent odd results: (a) the unsupervised algorithm will determine a maximum of 20 independent planes for each building. (b) the points that are more than 10 cm away from the detected shapes are considered to be outliers. These two considerations increase the robustness of the approach. The results for each building provide the number of flat planes, the percentage of flat area in a building footprint and the average height of the building.

Apart from the slope of the roofs, the building must have reserved structural capacity for accommodating a green roof. Buildings with a concrete structure have enough strength to adopt a green roof, whereas not all the buildings with a steel structure have

the required reserved structural capacity. It is observed that taller buildings in Liège are made of concrete. Therefore, based on our knowledge, we assume that buildings with a height greater than or equal to 20 m have a concrete structure, whereas the buildings with height less than 20m to have a steel structure. We determine the height of building based on the average height that we computed using the LiDAR and the DEM data at 1 m resolution obtained from SPW.

To identify the buildings made of steel with adequate strength, we analysed the building standards in Europe and Belgium since 1900. Based on these standards, we determined the reserve structural capacity of the building to accommodate green roofs. The structure of the buildings was indeed according to the norms that were in force during the period of construction. The buildings constructed before 1977 have strength more than required as they were built according to old standards, which were more conservative given their lower accuracy [133]. Developing green roofs on these recent buildings without major structural changes is impossible. Also, the buildings constructed before 1977 are more than 40 years old, indicating the need for in-depth renovations which can be an opportunity to develop green roofs on the top of these buildings. Therefore, we consider buildings with steel structure that are constructed before 1977 to be structurally suitable for developing green roofs.

After identifying the potential buildings that conform to the criteria explained above, we classified the potential roofs based on the area and the percentage of area of the roofs that can be mobilized for green roofs. Figure 2.1 shows the flow of methodology used in this study.

2.2.3 Prioritizing the areas for implementing green roofs

Green roofs are argued to provide several ecosystem services including mitigation of urban heat island effect, stormwater management and improve air quality along with improvement in the quality of life and environment. However, based on the available datasets and importance of these services, we focus on three main ecosystem services: increase in urban green areas, regulation of temperature and improving the quality of life in socio-economically deprived regions. Thus, we identified the areas with higher surface temperature, lower green areas, and socio-economically deprived regions to identify the priority zones for developing green roofs where the benefits of green roofs can be maximised.

To identify existing greens, we computed normalised difference vegetation index (NDVI). NDVI quantifies the vegetation by measuring the difference between near-infrared and red bands (Eq.1). We used images from European Space Agency (ESA) taken by Sentinel-2 (10 m resolution) satellite on April 22nd, 2020 to compute NDVI.

We used the bands that capture red (0.665 mm) and near infrared-NIR (0.842 mm) colours with band 4 and 8, respectively.

$$NDVI = \frac{NIR - RED}{NIR + RED} \tag{2.1}$$

To calculate the surface temperature, we utilise LANDSAT-8 level 1 image captured on 27th June 2019. The data was procured from United states geological survey (USGS) at a resolution of 30 m and thermal band 11 was used. We computed the surface temperature (K) using equations 2 and 3 (USGS, 2019). We further converted the temperature values into degree Celsius (°C)

$$L_\lambda = M_L Q_{cal} + A_L \tag{2.2}$$

L_λ = TOA spectral radiance (Watts/($m^2 * srad * \mu m$)) ML =Band-specific multiplicative rescaling factor from the metadata, AL=Band-specific additive rescaling factor from the metadata, Q_{cal} = Quantized and calibrated standard product pixel values (DN)

$$T = \frac{K_2}{ln(\frac{K_1}{L_\lambda} + 1)} \tag{2.3}$$

T = Top of atmosphere brightness temperature (K) where: K1 =Band-specific thermal conversion constant from the metadata, K2 =Band-specific thermal conversion constant from the metadata

Areas with higher NDVI values can correspond to lower land surface temperature, mainly due to the influence of humidity on ground and evapotranspiration of plants on the surface [134, 135]. Thus, we checked the correlation between the surface temperature and NDVI values using Pearson's correlation coefficient. For the correlation, we resampled the surface temperature raster to 10 m resolution. The correlation test suggests that the correlation between NDVI and surface temperature is significant (at 95% confidence interval), and they are negatively correlated. Figure 2.2 also suggests that there is a negative correlation between NDVI and surface temperature. Thus, we included only the NDVI parameter in the analysis as we have it at a finer resolution as compared to surface temperature.

For socio-economically deprived regions, we use the socioeconomic difficulty index developed by Bianchet et al. [136] for entire Walloon region at statistical sectors level. The index was developed using Principal Component Analysis (PCA) which included a comprehensive list of indicators related to the origin of inhabitants, income, employment, and working conditions. The socio-economic deprivation index is converted from statistical sector level and resampled to a raster of 10 m resolution.

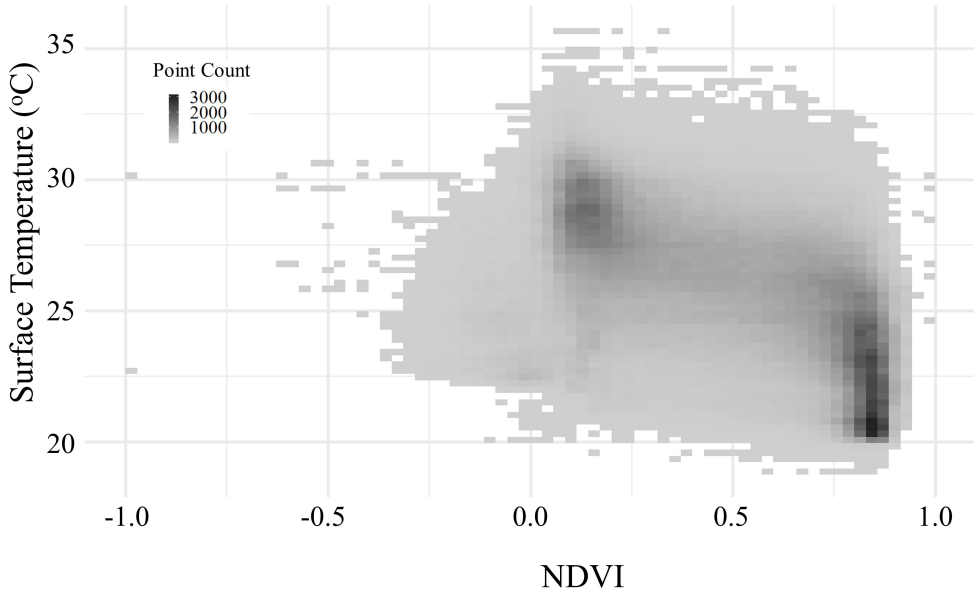

Figure 2.2: Collinearity between NDVI and Surface Temperature

We normalised the values of NDVI and socioeconomic deprivation index from 0 to 1 based on the priority. For instance, areas with lower greens or higher temperature and a higher deprivation index are considered to be 1. Thereafter, we performed a spatial multi-criteria analysis (SMCA), in which we multiplied the values of parameters giving equal weightage. We then divided the entire city into three zones namely, low, medium and high priority zones based on the scores obtained in SMCA. The threshold for categorizing the city into three categories are decided based on the interquartile range as given in table 2.1.

Table 2.1: Categorization of SMCA score

Category	Values
Low	<25th percentile
Medium	25th – 75th percentile
High	>=75th percentile

2.3 Results and discussion

In this section, we present the results of the study. Firstly, we introduce the potential of green roofs in the city of Liège. For which we present the priority zones where the green roofs can be retrofitted to obtain maximum benefits.

2.3.1 Potential of green roofs

Our analysis suggests that around 22% (31004) of the buildings have roofs that are partially or entirely flat (0 – 10°). The total area of roofs which is flat is around 486 hectares. Out of these buildings, around 516 buildings are with a concrete structure and rest of the buildings have a steel structure. Around 26,908 (328 ha) buildings with a steel structure having flat roofs are constructed before 1977. Thus, a total of 27,424 (20%, 351 ha) buildings in Liège are having roofs that are completely or partially flat and a structure that can support roof greening. In our analysis of flat roof detection, we also identify the percentage of area that is flat in each of the building roof. Table 2.2 suggests that around 3425 (2%) buildings have their roofs completely flat which occupy 209.87 hectares of area. Additionally, around 19,900 (15%) buildings have roofs with more than 50% flat area. Rest of the buildings (4098, 3%) have less than 50% of their roof area as flat. As we have considered the planes greater than 10 m^2 for detection of flat roofs, the selected building roofs, irrespective of percentage of flat area in each roof, have a flat region greater than 10 m^2. Therefore, all these buildings (27,424, 20%) can be retrofitted with green roofs considering the available flat area and reserved structural capacity to support additional weight of green roof.

The distribution of potential roof sizes for roof greening in the city is as follows. We categorize the roofs in three categories as shown in figure 2.3. In general, the average size of potential roofs for greening is 128 m^2 and around 50% of the buildings with potential for roof greening have an area greater than 41 m^2 which can be retrofitted with green roofs. The spatial distribution of potential of roof is shown in figure 2.5.

Table 2.2: Number and area of building roofs classified according to percentage of area occupied by flat plane

	Percentage of flat area in each roof		
	<50%	50 - 100%	100%
Number of buildings	4098	19901	3425
Area occupied by flat planes	14.56	157.52	209.87

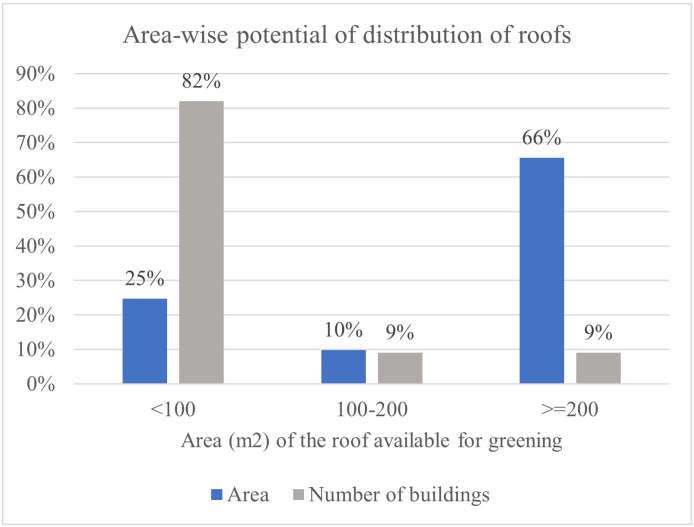

Figure 2.3: Area-wise percentage of total potential roofs (Area and number of buildings)

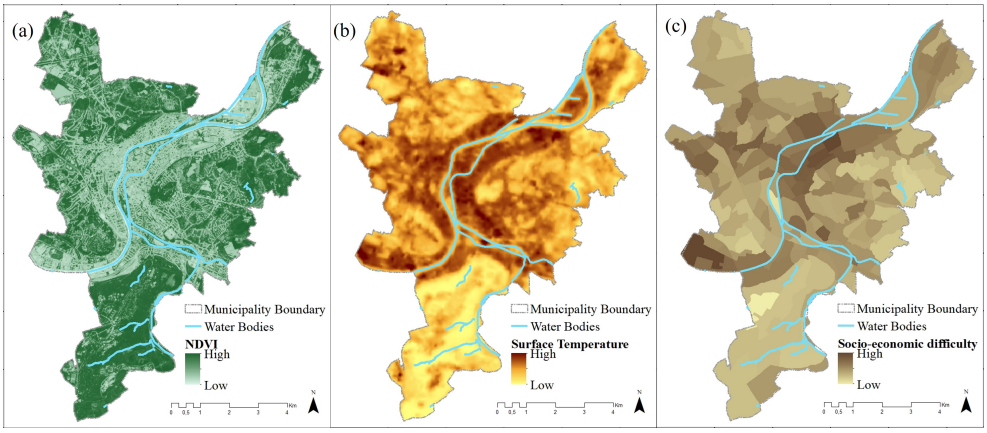

Figure 2.4: Spatial distribution of (a) NDVI, (b) Surface temperature (c) Socio-economic deprivation index in Liege

2.3.2 Prioritizing the areas for green roofs

The city of Liège has substantially low green spaces in the central part which has high built-up density (Figure 2.4a). Thus, surface temperatures are also observed to be relatively higher in the central region (Figure 2.4b). Additionally, the socio-economic

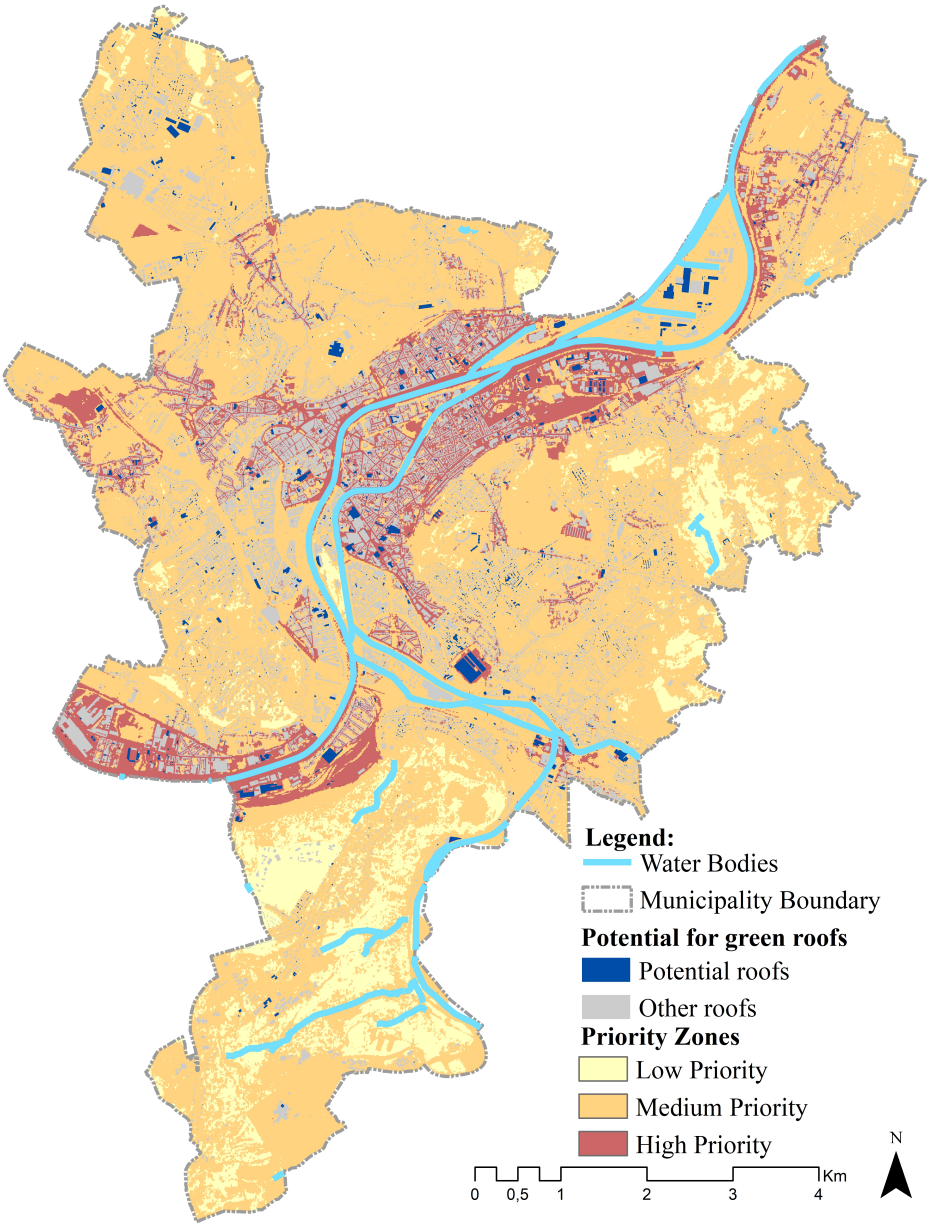

Figure 2.5: Potential of green roofs in the city of Liege along with priority zones

difficulty index is also observed to be high in the sectors near the city centre along the river and the eastern part of the city (Figure 2.4c). Based on these parameters, we delineated the regions with high, medium, and low priority as mentioned in section 2.3 (Figure 2.5)

. Around 1700 hectares of the city area comes under the high priority zone, in

Table 2.3: Priority-wise percentage of total potential roofs in terms of total area of roofs and number of buildings in each category with respect to percentage of flat roof area.

Priority zone		**% of roof area which can be greened**		
		<0.5	**0.5-1**	**1**
Low	No. of buildings	67 (0.05%)	393 (0.3%)	96 (0.07%)
	Area (ha)	0.3	3.6	8.14
Medium	No. of buildings	1921 (1%)	10927 (8%)	1747(1%)
	Area (ha)	6.8	82.7	98.5
High	No. of buildings	2110 (2%)	8581 (6.3%)	1582 (1%)
	Area (ha)	7.4	71.1	103.1

which there are around 44% of the total buildings. Around 20% (12,273 buildings, 167 hectares) of these buildings have the potential to retrofit green roofs. Around 3423 hectares area comes under the medium priority zone, which consists of 52% of the total buildings in the city. Around 20% (14,595, 173 hectares) of these buildings have the potential for retrofitting green roofs. The low priority zone accounts for around 1700 hectares which has around 4485 buildings. Around 12% of these buildings have the potential for roof greening.

Table 2.3 shows the distribution of potential roofs with respect to percentage of flat area in a roof, in terms of total area and number of buildings in each of the priority zone. In comparison to other zones, high priority zone has the largest area of buildings with roofs that are completely flat (103 hectares). Apart from this, classification of potential roofs in terms of area of roof available for greening suggests that there is a large number of buildings with area less than 100 m^2 (figure 2.6). It is evident that although the buildings with roof area greater than 200m^2 are a few (figure 2.6), developing them can provide a larger area with green roofs. A significant number of these roofs with large areas are in priority zones. It is easier to develop green roofs in such conditions as the number of building owners is reduced and greening large areas may lead to economies of scales.

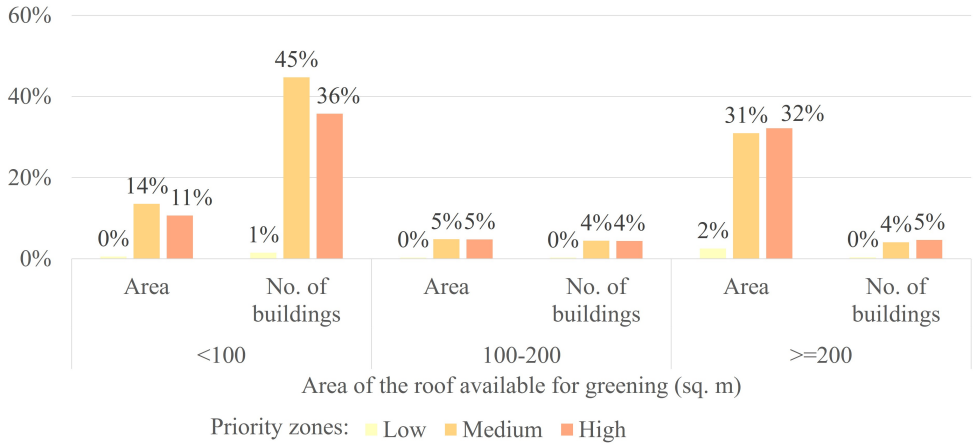

Figure 2.6: Potential of green roofs in the city of Liege along with priority zones

2.3.3 Discussion

Around 20% (351 hectares) of the buildings in Liège have a potential for greening. Around 12% of these buildings have complete flat roofs and rest of the buildings roofs that are partially flat. Even though partially flat, the roof sizes are above 10 m^2. Although there are around 20% buildings with potential of greening, around 88% of these buildings are composed of roofs which are partially flat. As per our methodology, we only identify the planes which are between 0 – 10 degrees and are greater than 10 m^2 area. The area values are summed up in the end to provide the area available for greening. There is a possibility that the planes are not adjoint and are away from each other. Therefore, the roofs that are reported to have a larger area for greening might have 2 small areas which are disjoint. Disjoint flat roofs, though, might not be problematic, can bring maintenance issues. Thus, further investigation for roofs that are partially flat is needed.

Apart from this, most of the buildings in the city of Liège have pitched roofs. The potential of roof greening is relatively lower than other cities [126, 137], mainly due to less number of flat roofs. Building stock in Wallonia region in general and in Liège is very old [138], resulting in large number of pitched roofs. It has been argued that green roofs can also be developed on slightly pitched roofs (below 20°) [45]. Thus, there may be more potential for developing green roofs than what is analysed in the paper. However, it is important to note that the installation and maintenance costs for pitched roofs are much higher as compared to flat roofs [139].

Additionally, our study also highlights that there are around 77% of the buildings

with a roof area greater than or equal to 10 m^2 which are constructed before 1977. Out of these, some of the buildings have flatter roofs, however most of them are observed to have a pitched roof. Nevertheless, most of these buildings are more than 40 years old, indicating the need for in-depth renovations which can be an opportunity to develop green roofs on top of these buildings.

Apart from this, the identification of priority regions suggests that the potential of green roofs is lower in high priority region as compared to the medium priority region when analysed in terms of number of roofs, but it is quite significant when analysed in terms of total area. The roofs that are completely flat which are in high priority region account for 103 hectares of area for retrofitting green roofs. It is important to note that high priority zone which are socio-economically deprived to an extent might not be able to support the cost of implementing the green roofs, especially for smaller roofs owned by households. On the contrary, large roofs are typically owned by companies. It is essential to identify solutions to make green roofs cost effective especially for larger ones. As the built-up density is relatively higher in the high priority region, implementation of green roofs on the potential buildings can be beneficial.

2.3.4 Limitations and future scope

The present study proposes a simple approach for identifying the green roofs and prioritizing the zones for their implementation. In this study, we identified the potential of green roofs with the help of three parameters, area and slope of the roofs and structure of the building. However, more parameters such as identifying the shaded areas and the building use can enhance the analysis.

Apart from this, as mentioned earlier, roofs that are partially flat need to be further investigated. Moreover, we considered the buildings with a height greater than 20m to be made of concrete. However, a validation of roof slopes and structure is still required to fine-tune the results. Furthermore, we considered roof area greater than $10\mathrm{m}^2$ to have potential to develop green roofs. However, due to obstructions such as chimneys and elevator shafts, there is a need to identify the net available area on each roof for developing the green roofs.

Additionally, in this study, we also prioritized the zones where green roof implementation can yield benefits in terms of environment and socio-economic development. For this we used NDVI, surface temperature and socio-economic deprivation index. As NDVI includes all the greens in the city, it is difficult to gauge the spatial distribution of existing public green spaces in the city. Due to lack of data on existing public green spaces, parameter related to access to green spaces in the city has not been considered. An approach similar to Oehrlein et al., [140] can be used in

increasing the accessibility to green spaces. Apart from this, city of Liège is situated on the banks of river Meuse. With increase in climate change, the risk of flooding can increase. Considering a parameter related to stormwater management in prioritizing the installation of green roof can enhance the analysis. Apart from this, the ecosystem services such as biodiversity enhancement, air quality and recreation are also provided by green roofs. The SMCA including versatile ecosystem services related parameters as done by Langemeyer et al. [42] can be integrated in our study in future.

2.4 Conclusions

UGIs are recognized as important instruments in addressing urban environmental problems by providing the ecosystem services. UGI such as green roofs are gaining popularity owing to their multiple benefits and their ability to provide these benefits in compact cities. In this study, we proposed a simplistic approach for identifying the potential of green roofs along with identification of priority regions in the context of Liège, Belgium.

Our analysis concludes that Liège offers a green roof potential area of about 350 hectares on 20% of the total buildings in the city. According to the analysis for priority zones, we observed that the high priority zone mainly comprises of regions in the city centre near the river and in some parts in the east. Based on the discussed benefits in the literature, developing green roofs in this zone can yield maximum benefits. We observed that the potential of green roofs in the high priority zones as compared to the moderate priority zone is low in terms of number of roofs but is significant in terms of area of roofs. Moreover, the high priority zone of Liège, especially the region in the centre of the city has significantly high built-up density, which makes green roofs implementation extremely relevant. The results also indicate the importance of cost-effective green roof solutions as high priority zones also experience socio-economic deprivation to an extent. However, owing to their multiple benefits, developing green roofs on the potential roofs can have a significant impact on the urban environment. Additionally, green roofs can be combined with other UGIs for better ecosystem services.

The methodology used in this study is straightforward but depends upon the availability and quality of datasets. Moreover, the benefits of green roofs can be analysed with the help of modelling techniques. However, our approach can act as a preliminary decision-making tool for urban planners to analyse the potential of green roofs and prioritize them in deprived areas. Moreover, this approach can be used for other cities in Belgium and Europe with contextual modifications.

2.5 Key contributions

- Liège offers a green roof potential area of about 350 hectares on 20% of the total buildings in the city.
- If only flat roofs with area greater than 100 m^2 are considered, around 21% of buildings with 436 hectare area can be retrofitted with green roofs. We use these potential roofs as a realistic potential of green roofs in analysing their impact on ecosystem services.
- We also analyse the proportions of potential buildings in priority zones based on socio-economic deprivation and lack of green spaces spatially.
- Developing green roofs in the high-priority zone (city centre and the eastern region) can yield maximum benefits.

Part II

UHI mitigation potential of green roofs

3

Employing a highly resolved WRF-LCZ model to identify the influence of realistic potential of green roofs in mitigating heatwave[1]

Given their multifold benefits, green roofs are often considered to mitigate the urban heat island (UHI) effect. Most mesoscale studies consider 100% green roof fraction or the same green roof fraction in each land use while analysing the influence of green roofs on the UHI effect, which is unrealistic. Consequently, the impact of green roofs evaluated in these studies may not be suitable for informing policy. Furthermore, the effect of morphologies on temperature reduction due to green roofs has not been previously studied. To address this gap, in this paper, we evaluate the impact of a realistic fraction of green roofs on the UHI effect during a heatwave in Liège, Belgium, employing a high-resolution WRF study using the BEP-BEM parameterisation with local climate zone (LCZ) land use classification. We run the WRF simulation for the base scenario (without green roofs), extreme scenario (100% green roof fraction), and a realistic scenario. We assume existing flat roofs computed using remote sensing in LCZ as an indication of potential green roofs in a realistic scenario. The results indicate a limited reduction in near-surface

[1] Published as: **M.Y.Joshi**, and J.Teller, *Employing a highly resolved WRF-LCZ model to identify the influence of a realistic potential of green roofs in mitigating heatwave* (2023). Science of Total Environment. (Under review)

air and surface temperature in a realistic scenario, with a nighttime increase in temperature. Additionally, in the extreme scenario, the reduction in temperatures largely depends on the morphology. However, in a realistic scenario, it depends on the green roof fraction. Other indicators like heat index and UHI intensity also is not reduced much with realistic greening. Therefore, realistic roof greening alone will not be sufficient to achieve an impact on a city-scale. An combination of different mitigation strategies are needed for a substantial regional scale impact.

3.1 Introduction

Climate change is causing frequent and extreme heat events such as heat waves, resulting in high heat-stress-induced mortality and increased energy consumption in urban areas [141–143]. Along with urbanisation, this has led to higher temperatures in urban areas than their rural counterparts, causing the Urban heat island (UHI) effect. Heat waves could exacerbate the impacts of the UHI effect [144, 145] by altering the sensible and latent heat flux asymmetrically [146] and changing the wind speeds [147]. Therefore, mitigation of the impacts of heat waves and the UHI effect is crucial.

Several mitigation strategies have been proposed to reduce the extreme impacts of heat waves, such as green-blue infrastructure [148], green spaces [149, 150] and cool reflective materials [151, 152]. Compared to usual mitigation strategies such as trees, water ponds, or parks, roof-based strategies such as green roofs and cool roofs are gaining more popularity in urban areas [120, 152–154] due to the lack of other free spaces. Moreover, since the roofs also receive large amounts of solar radiation, the roof-based strategies can reduce the effects of heat [153, 154]. Unlike cool roofs, green roofs provide multiple ecosystem services such as UHI mitigation, enhancing urban biodiversity, stormwater management, and quality of life [38, 52]. Thus, retrofitting green roofs on the building roofs could be a logical strategy, given the additional benefits.

The advantages of green roofs have been convincingly demonstrated at a building or neighbourhood scale [52]. However, the translation of the mitigation potential of green roofs at these scales to city scale is complex and challenging because of the influence of surface heterogeneity on local microclimate [153, 155, 156]. Moreover, the impacts of individual building green rooftops on air temperatures outside the urban canopy may not be captured [153, 157]. In this aspect, numerical weather prediction (NWP) models aid in upscaling and quantifying the impacts of green roofs at a city or regional scale.

Several studies have used NWP models, such as the weather research and forecasting (WRF) model, to assess the influence of green roofs on the UHI effect during

extreme heat events [153, 158–161]. A major drawback of these studies is that they do not take into account the surface heterogeneity represented as local climate zones (LCZs). Urban canopy parameterisations in NWP models require the most detailed input data, such as land cover and urban morphology, to capture the study area's urbanisation appropriately. Regional scale data on urban morphology is challenging to obtain but is crucial in improving the modelling capacity. LCZs, defined by [162], facilitate the incorporation of urban morphology into the complex modelling of WRF. LCZs are homogenous regions in terms of surface cover, structure, material and human activity that stretch over hundreds of meters to several kilometres horizontally. As LCZ data explains the urban morphology in sufficient detail, we utilise LCZ classes to describe the landscape of the study area.

Apart from this, most WRF studies investigate the potential of green roofs at their maximum capacity (100% green roof fraction) in mitigating the UHI effect [141, 152, 157, 163]. 100% green roof scenarios are unrealistic, especially in European cities where many buildings may have sloped roofs. It is possible to install green roofs on sloped roofs; however, the installation and maintenance costs for this are extremely high [43–45]. Installing them on flat roofs is more feasible. In order to realistically model the effect of green roofs at a city scale, however, NWP studies should combine both realistic fractions of green roofs and LCZs. By realistic, we mean the existing flat roofs that may be transformed into extensive green roofs without severely altering the building. Such studies are lacking in the literature.

Another assumption in most WRF studies of green roofs is the use of the same green roof fraction across all LCZs. Assuming a similar green roof fraction across different land uses is unrealistic since the type of buildings varies across the land uses and LCZs. For instance, residential buildings mainly have sloped roofs in European cities [46–48], and since they are privately owned, implementing green roofs on them could be challenging [49,50]. However, installing green roofs on commercial buildings such as malls, industrial buildings, or public buildings like schools or hospitals can be relatively easier since the buildings are often maintained by municipalities [51]. Therefore, in this study, we provide a method to assess the impact of a realistic fraction of green roofs on the UHI effect, which is based on the availability of flat roofs in each LCZ class, identified using remote sensing.

Furthermore, while WRF studies with LCZ classification and BEP–BEM (Building Energy Parameterisation and Building Energy Modelling; most sophisticated parameterization setting of WRF. For more details, refer section 3.2) parameterisation is available for other parts of the world [157, 164–166], such a study has never been employed for North-Western European cities with temperate climates to assess the role of green roofs or any other mitigation strategy. These cities are experiencing

recurring severe heat waves with a longer duration each passing year during summer [87]. Therefore, assessing the potential of mitigation measures like green roofs in such cities is necessary. Consequently, we perform this study in the context of Liège, Belgium. To the best of our knowledge, such a study has never been conducted for a Western European city like Liège.

Thus, in this paper, we perform a high-resolution WRF study using the BEP-BEM parameterisation with LCZ land use classification to assess the impact of a realistic fraction of green roofs on the UHI effect during a heatwave in Liège City. There are three main novelties in the paper:

1. By using a fraction of flat roofs obtained using remote sensing as an indication of potential green roofs in each LCZs, we assess the impact of a realistic percentage of green roofs on the UHI effect.
2. We do this by analysing the spatial and temporal variability of observed effects in terms of temperature and UHI indicators.
3. We assess the impact of green roofs in different LCZs by evaluating the typological variability of air and surface temperatures.
4. Lastly, for the first time in the WRF studies, this paper analyses a North Western European city with a temperate climate like Liège.

We mainly run three simulations for the study area; i) without green roofs (base scenario), ii) with a realistic fraction of green roofs (realistic scenario) and iii) with 100% roof greening for all LCZs (extreme scenario).

The remainder of this paper is organised as follows. Section 3.2 explains the WRF model along with the BEP-BEM parameterisations and the inputs and outputs from the model in detail. Section 3.3 presents the model validation and the results from three simulation runs. Finally, section 3.4 draws the concluding remarks of our paper.

3.2 Methodology

3.2.1 WRF model

The WRF model is an NWP and atmospheric simulation model intended for both research and operational applications. In this paper, we employ the WRF version 4.4.1. WRF model has a dynamic solver that incorporates compressible and non-hydrostatic Euler equations with several physical and dynamic options designed for regional scale. However, as there is an increasing interest in simulating the urban atmosphere, urban canopy schemes are developed and integrated into WRF due to the complex

dynamics of urban climate. Urban canopy schemes such as BEP-BEM are included in WRF as physics options to represent better urban morphology, such as building and street geometry and the surface characteristics such as albedo, emissivity, and urban/vegetation fraction [92].

WRF has three urban canopy parameterizations: Single layer urban canopy model (SLUCM), multi-layered urban canopy model (MLUCM) with building energy parameterisation (BEP), and MLUCM with BEP-BEM (Building energy modelling). The SLUCM assumes infinitely long street canyons that represent urban geometry. The MLUCM BEP model represents more sophisticated urban modelling in WRF. It divides the urban canopy into several vertical layers at various heights. It independently solves fluxes and meteorological variables in each layer, enabling the characterisation of building height distribution in high-density built areas.

Coupling with BEM, using BEP-BEM, WRF models the anthropogenic quantities (including emissions from air conditioners or equipment and indoor-outdoor air exchange) at different heights independently as heat or moisture fluxes. As BEP-BEM is the most sophisticated UCM model, we utilise the BEP-BEM parameterisation in this paper to simulate the diurnal variation of near-surface air temperature ($\mathrm{T_{air,2m}}$), surface temperature ($\mathrm{T_{se}}$) and relative humidity ($\mathrm{RH_{2m}}$) over the city. The BEP-BEM model computes the surface momentum, heat exchanges, humidity, and turbulent kinetic energy fluxes to the atmospheric dynamics governing equations. Compared to SLUCM, the BEP-BEM system includes [92, 167, 168]:

(a) the 3D urban structure in the model using multiple layers and the origins and skins of momentum and heat in the vertical layers within the urban canopy layer,
(b) the impact of horizontal and vertical surfaces such as roads and walls on the momentum, turbulent kinetic energy and potential temperature,
(c) the shading, reflection and blocking effect of horizontal and vertical surfaces on net solar radiation within the urban canopy layer,
(d) exchange of heat between building walls, rooftops, and floors
(e) heat discharged by people and domestic electrical appliances and
(f) air-conditioning cooling, heating, and ventilation

Advanced urban geometry must be described accurately to evaluate the physical processes within the urban region. In the recent versions of WRF, there is an option to integrate the 11 urban LCZs to classify the urban landscape of the study area using the MLUCP BEP-BEM parameterisation. Many studies have implemented this method to assess the urban climate (Brousse et al., 2016; Zonato et al., 2020; Hammerberg et

al., 2018; McRae et al., 2020; Patel et al., 2020) and also to assess the strategies for regulating the urban climate. This study uses the LCZ map for Europe generated by WUDAPT [169, 170].

3.2.2 Surface energy balance

The surface energy balance of a surface in WRF is represented by:

$$\mathrm{SW_{net}} + \mathrm{LW_{net}} + \mathrm{AH} = \mathrm{LH} + \mathrm{SH} + \mathrm{G}, \tag{3.1}$$

where $\mathrm{SW_{net}}$ is the net shortwave radiation at the surface, $\mathrm{LW_{net}}$ is the net longwave radiation at the surface, AH is the anthropogenic heat flux, LH and SH are the latent and sensible heat fluxes, and G is the ground heat flux. For BEP-BEM, the AH comes from air-conditioning, heat exchanges between building interior and exterior air, and the heat released by equipment and people within the buildings. The BEP-BEM parameterisation does not include the AH from traffic or industry.

A traditional roof transfers all net radiation into sensible heat flux and heat entering the building, raising the $\mathrm{T_{se}}$ and $\mathrm{T_{air,2m}}$. Green roofs lower the net radiation at the roof by predominantly releasing the latent heat flux from the vegetation and soil. The green roof modeling in WRF is explained briefly in the next section.

3.2.3 Numerical Modeling of Green Roofs

WRF parameterises the green roofs with land-surface scheme developed based on [171] and [172]. It considers the incoming net radiation, water input from precipitation and irrigation, evapotranspiration from vegetation, heat exchange with the atmosphere, and diffusion of energy and moisture throughout the soil to compute the energy and water budgets. This model is one dimensional, as horizontal transport and subsurface flows are neglected.

In WRF, a green roof consists of 10 layers ($\sim$ 30 cm), with five levels representing the organic matter substrate (8 cm), one level representing the drainage layer (5 cm) and four levels describing the insulation layer (16.6 cm). More details can be found in [173].

Hydrology and thermodynamics of green roofs

The latent heat flux (LE) from green roofs comprises of evaporation from soil moisture and evapotranspiration through the leaves as follows:

$$LE = \frac{\rho_a L(q_{surf,S} - q_a)}{R_a + R_S}, \tag{3.2}$$

where ρ_a is the air density, L is the latent heat of vaporisation, $(q_{surf,S} - q_a)$ is the difference between the specific humidity of saturated soil and the actual air humidity around the plants [171], R_a is the aerodynamic resistance [174] and R_s is the stomatal resistance. The details of calculating R_s can be found in [175] and [173].

The heat transfer between green roof layers is calculated using the Fourier diffusion equation for soil temperature:

$$\frac{\partial T}{\partial t} = \frac{\partial}{\partial z}\left(\lambda \frac{\partial T}{\partial z}\right) + F_T \tag{3.3}$$

where F_T stands for source and sink terms. F_T is calculated from the surface energy balance for the topmost layer:

$$\frac{F_T}{\Delta z \lambda} = \mathrm{SH} - \mathrm{LE} + (1 - \alpha_{\mathrm{GR}})\,\mathrm{SW}_{\mathrm{net}} + \mathrm{LW}_{\mathrm{net}}, \tag{3.4}$$

where α_{GR} is the albedo of the green roofs, λ is the thermal diffusivity of the substrate layers and the $\mathrm{LW}_{\mathrm{net}}$ changes based on the temperature and emissivity of the green roof which is 0.93. For the layer close to the conventional roof, F_T is the heat conduction flux calculated using the temperature gradient between the bottom layer of the green roof and the uppermost layer of the structural roof, using a weighted average of their thermal diffusivity values. The thermal diffusivity for natural roof layers depends on soil moisture. More details can be found in [173].

3.2.4 Model set-up

Simulation domain

The study area targets Liège City and the surrounding area centred on 50°38'1.43" N 5°34'2.96" E. Four one-way nested domains were used with 150 x 150 grid points in domain 1, and 151 x 151 grid points in domains 2 and 3, respectively and 175x175 grid points in domain 4, with a grid spacing of 9, 3, 1, 0.333 km in WRF 4.4.1, respectively (Figure 3.1(a)). The outer domain includes the North Sea and Western Europe, whereas the innermost domain contains the Arrondissement of Liège in the centre surrounded by the Arrondissement of Tongres, Huy, Waremme, Verviers along with a small part of South-Limburg in the Netherlands. Arrondissements in Belgium are sub-divisions of provinces. The LCZ classification is substituted as Land-use classification in the innermost domain (d04) by updating the surface parameters for every grid. The other domains are initialised using MODIS land use data. The innermost domain has 11 urban LCZ categories to enable WRF to utilise detailed urban morphologies for the chosen BEP-BEM parameterization. The details to integrate the LCZ into WRF can be found in [176].

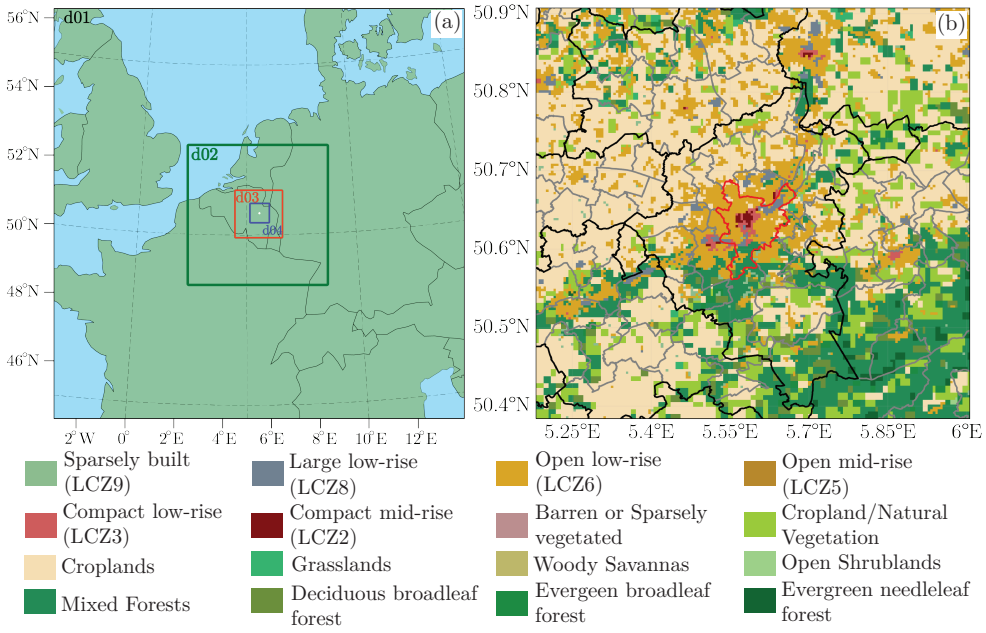

Figure 3.1: (a) WRF domain configuration. The outer domain (d01), the second domain (d02), the third domain (d03) and the innermost domain (d04) have a resolution of 9 km, 3km, 1km and 333 m, respectively. (b) Urban land-use categories after the incorporation of local climate zones (LCZs) from WUDAPT data over domain d04.(Black borders represent provinces, grey borders represent municipality, red border is the Liège municipal boundary)

Parameter settings

In this study, we use the LCZ data produced for Europe by [169, 170] for the innermost domain. The non-urban land covers are based on the MODIS (Moderate Resolution Imaging Spectroradiometer) data 21-class product [177]. The innermost domain mainly contains only six urban LCZ classes, which are LCZ-2 (Compact mid-rise), LCZ-3 (Compact low-rise), LCZ-5 (Open midrise), LCZ-6(Open low-rise), LCZ-8(Large low-rise), and LCZ-9 (Sparsely built)(Figire 3.1(b)). We use 45 vertical levels in [92] from surface to 50 hPa [164] with six levels within the urban canopy layer of 5-10 m each. The first point is sufficiently close to the ground (at 2.5m), which satisfies the requirement of the BEP-BEM model [164, 178]. The integration time-step was 40 s for the outermost domain, and we collected the simulation outputs every hour for the innermost domain. The initial and boundary conditions were taken from

European Centre for Medium-Range Weather Forecasts (ECMWF) reanalysis v5 (ERA5) data [179] with an update interval of 3 hours. Apart from this, in this work, we used the unified Noah land-surface model for the land-surface scheme [180, 181] and the Mellor-Yamada-Janjic scheme for the planetary boundary layer [182]. We use the Thompson microphysics scheme [183] and the Rapid Radiative Transfer Model for Global Circulation Models (RRTMG) for longwave and shortwave radiation [184]. For the surface layer scheme we use the Monin-Obukhov-Janjic approach [182]. Lastly, we used the Modified Tiedtke scheme for cumulus parameterisation [185]. The length and time frame of the simulation is decided based on the occurrence of the most severe and longest heatwave in Liège city. The method used for identifying heatwaves is described in section 3.2.4.

Realistic potential of green roofs in LCZ

For this study, we estimate a realistic potential of roof greening in Liège city using remote-sensing and geoinformation systems (GIS). We simulate the green roofs only where the existing flat roofs are present to ensure practical greening. We identified flat roofs using LiDAR point cloud data with a point density of 0.8 points/m^2 for Liège. Employing the RANSAC algorithm to process LiDAR point cloud, we obtain the number of planes within a building footprint. Assuming flat roofs to have less than a 10° slope, we identify planes that are flat with an area of at least 10 m^2 for each building. This way, we identify the buildings with flat roofs in Liège. The details of this methodology can be found in [88]. Based on this, we consider buildings with flat roofs for roof greening.

To compute a realistic percentage of green roofs in each LCZ, firstly, we rasterise the building layer and buildings with green roofs layer to 1 m resolution raster. Thereafter, we aggregate the pixels to 100 m (same resolution as LCZ) by summing, to understand the proportion of potential green roofs per 100×100 m pixels.

We calculate a realistic percentage of green roofing in each LCZ as:

$$\mathrm{GR}_{\mathrm{LCZ}} = \frac{\mathrm{GR}_{\mathrm{mean}}}{\mathrm{BU}_{\mathrm{mean}}}, \tag{3.5}$$

where GR_{mean} is the average area of potential green roofs in one LCZ class and BU_{mean} is the average of building area in the LCZ class. To compute GR_{mean} and BU_{mean}, we use QGIS *Raster layer zonal statistics* tool.

Based on this, figure 3.2 shows the roof greening potential in each LCZ in Liège city. The percentage of roof greening potential is the highest for LCZ-8, followed by LCZ-5, 9, 2, 3 and 6.

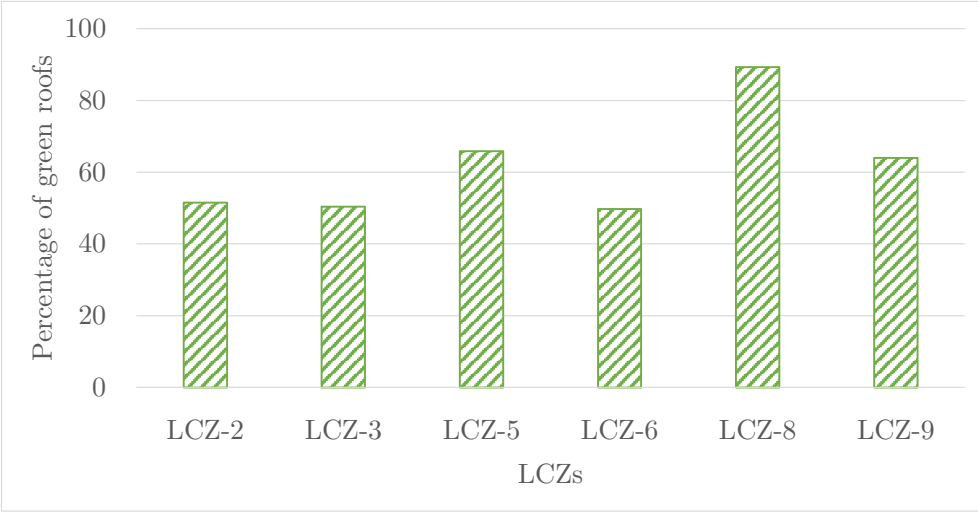

Figure 3.2: Percentage of green roofs

Identifying the heatwave

We identify the longest and the most severe heatwave observed in Liège in the last 20 years to decide the length and time frame of the simulation based on [3]. The meteorological data used for identifying heatwaves is obtained from the weather station nearest to Liège city. The approach is mainly based on high quantiles of distributions of daily temperatures. Figure 3.3 shows how the heatwave can be characterised for a given period of time using the three settings, namely, *Spic, Sdeb and Sint*. *Spic* refers to the temperature threshold beyond which an event is detected, whereas, *Sdeb* is the threshold that defines the beginning and the end of the heatwave. *Sint* is the interruption threshold which enables merging two consecutive occurrences without a significant drop in temperature.

The heatwave event starts when the temperature is above the *Sdeb* threshold. The heatwave is interrupted if the daily temperature goes below the *Sdeb* threshold for at least three consecutive days or drops to values below the *Sint* threshold. The values of *Spic, Sdeb and Sint*, which are 99.5, 97.5 and 95th percentile, respectively, are computed on the daily mean air temperatures for a given period. These values are a result of a detailed preliminary analysis of EURO-CORDEX data [3, 186], which led to heatwave identifications close to the application of the operational method. This method is beneficial as it considers the local climate of the study area. We compute the number of heatwaves, their intensity and duration and select the heatwave with the highest

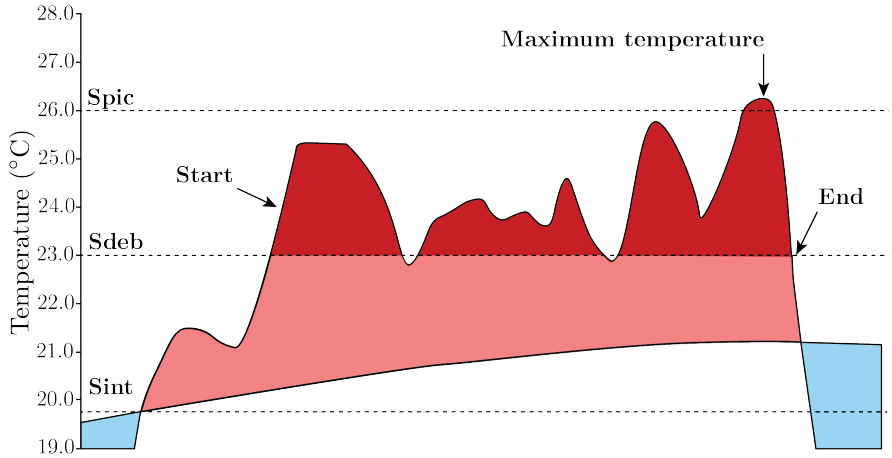

Figure 3.3: Characterisation of a heat wave from a daily mean temperature indicator: Duration (start and end), maximal temperature and global intensity (red area of the plot). Temperatures above (below) climatological line (2000-2020 reference period) are represented by pink (blue) area. Graphic adapted from Ouzeau et al. [3].

intensity and duration. We run the simulation for the entire heatwave in this study.

3.2.5 Indices for assessing UHI effect

UHI intensity

There are several ways to estimate the UHI intensity (UHII) [187–189]. In this paper, we use the linear equation between urban fraction ($\mathrm{Urb_{frac}}$) and temperature given by [188].

$$\mathrm{T} = \mathrm{Urb_{frac}} \times \mathrm{UHII} + \mathrm{T_{rural}} \tag{3.6}$$

Here, the $\mathrm{Urb_{frac}}$ is the independent variable, and the slope of this equation is the UHII. The intercept, in this case, is the temperature in the previous area, which is the non-urban (rural) area. We exclude the areas with open water bodies and consider only the urban LCZ pixels. The $\mathrm{Urb_{frac}}$ is obtained from MODIS and LCZs. This mainly indicates the level of urbanisation with a proportion of impervious areas.

Heat index

The UHI effect also deteriorates human thermal comfort influencing the health of people. Therefore, we examine heat index (HI) using a regression analysis by [190],

which is used by many recent studies. The Steadman's HI is widely used as a metric for measuring thermal comfort that includes temperature and relative humidity. It primarily describes the perception of heat felt by a human body under a given weather. The calculation of HI is as follows [191]:

$$\begin{aligned} \mathrm{HI} = & -42.379 + 2.04901523 \times \mathrm{T} + 10.14333127 \times \mathrm{RH} - 0.22475541 \times \mathrm{T} \times \mathrm{RH} \\ & - 0.00683783 \times \mathrm{T}^2 - 0.05481717 \times \mathrm{RH}^2 + 0.00122874 \times \mathrm{T}^2 \times \mathrm{RH} \\ & + 0.00085282 \times \mathrm{T} \times \mathrm{RH}^2 - 0.00000199 \times \mathrm{T}^2 \times \mathrm{RH}^2 \end{aligned} \tag{3.7}$$

where the HI is calculated in °F but is transferred to °C for consistency. T is the dry-bulb temperature, and RH is the relative humidity. In our study, the HI was calculated based on $\mathrm{T}_{\mathrm{air,2m}}$ and $\mathrm{RH}_{\mathrm{2m}}$ from WRF outputs. We also showcase the details of the boundary layer within 2 km by describing the vertical profile of $\mathrm{T}_{\mathrm{air}}$, RH and V.

3.3 Results and Discussion

3.3.1 Selected heatwave in Liege

In this section, based on the methodology for heatwave detection by [3], we select the most intense and longest heatwave in Liège. Figure 3.4(a) shows the intensity and duration of the heatwaves in Liège between 2000-2020. We observe that there have been six heatwaves in Liège during this period. Moreover, the intensity of heatwaves is increasing with time. Most heatwaves have a duration of more than eight days. We can see that the heatwave of the year 2018 is the longest heatwave with a severe intensity. Therefore, we choose this heatwave for this work and run the simulation from 23rd July to 7th August. Figure 3.4(b) demonstrates the daily mean temperatures for 16 days of this heatwave which was observed from 23rd July to 7th August 2018. The daily mean temperature is the highest for the 27th of July.

3.3.2 Comparison of WRF results with meteorological measurements

We validate the values of 2-meter air temperature $\mathrm{T}_{\mathrm{air,2m}}$, 2-meter relative humidity $\mathrm{RH}_{\mathrm{2m}}$, and 10-meter wind speed $\mathrm{V}_{\mathrm{10m}}$ obtained from the WRF model with the weather station data nearest to Liège over the entire simulation period of 16 days (23rd July to 8th August 2018). Figure 3.5 suggests that the model results show a good agreement with the observations. The diurnal variation of the temperature and humidity obtained from the model shows good agreement with the observations. Furthermore,

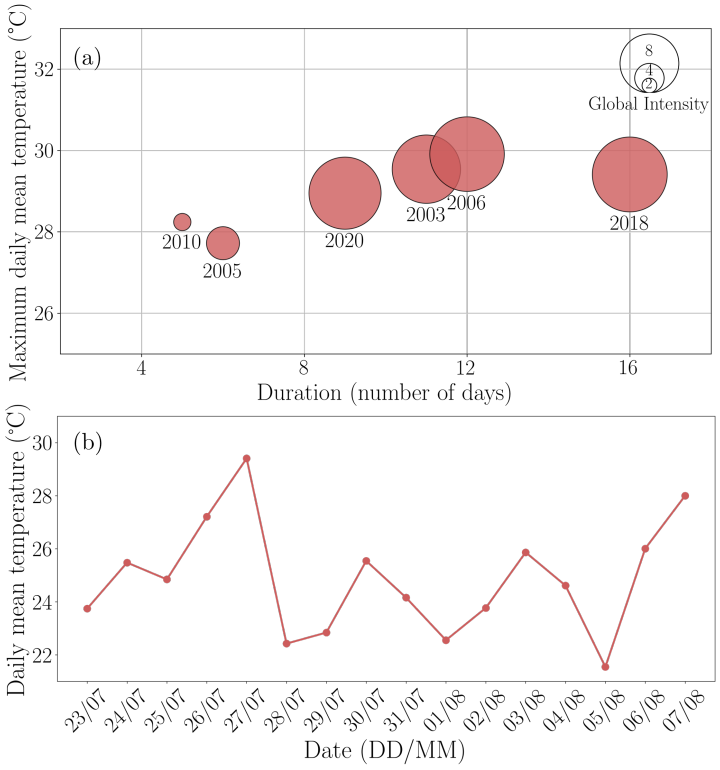

Figure 3.4: (a) Intensity and duration of heatwaves in Liège from 2000 to 2020 (b) Daily mean temperature during the longest and most intense heatwave in Liège ((a) is made using the code provided by [4, 5]

the wind velocity (Fig. 3.5(c)) also matches well; considering the difficulties involved in accurately modelling turbulence to predict the wind speed, the results shown in the figure satisfactorily predict the required quantities of interest.

On certain days, the simulation results show a cold and wet bias during the day and night, with a higher bias at night compared to the day (Table 3.1). The RMSE values are also lower during the day. The wind speeds follow a similar trend to the observations from the weather station with slight over and underestimations. Previous studies also report similar biases as systematic biases of the model [157, 192–196]. However, the goal of the present study is to do a comparative study of the scenarios with and without green-roofs and as such, the current predictions are indeed enough for such a study.As the simulations of all scenarios use the same physical parameterisations and configurations; they are comparable in performance and can be compared to

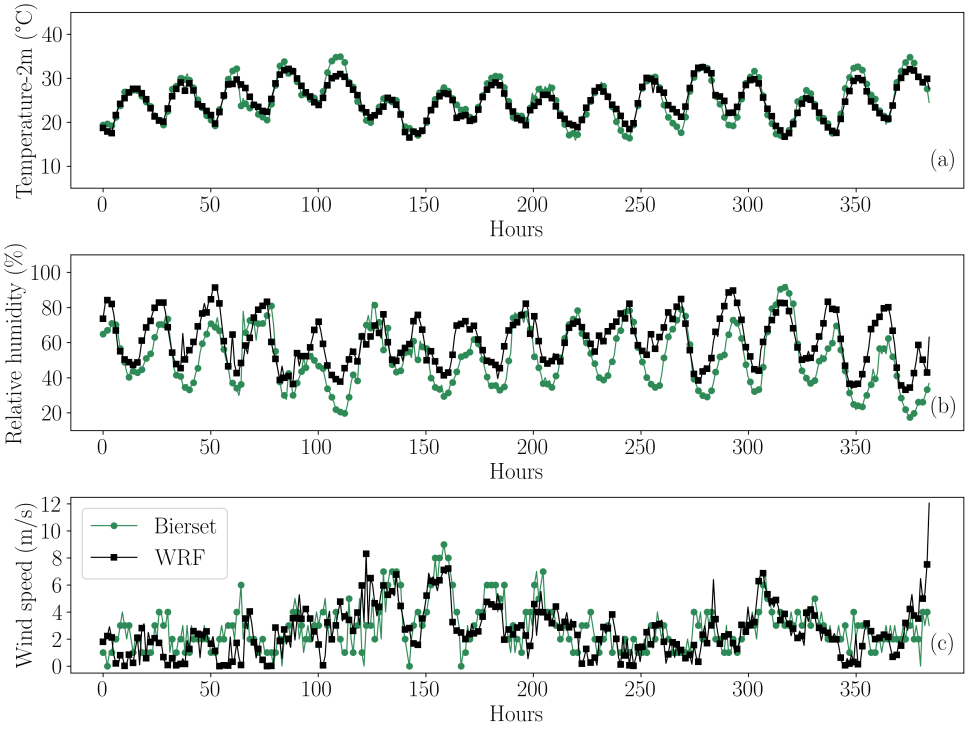

Figure 3.5: Time series of (a)2-m temperature (in °C) and (b)relative humidity (%) (c)10-m wind speed (in ms^{-1}) for weather station (green) and output from WRF (black)

Table 3.1: Summary of mean absolute error (MAE) and root mean squared error (RMSE) for simulated and weather station data of $\mathrm{T_{air,2m}}$, $\mathrm{RH_{2m}}$, and $\mathrm{V_{10m}}$ during day (04:00-18:00) and night (19:00-4:00) for entire simulation

	MAE			RMSE		
	Day	Night	Total	Day	Night	Total
$\mathrm{T_{air,2m}}$	-0.08	-0.17	-0.167	0.741	1.6865	1.659
$\mathrm{V_{10m}}$	-1.29	-0.20	-0.244	1.88	1.72	1.731
$\mathrm{RH_{2m}}$	4.13	10.14	9.91	7.23	14.46	14.25

obtain insights into scenarios with and without green roofs.

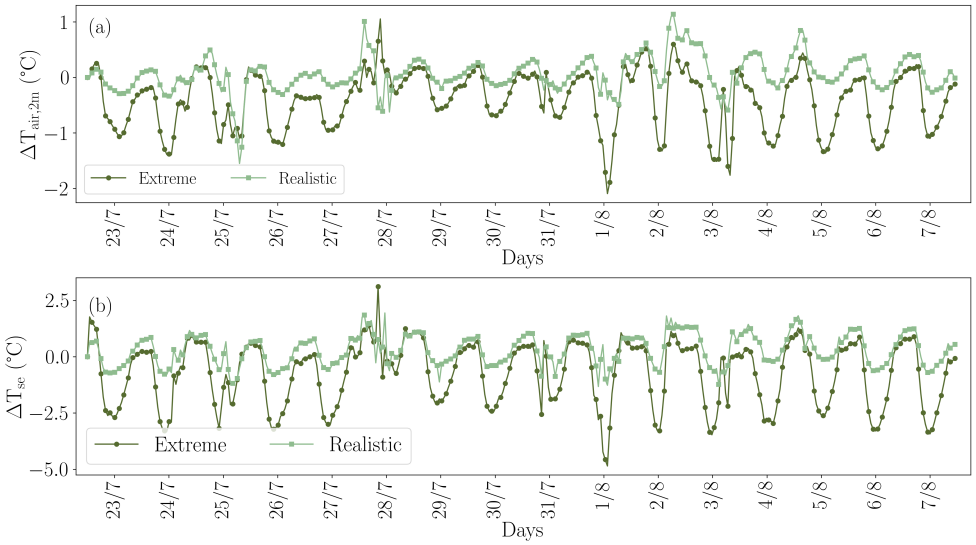

Figure 3.6: Temporal variation of difference in (a) near-surface air temperature ($\Delta T_{air,2m}$) and (b) surface temperature (ΔT_{se}) in realistic and extreme scenario averaged over the innermost domain

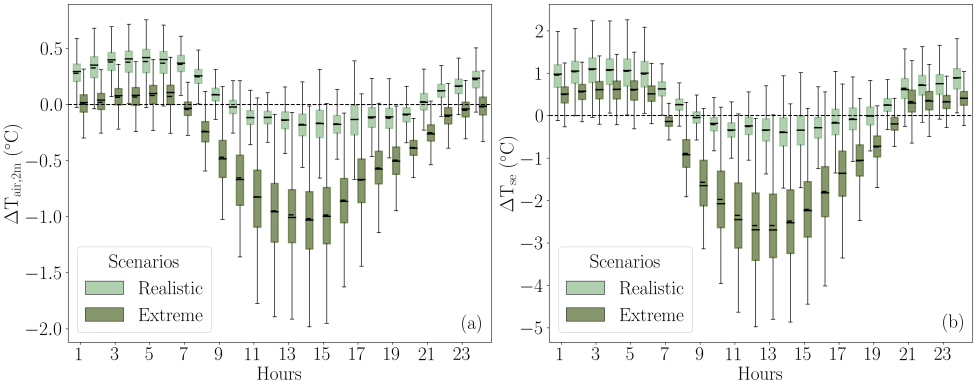

Figure 3.7: Spatial variation of difference in (a) near-surface air temperature ($\Delta T_{air,2m}$) and (b) surface temperature (ΔT_{se}) in realistic and extreme scenario averaged over the innermost domain

3.3.3 Impact of green roofs on temperature

Figure 3.6 presents the temporal variation of differences in near-surface air temperature ($\Delta T_{air,2m}$) and surface temperature (ΔT_{se}) spatially averaged over the innermost domain for only the urban grid cells. We observe that the $\Delta T_{air,2m}$ and ΔT_{se} follow a typical diurnal cycle for each day during the entire simulation period. The $T_{air,2m}$ and T_{se} decrease during the day and slightly increase during the night. The reduction in temperatures during the day is higher in the case of the extreme scenario compared to a realistic scenario. Understandably, due to the non-linear nature of the interactions between turbulence, heat, and moisture the reduction in temperature is not the same over all the days. Furthermore, we observe that the surface temeperature has similar values over different days, however the air-temperature has more variations (Figure 3.6). This can be explained by the fact that the near-surface turbulence plays a major role in deciding the air-temperature which is more sensitive than the surface temperature which majorly depends on the surface energy balance caused by the radiation. While the maximum reduction in $T_{air,2m}$ is around 0.5°C for a realistic scenario, it reduces up to 2°C for the extreme scenario. The maximum reduction in T_{se} is around 1.5°C in a realistic scenario, whereas it is around 4.5°C in the extreme scenario. During the night, the increase in $T_{air,2m}$ is around 0.2°C and 0.5°C in extreme and realistic scenarios, respectively.

To quantify the average spatial and temporal variation of green roofs on temperature reduction, we calculate the average reduction in temperature over a 14-day period. We neglect the first two days of simulations to account for the spin-up effects. In Figure 3.7, we demonstrate the temporally averaged spatial variation in temperature for 24 hours, to examine whether the impact of green roofs varies spatially in both scenarios. While most of the $\Delta T_{air,2m}$ values are between 0.2-0.4°C in a realistic scenario, the values vary between 0.75-1.2°C in the extreme scenario. Similarly, in terms of T_{se}, the range of ΔT_{se} is greater for the extreme scenario compared to a realistic scenario. Most (values between 25th to 75th percentile, 50%) of the ΔT_{se} values range from 0-1°C and 1.5-3.5°C for realistic and extreme scenarios, respectively. Spatially also, the increase in temperatures during the night in a realistic scenario is similar to the decrease in temperatures during the day.

Figure 3.8 and 3.9 show the spatial variation averaged over 24 hours. We observe that on average, there is a decrease in air and surface temperature overall. This is due to the longer days during summer in Europe. We also observe that the decrease in both T_{air} and T_{se} is slightly higher on the western side of Liège (outside the city boundary) in both scenarios. In the city center, the decrease in T_{air} and T_{se} is lower.

This suggests that the T_{se} and $T_{air,2m}$ reductions are limited for a realistic scenario where a certain percentage of building roofs are greened. Moreover, in a realistic

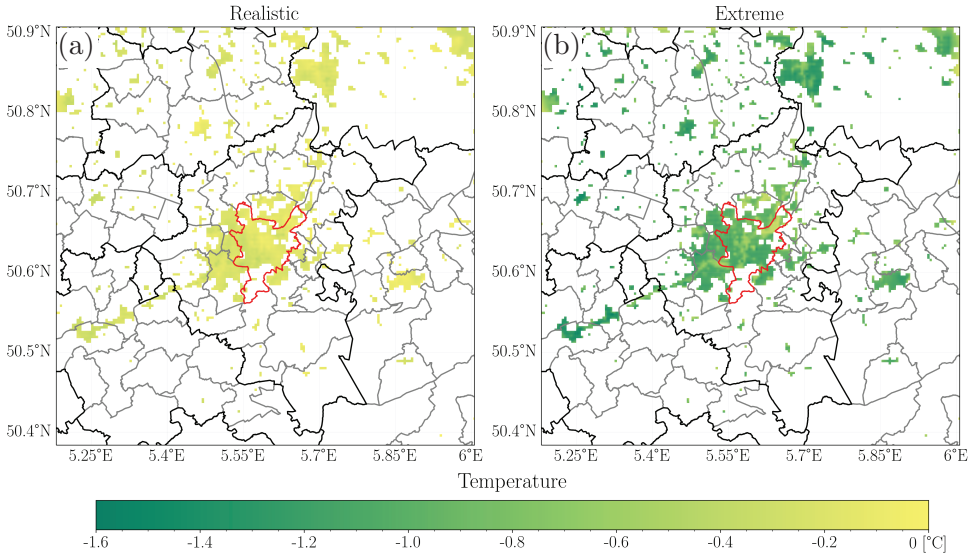

Figure 3.8: Spatial variation of temporally averaged differences in air temperatures (a)Realistic scenario (b)Extreme scenario

scenario, there is also warming of a similar magnitude. As the temperature changes differ spatially (Figure 3.8 and 3.9), it may vary in different LCZs. Moreover, LCZs vary in terms of green roof potential and morphology. Therefore, in the next section, we explore the impact of realistic and extreme green roofing scenarios in each LCZ.

3.3.4 Green roofs and Local Climate Zones

Figure 3.10 and 3.11 shows the spatial variation of ΔT_{air} and ΔT_{se} for each urban LCZ within the study domain.

Near-surface air temperature

In the extreme scenario, during the day, the largest $\Delta T_{air,2m}$ is observed in the compact low-rise LCZ-3, followed by the open low-rise LCZ-6, compact mid-rise LCZ-2, open mid-rise LCZ-5, large low-rise LCZ-8 and sparsely built LCZ-9. Although the maximum value of $\Delta T_{air,2m}$ is observed in LCZ-6, more (around 75%) values of $\Delta T_{air,2m}$ in LCZ-3 are greater than 1°C, whereas only 30-50% of the values of $\Delta T_{air,2m}$ are greater than 1°C in LCZ-6. Therefore, green roofs are more effective in LCZ-3

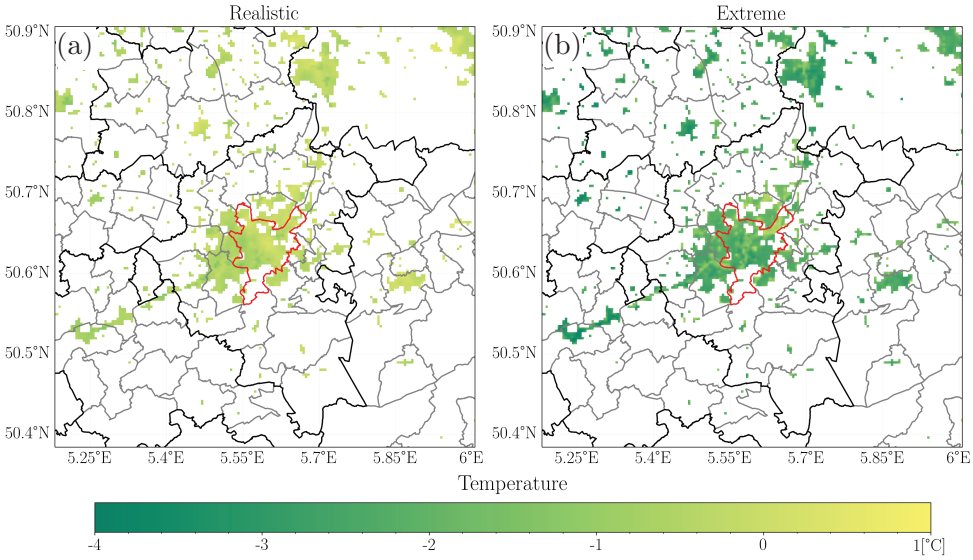

Figure 3.9: Spatial variation of temporally averaged differences in surface temperatures (a)Realistic scenario (b)Extreme scenario

compared to LCZ-6. The extent of reduction in $T_{air,2m}$ depends on the morphology of the LCZ. For instance, the highest $\Delta T_{air,2m}$ is observed in compact LCZs (LCZ-2 and 3). So, a larger built-up area means a higher percentage of roofs to green and a higher reduction in $T_{air,2m}$. The reduction in $T_{air,2m}$ is also higher for LCZs with low-rise buildings compared to high-rise ones.

Contrary to the observations in the extreme scenario, during the day, we observe the highest reduction in $T_{air,2m}$ in the large low-rise LCZ-8, in a realistic scenario. This could be due to the highest percentage of flat roofs available for greening compared to the other LCZs. This LCZ (large low-rise) is characterised by large-sized commercial or industrial buildings, which usually have large flat roofs. Compact mid-rise and low-rise, along with open mid-rise LCZs (LCZ-2,3 and 5), experience a similar range of reduction in $T_{air,2m}$, followed by open low-rise and sparsely built LCZs (LCZ-6 and 9). In a realistic scenario, we observe that building heights or density do not affect the reduction in $T_{air,2m}$. The reduction in $T_{air,2m}$ is largely dependent on the roof greening potential in each LCZ.

It is important to note that the reduction in $T_{air,2m}$ is less than 0.5°C for most of the region within LCZ-8, with some areas experiencing a reduction in $T_{air,2m}$ of greater than 0.5°C. Almost entire regions of other LCZs experience a reduction of

less than 0.5°C in $T_{air,2m}$. Therefore, realistic roof greening may not be beneficial in reducing the $T_{air,2m}$ in most urban areas. However, it may be beneficial in some of the areas of large low-rise LCZ-8.

Surface temperature

Similar to $T_{air,2m}$, in the extreme scenario, the highest reduction in T_{se} is observed in compact low-rise LCZ-3, followed by open low-rise LCZ-6, compact mid-rise LCZ-2, open mid-rise LCZ-5, large low-rise LCZ-8 and sparsely built LCZ-9. This means that greening the roofs in compact and low-rise types of LCZs can be beneficial in reducing the T_{se}. Similarly, in a realistic scenario, the highest reduction in T_{se} is observed in large low-rise LCZ-8 (similar to the trend for $\Delta T_{air,2m}$ in a realistic scenario). Almost more than 50% of the LCZ-8 experiences a reduction of greater than 1°C in T_{se} with realistic roof greening. Realistic roof greening in compact low-rise and open low-rise (LCZ-3 and 6), although reduces the T_{se} more than the compact and open mid-rise

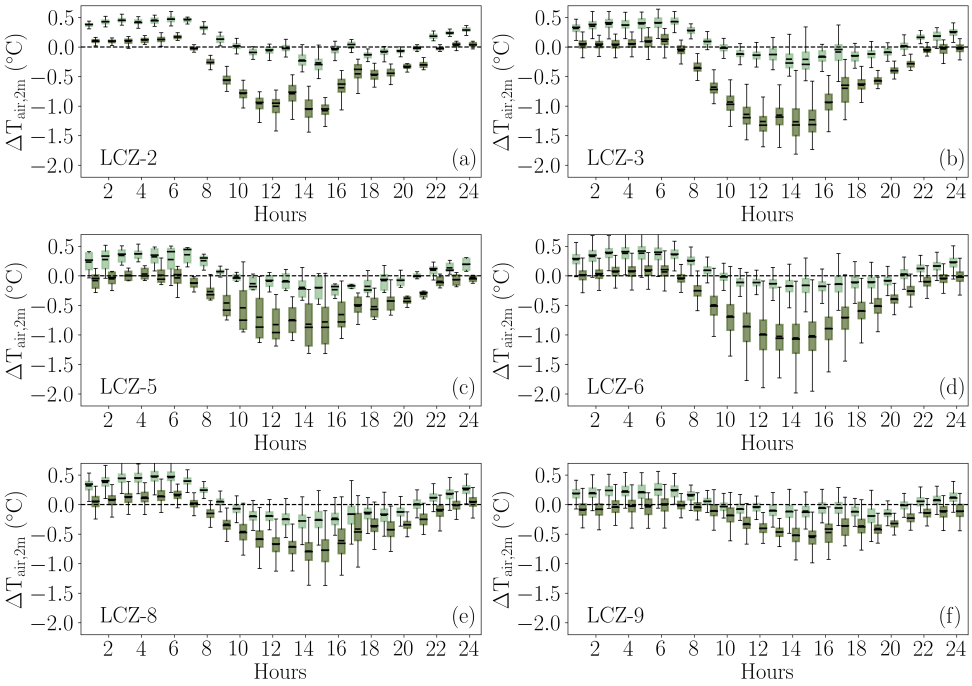

Figure 3.10: Diurnal spatial variation of ΔT_{air} for (a)LCZ-2, (b)LCZ-3, (c)LCZ-5, (d)LCZ-6, (e)LCZ-8, (f)LCZ-9

(LCZ-2,5), the reduction in T_{se} is less than 1°C for most of the region in these LCZs. Therefore, realistic roof greening is not beneficial in LCZ-2,3,5 and 6. Sparsely built LCZ-9 has the lowest reduction in T_{se} because of the lowest built-up available for roof greening.

Similar to T_{air}, T_{se} also increases at night in all LCZs, with the same amount of increase at night as the decrease in T_{se} during the day. The increase in T_{se} at night is also higher than the decrease in T_{se} during the day for LCZ-2,3,5 and 6.

Altogether, the impact of green roofs on $T_{air,2m}$ and T_{se} in LCZs is distinctive. It depends on morphological factors such as building density and height when the percentage of roof greening is the same in all LCZs. However, when a realistic scenario is investigated, the impact of green roofs is better in large low-rise LCZ where the percentage of potential roof greening is higher. It is important to note that the reduction in temperatures in a realistic scenario is not significant in other LCZs. Moreover, night-time warming is observed in all LCZs.

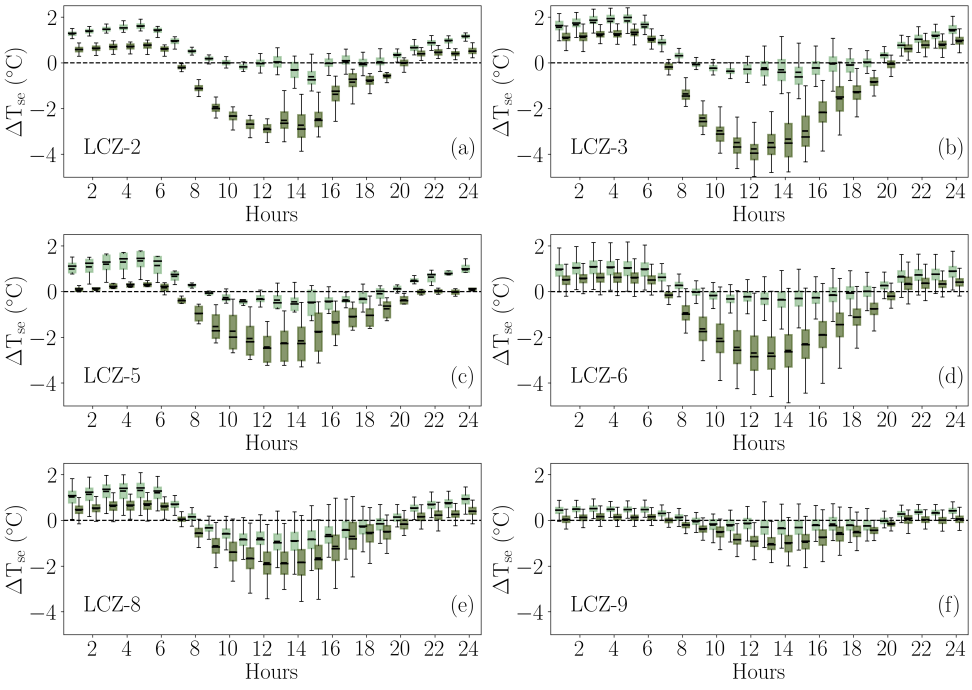

Figure 3.11: Diurnal spatial variation of ΔT_{se} for (a)LCZ-2, (b)LCZ-3, (c)LCZ-5, (d)LCZ-6, (e)LCZ-8, (f)LCZ-9

3.3.5 Impact on UHI effect

We measure the impact of green roofs on the UHI effect using UHI intensity (UHII) during the daytime. Figure 3.12 shows the air and surface UHII computed for the innermost domain. We observe that the air UHII is reduced by 1°C and surface UHII is reduced by 3.5°C with extreme roof greening, whereas the air UHII is reduced by 0.25°C and surface UHII is reduced by 0.5°C with realistic roof greening. We also observe that with an increase in urban fraction, there is an increase in both T_{se} and $T_{air,2m}$, suggesting a connection between UHII and urbanisation, even in the extreme roof greening scenario. However, the increase in UHII with urbanisation is lesser with the introduction of green roofs in the study domain. The reduction in UHII is insignificant with realistic greening.

3.3.6 Heat Index

As explained in section 2.5.2, HI is widely used as a metric for measuring thermal comfort that includes temperature $T_{air,2m}$ and relative humidity RH. It primarily

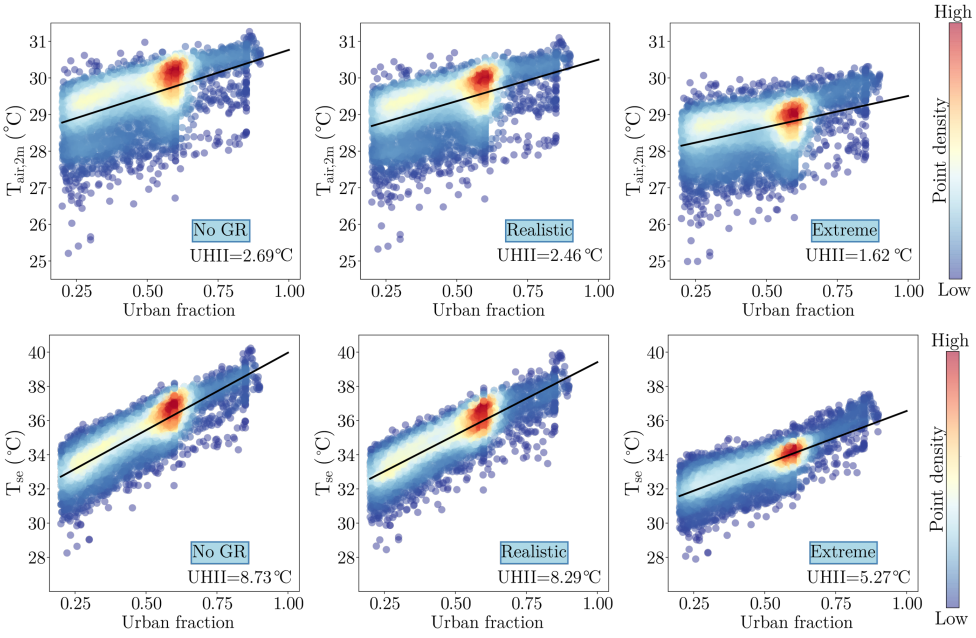

Figure 3.12: Relationship between daytime T_{air} (°C) and the urban fraction with linear fitting ((a),(b),(c)), and daytime T_{se}

describes the perception of heat felt by a human body under a given weather, with increasing HI thermal comfort reduces. Figure 3.13 (a) shows the temporal variation of RH over the simulation period. RH increases during the day in both realistic and extreme scenarios. Looking at the spatial variation (Figure 3.14(a)), we observe that the RH reduces at night for most of the region in a realistic scenario, whereas, it increases for half of the region during the night and decreases for the other half of the region in the extreme scenario. The RH increases more in the extreme scenario than in a realistic scenario during the day. The results clearly show that green roofs increase the relative humidity in extreme scenario and therefore can affect thermal comfort.

Figure 3.13(b) shows the temporal variation of HI spatially averaged over the innermost domain urban grid cells. ΔHI follows a similar trend as observed for the $T_{air,2m}$ (Figure 3.7(b)). Based on this, we observe that it decreases during the day and increases during the night for both realistic and extreme scenarios. The highest reduction in HI during the day is around 1.5°C in the extreme scenario and 0.5°C in a realistic scenario. On average, the reduction in HI is 0.2°C and 0.8°C for realistic and extreme scenarios, respectively.

As mentioned previously, an increase in RH at a constant temperature reduces the thermal comfort. However, in our simulations though the RH has increased during

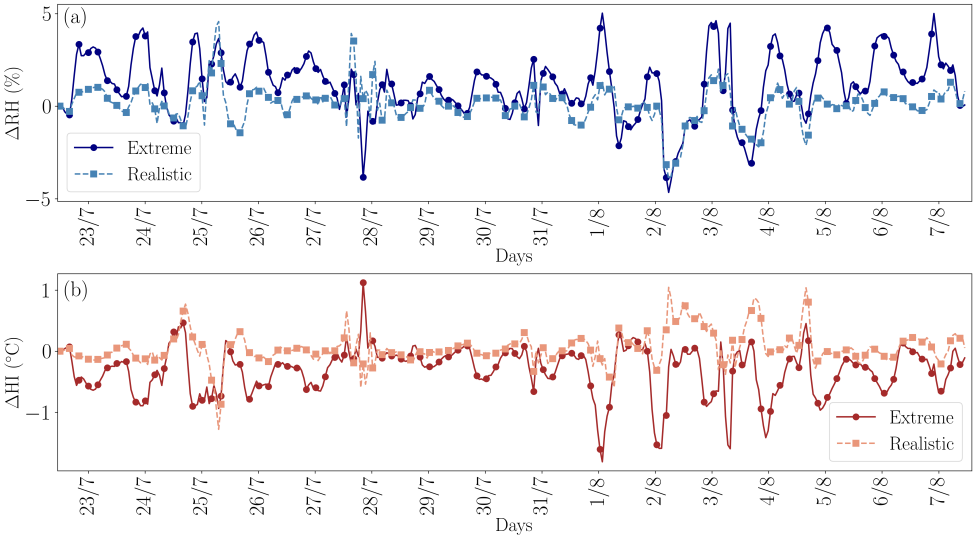

Figure 3.13: Temporal variation (spatially averaged for each hour) of differences in (a) relative humidity and (b) heat index for realistic and extreme scenarios

the day for the extreme scenario, there is a corresponding larger reduction in $T_{air,2m}$, which causes a net reduction in the HI in the extreme scenario. On the other hand, in a realistic scenario, some of the areas experience an increase in HI during the day. This could be due to an increase in $T_{air,2m}$ in some parts of the region. Since the $T_{air,2m}$ increases during the night, the HI also increases during the night. Moreover, the increase in HI during the night is more than the decrease observed during the day in a realistic scenario. Therefore, even in terms of thermal comfort, realistic roof greening has limited benefits.

3.3.7 Impacts on boundary layer

To further understand the effect of realistic and extreme green roofing scenarios on UHI, we investigate their impact on the boundary layer. For this, we show the time series of differences in vertical profiles (2 km above ground level (AGL)) of ΔT_{air}, ΔRH and wind speed for both realistic and extreme scenarios. We observe a reduction in T_{air} almost every day between 0.5-1.5 km. The reduction is also observed below 0.5 km during the day, but there is an increase in the night (Figure 3.15 (a) and (b)). The T_{air} reduction is higher in the extreme greening scenario compared to a realistic scenario. While, the reduction in T_{air} is less than 0.5°C in a realistic scenario, the reduction in T_{air} is nearly zero on 27th July (highest daily temperature) in a realistic scenario. Additionally, the increase in T_{air} near the surface during the night time is around 0.5-1.5°C in a realistic scenario for almost all days. The increase in T_{air} during the night near the surface is also observed in the extreme scenarios for a few days

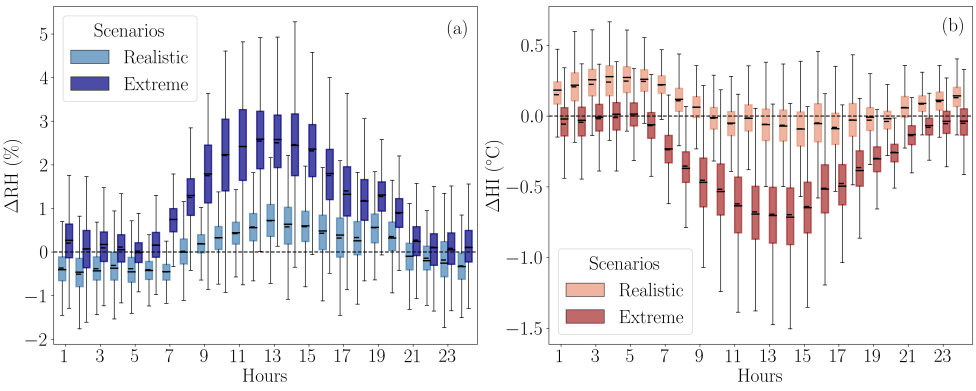

Figure 3.14: Spatial variation (temporally averaged for each hour) of differences in (a) relative humidity and (b) heat index for realistic and extreme scenarios

but is less than 1°C. Moreover, the reduction in T_{air} in the extreme scenario is much higher compared to a realistic scenario between 0.5-1.5 km height.

Over most of the days during the warm afternoon we observe a decrease in horizontal wind speed (Figure 3.15 (c) and (d)) near the surface (<0.5 km) because of the reduced vertical mixing due to a reduction in T_{air}. Decrease in the temperature increases the stability of the boundary layer, which in turn causes a reduction in the turbulent intensity [197] causing a reduced vertical mixing. The vertical mixing increased above 0.5 km for this period for both scenarios, with higher vertical mixing in the extreme scenario. The reduced vertical mixing near the surface led to stronger airflow over the higher levels with a reduction in momentum shift from higher to lower levels. This reduces the wind speeds near the surface generating stronger (weaker) wind speeds at higher (lower) levels.

Delving into the vertical profile of ΔRH (Figure 3.15 (e) and (f)), we observe that

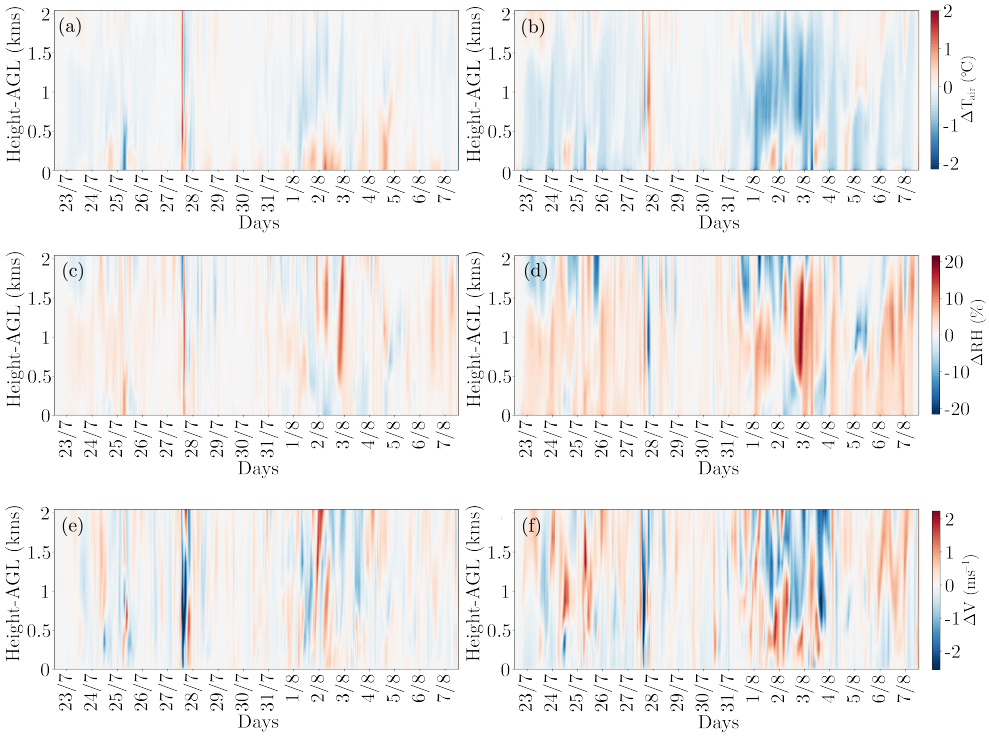

Figure 3.15: Vertical profile of differences in air temperature, relative humidity and wind speed, for realistic ((a),(c),(e)) and extreme ((b),(d),(e)) scenarios with spatially averaged values for urban innermost domain from July 23-August 7, 2018

the RH increases with retrofitting green roofs for most of the vertical profile. However, the increase is lower in a realistic scenario compared to the extreme scenario. This increase can be attributed to the higher evapotranspiration with roof greening and lower wind speeds. Largely, since the T_{air} is not reduced significantly and also increases during the night, with a slight rise in RH, the heatwave is not mitigated but the effects are worsened in a realistic scenario near the surface. For the same time period, however, the extreme scenario has reduced T_{air} but increased RH. This scenario could be beneficial to reduce the T_{air}, but may exacerbate the RH in the region. It is important to note that the increase in RH here is without irrigation on the green roofs. With irrigation, the T_{air} may be reduced but the RH may increase even more.

There have been concerns in various studies regarding the exacerbation of relative humidity in the atmosphere after implementing green roofs on a large scale. Our analysis also points out the increase in relative humidity, which is related to the effects induced by changes in vertical mixing and evapotranspiration of green roofs. Studies have shown that after introducing green roofs, the sensible heat flux decreases, which increases the stability of the atmosphere and hence decreases the vertical mixing over the city [120, 153]. Generally, in urban areas, when the sensible heat flux from urban areas increases, the developed internal boundary layer (with the atmospheric flow from rural to urban) grows faster and the urban atmosphere is more affected by urban surface conditions, and hence the impact of advection by the synoptic or mesoscale wind is diminished [153]. However, when the vertical mixing over urban areas is weaker (due to green roofs), the developed internal boundary layer expands slowly. Hence, at a certain height over urban areas, the atmosphere is less affected by ground surface conditions and more affected by the upwind surfaces. This advection of moist air from rural to urban areas can increase the relative humidity in urban regions.

3.4 Conclusions

In this study, we evaluate the impact of a realistic fraction of green roofs on the UHI effect during a heatwave in Liège city, employing a high-resolution WRF study using the BEP-BEM parameterisation with LCZ land use classification. We ran the WRF simulation for a base scenario (without green roofs), a realistic scenario (green roof fraction derived from remote sensing) and an extreme scenario for the longest and most severe heatwave in Liège from 23rd July to 8th August 2018. We observe a reduction in near-surface air and surface temperatures after introducing green roofs in the study domain. Our results in the extreme scenario are in line with other green

roof studies [120, 157, 198]. These studies also suggest a nighttime warming due to green roofs, which is mainly because of the accumulation of extra solar radiation during the daytime by rooftop soil layers which is discharged at night [120, 198].

Comparing realistic and extreme scenarios, we observe that the effect of realistic roof greening is much less in reducing the near-surface air (0.5°C maximum) and surface temperature (1.5°C maximum) throughout the simulation period compared to the extreme scenario. In a realistic scenario, the increase in air temperature during the night is similar to the decrease in air temperature during the day. Therefore, on an average, there is a slight decrease in temperatures in realistic scenario.

Further investigating the impact of green roofs in each LCZ in Liège, we observe that the decrease in air and surface temperature depends on the urban morphology when the green roof fraction is the same for all LCZs. For instance, the decrease in temperatures is higher in compact, low-rise, and highly dense LCZs when all the roofs are green. This result is similar to the idealised two-dimensional experiments by [173], which suggest that the mitigation effect from green roofs on air temperature varies linearly with building density during summer. They also report that the mitigation effect is higher for low-rise buildings. In realistic roof greening, the magnitude of the effect is mainly dependent on the green roof fraction. Therefore, the large low-rise LCZ (LCZ-8) characterised by large industrial or commercial buildings in Liège City has a higher temperature reduction than other LCZs. It is important to know that the decrease in temperature in LCZ-8 is also limited in a realistic scenario.

Since the green roofs reduce the temperatures during the day, we also investigate the reduction in UHI intensity (UHII) during the day. We observe that the air and surface UHII reduce with the deployment of green roofs. The reduction is higher with extreme roof greening compared to a realistic one. However, the surface and air UHII reduction with realistic roof greening is only 0.2 and 0.5°C, respectively, which is very low. Another thing to note is that, even in both green roof scenarios, the air and surface temperatures increase with the increase in urban fraction. [157] reports a similar result regarding green roofs and suggests that deploying cool roofs can be better since the temperature is lower with an increase in urban fraction. Our study indicates that green roofs effectively reduce air and surface temperatures when all buildings are retrofitted with green roofs. However, such a scenario is impossible, and realistic roof greening has limited effectiveness at a city scale in reducing the temperatures during the day.

Since human thermal comfort is also an indicator of the UHI effect along with temperatures, we calculate the heat index, which relates air temperature and relative humidity, and observed that green roofs reduce the heat index. Green roofs increase the relative humidity during the day because of the evapotranspiration. Nevertheless,

since the reduction in temperature is higher, the heat index is reduced even with a higher increase in relative humidity in the extreme scenario. In the extreme scenario, the nighttime heat index is also not increased for half of the region, suggesting the effectiveness of green roofs in the extreme scenario. In a realistic scenario, however, the heat index does not reduce as much as it increases at night. So, realistic green roofing worsens the heat index for most parts of the city at night. Additionally, after looking at the vertical profiles of relative humidity, air temperature and wind speeds, we notice that green roofs may exacerbate the relative humidity in the urban area in the long run.

Altogether, we conclude that realistic roof greening in Liège may not be sufficient to reduce the UHI effect at a city scale. Other mitigation strategies may be required to have a regional-scale impact on the UHI effect. Future studies can include multiple mitigation strategies in one scenario to evaluate this. Our study shows the importance of considering realistic green roof fractions in analysing their impact on the UHI effect. In this study, for Liège, we consider all the flat roofs as the roofs that can be greened. However, building roofs are often flat in tropical and Mediterranean urban regions. Hence, the impact of realistic greening could be higher and, therefore, must be evaluated.

3.5 Key contributions

- Unlike most studies that solely focus on averages, this analysis presents air and surface temperatures with consideration for spatial, temporal, and typological variability.
- Realistic roof greening may not be sufficient to significantly reduce the UHI effect at city scale, especially for reducing air temperature.
- Decrease in air and surface temperature in LCZs depends on the urban morphology along with the percentage of roof greening.
- As LCZs are generic, they may lack a detailed representation of typological variability. Therefore, a more specific analysis of LCZs tailored to the study area is essential to capture nuanced variations, which is done in chapters four and five.
- A combination of various mitigation strategies must be tested at the city scale with realistic fractions.

4

Identifying urban morphological archetypes for microclimate studies using a clustering approach[1]

Urban morphology relates to the form, structure, physical characteristics, and arrangement of buildings affecting the urban microclimate. As the morphological characteristics vary across the city, small units such as urban blocks are analysed for microclimate estimation. However, microclimatic analysis of all the blocks in a city is computationally challenging and time-consuming. Therefore, it is vital to identify representative blocks in a city to obtain a general overview of the microclimate. Urban morphological archetypes are the representative units of a homogenous group of blocks based on morphological parameters. Here, we propose a systematic approach for identifying urban morphological archetypes suited for microclimatic analysis. Specifically, we employ a well-defined, PCA-based k-means clustering approach supported by validation using external criterion analysis. We use urban morphological parameters based on form, shape, arrangement, and variations within a block in Liege, Belgium. We use the cubic clustering criterion and pseudo F statistic to identify nine distinct homogenous clusters. Then, we propose a validation approach in the absence of existing typologies using ANOVA analysis on the external criterion of land surface temperature, a proxy for measuring microclimate. The validation

[1]Published as: **M.Y.Joshi**, A.Rodler, M.Musy, S.Guernouti, M.Cools and J.Teller, *Identifying urban morphological archetypes for microclimate studies using a clustering approach*. Building and Environment. **224**, Article 109574 (2022), doi:10.1016/j.buildenv.2022.109574

suggests that the clusters are significantly different, indicating successful clustering. We also compare our classification to the existing local climate zone (LCZ) classification. We identify relevant sub-classes within the broader LCZ classes essential for capturing microclimatic variation. Finally, the study provides realistic archetypes for performing microclimatic simulations at a city scale. The proposed approach can be effectively applied to other cities for urban microclimate studies.

4.1 Introduction

Urban settlements alter the natural environment surrounding them, creating a unique microclimate [199]. Urban microclimates tend to produce and retain more heat, resulting in comparatively higher temperatures than their rural counterparts. This phenomenon is known as the urban heat island (UHI) effect [2, 200]. The overall air and surface temperature in cities have risen gradually over the years, resulting in a significant air UHI and surface UHI effect, respectively [201, 202]. The spatial variation of the UHI effect largely depends on urban morphological factors such as built-up intensity, presence of vegetation, building heights, albedo and sky-view factor (SVF) [203, 204]. Therefore, microclimates encompassing buildings and urban blocks are studied to understand and mitigate the UHI effect.

The urban microclimate is the outcome of dynamic interactions between the macroclimate and urban morphology [205, 206]. Thus, urban morphology is a vital part of UHI-related microclimatic studies owing to its importance also for assessing mitigating solutions for the UHI effect [207, 208]. Urban morphology relates to the form and the structure of an urban area and the buildings' physical characteristics and arrangement. Urban morphological parameters influence the urban microclimate in several ways. For example, building density reduces the average wind velocity worsening the urban ventilation and intensifying the UHI effect [209, 210]. Longwave radiation gets blocked in the streets due to low SVF on the streets, retaining more heat in the region and escalating the UHI effect [211, 212].

Urban morphological parameters, such as the size of the building façades, also impact wind velocity, thus intercepting solar radiation and contributing to solar trapping, which primarily causes the UHI effect [213]. Sometimes, urban morphological factors can also help in regulating the UHI effect. For example, arrangements of buildings in a block, such as U-shaped blocks, blocks with courtyards, or multiple courtyards, have improved microclimates compared to detached, attached and linear blocks [214]. Additionally, a block's variation in the height of buildings is also observed to reduce outdoor temperatures better than the blocks with uniform building heights [210]. In winters, mid-rise blocks are more suitable than high-rise blocks

with open spaces to block the cold winds [206]. These studies demonstrate that urban morphological patterns largely influence microclimate.

The morphological patterns within the city vary based on building properties, street-related properties, and properties of urban blocks. Due to such variations in the city, many researchers suggest analysing individual urban units, such as urban blocks, to study the UHI effect at the microscale [215, 216]. Evaluating microclimate in urban blocks also allows the urban planners and designers to play a pivotal role in providing balanced strategies and techniques related to its local context [217]. However, analysing the microclimate of all the blocks in the city can be computationally challenging and time-consuming. In this scenario, identifying typical urban morphological archetypes representing a homogenous group of blocks [218, 219] in a city can simplify microclimatic studies and aid in generalising the results at a city scale. Therefore, we propose a systematic approach to identifying urban morphological archetypes suited for microclimatic studies.

Typically, the first step in identifying urban morphological archetypes involves classifying the entire city into different types. There have been previous attempts to classify the urban areas into homogenous units for UHI-related studies. Stewart and Oke [162] introduced the local climate zones (LCZs) as homogenous regions in terms of surface cover, structure, material and human activity that stretch over hundreds of meters to several kilometres horizontally. Based on LCZ, several researchers have generated LCZs specific to their areas, substituting or adding a few parameters in the process [220–222]. Although generating LCZs is the widely used approach, Stewart and Oke [162] highlight that the LCZ system is generic and cannot capture the peculiarities of every urban area and is adapted to catch the microclimate effect at the scale of a few hundred meters. Thus, they suggest that users can create new sub-classes in the city if needed. Apart from this, the LCZ parameters often remain insufficient while describing the urban canopy in detail, especially when the end goal is to analyse the UHI effect at the microscale [203]. Therefore, additional morphological parameters that describe the urban canopy in detail are necessary for classifying the urban area into morphological archetypes. Apart from this, as the basic unit of design for urban planners and designers is an urban block, rasterised output like LCZs does not provide precise typologies at the block level [223, 224].

Other approaches have been employed previously, such as rule-based classification, machine learning based classification algorithms, and classification using spatial multi-criteria analysis to identify urban morphological archetypes [225–227]. While these methods are systematic and replicable, they are only applicable in the case of predefined urban morphological archetypes. In the absence of predefined archetypes, the clustering approach can be helpful as it is data-driven [215, 228–231]. Further-

more, clustering allows simultaneous assessment of various variables by grouping the elements based on similarities [231]. Thus, the clustering approach is more logical and effective in identifying urban morphological typologies. However, prior studies have not employed the clustering approach with external validation to form urban archetypes to identify local climate zones for microclimate analysis. Therefore, in this study, we propose a clustering approach to identify the urban morphological archetypes based on important urban morphological parameters.

Once the clusters are generated, we need to check whether the clustering has delivered unique and distinct archetypes. One way to check if the clusters are significantly different is with the help of predefined or pre-existing rules for archetypes. But, in many cases, there is a lack of predefined rules wherein the validation requires some logical basis. An approach popular in the statistical community but not widely used in clustering urban blocks is the external validation criterion using ANOVA analysis. However, such a validation requires an external parameter not used in clustering [232], which, in this case, is a non-morphological parameter (i.e. a parameter not related to building geometry) to prove that significant differences exist between the clusters. Therefore, in this study, we propose a validation using an external parameter to confirm the adequacy of the clusters' diversity.
Summing up, in this paper, we propose a systematic approach to identifying the urban morphological archetypes particularly suited for UHI-related microclimatic analysis. The approach involves:

1. Clustering: classifying city blocks based on urban morphological parameters.
2. Validation of the clustering-based classification using an external criterion.
3. Determining the unique urban morphological archetypes that represent the different clusters in the city.

We also compare the clustering-based classification results with the LCZ data created for Europe by the world urban database and access portal tools (WUDAPT) [169, 170]

The present approach provides realistic urban blocks for microclimate analysis, including CFD simulations instead of a simplistic representation of urban blocks. Furthermore, it reduces the computational time for analysing the microclimate at a higher resolution as it alleviates the need for simulating the microclimate of an entire city. Instead, the simulations can be carried out on the identified archetypes to arrive at a general overview of the microclimatic situation in the city. Moreover, the properties of these archetypes can be helpful to further generate modelled blocks in the city that will be a better representation of reality.

4.2 Methodology

4.2.1 Study area and dataset

In this study, we examine the city of Liege in the Wallonia region of Belgium. It is the third most populous city in the country, with 196,296 inhabitants [83] and an area of 69 km^2. The city is densely occupied by buildings in the centre, leaving few open green spaces. The surface temperatures in the city are observed to be high during the summer, indicating a significant surface UHI effect [88].

The dataset includes the building footprints from the PICC (Projet Informatique de Cartographie Continue) dataset, which has an accuracy of less than 25 cm. This data is retrieved from the geoportal of Wallonia (https://geoportail.wallonie.be). We also use the parcels from cadastre data (2018) for block generation. For the height of the buildings, we use the LiDAR point cloud data from 2014 with a point density of 0.8 $\mathrm{points}/\mathrm{m}^2$, retrieved from the geoportal of Wallonia.

4.2.2 Selection of blocks

Urban blocks are an area with one building or a group of buildings surrounded by streets [226, 229]. Thus, firstly, the city is divided into several blocks using the parcels in the cadastre data. The border of the enclosing streets delineates a block, and cadastral information on streets or parcels can help in demarcating the blocks. Blocks can also be derived if the street width information is available in a city [229].

For Liege city, cadastral information is readily available; therefore, we use parcels to define the blocks for this study. The parcels are the plot boundaries for each building in the city, as depicted in Figure 4.1(a). We merge all the parcels and transform them into blocks using ArcGIS Pro (Version 2.9.1) (Figure 4.1(b)).

Blocks with fewer buildings and larger open spaces are not relevant for this study. Thus, the first selection criteria for the blocks in this analysis is the ground space index (GSI). GSI refers to the area occupied by buildings (A_{bu}) in the block per area of the block (A_{bl}) as illustrated in the following equation [233]:

$$GSI = \frac{\sum_{i=1}^{n} A_{bu(i)}}{A_{bl}} \tag{4.1}$$

We only consider the blocks with GSI greater than 0.2 as we focus on urban climate zones [162]. In addition, we choose the blocks with at least three buildings within their perimeter to filter smaller blocks with just one or two buildings.

Another criterion for selecting the blocks is their shape. Sometimes, the block shapes in a city can be irregular, as shown in figure 4.2. Such blocks usually have very

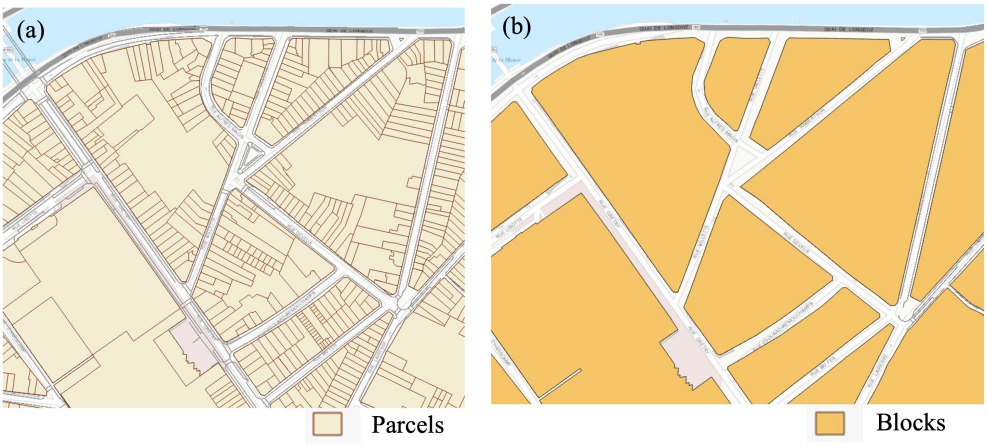

Figure 4.1: (a) Parcels based on cadastral data (b) Defined blocks with the help of parcels

few or no buildings or contain large landscapes. However, some blocks might have a significant number of buildings that are widely spaced. We use the shape factor (SF) as defined in Ma et al. [215]. To calculate SF, we first construct the minimum bounding circles around the blocks using ArcGIS's minimum bounding geometry tool. Thereafter, we compute SF using the following equation:

$$SF = \frac{A_{bl}}{\pi r_{circle}^2} \tag{4.2}$$

where A_{bl} is the area of the block and r_{circle} is the radius of minimum bounding circle around the block. Preliminary statistical analysis of the blocks in the city indicated that 95% of the blocks have a shape factor greater than 0.15. Further observation of blocks with SF less than 0.15 indicates that these blocks are irregular and non-repeating. Therefore, we consider blocks with SF greater than 0.15 in this study.

4.2.3 Parameters affecting microclimate

In this paper, we consider 17 morphological parameters that can potentially affect the microclimate (Table 4.1). Along with the parameters proposed for classifying LCZs by [162], we identify the parameters based on the categories that broadly define the morphology of a block, namely, form, shape, arrangement, and variations within the block. We also utilise the parameters that influence the wind flow in the urban area.

Figure 4.2: Blocks with irregular shapes

These parameters are observed to influence urban microclimate in the literature, as mentioned in Table 4.1.

LCZ parameters

The parameters used for classifying LCZs are the sky view factor (SVF), aspect ratio (AR), building surface fraction (BSF), impervious surface fraction (ISF), and pervious surface fraction (PSF), the height of roughness elements (HRE) and terrain roughness class. We do not consider the terrain roughness class (TRC) parameter of LCZ classification as the blocks fall into the 'very rough' class of Davenport classification of effective terrain roughness, where the roughness length is 0.5 m [162]

Sky view factor:

SVF indicates the amount of sky visible from the ground at a given position, referring to the proportion of sky not obstructed by the surrounding built-up [204,245–247]. We calculate the SVF using the Relief Visualisation Toolbox of QGIS 3 [248, 249].

We use the digital surface model (DSM) and the building footprint dataset to generate the raster with building height information. We consider the open spaces and roads along with the bottom of the buildings at 0 m. Moreover, for better accuracy in urban areas, we only consider the building heights and the obstructions like trees are non-existent in this analysis. We consider a search radius of 100 m and the number of directions as 16 based on [246] for SVF calculation.

Table 4.1: Urban morphological parameters

Categories		Parameter	References
Parameters used for LCZ	*SVF*	Sky view factor	[162]
	AR	Aspect ratio	[162]
	GSI	Ground space index/Building surface factor	[213] [215] [234]
	ISF	Impervious surface fraction	[162]
	PSF	Pervious surface fraction	[162]
	HRE	Height of roughness elements	[214] [235] [236]
Arrangement (Density and arrangement of the buildings within the block)	*OSR*	Open Space Ratio	[237]
	MA	Mean building areas	[215] [238]
	NB	Number of buildings per unit area of the block	[239] [220]
Variation (Variations between the buildings within a block)	*SH*	Standard deviation of building heights	[210] [240]
	SA	Standard deviation of building areas	[215] [238]
Form (Compactness/sprawl of buildings within a block)	*DB*	Average distance between the nearby buildings	[214] [215]
	DCR	Ratio of distance from the centroid to buildings to the radius of minimum bounding circle to block ratio	[215]
Shape (Shape factor of the block)	*SF*	Block shape factor	[215] [241]
Wind flow	*FAI*	Frontal area index	[242]
	AH	Average height of the buildings	[243]
	Po	Porosity	[244]

Based on the output from the relief visualisation toolbox, we aggregate the SVF values in the output raster for every block. Therefore, it is crucial that we consider SVF values in streets and open spaces. However, as the blocks do not consist of streets

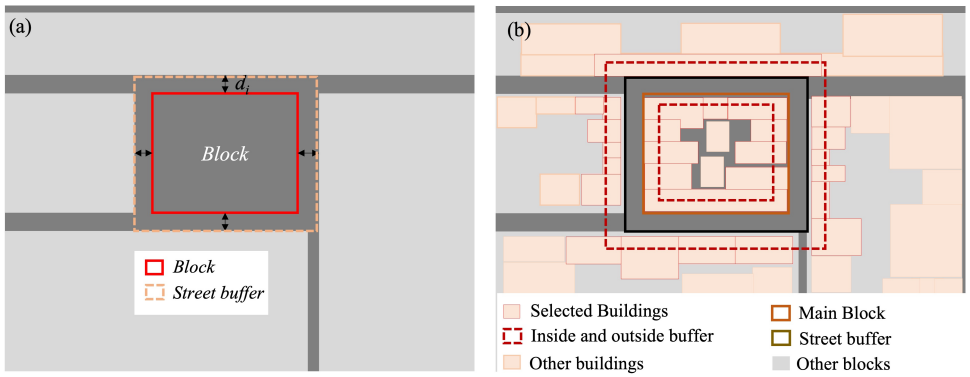

Figure 4.3: (a) Street width between the block (b) Buffers creates for selecting the buildings on both sides of roads

surrounding them, we create a buffer zone to include the SVF values at street level on the streets surrounding the block. To create the buffer zone, firstly, we calculate the distance of each block from the nearest four blocks located within 33 meters of the block. Thirty three meters is the maximum street width of major streets in the Walloon region [250]. We consider the buffer as follows:

$$D_{\text{buffer}} = max(d_i), \tag{4.3}$$

where, d_i is the block's distance from the adjacent block, and n is the number of adjacent blocks within 33 meters of the block Figure 4.3(a).

Next, we remove the buildings from the obtained SVF raster by setting the raster values corresponding to the building footprint as null. Thereafter, we consider the average SVF values on open spaces and streets in the buffer block as the SVF of that particular block. We aggregate the SVF values to the blocks using the zonal statistics as table tool in ArcGIS Pro 2.9.1.

Aspect Ratio:

Aspect ratio (AR) is the building height to street width ratio (H/W). As streets surround blocks on all sides, we consider the average value of AR of all streets surrounding the block. We compute the street width based on the distance of blocks from the adjacent blocks d_i as shown in figure 4.3(a). For AR, we consider the average street width calculated as follows:

$$w_{\text{avg}} = \frac{1}{n}\sum_{i=1}^{n} d_i \tag{4.4}$$

where, n is the number of adjacent blocks within 33 meters of the block.

To estimate the building height, we first identify the buildings on both sides of the road. To do this, we create a buffer of 5 m inside the block and 3 m outside the street buffer, as shown in figure 3(b). Then, we select the buildings that are crossed by the outline of these buffers using ArcGIS Pro 2.9.1. After that, we calculate the average height of the selected buildings as follows:

$$h_{avg} = \frac{1}{n}\sum_{i=1}^{n} h_i \tag{4.5}$$

where, h_i is the height of the building on either side of the road, and n is the number of buildings that are on both sides of the road surrounding the block. Subsequently, we calculate the AR of a block as follows:

$$AR = \frac{h_{\text{avg}}}{w_{\text{avg}}} \tag{4.6}$$

Impervious surface fraction (ISF):

ISF indicates the area occupied by impervious surfaces such as pavements, rocks, and buildings. Zha et al. [251] defined the normalised difference built-up index (NDBI) to determine urban and built-up areas. It is used to express the intensity of urbanisation [252] and can be used as a substitute to indicate urban impervious surfaces [253]. Thus, in this paper, we use NDBI as a proxy for ISF. We calculate NDBI using the Sentinel-2A satellite imagery captured on 21st July 2021 from the United States geological survey (USGS). We choose the image on this date as July and August experience higher temperatures. Moreover, among the images available for this time frame, the selected image had the lowest and most acceptable cloud coverage of less than one per cent. The NDBI was calculated as follows:

$$NDBI = \frac{SWIR1 - NIR}{SWIR1 + NIR}, \tag{4.7}$$

where SWIR1 is the shortwave infrared band (Band 11) with a resolution of 20 m, and NIR is the near-infrared band (Band 8) with a resolution of 10 m. For calculating the NDBI, we resample the SWIR1 band to 10m and compute the NDBI at 10 m resolution. To estimate the NDBI of a block, we calculate the average NDBI of a block as

ISF using the zonal statistics as table tool in ArcGIS Pro 2.9.1.

Pervious surface fraction (PSF):

PSF refers to the area occupied by pervious surfaces like bare soil, vegetation or water. Normalised difference vegetation index (NDVI) is used to detect bare soil and vegetation [254,255]. Thus, in this study, we consider NDVI to inform the perviousness in the block. We calculate the NDVI using the Sentinel-2A image used for calculating NDBI. It is computed as follows:

$$NDVI = \frac{NIR - R}{NIR + R}, \tag{4.8}$$

where NIR and R are the near-infrared (band 8) and red (band 4) bands with a resolution of 10 m. Similar to NDBI, we calculate the average NDVI of a block as the PSF using the zonal statistics as table tool in ArcGIS Pro 2.9.1.

Height of roughness elements (HRE):

As the roughness of the neighbourhood can influence the aerodynamic properties, we compute the HRE for the buffer around the block as used in the SVF calculation [242, 256]. HRE is the average of building heights in the urban canopy. Here, we calculate it as follows :

$$HRE = \frac{\sum_{i=1}^{n} A_{bu(i)} \times h_{bu(i)}}{A_{buffer}} \tag{4.9}$$

where A_{bu} is the area of building and h_{bu} is the height of the buildings within the outer buffer of the block as shown in figure 3 (b), Abuffer is the area of the outer buffer and n is the number of buildings within the block. We calculate the height of buildings using digital surface model (DSM) data provided by the geoportal of Wallonia.

Parameters informing arrangement

The parameters in the arrangement category represent the parameters that inform the open spaces and area and the number of buildings. Open space ratio (OSR) is defined as the ratio of open areas to the built area, and it describes the intensity of use of non-built ground [237]. We compute it as follows:

$$OSR = \frac{1 - GSI}{GSI} \tag{4.10}$$

MA is the average area of buildings within the block. NB is the number of buildings per unit area in a block. We compute it as follows:

$$NB = \frac{n}{A_{bl}}, \tag{4.11}$$

where n is the number of buildings within the block.

Parameters informing variation

The variation category consists mainly of two parameters. Studies have indicated that variation in heights can influence the microclimate [210, 240]. In computational fluid dynamics (CFD) studies, the area of the object also affects the wind direction [238]. Thus, we also consider variation in building area in this study as there is a potential effect on the UHI. SH is the standard deviation in building heights, and SA is the standard deviation in building areas within the block. Since height informs the roughness of the block and its neighbourhood, we consider SH to be the standard deviation of building heights within the outer buffer of the block as considered for SVF calculations.

Parameters informing the form

The form represents the compactness or sprawl of buildings within the block. GSI can also demonstrate the form, but there can be variations in the patterns. Therefore, we consider parameters like DB and DCR. DB is the average distance between the adjacent buildings in a block. We calculate as follows:

$$D_{\min} = \frac{1}{n} \sum_{i=1}^{n} \min_{1 \le j \le n-1} (D_{ij}) \tag{4.12}$$

where D_{ij} is the distance between one building to the rest of the buildings, n is the number of buildings in the block (Figure 4.4 (a)).

DC is the average distance between the block's centre and the building's centre (Eq. 13). As the value of DC depends upon the block's size, we normalise the parameter using the radius of the minimum bounding circle (Eq. 14). Thus, DCR is the parameter indicating the average distance of buildings from the block's centre.

$$DC = \frac{\sum_{i=1}^{n} D_{c(i)}}{n}, \tag{4.13}$$

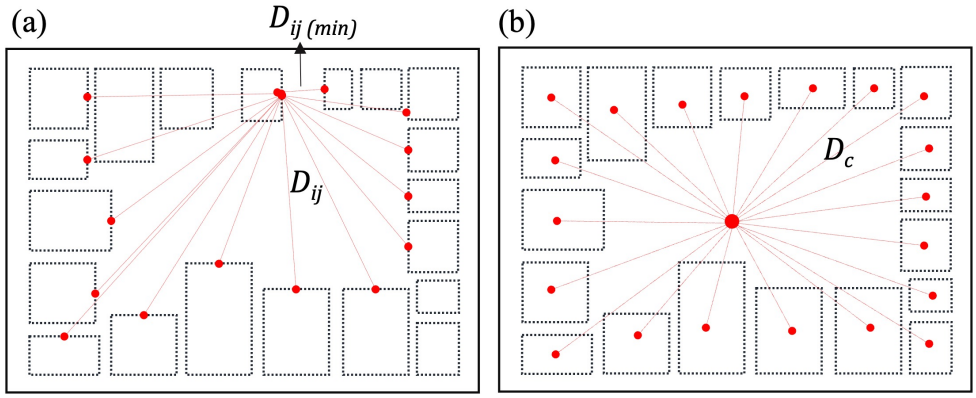

Figure 4.4: (a) Distance between the buildings (b) Distance from the centre of the block to the building

$$DCR = \frac{DC}{r_{circle}}, \tag{4.14}$$

where, $D_{c(i)}$ is the distance from the block's centre to the building's centre, and n is the number of buildings in a block.

Parameters for block shape

As mentioned in section 2.2, SF informs the shape of the block. Moreover, there might be differences in the blocks based on the shape of the block. Thus, we use this parameter as well in our analysis.

We calculate the parameter values for blocks using the Geopandas package in python (https://geopandas.org/en/stable/). We convert each shapefile to a geodata frame to proceed with further analysis.

Parameters influencing the wind flow

Urban morphology influences the urban air ventilation environment [242, 243]. Several indicators such as GSI, SH, HRE, average height (AH), frontal area index (FAI) and porosity (Po) are considered in analysing the urban wind environment as they indicate surface roughness [243,257,258] . In this paper, GSI, SH and HRE parameters are already considered in other categories of urban morphology. Therefore, in this section, we explain the remaining parameters such as AH, FAI and Po. As AH, FAI and Po indicate roughness in the urban block, we consider the buildings in the buffer

area (Figure 3(a)) for calculating the indicators.

AH is the average height of buildings within the buffer of the block.

FAI measures building walls facing the wind flow in a particular direction [244]. We compute FAI using the methodology from [65] in this paper. The method involves rasterisation of the building height and area and computing the FAI at 100m resolution. The FAI is only calculated for northerly/easterly winds. We computed the FAI for the blocks using zonal statistics as table tool in ArcGIS Pro 2.9.1 and considered the mean of FAI pixels overlapping the buffer block as FAI of the block.

Po is the ratio of the empty volume in an urban canopy to the volume of the urban canopy. In this paper, we consider the volume of the urban canopy of a block (UCLV) as follows [259]:

$$UCLV = max(h_i) \times A_{buffer}, \tag{4.15}$$

where hi is the height of the buildings in the buffer block. The building volume (BV) in the buffer block is computed as follows:

$$BV = \sum_{i=1}^{n} A_i \times h_i, \tag{4.16}$$

where A_i is the area of buildings located in the buffer block. Therefore, Po is defined as:

$$Po = \frac{UCLV - BV}{UCLV} \tag{4.17}$$

4.2.4 Clustering approach

We use k-means clustering in this paper for the reasons explained below:

- Firstly, Liege city does not have any pre-existing classification of urban built form.
- Secondly, the k-means clustering algorithm is a hard clustering method that provides distinct clusters.
- Lastly, it is very efficient for large and high-dimensional datasets.
- Moreover, several studies [228–230] have demonstrated that k-means have provided logical results for identifying urban typologies.

Pre-processing of data

It is crucial to scale and normalise the data before performing the k-means clustering [231,260], as the presence of outliers or skewed distributions can influence the optimal number of clusters generated by algorithms. Therefore, first, we scale the data to

guarantee that no particular weight is given to any specific variable or feature.

Researchers often couple principal component analysis (PCA) with k-means in order to reduce dimensionality and ensure non-collinearity among the variables [187, 230]. Moreover, PCA-based k-means are observed to generate a better clustering result [261]. A PCA is a linear transformation of variables into reduced dimensional space while retaining the maximum variance [230, 231].

In this paper, we are not confronted with a large number of dimensions. However, there may be collinearity between the variables. As collinearity may influence the results, we do a PCA analysis to obtain principal components (PCs) that are non-collinear and explain maximum variance in the data. We transform the data into PCs using classical PCA and decide on the number of PCs based on Kaiser criteria [262]. Thus, we select the PCs based on the cumulative variance explained by each component that has an eigenvalue greater than one. We further discuss the loading of each parameter on the chosen PCs using varimax rotation to estimate their influence on the clustering outcome. We consider the rotated principal component (RC) scores as input for the k-means clustering. We use the R stats package version 4.0.3. for PCA analysis.

K-means clustering

K-means clustering algorithm is an unsupervised clustering technique that attempts to determine k non-overlapping clusters to maximise the distance between the clusters and minimise the distance within the cluster. Given the set of n data points and a predefined number of clusters (k), the algorithm randomly selects k cluster centres initially. It classifies the data points to the nearest cluster centre. Then, it calculates the within-cluster sum of squares and reassigns the cluster centres to result in a final partition that optimises the clustering quality by minimising the intracluster sum of squares distances of any data point to its nearest cluster centre as defined by the following equation [263]:

$$J(C) = \sum_{i=1}^{k} \sum_{j=1}^{n} \parallel x_j - c_i \parallel^2 \tag{4.18}$$

K-means algorithm generally picks up the centroids randomly. Thus, the result depends upon how the initial centroids were selected. Therefore, to avoid this problem, we use the k-means ++ initialisation which is a smart centroid initialisation technique. With this technique, the best possible initial centroid is selected and the replicability of results is ensured with significant iterations [264]. We use the clusterR package of R version 4.0.3 for clustering the data using the k-means algorithm.

Determining the number of clusters

There are numerous varieties of methods available to identify the number of clusters. However, identifying the optimal number of clusters is always challenging for clustering analyses. Thus, many studies use more than one method to determine an optimal number of clusters [265, 266]. In this paper, we use the cubic clustering criterion (CCC) and pseudo F statistic to select the optimal number of clusters.

CCC is a test statistic developed by the SAS programming package [267] for identifying an optimal number of clusters. This index is the measure of within-cluster homogeneity compared to between-cluster heterogeneity. For identifying the optimal number of clusters, the values of CCC are plotted against the number of clusters and the peak value is chosen as appropriate. However, the peak value of CCC should be positive and preferably greater than two or three [268].

Caliński and Harabasz [269] developed the pseudo F statistic and defined it as the ratio of between-cluster variance to within-cluster variance. Similar to CCC, the pseudo F values are plotted against the number of clusters and the peak value is chosen as the optimal number of clusters. The large peaks in the pseudo F statistic are indicators of greater cluster separation.

Milligan and Cooper [268] examined 30 indexes developed to identify the number of clusters. According to the study, CCC performed at a competitive rate; however, it may suggest too many clusters in some cases. Additionally, pseudo F statistic has performed well and is less prone to errors, according to Milligan and Cooper [268]. Thus, we compare these two indices and decide the optimal number of clusters. To compute these indices, we use the NbClust package of R.

Validating the clusters

For external criterion analysis, standard parametric analyses such as analysis of variance (ANOVA) or multivariate analysis of variance (MANOVA) are used to validate the clustering result using a variable excluded from clustering analysis [232].

Differences in surface temperature are related to different microclimates. So, the average surface temperature of the blocks can be one of the proxies for measuring microclimate conditions [254, 270]. In this study, the external variable cannot be a parameter that influences or informs urban morphology. Thus, we choose the block's average land surface temperature (LST) as a dependent variable for external criterion analysis. We compute it using zonal statistics as table tool in ArcGIS Pro 2.9.1. We consider using a one-way ANOVA analysis to validate the clustering result as we have one parameter. Moreover, several studies have effectively used one-way ANOVA for validating the clustering analysis results [271–273]. Therefore, we validate the

clustering result with the help of a one-way ANOVA to see whether the mean land surface temperature (LST) of the blocks varies across the clusters.

We calculate the land surface temperature (LST) using the LANDSAT-8 level 1 image captured on 18th July 2022. We choose the image on this date as July and August experience higher temperatures. Among the images available for July and August, the image on this date had the lowest and most acceptable cloud coverage of less than one per cent. In addition, we procured the image from the USGS at a resolution of 30 m. We use the thermal band 10 to compute the LST (in Kelvin (K)) using the following equations [274]:

$$L_\lambda = M_L Q_{cal} + A_L, \tag{4.19}$$

where L_λ = TOA (Top of Atmosphere) spectral radiance (Watts/(m^2 * srad * μm)), M_L = Band-Specific multiplicative rescaling factor from the metadata, A_L = Band-specific additive rescaling factor from the metadata, Q_{cal} = Quantized and calibrated standard product pixel values (DN).

$$T = \frac{K_2}{ln\left(\frac{K_1}{L_\lambda} + 1\right)}, \tag{4.20}$$

where T = TOA brightness temperature (K), K_1 = Band-specific thermal conversion constant from the metadata, K_2 = Band-specific thermal conversion constant from the metadata We further convert the LST values to degrees Celsius (°C).

ANOVA analysis enables comparing variances of more than two populations to determine equality of means. The F-test is performed against the null hypothesis, where the means of LST of each cluster are equal. The alternate hypothesis would be that not all the means of LST are equal. If the p-value of the F-statistic (Pr (>F)) is less than 0.05, then the null hypothesis will be rejected, and the alternate hypothesis will be accepted.

4.2.5 Determining predefined LCZ for blocks

To compare the clustering results with LCZ, we first determine the LCZ of the blocks using the LCZ map by WUDAPT [170] for entire Europe. The LCZ map [169] is at a resolution of 100 m, with each pixel indicating the type of LCZ. We use zonal statistics as a table tool of ArcGIS Pro 2.9.1 and identify the value of the majority of pixels in the block as LCZ.

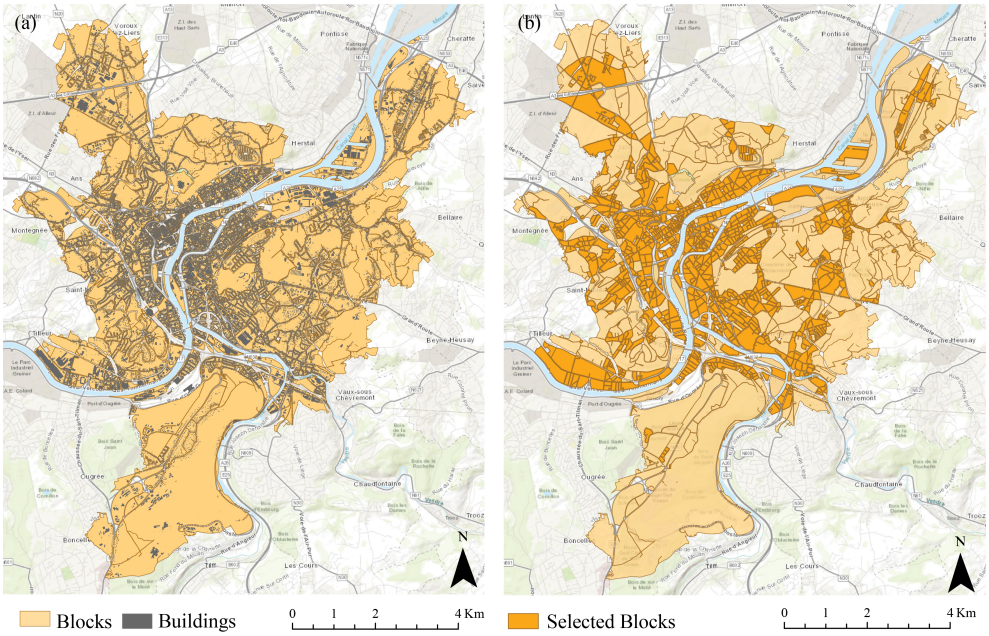

Figure 4.5: (a) Blocks in the city of Liege (b)Selected blocks for this study

4.3 Results and discussion

4.3.1 Selected blocks

Figure 4.5(a) depicts the total blocks in the city of Liege. There are a total of 1,441 blocks in the city. Out of these blocks, we select 1007 blocks in total for the analysis based on the selection criteria explained in section 2.1. Figure 4.5(b) illustrates the selected blocks in the city. From figure 4.5(b), we observe that the larger blocks with fewer buildings are effectively filtered along with irregularly shaped blocks.

4.3.2 Principal component analysis

Pairwise correlation of the 17 parameters indicates a high (>50%) and significant correlation between some variables, as shown in figure 4.6. The correlated variables may influence the clustering results, given the higher magnitude. Therefore, PCA analysis is relevant in this case.

We observe from figure 4.7 that first four principal components have eigenvalue greater than one. Moreover, these four PCs explain around 75% of the variance in

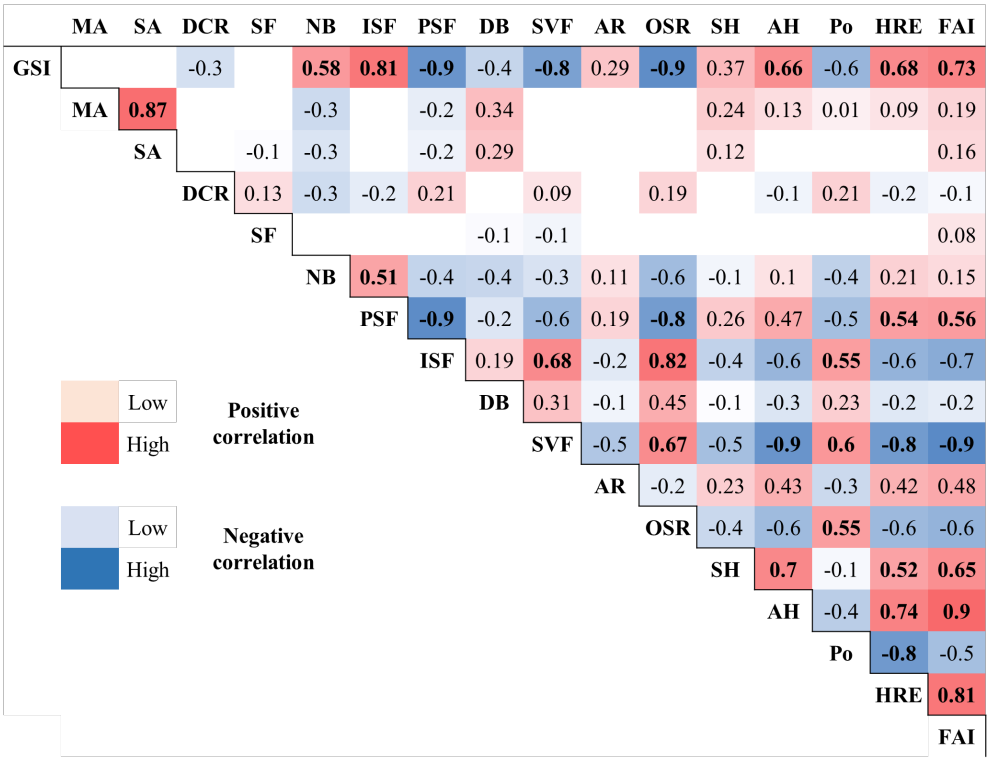

Figure 4.6: Correlation Matrix

the dataset. Therefore, we select these four PCs as variables for clustering. Table 4.2 and 4.3 shows principal component loadings and rotated component loadings obtained with varimax rotation. We observe that it is difficult to interpret the loadings from the PCs as some parameters have significant loadings on more than one PC (for example, GSI, DCR and OSR). The Varimax rotated solution (RCs) results in large loadings on a single component and small cross-loadings on the other components, facilitating the interpretation.

The RC1 and RC3 account for the higher variance in the data, which is about 28% and 26%, respectively. Thus, the following parameters, such as GSI, PSF, ISF, SVF, AR, HRE, OSR, NB, SH, AH, and FAI, influence the clustering the most. These parameters mainly correspond to the LCZ parameters, the parameters informing the arrangement and the parameters related to the wind environment. Parameters related to variation in the block, form and shape account for 21% of the variance (combined variance of RC2 and RC4), indicating their significance as well.

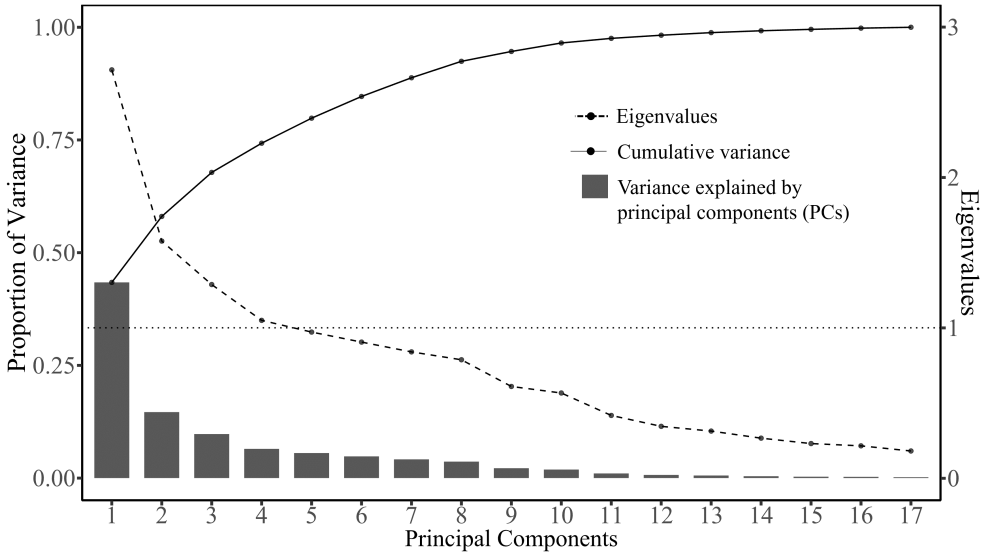

Figure 4.7: Principal Components Analysis

4.3.3 Number of clusters (k)

Figure 4.8 demonstrates the CCC and pseudo F statistic values for the number of clusters (k = 1 to 30). The value of CCC peaks first at k= 11, then at k=13, followed by k=23 and lastly, k= 27. As per Sarle [267], the highest value of CCC corresponds to the optimal number of clusters. However, in the case of distinct non-hierarchical elliptical clusters, the graph often shows a sharp rise to the correct number of clusters, followed by a gradual increase and eventually a gradual decline. In the plot of CCC (figure 4.8), a sharp rise is observed at k=9.

The pseudo F statistic value, on the other hand, peaks at k=5, then at k= 9, followed by k=9, k=11, k=13, k=23 and k=27. As the suitable value matches at k=9, we choose the number of optimal clusters as 9.

4.3.4 Validation – ANOVA analysis

Figure 4.9 demonstrates the mean LSTs of blocks within each cluster, whereas figure 4.10 depicts the spatial variation of the mean LST of blocks. We observe from figure 4.9 that there is a variation in the average mean LST across the clusters. Moreover, the variation can also be observed in figure 4.10 as the blocks in the city centre have higher LST as compared to the blocks in the outskirts of the city.

Table 4.2: Loadings of parameters on PCs

PC loadings					
Parameters		**PC1**	**PC2**	**PC3**	**PC4**
LCZ	GSI	0.338	-0.099	0.162	-0.068
	PSF	-0.318	-0.022	-0.242	0.164
	ISF	0.293	-0.092	0.288	-0.195
	SVF	-0.332	-0.047	0.216	-0.019
	AR	0.164	0.051	-0.278	0.394
	HRE	0.314	0.08	-0.138	0.135
Arrangement	OSR	-0.315	0.119	-0.19	0.2
	MA	0.031	0.536	0.312	-0.058
	NB	0.163	-0.409	0.282	0.04
Variations	SH	0.2	0.277	-0.277	-0.009
	SA	0.017	0.498	0.344	-0.104
Form	DCR	-0.087	0.111	-0.309	-0.518
	DB	-0.135	0.318	0.162	0.169
Shape	SF	0.027	-0.031	-0.246	-0.615
Wind environment	AH	0.305	0.153	-0.252	0.081
	Po	-0.262	0.087	-0.06	-0.129
	FAI	0.328	0.176	-0.18	0.049
Eigen Values		2.717	1.577	1.288	1.05
Explained variance		43%	15%	10%	6%
Cumulative variance		43%	58%	68%	74%

Table 4.4 provides the details of the ANOVA test. The p-value of the F-statistic is less than 0.01, implying that the means of LST in clusters A to I are not equal, indicating that the clusters are different from each other. Therefore, the ANOVA analysis validates the result of clustering. Altogether, the clustering result is acceptable, and the clusters are different from each other.

4.3.5 Features of morphological clusters

After applying k-means to the four RCs, we obtain 9 clusters in the city of Liege. Clusters D, E, F and G have the largest number of blocks in Liege city, followed by the clusters C, B and A. The clusters H and I have the lowest number of blocks (Figure 4.11). Therefore, we consider blocks closest to the cluster centres and identify them as morphological archetypes. Given the intra-cluster homogeneity, these blocks can

Table 4.3: Loadings of parameters on RCs

RC loadings					
Parameters		RC1	RC2	RC3	RC4
LCZ	GSI	**0.851**	0	-0.433	0
	PSF	**0.885**	0	-0.223	0
	ISF	**-0.838**	-0.176	0.374	0
	SVF	-0.481	0	**0.808**	0
	AR	0	-0.147	**-0.656**	0.227
	HRE	0.446	0	**-0.771**	0
Arrangement	OSR	**-0.875**	0	0.319	0
	MA	0	**0.935**	-0.107	0
	NB	**0.698**	-0.413	0.12	0.275
Variations	SH	0	0.211	**-0.725**	-0.19
	SA	0	**0.906**	0	0
Form	DCR	-0.269	0	0	**-0.683**
	DB	-0.362	0.526	0.144	0.18
Shape	SF	0	-0.123	0	**-0.707**
Wind environment	AH	0.332	0	**-0.86**	0
	Po	**-0.56**	0.113	0.432	-0.191
	FAI	0.428	0.114	**-0.854**	0
Eigen Values		4.723	2.297	4.386	1.222
Explained variance		28%	14%	26%	7%
Cumulative variance		28%	41%	67%	74%

Table 4.4: Model summary of ANOVA

	Df (degrees of freedom)	*Sum of squares*	*Mean sum of squares*	*F-statistic*	*Pr(>F)*
Clusters	8	1117	139.59	79.36.95	0.000

effectively represent the clusters. Figure 4.12 provides a two-dimensional view of the morphological archetypes in Liege obtained based on the clustering. Table 4.5 provides the values of parameters of the archetypes. Figure 4.13 (a) demonstrates the spatial distribution of clusters in the city.

The clusters in the city centre consist of compact blocks with low-rise to high-rise buildings (Clusters A, B, C and D). The clusters on the fringe of the city are open and sparsely built compared to the clusters in the inner city (Clusters E, F, and G). Other

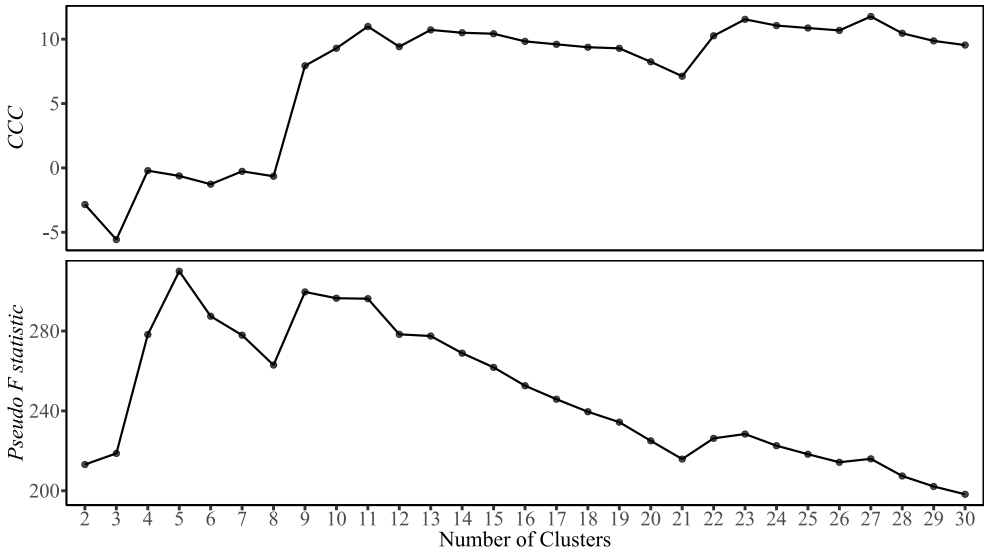

Figure 4.8: CCC and pseudo F statistic values for different numbers of clusters (k)

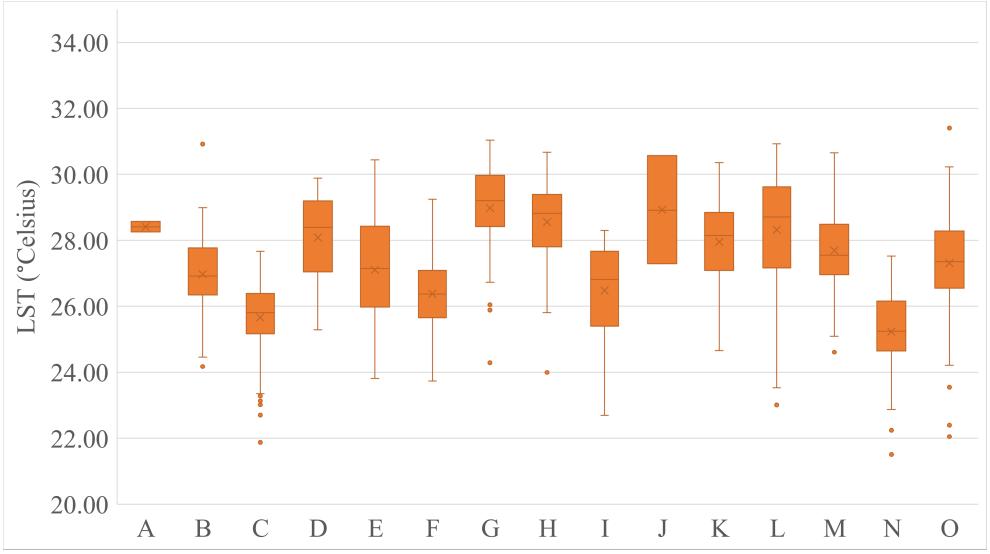

Figure 4.9: Cluster-wise mean LSTs of blocks

clusters (clusters H and I) are spread across the city, and the blocks in these clusters have large-sized and a few buildings, with mostly homogenous mid-rise to low-rise

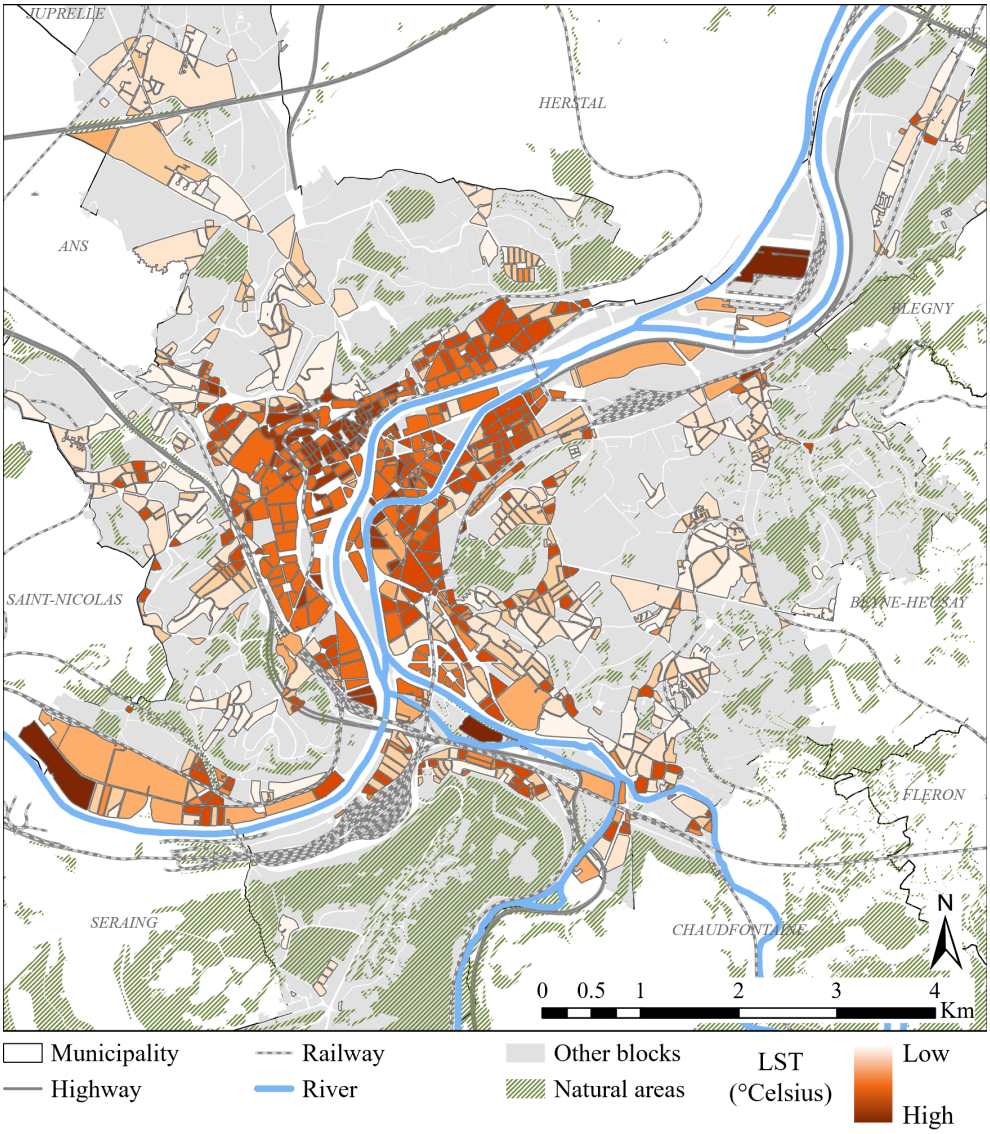

Figure 4.10: Spatial variation of mean LST of clusters

buildings. Significant variation between the clusters in terms of morphological parameters can be observed in figure 4.14. Based on these characteristics and the LCZ nomenclature provided by Stewart and Oke [162], we name the clusters as given in figure 4.12.

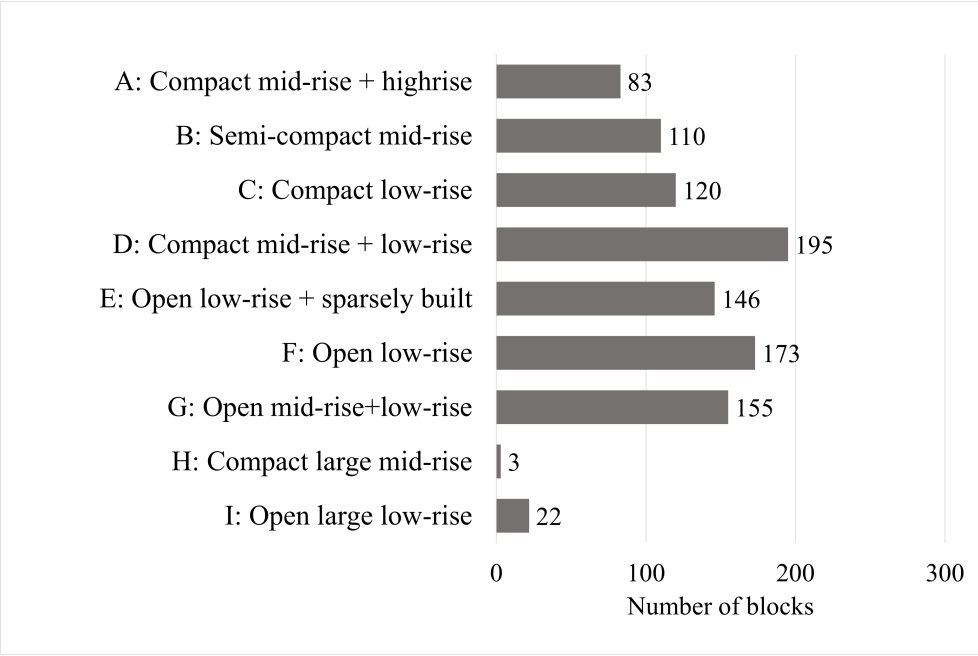

Figure 4.11: Number of blocks per cluster

4.3.6 Comparing clusters with LCZ

As per figure 4.13 (b), Liege city is classified mainly into four LCZs: Open low-rise, compact low-rise, compact mid-rise, and large low-rise. A few blocks in the city are classified into open, mid-rise and sparsely built. According to LCZ classification, clusters A and B blocks are predominantly compact mid-rise (Table 4.6). As cluster A has the largest GSI and a significantly higher HRE, it fits the description of the corresponding LCZ. However, cluster B has a moderate GSI value but a comparable HRE. Therefore, an almost equal share of blocks in this cluster corresponds to the compact low-rise classification of LCZ. Moreover, around 39% of the blocks in cluster A are classified as compact low-rise.

Clusters C and D are the clusters with blocks mostly on the city's outskirts. The GSI range of these clusters largely falls within the specified range of LCZ class of compact low-rise (table 4.7). However, there are variations between the clusters in terms of the arrangement (NB) and the shape of the blocks (SF). There are also slight differences in terms of building heights. For example, blocks in cluster D have taller buildings than the blocks in cluster C. Consequently, the AR values are higher for blocks in cluster D as compared to blocks in cluster C. Additionally, an almost equal

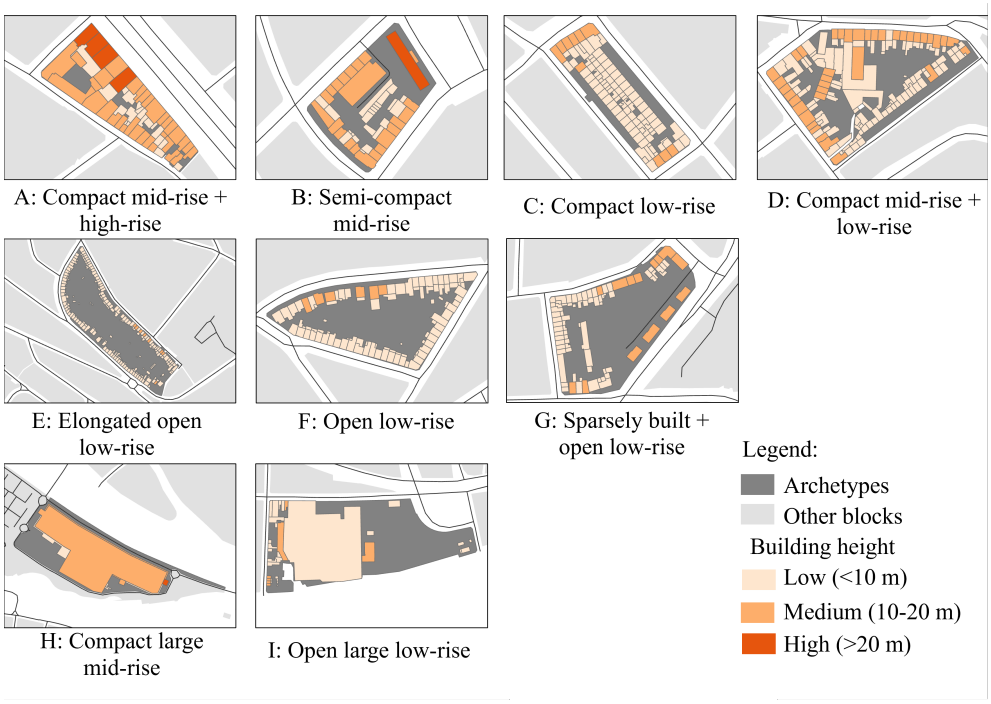

Figure 4.12: Two-dimensional view of morphological archetypes based on clustering

share of blocks of cluster C corresponds to open low-rise as per LCZ classification (table 4). Thus, clusters C and D represent distinct sub-classes within the LCZ of open low-rise.

Blocks in clusters E, F, and G are predominantly open low-rise as per LCZ classification. Around 80% of these blocks in the cluster fall into the open low-rise LCZ category (Table 4). However, they are different in terms of the shape of the block (SF) and open space in the block (OSR). Therefore, these clusters form essential sub-classes within the LCZ type of open low-rise.

The blocks in clusters H and I mainly belong to the large low-rise type of LCZ. These clusters have blocks with a large building area. However, cluster I has a GSI of 0.65, whereas the blocks in cluster H have a lower GSI. Thus, cluster I is more compact as compared to cluster H. The main characteristic of the blocks in these clusters are the large-sized buildings, so they are the essential sub-classes of the large low-rise LCZ classification. Figure 4.15 shows the proportion of clusters (sub-classes) in the existing LCZ classification. The distribution of sub-classes in compact mid-rise, compact open low-rise and large low-rise types of LCZ is almost equal. However, the

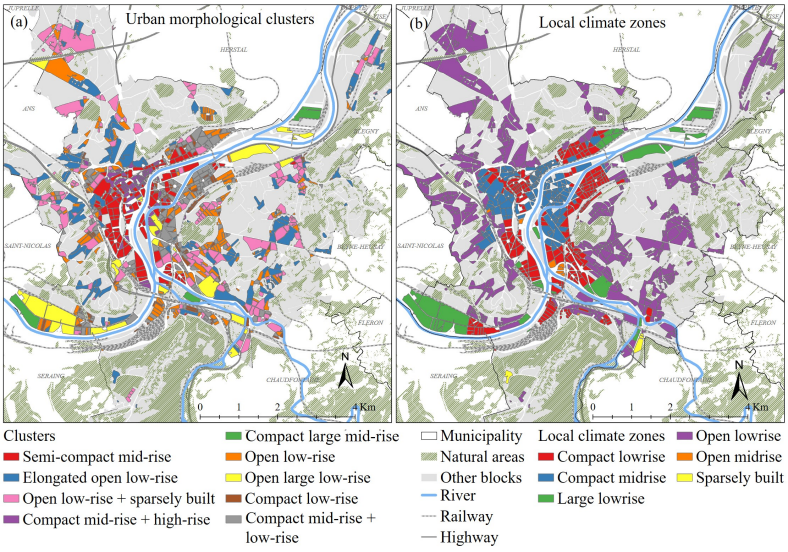

Figure 4.13: (a) Spatial distribution of clusters (b)Spatial distribution of LCZs

dominant sub-class in the compact low-rise type of LCZ is the semi-compact low-rise cluster.

Altogether, we observe that the classification in this paper broadly corresponds to the LCZ classification. However, our approach provides more detailed sub-classes, which are necessary to capture the microclimatic variations in the city (figure 4.14). We also observe that there are a few of the blocks misclassified as open low-rise when they are supposed to be in the compact mid-rise or low-rise category and vice versa. Furthermore, the differences in terms of morphological parameters within the sub-classes of each LCZ are noteworthy and can affect the microclimate and UHI. Thus, the clustering approach has produced more meaningful homogenous clusters which deliver logical LCZs and sub-classes of LCZs suited to the region.

4.4 Discussion and Conclusions

Urban morphological archetypes are the urban blocks that represent a homogenous group of blocks in terms of urban morphology, identification of which is vital for microclimatic analyses. In this paper, we propose a well-defined PCA-based k-means clustering approach supported by an external criterion validation using ANOVA analysis to identify urban archetypes. We choose the k-means clustering approach as it

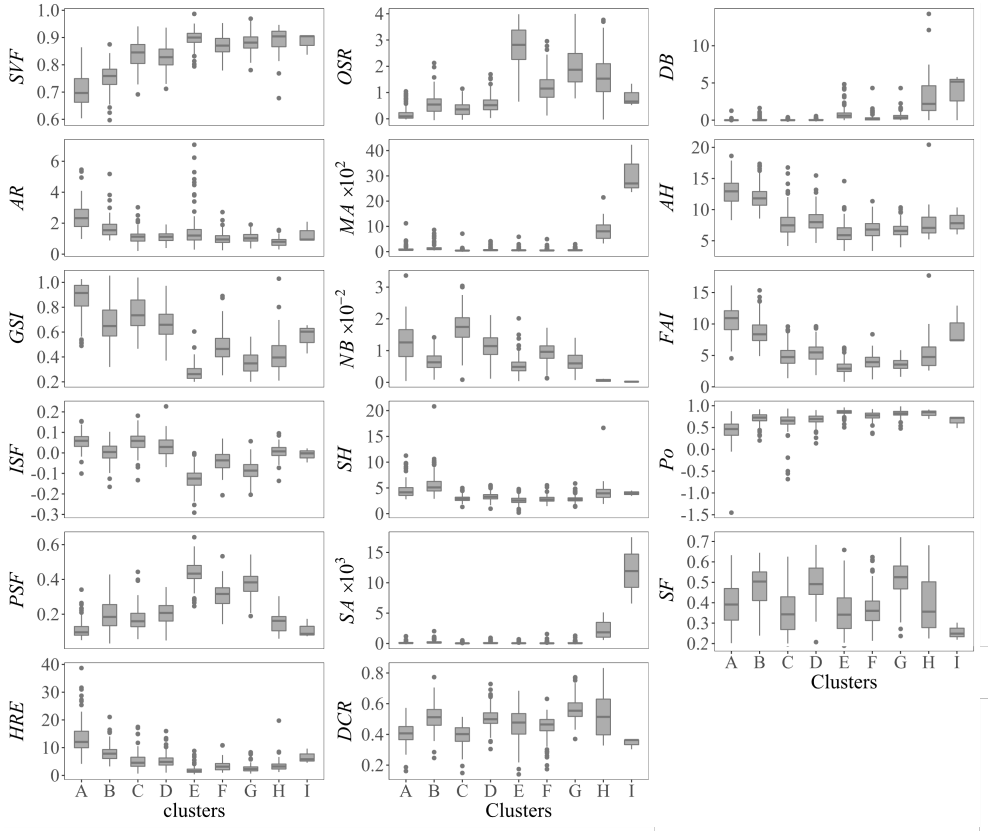

Figure 4.14: Variations in the values of parameters for different clusters

is an unsupervised data-driven algorithm that is robust in the absence of an existing classification of built-form in the city. We use seventeen urban morphological parameters based on LCZ, the categories such as form, shape, arrangement, and variations within the block, along with the parameters influencing the wind flow, defining the morphology of the block. Moreover, we support the choice of morphological parameters by identifying their influence on the microclimate, as mentioned in the literature. We propose the following steps to identify urban morphological archetypes for microclimate studies.

1. Filter the urban blocks based on building density, regularity of block shape and the number of buildings per block to identify blocks fit for analysis.
2. To reduce the dimensionality and verify non-collinearity among the variables,

Table 4.5: Characteristics of morphological archetypes belonging to each cluster

Cluster	SVF	AR	GSI	ISF	PSF	HRE	MA	SA	DCR
A	0.69	2.85	0.9	0.05	0.09	13.3	80.63	71.37	0.43
B	0.78	0.88	0.57	-0.01	0.2	9.7	109.8	149.2	0.41
C	0.81	1.08	0.72	0.04	0.19	6.52	33.61	18.21	0.42
D	0.81	1.54	0.63	0.03	0.21	4.29	46.65	61.27	0.58
E	0.88	1.48	0.29	-0.15	0.45	1.94	41.44	24.87	0.54
F	0.86	0.72	0.44	-0.07	0.33	2.91	45.49	27.6	0.49
G	0.87	0.98	0.33	-0.08	0.39	2.46	54.61	45.16	0.56
H	0.9	2.09	0.65	-0.05	0.17	5.82	4234	11929	0.3
I	0.92	0.74	0.49	-0.02	0.17	3.08	807.4	3790	0.7

Cluster	DB	SF	NB	OSR	SH	AH	Po	FAI
A	0	0.35	0.01	0.11	4.55	12.57	0.51	10.24
B	0	0.55	0.01	0.75	6.76	10.69	0.76	7.68
C	0	0.35	0.02	0.39	3.08	7.54	0.63	5.84
D	0.01	0.44	0.01	0.58	2.99	7.78	0.7	5.31
E	0.48	0.28	0.01	2.43	2.42	6.09	0.83	3.58
F	0.2	0.33	0.01	1.29	2.37	6.72	0.8	4.45
G	0.48	0.48	0.01	2.03	3	7.18	0.82	3.39
H	0	0.22	0	0.53	4.5	10.35	0.74	7.35
I	2.6	0.35	0	1.03	3.17	8.4	0.79	4.61

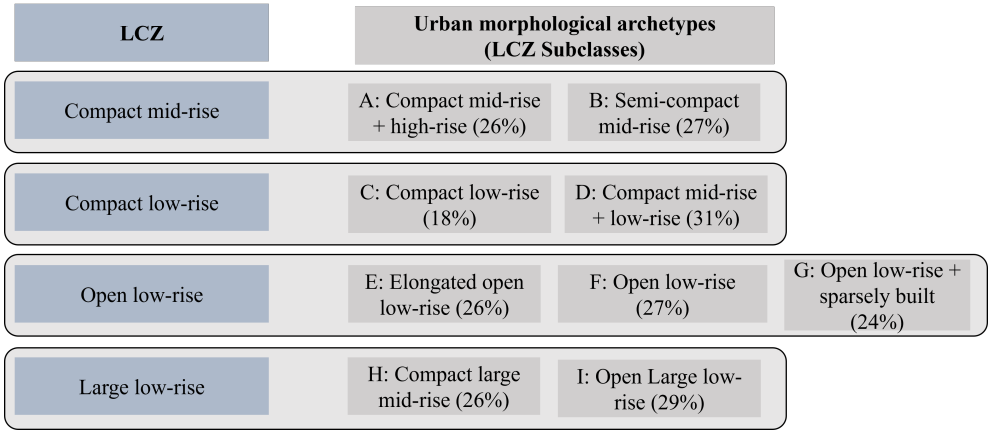

Figure 4.15: Proportion of clusters (sub-classes) in the existing LCZ classification

Table 4.6: Percentage of blocks in a cluster classified as an LCZ

Morphological clusters	Compact mid-rise	Compact low-rise	Open mid-rise	Open low-rise	Large low-rise	Sparsely built
A: Semi-compact mid-rise	44%	41%	5%	6%	1%	
B: Compact mid-rise + high-rise	57%	39%		2%	2%	1%
C: Compact low-rise	18%	39%		38%	3%	
D: Compact mid-rise + low-rise	23%	40%	1%	29%	5%	
E: Elongated open low-rise	2%	1%		96%	1%	
F: Open low-rise	4%	20%		73%	3%	
G: Open low-rise + Sparsely built	2%	8%	1%	86%	1%	
H: Compact large mid-rise				33%	67%	1%
I: Open large low-rise	18%	14%		23%	45%	1%

Table 4.7: Comparing parameter values of LCZs and archetypes

LCZs	Clus -ters	GSI	BSF (LCZ)	HRE	HRE (LCZ)	AR	AR (LCZ)	SVF	SVF (LCZ)
Compact mid-rise	A	0.89	0.4 - 0.7	13.29	10 - 25	2.85	0.75 - 2	0.69	0.3 - 0.6
	B	0.57		9.69		0.88		0.78	
Compact low-rise	C	0.72	0.4 - 0.7	6.52	3 - 10	1.08	0.3 - 0.75	0.808	0.2 - 0.6
	D	0.63		4.29		1.54		0.812	
Open low-rise	E	0.29	0.2 - 0.4	1.94	3 - 10	1.47	0.3 - 0.75	0.876	0.6 - 0.9
	F	0.43		2.9		0.72		0.864	
	G	0.32		2.45		0.97		0.869	
Large low-rise	H	0.65	0.3 - 0.5	5.81	3 - 10	2.09	0.1 - 0.3	0.9	> 0.7
	I	0.49		3.07		0.74		0.92	

use varimax rotated PCA to transform the urban morphological parameters into principal components that explain the most variance present in the data.

3. Cluster the RCs using the k-means clustering algorithm with k-means ++ ini-

tialisation; identify the best number of clusters using the CCC and pseudo F statistic.
4. Validate the clusters using ANOVA analysis using the mean LST of blocks as a dependent variable, which is one of the proxies for measuring microclimate quality.
5. Identify the blocks that are nearest to the cluster centre as an urban morphological archetype.

We apply the aforementioned steps to the city of Liege in Belgium. Firstly, by filtering the city blocks using GSI and SF, we obtain 1007 blocks qualifying for the analysis. Subsequently, we obtain four principal components based on the PCA, which are rotated using varimax rotation before clustering them using the k-means algorithm. We determine the number of clusters based on the best values of indices CCC and pseudo F statistic, resulting in nine homogenous clusters different from each other. Lastly, the validation indicates that the clustering is also successful in terms of LST, making the clusters logical for analysing the microclimate. Finally, we put forward a representative block from each cluster resulting in nine urban morphological archetypes that can be used as input for microclimatic analyses. We also compare the clusters with the existing LCZ map for Europe. The clustering-based classification in this study broadly corresponds to the LCZ classification. However, LCZ fails to capture morphological variety that can influence the microclimate. The approach used in this study identifies the relevant sub-classes that fall within the broad LCZ classes.

Although LCZ maps are available for Europe, the method proposed in this study is advantageous for the following reasons: the classification accuracy of LCZ maps is 70% [170] and using them directly might include misclassifications, as explained in section 3.7. Researchers also compute LCZs for specific regions for better accuracy [220, 275]; however, implementing a methodology to estimate LCZs in a city is not straightforward. Due to the wide-ranged parameter values of LCZ, there are often overlaps in the LCZ categories. Thus, sub-classes or combinations of various LCZ classes are often proposed as it gets extremely challenging to assign LCZ class to a block [204]. Moreover, the LCZ dataset is insufficient as the urban canopy must be described explicitly for analysing microclimate [203]. Furthermore, integrating raster-based LCZs into urban planning can be challenging as urban blocks are the urban design unit for urban planners and architects [223]. The urban block scale is also considered appropriate to analyse the heterogeneity of microclimate within the urban fabric [276]. Therefore, urban blocks are the appropriate units for identifying homogenous climate zones in a region.

The archetypes identified using this method can be used as a database to inform urban planners in optimising the urban forms to regulate the microclimate [277]. The

approach used in this study is also helpful in the absence of predefined typologies or classifications. It can effectively be applied to other cities worldwide for analysing the microclimate based on urban morphology. For instance, we apply it to Liege city, but the approach can be applied to the entire Wallonia region or Belgium to identify local archetypes for microclimate analysis. Although the approach is straightforward, it is essentially dependent on the data availability. Thus, preparing the data can be challenging when the datasets are not readily available. Approaches such as the Geoclimate tool by [257] can help derive LCZ parameters. Further studies can include developing data using open-access datasets to identify urban morphological parameters.

The present approach aids the microclimatic analysis by providing realistic urban blocks for microclimate analysis, including CFD simulations instead of a simplistic representation of urban blocks. Furthermore, it reduces the computational expense of analysing the microclimate at a higher resolution as it alleviates the need for simulating the microclimate of an entire city. Instead, the simulations can be carried out on the identified archetypes to arrive at a general overview of the microclimatic situation in the city. Moreover, the properties of these archetypes can be helpful to further generate modelled blocks in the city that will be a better representation of reality.

4.5 Key contributions

- Urban block is an appropriate scale of analysis for both capturing microclimate characterisation and variability and policy implementation.
- A novel systematic clustering approach for identifying urban morphological archetypes is proposed.
- We use 17 urban morphological parameters that define the geometries of an urban block in detail.
- Nine distinct morphological archetypes were identified for Liège city.
- Through comparative analysis with WUDAPT's LCZs, we identified pertinent sub-classes within the broader LCZ classification. These sub-classes effectively capture essential microclimatic variations, rendering the archetypes superior to existing LCZs.
- Morphological variation among the archetypes can influence the impact of green roofs on microclimates in them.
- Approach can be effectively used for other cities or regions.

5

Influence of urban morphology on the potential of green roofs in regulating local microclimate[1]

Urban heat island (UHI) mitigation strategies such as green roofs have become relevant owing to the abundance of impervious roofs in urban areas. As the UHI effect varies locally based on the urban morphology in a city, it is vital to assess the impact of green roofs on the local microclimate in different typical urban morphologies. Therefore, in this paper, we explore the role of roof greening in regulating the local microclimate in Liège, Belgium, for nine realistic and unique urban morphological archetypes, during a heatwave. For Liège city, we obtain the urban morphological archetypes based on a systematic data-driven approach using an extensive list of urban morphological parameters. We simulate nine scenarios without green roofs (base scenario) and nine scenarios with green roofs using the Solene-microclimat model. We introduce green roofs only on the existing flat roofs identified using remote sensing to analyse the realistic impact of roof greening. Results of the base scenario suggest that due to morphology, archetypes vary in terms of air and surface temperature. Because of the distinct morphologies in the archetypes, we observe that the impact of roof greening on these archetypes is also distinctive. For instance, green roofs can reduce the surface temperature effectively in compact/semi-compact

[1] Published as: **M.Y.Joshi**, A.Rodler, M.Musy, S.Guernouti, and J.Teller, *Influence of urban morphology on the potential of green roofs in regulating local microclimate: A case study of Liège, Belgium. Urban Climate. (under review) (2023)*

high-rise archetypes, whereas green roofs' potential to reduce air temperature is limited. While green roofs can effectively reduce surface and air temperature in compact low-rise archetypes, most compact low-rise archetypes are residential and have fewer flat roofs to green. However, large low-rise archetypes, which are predominantly industrial or commercial, can be retrofitted with green roofs, given the large potential of roof greening. This study provides insight into the interplay between urban morphology, realistic roof greening potential, and the UHI effect on local microclimate, improving our understanding of microclimate regulation with green roofs.

5.1 Introduction

Climate change is causing exceptionally high temperatures in urban areas resulting in heat strokes, higher mortality rates, and increased power consumption due to air conditioning [142, 278, 279]. Such adverse effects of extreme heat are particularly intense in urban areas compared to the neighbouring rural areas, causing the so-called urban heat island (UHI) effect [2]. Presently, factors such as urbanisation, urban densification and climate change have amplified the frequency and intensity of heatwaves, worsening the impacts of UHI [280]. Therefore, identifying strategies to curtail the adverse effects of extreme heat stress is necessary.

Strategies such as the use of high albedo materials in the construction of roofs, shading urban areas with trees, introducing city-scale green spaces like parks, and greening urban surfaces using green roofs and walls are frequently utilised for UHI mitigation [281–284]. As cities predominantly have high built-up densities with less open spaces and greening, solutions such as cool roofs, green roofs and green walls are highly relevant for UHI mitigation [285, 286]. Green roofs and walls are considered to have more advantages than cool roofs, given their multi-fold benefits, such as improving urban biodiversity, stormwater management, and quality of life, in addition to UHI mitigation [38]. Since green walls have a high financial cost for installation and maintenance compared to other alternatives [287], constructing green roofs can be a practical strategy to reduce extreme heat stress in urban areas.

UHI effect in urban areas varies locally based on the land cover and urban morphology [288]. Urban morphology relates to the form and structure of an urban area and the physical characteristics and arrangement of buildings [237, 289]. It influences the urban microclimate in several ways. For instance, higher building density, lower sky view factor, and larger building facades intensify the UHI effect [210, 211, 213]. Higher building density reduces the average wind velocity deteriorating urban ventilation [209], whereas lower SVF blocks the longwave radiation on the streets [212], retaining more heat in the region. Larger building facades impact wind velocity intercepting solar radiation and contributing to solar trapping [213].

Other factors, such as building arrangement and height variation, help regulate the microclimate [210, 214]. For instance, U-shaped blocks, blocks with courtyards, or multiple courtyards, have improved microclimates compared to detached, attached or linear blocks [214]. Additionally, a variation in building heights reduces the temperatures better than the area with uniform building heights due to the shading effect [210]. Consequently, the impact of green roofs can vary in different city regions with distinct morphological characteristics, which necessitates a detailed study of urban microclimate. Therefore, it is crucial to understand the role of urban morphology and the contribution of green roofs in mitigating the UHI effect during extreme heatwaves. In this study, we focus on the city of Liège in Belgium.

The morphological patterns in a city vary based on building and street-related properties. Because of such variations, researchers suggest analysing individual urban units, such as urban blocks, to study the UHI effect at the microscale [215, 290]. Analysing microclimate in urban blocks also allows urban practitioners to propose relevant strategies and techniques for the local context [217]. However, analysing a city with thousands of such urban blocks is computationally challenging and time-consuming. In such a scenario, identifying typical urban morphological archetypes representing a homogenous group of blocks can simplify the microclimate analysis at a city scale [218, 219, 289].

Urban areas can be classified into distinct microclimatic zones or archetypes based on morphology and related variables. For example, Stewart and Oke [162] introduced the local climate zones (LCZ) as homogenous regions in terms of surface cover, structure, material and human activity that stretch over hundreds of meters to several kilometres horizontally. Such LCZ maps are available for Europe and America [169]. Moreover, several researchers have generated LCZs specific to their areas, substituting or introducing additional parameters. Although the LCZ approach is widely used, Stewart and Oke [162] highlight that the approach is generic and cannot capture the peculiarities of every urban area. It is mainly adapted to the microclimate effect at the scale of a few hundred meters. Thus, they suggest creating new sub-classes unique to the urban areas of interest. Moreover, the LCZ parameters often remain insufficient to describe the urban canopy in detail, especially when the end goal is to analyse microclimate at the microscale. Apart from this, as the basic unit of design for urban planners is an urban block, rasterised output like LCZs do not provide precise typology at the block level [223, 224, 289].

Other approaches to identify urban morphological archetypes, such as rule-based classification, machine learning-based classification and classification using spatial multi-criteria analysis, have been employed previously [225–227]. While these methods are systematic and replicable, they can only be applied when predefined urban

archetypes exist in an area. For the city of Liège, since there are no predefined urban archetypes and LCZ maps proved inadequate to capture the unique morphological features of the city, Joshi et al. [289] proposed an alternative method that identifies urban morphological archetypes using a data-driven approach of PCA-based k-means clustering on different urban morphological parameters. This method provided nine realistic urban morphological archetypes for the city that are distinct from one another. These archetypes can help analyse the mitigation solutions, such as green roofs at a microscale, with the further intention to generalise the results at a city scale. Therefore, in this study, we employ the method proposed by Joshi et al. [289] to obtain realistic archetypes.

Many of the exploratory studies of the impact of green roofs on urban microclimate are limited to only a few chosen urban blocks in a city without focusing on the way morphology affects the microclimate [291–295]. In contrast, few studies analysed the impact of green roofs on different LCZs observed in their region of interest [243, 296, 297]. However, these studies employ simplified urban morphology; for example, Schibuola and Tambani [297] only consider compact mid-rise LCZ and change the heights of the buildings in it to generate high-rise and low-rise LCZs, instead of choosing existing realistic urban configurations. Additionally, Chen et al. [296] analyse three LCZs that are predominantly residential and have open spaces. Compact urban morphologies without open spaces are not analysed in these studies. In contrast, Wang et al. [243] focused their analysis only on the three compact LCZs in the city, while the other LCZs were not analysed.

The above studies show a research gap as all urban LCZs or archetypes are not usually analysed to examine their potential impact at the city scale. Moreover, compact urban blocks with no open space are not investigated. In other exploratory studies of green roofs [298–300], the green roof fraction is arbitrarily tested from anywhere between 0 and 100 per cent without considering the potential of existing buildings in the city on which green roofs can be installed. For instance, installing green roofs on existing flat roofs is more manageable than sloped roofs [43–45]. Moreover, one hundred per cent greening with green roofs is unrealistic, especially in European cities where historic buildings primarily have sloped roofs. In this study, we explore the impact of green roofs on the local microclimate during a heatwave by introducing green roofs on buildings with flat roofs in all the realistic archetypes of Liège, Belgium. To the best of our knowledge, such a complete study of realistic urban morphological archetypes with green roofs has never been previously reported.

Therefore, in this paper, we perform an exploratory study of the role of roof greening in regulating the local urban microclimate in Liège city using the Solene-microclimat model. For the first time in the studies assessing UHI mitigation so-

lutions, this paper analyses all the unique realistic morphological archetypes in a city during a heatwave for evaluating the impact of a realistic limit of roof greening identified using remote sensing in reducing the local air and surface temperatures. It provides insight into the interplay between urban morphology, realistic roof greening potential, and the UHI effect on local microclimate.

In section 2, we present the methodology of the study with a brief explanation of the microclimate model used, inputs and outputs from the model and the method for identifying heatwaves. In section 3, we present how air and surface temperature differs in different urban morphological archetypes, followed by the results of the impact of green roofs on the air and surface temperatures considering the realistic potential of roof greening in the archetype. And finally, we derive a cooling index (CI) to facilitate the comparison of cooling by green roofs in different archetypes. In section 4, we summarise the results and conclude them in section 5 based on the study.

5.2 Methodology

In this section, we provide details on the study area and elaborate on the Solene-microclimat model for microclimate analysis (Sections 2.1 and 2.2). We briefly explain the identification of heatwaves and urban morphological archetypes (Sections 2.3.1 and 2.3.2). We also describe the method for generating realistic morphologies and the surface properties used in Solene-microclimat. Lastly, we explain the total cases run and the expected outputs from the model.

5.2.1 Study Area

In this study, we examine the city of Liège in Belgium. It is the third most populous city in the country, with 196,296 inhabitants [83] and an area of 69 km^2. The city is densely occupied by buildings in the centre, leaving few open green spaces. The surface temperatures in the city are observed to be high during the summer, indicating a significant surface UHI effect [88].

5.2.2 Solene-microclimat Model

In this study, we employ the Solene-microclimat model [93] for computing realistic urban morphological archetypes' outdoor air and surface temperature. With Solene-microclimat, a researcher can investigate the model in depth and propose changes relevant to its study area as it is editable [94]. It also has the advantage of describing

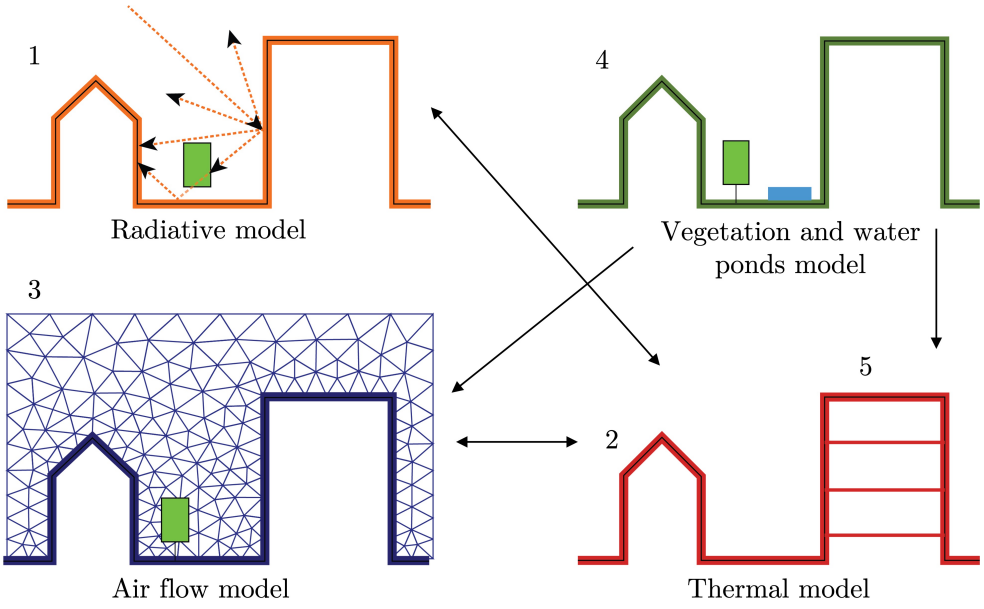

Figure 5.1: The coupling of the three different models included in Solene-microclimat: Radiative model (1) = SOLENE, Thermal model for urban surface s(2) and buildings (5), and Airflow model = code-Saturne (3). The sub-models (4) locally modify the surfaces and volumes properties in (2) and (5) to represent vegetation and water ponds. The arrows represent results passed from one model to another, and the green rectangle symbolises a tree. The figure is adapted from Robineau et al. (2022).

an urban block realistically due to tetrahedral meshing. Solene-microclimat can simulate the microclimate at the district scale with a high resolution (up to 1 m). It has been previously used to assess the impact of adaptation strategies such as green roofs and walls on outdoor and indoor thermal comforts and building energy consumption [95, 96].

The modelling approach of Solene-microclimat is based on the coupling of radiative, thermal and CFD (Computational Fluid Dynamics) models (Figure 5.1). Vinet et al. [301] originally developed the Solene-microclimat model for outdoor comfort assessment. Eventually, the addition of new sub-models facilitated the inclusion of radiative transfers, including longwave radiation, conduction and storage in walls and soils, airflow and convective exchanges, evapotranspiration from natural surfaces (like vegetation and water ponds or watering systems) and energy balance for a building in the simulated area. The model is coupled with an OpenSource CFD

software Code-Saturne 3.0, utilising the Reynolds Averaged Navier Stokes (RANS) approach with the k-epsilon turbulence model. Code-Saturne solves for wind velocity, air temperature and humidity. The anthropogenic fluxes simulated by the model are those associated with the heating and cooling of buildings but not with the traffic, for instance.

The model can simulate an extensive range of mitigation solutions. Different kinds of vegetation can be considered: trees [302], green roofs and green walls [303], as well as lawn surfaces [304]. All models used by Solene-microclimat have been compared independently to measured data [93] (Refer to section 2.2.1 for details). Apart from this, the spatial resolution of the model depends on the meshes and can be up to 1m. The simulation can be launched for hourly or sub-hourly time steps. As Solene-microclimat can simulate realistic 3D urban settings, explicit descriptions of objects like buildings and trees can be the input in the model. The primary outputs of the sub-models are their impact on sunlight, wind, air temperature and humidity, and surface temperature [94, 305].

Complementing equations were added to the wall to simulate green roofs in the model to represent foliage's role in the surface-to-air interface. Foliage acts as a partial barrier to radiation. It exchanges with the surface that supports it (the substrate when present or directly the wall in case of climbing plants) and the surrounding surfaces. It also exchanges convective and latent heat fluxes. For these kinds of surfaces, the latent heat flux of the substrate is considered in the model [94]. The method adopted to calculate evapotranspiration (ETP) is based on the Penman-Monteith equation, as the Food and Agriculture Organization (FAO) advised [306–308]. The model uses latent heat fluxes from vegetation and its substrate to calculate the mass rate of moisture released into the air and taken into account in the CFD model.

This method calculates the crop irrigation needs under the assumption of ideal water availability [93, 307]. Therefore, the model uses evapotranspiration rate (f) for considering the occurrence of water stress, which was conceptualised by Malys et al. [307]. The distribution of this flux between the foliage and the substrate is realised through the coefficient α_{lat} and the latent heat flux (φ_{lat}) is computed with equation (1) for the foliage and equation (2) for the soil surface.

$$\varphi_{\mathrm{lat,f}} = \alpha_{\mathrm{lat}} f \mathrm{ETP} \tag{5.1}$$

$$\varphi_{\mathrm{lat,es}} = (1 - \alpha_{\mathrm{lat}}) f \mathrm{ETP} \tag{5.2}$$

Furthermore, the evapotranspiration calculation depends on both solar and infrared radiation along with leaf surface temperature, air temperature in the foliage, air humidity and wind speed [94].

Lastly, Solene-microclimat is a comprehensive model used for simulating microclimates. It is similar to Envi-Met in terms of capabilities but with the added feature of using tetrahedral meshes to represent urban morphologies better. Moreover, the Solene-microclimat model has clear documentation on the equations and sub-models, making the tool well-suited for research.

Model Validation

Solene-microclimat model is previously validated for each of its sub-models and features. [309] has carried out a validation of the model on a street canyon composed of containers, showing good agreement for both air temperature and velocity on the street. Musy et al. [93] validated the ground, roof and wall modules included in Solene-microclimat using the data from the FluxSap campaign [310] for a neighbourhood in Nantes, France. Additionally, latent fluxes from vegetation and its substrate, which the model uses to calculate the mass rate of moisture released into the air and considered in the CFD model, are calibrated by Malys et al. [307] using monitored experimental data recorded on the roof of HEPIA school of Geneva (Switzerland), LEEA Laboratory. After this calibration, the model showed a good agreement with the measurements [303, 307]. The results on the direct and indirect effects of green roofs in a neighbourhood in Nantes, France, from [95] also conform with the results from other studies, indicating that Solene-microclimat can be used to assess several green adaptation strategies [93].

Apart from this, Rodler et al. [311] assessed the detailed building thermal model performance, and Azam et al. [312] substantiated the precise soil model performance in an open space (a car park). More details about the case studies and the validation steps are available in Musy et al. [94]. Most of the validation has been done in the temperate climate zone of Nantes, France [94]. As Liège city also falls in the same climate zone, we refer to the above studies for the validation of different modules used in Solene-microclimat.

5.2.3 Inputs for Solene-microclimat

We simulate the microclimate in urban blocks in Solene-microclimat for one day (24 hours). The meteorological data, namely air temperature, wind velocity, wind direction, global radiation, direct and diffused radiation, infrared radiation, relative humidity and pressure, are obtained from the observations of the Royal Meteorological Institute, Belgium (RMIB). For simulation, we identify and consider the hottest day of an intense heatwave observed in Liège in 20 years (from 2000-2020).

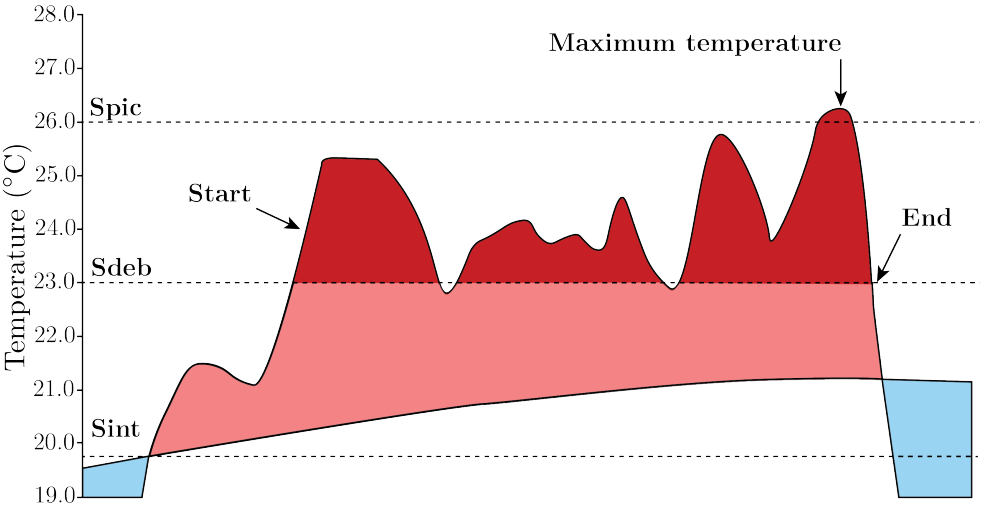

Figure 5.2: Characterisation of a heatwave from a daily mean temperature indicator: Duration (start and end), maximal temperature and global intensity (red plot area). The pink (blue) area represents the temperatures above (below) the climatological line (2000-2020 reference period). Graphic adapted from [3]

Heatwave identification

The meteorological data used for this study is obtained from the weather station nearest to Liège city. We utilise the method Ouzeau et al. (2016) advised to identify the heatwave. The approach is based on high quantiles of daily temperature distributions. Figure 5.2 demonstrates the characterisation of heatwaves for a given period of time. Three settings, namely, *Spic*, *Sdeb* and *Sint*, are involved in heatwave identification. *Spic* is the temperature threshold beyond which an event is detected. *Sdeb* is the threshold that defines the beginning and the end of the heatwave, and *Sint* is the interruption threshold which allows merging two consecutive occurrences without a significant drop in temperature.

When the temperature is above the *Sdeb* threshold, it is the start (first day) of the event. The heatwave is interrupted if the day's temperature goes below the *Sdeb* threshold for at least three consecutive days or drops to values below the *Sint* threshold. The values of *Spic*, *Sdeb*, and *Sint* are 99.5, 97.5 and 95th percentile, respectively, computed on the daily mean air temperatures for a given period. These percentiles are a result of a detailed preliminary analysis of EURO-CORDEX data [3, 313], which led to heatwave identifications close to the application of the operational method. This

method is beneficial as it considers the local climate of the study area. We compute the number of heatwaves, their intensity and duration and select the heatwave with the highest intensity and duration. Subsequently, we consider the hottest day in the selected heatwave period for simulations.

Urban surface properties

We use the values in Table 5.1 for albedo and emissivity of surfaces in the urban block. The values are based on the materials of surfaces in the existing literature and previously validated studies of Solene-microclimat [93, 95, 314]. Figure 5.3 denotes the surfaces in all nine blocks.

We assign the evapotranspiration constant f value for green surfaces as 0.5 for each hour, assuming green roofs have 50% water content each hour. Moreover, the albedo value of green roofs is 0.3, considering the green roofs are extensive green roofs.

Table 5.1: Surface Properties such as albedo and emissivity used to model archetypes in Solene-microclimat

Surfaces/Models	Materials	Albedo	Emissivity	Reference
Road	Asphalt	0.25	0.9	[93, 205]
Parcels (ground)	Asphalt	0.25	0.9	[93, 205]
Walls	Concrete	0.37	0.9	[311, 315]
Roofs	Concrete	0.3	0.9	[93, 311, 316]
Green roofs	-	0.3	0.9	[95]
Lawns	-	0.25	0.9	[96]

Generating realistic urban blocks

We employ the systematic principal component analysis (PCA)-based k-means clustering approach proposed by Joshi et al. [289]. In this method, 17 morphological parameters have been used. Along with parameters used for classifying LCZs [162], parameters informing form, arrangement, shape and variations within the urban block are utilised. More details about parameters can be found in [289]. We obtain nine realistic urban morphological archetypes for Liege using the 17 parameters (Figure 5.3). The nine classes derived from the clustering broadly correspond with the LCZ classification of Europe by [170]. Still, they provide essential sub-classes that

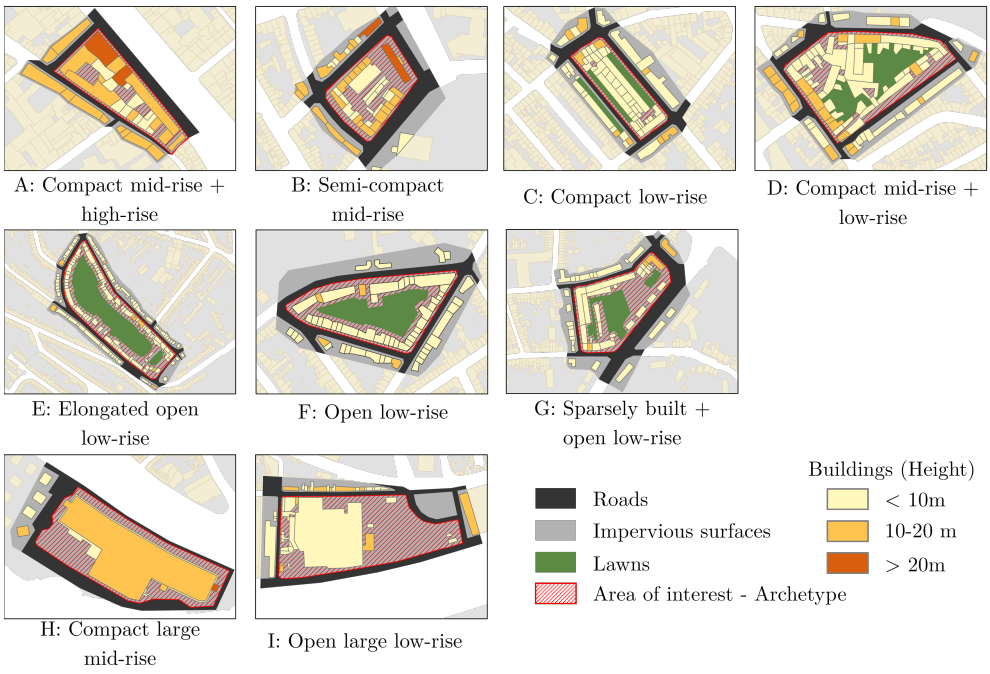

Figure 5.3: Detailed geometries used in the Solene-microclimat simulation based on urban morphological archetypes

better capture the morphological variety in the city.

We retain the geometries of the archetypes to be as realistic as possible. For practical purposes, we remove the buildings that are less than or equal to 20 m^2. We also simplify the building edges such that they are at least 2 m long. Figure 5.3 shows the 2-dimensional geometric configuration we used as an input in Solene-microclimat. Figure 5.4 shows the basic morphological properties of these archetypes, such as the percentage of area occupied by buildings, impervious open space and green open space.

With all these conditions, we generate realistic geometries using SketchUp Pro 2021. Further on, we create the domain of 700 x 700 m for archetypes A, B, C, D, F, and G and 1000 x 1000 m for blocks E, H and I (larger block area) with a height of 100 m each surrounding the urban area of blocks using open-source CAD modelling tool - Salome-7.6.0. The resolution used for the model is 2 m, as the Solene-microclimat model has been validated for mitigation strategies for similar geometries [95]. Furthermore, with 2 m resolution, approximately 10000 core hours on a supercomputer

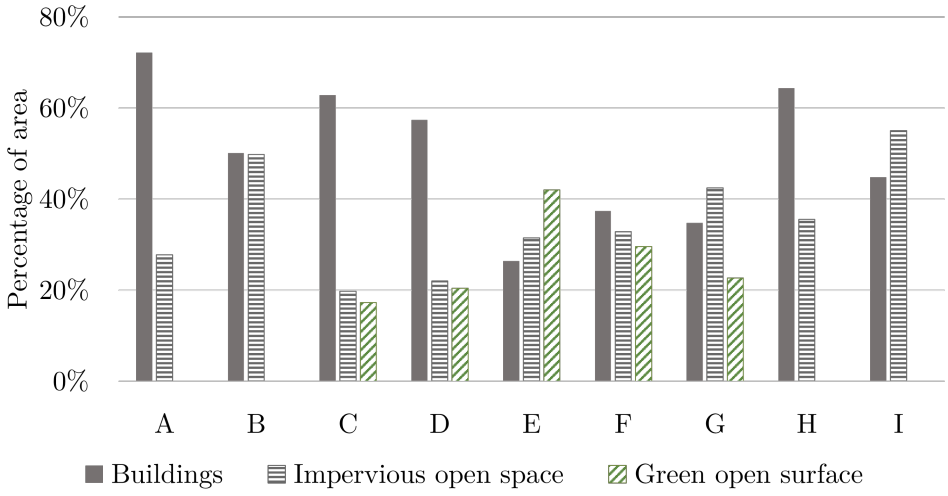

Figure 5.4: Basic Properties of Archetypes

were required to run all the cases in this study, with 16 cores per case. Therefore, increasing the resolution is computationally expensive and memory-intensive.

We define the surfaces within the archetype based on Figure 5.3 and Table 5.1 and generate the 2D and 3D tetrahedral meshes using Gmsh 2.8.3. As urban blocks do not exist in isolation, we insert buildings along the road surrounding the archetype to get the effect of context on the blocks.

5.2.4 A suite of Solene-microclimat simulation cases

We run two cases for each archetype, one with green roofs and one without (base scenario). Totally, we run 18 cases (nine cases for the base scenario, nine cases for scenarios with green roofs). Moreover, we simulate the green roofs only where the existing flat roofs are present to ensure realistic greening. We identified flat roofs using LiDAR point cloud data with 0.8 points/m^2 for Liège. Employing the RANSAC algorithm to process LiDAR point cloud, we obtain the number of planes within a building footprint. Assuming flat roofs to have less than a 10° slope, we identify flat roofs with an area of at least 10 m^2 for the entire city. The details of this methodology can be found in Joshi et al. [88]. Based on this, we consider buildings with flat roofs for roof greening. Figure 5.5 shows the percentage of flat roofs that can be greened in each archetype, and Figure 5.6 shows the spatial location of the flat roofs where we place the green roofs for simulations.

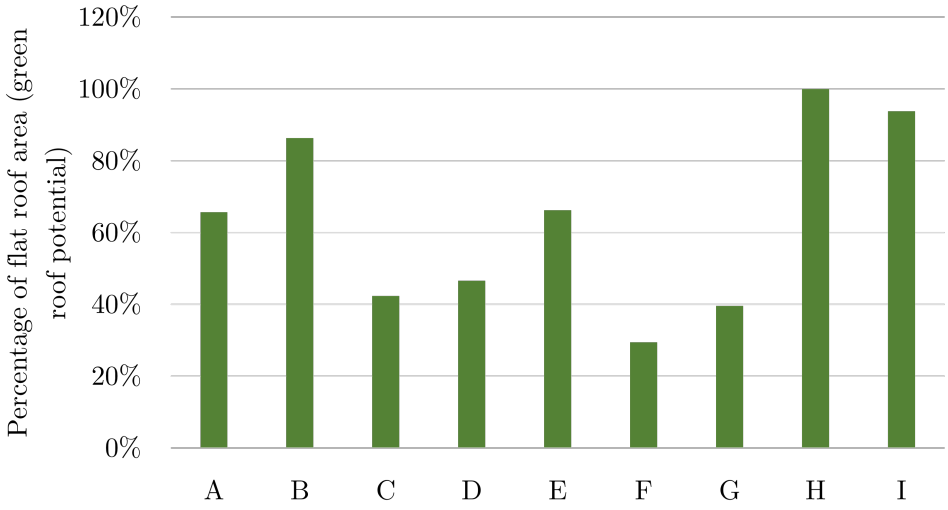

Figure 5.5: Green roof potential in each archetype

5.2.5 Outputs from the model

The model generates several outputs, such as hourly air and surface temperature, along with all the energy budget components of the archetype in W/m^2.

Surface energy balance

Surface energy balance gives us insight into the way dominant physical processes such as radiation, convection, conduction, and evapotranspiration affect surface and air temperatures. Morphology affects the surface energy balance, as the height of the buildings, green spaces in the archetype, and other factors affect the net energy received by the urban surfaces by modifying shading, inter-reflections, and wind velocity.

In the absence of evapotranspiration from green surfaces, the net radiation received by the urban surface is balanced by the sensible heat flux representing the convective heat exchange between the heated surface and the near-surface air, and the residual heat which enters the surface as the ground heat flux. When green roofs are introduced, during the daytime, if water is available, a large part of received solar radiation is used for evapotranspiration. This causes a drop in the net energy entering the substrate, essentially creating a cooling effect on the surface and in the convective heat flux transferred to the air that is less heated by the surface. Therefore, net energy

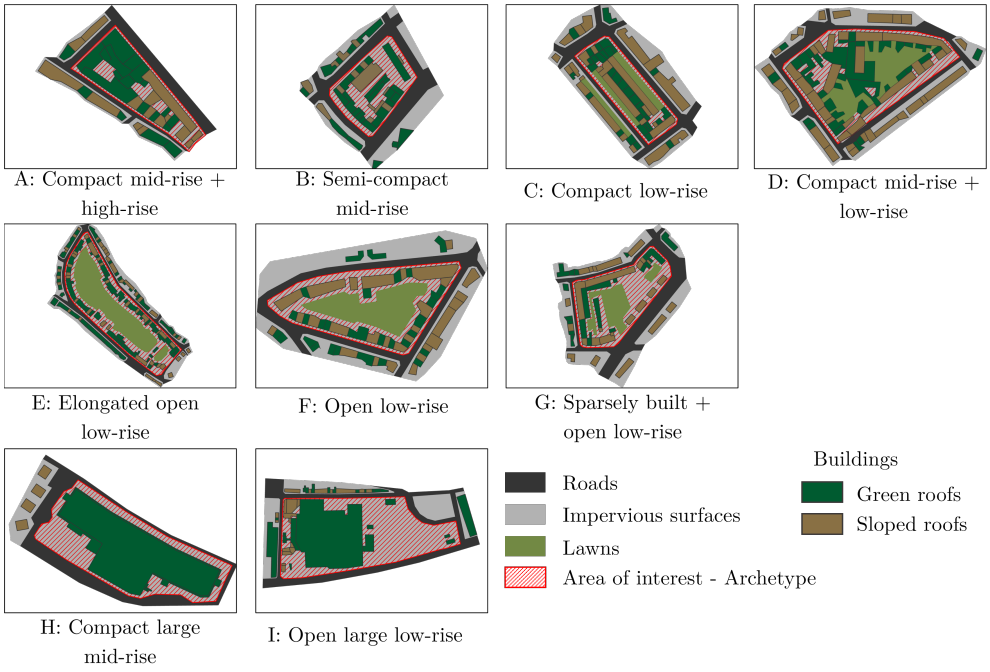

Figure 5.6: Green roof locations

budget/balance (φ_{net}) is the residual heat substrate that will enter a building; lower φ_{net} indicates lower overall energy consumed by buildings for cooling; in other words, lower the heat stress. The energy budget in the Solene-microclimat model consists of sensible heat flux and radiative flux for dry surfaces. For vegetation surfaces, latent heat flux is removed from the net energy budget. It is represented as follows:

$$\varphi_{\mathrm{net}} = \varphi_{\mathrm{sens}} + \varphi_{\mathrm{rad}} - \varphi_{\mathrm{lat}}. \tag{5.3}$$

Net radiative flux is computed as follows:

$$\varphi_{\mathrm{rad}} = \varphi_{\mathrm{SW}} + \varphi_{\mathrm{LW}}, \tag{5.4}$$

where φ_{SW} is the absorbed shortwave radiation, φ_{LW} is the net longwave radiation from the surface.

Sensible heat flux (φ_{sens})is calculated as follows:

$$\varphi_{\mathrm{sens}} = -\mathrm{h_c}\left(\mathrm{T_{se}} - \mathrm{T_{air}}\right), \tag{5.5}$$

where $h_c(\mathrm{Wm^{-2}K^{-1}})$ is the convective heat transfer coefficient (CHTC) and $\mathrm{T_{se}}$ and $\mathrm{T_{air}}$ are surface and air temperature, respectively. CHTC can either be derived either by a coupled thermo-aeraulic simulation or estimated through empirical correlations. The first method being expensive in terms of computational cost, building energy simulation models usually utilise correlations. Those correlations evaluate the CHTC from the wind speed (v_{air}) monitored at the studied surface [317]. We use the equation obtained by McAdams (1954) for low winds (v_{air} < 5 ms^{-1}) as follows:

$$\mathrm{h_c} = 5.7 + 3.8 v_{air}, \tag{5.6}$$

Latent heat flux is the flux transferred from a surface to the atmosphere with the evapotranspiration process. It is explained in section 2.2 in Equation 2.

Therefore, the net energy budget generally reduces when a surface is greened. By reducing the amount of energy available for sensible heat and releasing latent heat simultaneously, green areas can cool the surrounding area [318, 319]. In this study, we also explain the surface energy balance for all the archetypes in the presence of green roofs.

Area weighted average temperature

The $\mathrm{T_{air}}$ and $\mathrm{T_{se}}$ are obtained for each of the cell near a surface in the urban block. We start with investigating the surface temperature of roofs and ground in the urban block together to study the overall block temperature. Then, we investigate the near-surface air temperatures of roofs, ground and road surrounding the block. First, we compute the $\mathrm{T_{se}}$ or $\mathrm{T_{air}}$ at a surface by taking an average of $\mathrm{T_{se}}$ values on the triangular cells. Then, we compute the average $\mathrm{T_{air}}$ and $\mathrm{T_{se}}$ using the following equation:

$$\mathrm{T_{avg}} = \frac{\sum \mathrm{T_i A_i}}{\sum \mathrm{A_i}}, \tag{5.7}$$

where, $\mathrm{T_i}$ stands for $\mathrm{T_{se}}$ or $\mathrm{T_{air}}$ of a surface, $\mathrm{A_i}$ is the area of each surface and i is the total number of surfaces.

Difference in Temperatures and Cooling Index

For estimating the difference created by green roofs in each geometry, we compute the difference in average surface and air temperature between the base scenario and the green roof scenario as follows:

$$\Delta \mathrm{T} = \mathrm{T_{avg(basescenario)}} - \mathrm{T_{avg(greenroofscenario)}}. \tag{5.8}$$

Additionally, we show the spatial variation of changes in air and surface temperatures averaged over the mid-day (12:00-18:00) after introducing green roofs, which mainly shows the temperatures of each cell in the archetype.

We also compute the cooling index (CI) as follows:

$$\mathrm{CI}_{\mathrm{se/air}} = \frac{\Delta \mathrm{T}_{\mathrm{se/air}}}{\mathrm{GR}_{\mathrm{perc}}}, \tag{5.9}$$

where $\mathrm{GR}_{\mathrm{perc}}$ is the percentage of greened roof area to total roof area. CI represents the change in temperature per percentage of roof greening. This index removes the impact of different green roof percentages in each block and enables a fruitful comparison of differences between blocks.

5.3 Results and Discussion

In this section, we showcase the outputs obtained from running 18 cases. In section 3.1, we explain the selection of the hottest day during the most intense and longest heatwave in Liège. In section 3.2, we discuss the microclimate of each archetype and compare the archetypes with each other. Furthermore, in section 3.3, we present the impact of green roofs on regulating local microclimate in all the archetypes by explaining the changes in surface energy balance, surface and air temperature after realistic roof greening. Additionally, in this section, we elaborate on the impact of archetypes on the cooling index (CI).

5.3.1 Heatwaves in Liège

In this section, based on the methodology for heatwave detection by Ouzeau et al. [3], we select the hottest day in the most intense and longest heatwave in Liège. Figure 5.7 (a) shows the intensity and duration of the heatwaves in Liège between 2000-2020. We observe that there have been six heatwaves in Liège during this period. Moreover, the intensity of heatwaves is increasing with time. Most heatwaves have a duration of more than eight days. We can see that the heatwave of the year 2018 is the longest heatwave with severe intensity. Therefore, we choose this heatwave for this analysis. Figure 5.7 (b) demonstrates the daily mean temperatures for 16 days of this heatwave which is observed from 23rd July to 7th August 2018. The daily mean temperature is the highest for 27th of July. Therefore, in this study, we simulate the archetypes for the 27th of July, 2018.

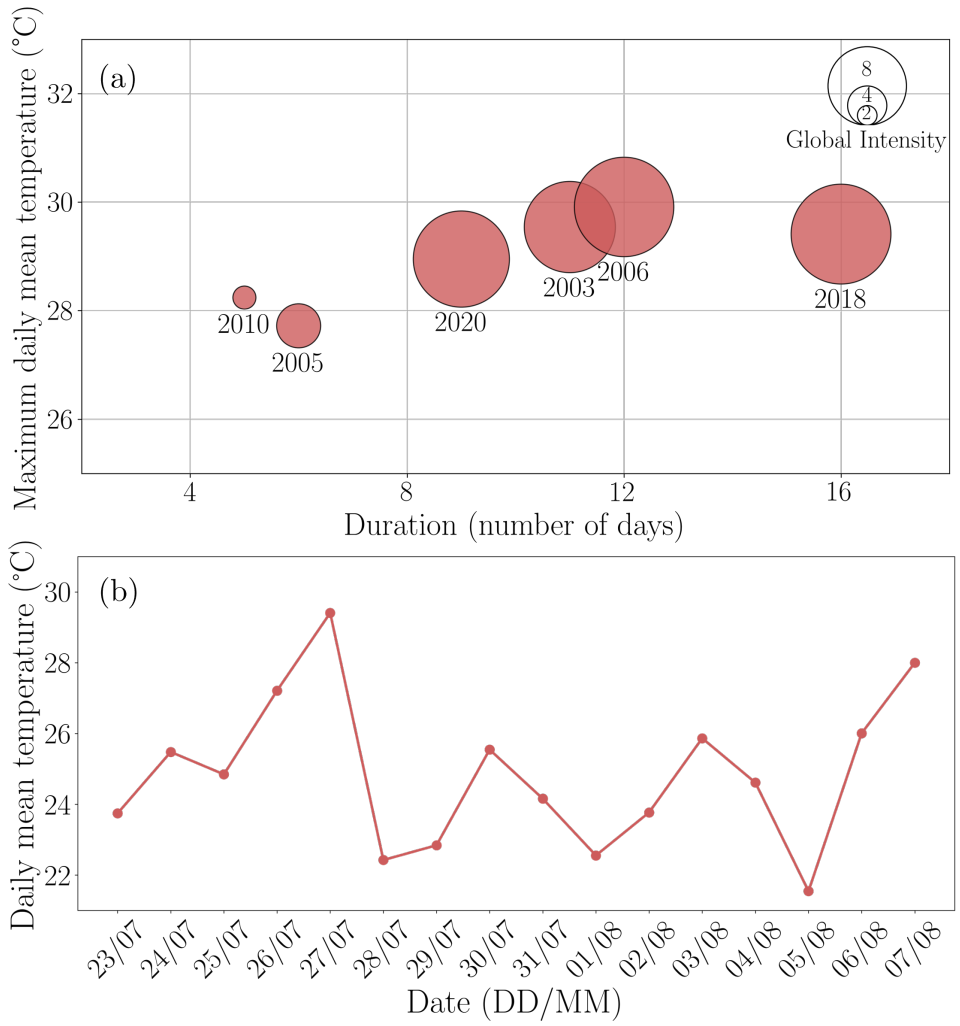

Figure 5.7: (a) Intensity and duration of heatwaves in Liège from 2000 to 2020 (b)Daily mean temperature during the longest and most intense heatwave in Liège

5.3.2 Microclimate of archetypes during the hottest day in heatwave

In this section, we present the average surface temperature (T_{se}) and near-surface air temperature T_{air}) of all horizontal surfaces belonging to the archetype (roofs of all buildings and ground, called 'all surfaces' from here on) for the nine urban morphological archetypes for 24 hours (Figure 5.8). We observe that both T_{se} and

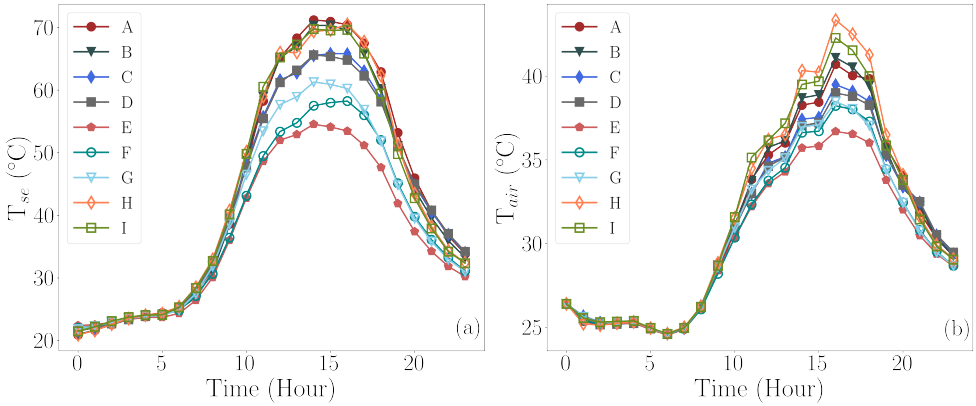

Figure 5.8: Diurnal variation of (a) Surface temperature (b) Air Temperature for all horizontal surfaces in Archetypes

T_{air} (Figure 5.8(a) and (b)) follow a typical diurnal cycle with low temperatures in the morning and higher temperatures in the afternoon during the heatwave, followed by lower temperatures at night. As expected, archetypes experience higher temperatures during the mid-day (12:00-18:00). We observe that the overall trend of T_{se} and T_{air} is similar for all archetypes from 0 to 24th hours in a day. Furthermore, in Figure 5.8(a) we see that the densely packed archetypes with no green space and archetypes with a large impervious surface area associated with them (Archetypes A, B, H and I) show maximum T_{se} and T_{air} indicating a high heat stress.

To delve deeper into the temperature variation during the hottest period of the day, we average T_{se} and T_{air} between 12:00 – 18:00 hours. Figure 5.9 shows the T_{se} and T_{air} averaged from 12:00-18:00 hours for all surfaces (roofs of all buildings + ground), at roof level and ground level. The T_{se} of archetypes ranges from 53°C to 71°C (Figure 5.9(a)), with a range of 76 - 84 °C at roof level (Figure 5.9(b)) and 44-56°C at ground level (Figure 5.9(c)). We observe higher temperatures at the roof level compared to the ground. Similarly, T_{air} of archetypes ranges from 35-41°C (Figure 5.9(d)), with a range of 37-41°C at roof level (Figure 5.9(e)) and 35-41°C at ground level (Figure 5.9(f)). T_{air} has a similar range at all levels, with slightly higher temperatures at roof level. This is because ground surfaces are more often shaded than roofs.

Surface temperature variation

Figure 5.9(a) shows that the compact high-rise/mid-rise archetype (A) is the hottest in terms of T_{se} of all surfaces due to taller buildings that are compactly located.

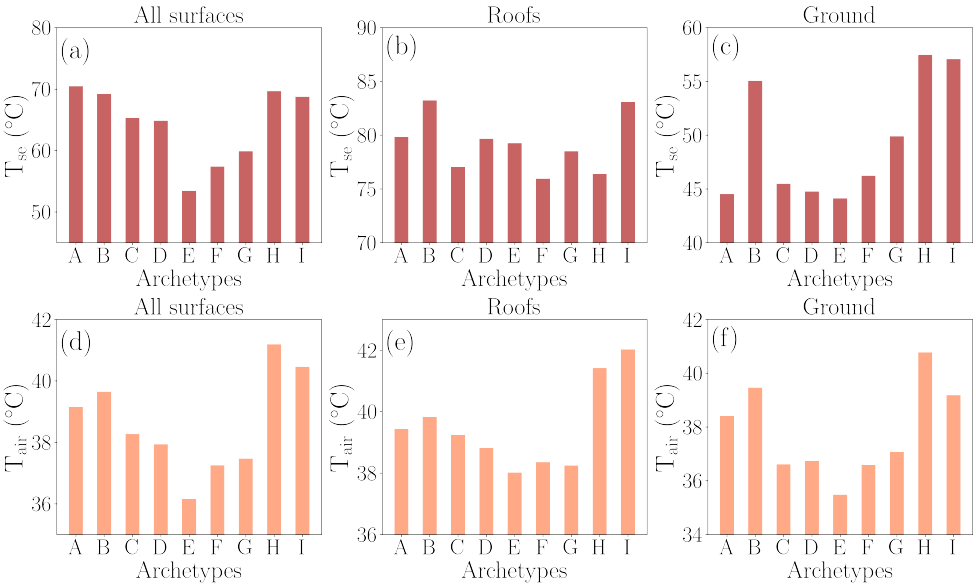

Figure 5.9: Average temperatures during mid-day (12:00-18:00) (a) T_{se}-all surfaces (b) T_{se}-roof level (c) T_{se}-Ground (d) T_{air}-all surfaces (e) T_{air}-Roof level (f) T_{air}-ground level

Archetypes similar to A such as B, H, and I which include a high proportion of impervious surfaces without any green areas have a comparable T_{se} (Figure 5.4). While the above-mentioned archetypes show similar higher T_{se}, the underlying cause is slightly different. For example, archetypes A and B have a high T_{se} as they have densely packed tall buildings, while archetypes H and I (large compact mid-rise and low-rise) have large buildings (areawise) with large, paved surfaces contributing to the heating of surfaces. It is also interesting to note that compact high-rise archetype (A) has a lower T_{se} at ground and roof level compared to archetype B, but overall, archetype (A) has higher T_{se}. This is because of the higher built-up percentage in archetype A.

Figure 5.9(a) also shows that archetype with large elongated central green space with low rise buildings (E) is the coolest (Figure 5.2). Similar archetypes with a mix of low-rise buildings and green spaces (C, D, G, and F) have lower T_{se} as compared to archetypes with no green areas (Archetypes A, B, H and I). Moreover, compact low/mid-rise archetypes (C and D) have almost similar average T_{se}. On the other hand, open low-rise archetype with sparsely located buildings (G) is almost 5°C lower in terms of average T_{se} of all surfaces, than similar low-rise archetypes C and D. This is possibly due to the loosely packed nature of buildings, with a large open area and a

green area in between. Open low-rise archetype (F) has a lower T_{se} than archetype (G) because of the larger green space in the archetype's open area and lower building heights.

Air temperature variation

Figure 5.9(d) shows that the T_{air} in the compact archetype with a large building (area-wise) and no open or green area (H) is the highest, followed by similar archetypes I, B, and A with higher impervious surfaces and building density. While the variation of T_{air} broadly follows the T_{se} variation, T_{air} is higher in archetypes H and I (than archetypes A and B) due to the presence of large-sized buildings. Moreover, archetype H is slightly warmer than archetype I because of its higher built-up percentage (Figure 5.4). Compact archetypes with taller buildings (A and B) also have similar air temperatures, but archetype B is slightly warmer than A because the open impervious space (in archetype B) provides more room for the warm wind to circulate. Another reason could be the shadowing on ground (in small open spaces) caused by taller buildings in archetype A.

Other low-rise archetypes (C, D and G) have 1-2°C lower T_{air} than high-rise and impervious surfaced archetypes (A and B). Compact low-rise archetypes (C and D) are slightly warmer than the sparsely built archetype (G) due to higher built-up percentage in the block. Open low-rise archetype (F) has around 1°C less T_{air} compared to the compact low-rise archetype (C) because of the larger green space. Lastly, elongated open low-rise archetype (E) has the lowest T_{air}, which is 1°C lesser than archetype F and significantly lesser than other archetypes because of the vast green space in the centre.

Based on the results, we observe that the archetypes are different from each other in terms of T_{se} and T_{air}. However, we notice that some archetypes have just around 1-2°C difference in average T_{se}. Like, compact archetypes A, B, H, and large low-rise archetype I have similar temperatures; however, they are different in terms of temperatures at roof level and ground level (Figure 5.9(b) and (c)). For instance, archetype A has around 11°C lower T_{se} on the ground than archetype B. Similarly, archetype B has a higher T_{se} at roof level than archetype H (almost 9°C difference). Semi-compact and large low-rise archetypes B and I have similar T_{se} values even at roof and ground level. But in this case, archetype B has almost 3°C lower T_{air} at roof level compared to archetype I (Figure 5.9 (e)). Similarly, compact low-rise archetypes C and D have comparable T_{se} but the T_{se} at roof level for archetype D is almost 2.5°C warmer than archetype C. Likewise, archetypes F and G have similar Tse, but archetype F has 3°C lower T_{se} at ground level.

To summarise, the results show that morphological variables affect the overall

surface and air temperatures in the archetypes, resulting distinct variation of T_{se} and T_{air}. This can influence the relative benefits of the green roofs in each archetype. Therefore, retrofitting green roofs on buildings in cities should consider the morphology and the results from one morphological archetype cannot be directly generalised to another.

5.3.3 Green roof's potential in regulating microclimates of archetypes

We present the impact of greening the flat roofs in the nine archetypes. Section 3.3.1 explains the changes observed in the surface energy balance of the archetypes after introducing green roofs. Section 3.3.2 presents the difference in T_{se} and T_{air} caused by realistic roof greening in the archetypes. Lastly, section 3.3.3 presents the impact of morphologies (archetypes) on the cooling index (CI).

5.3.4 Surface energy balance

Here, we present the changes in the surface energy balance of the archetypes after introducing green roofs on potential buildings. We observe from Figure 5.10(d) that the net energy budget (φ_{net}) reduces after roof greening in all the archetypes, indicating a lower energy entering the buildings. Lower (φ_{net} is due to the latent heat flux (φ_{lat}) (5.10(b)) introduced by the evapotranspiration of green roofs and a significant reduction in sensible heat flux (φ_{sens}) (5.10(a)), along with a slight decrease in φ_{rad} (Figure 5.10(c)). The φ_{sens} is proportional to the difference between the T_{se} and T_{air}. With the introduction of green roofs T_{se} is reduced which in turn affects the φ_{sens} and results in lower T_{air}. This shows that adding green roofs reduces both net energy entering the buildings and energy transferred to the air in the urban area.

Comparing the archetypes, we observe the most significant change in terms of φ_{net} for the compact mid-rise archetype (H) with a large building of maximum flat roof area i.e. with maximum greening potential (Figure 5.5). This is followed by archetypes A, B, I, D, C, E, G and F. The variation is also similar in the case of $\Delta\varphi_{rad}$, $\Delta\varphi_{sens}$, and $\Delta\varphi_{lat}$. We observe that the densely packed compact archetypes A and B and the large low-rise archetype with impervious open space (I) have comparable $\Delta\varphi_{net}$. Similarly, compact low-rise archetypes C and D have lower $\Delta\varphi_{net}$ compared to the compact and impervious archetypes (A, B and I) and have comparable values of $\Delta\varphi_{net}$. In archetypes with green spaces (C, D, E, F, and G), the $\Delta\varphi_{net}$ is considerably lower than other archetypes as these archetypes have green spaces in addition to green roofs, which already contribute to the $\Delta\varphi_{net}$ in these archetypes.

Overall, the net energy reduces for all the archetypes in general after introducing green roofs, but the reduction is lower in archetypes which already have the presence

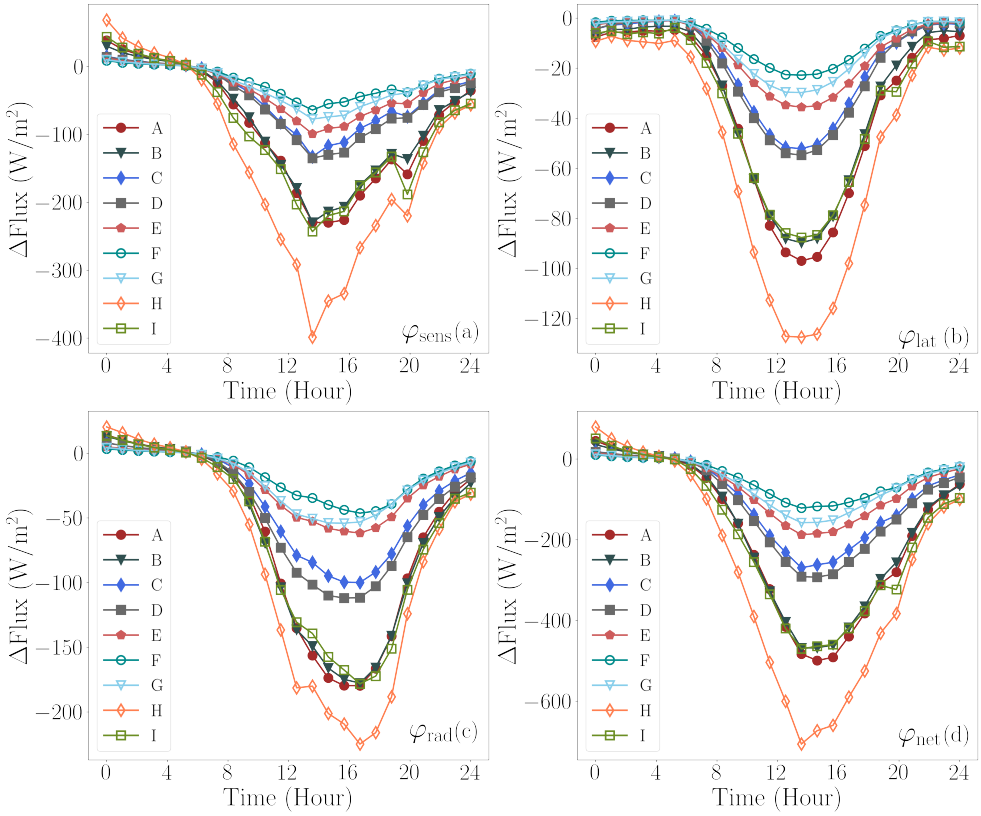

Figure 5.10: Changes in fluxes observed after adding green roofs to archetypes (a)Sensible heat flux (b)Latent heat flux (c)Radiative flux (d)Net energy budget

of other green spaces. But predominantly, the area of roof greening influences the change in net radiation flux.

Impact of realistic roof greening on Archetypes

Figure 5.11 demonstrates the ΔT_{se} (Figure 5.11 (a)) and ΔT_{air} (Figure 5.11 (b)) for 24 hours on an extreme heatwave day after adding green roofs to the existing flat roofs in the archetypes. We observe that the reduction in temperatures also follows a typical diurnal cycle with maximum reduction in the middle of the day during the heatwave with little or no reduction in temperature in the night. Furthermore, the results show a distinct difference in temperature reduction between different urban archetypes indicating the importance morphology in the roof greening analysis.

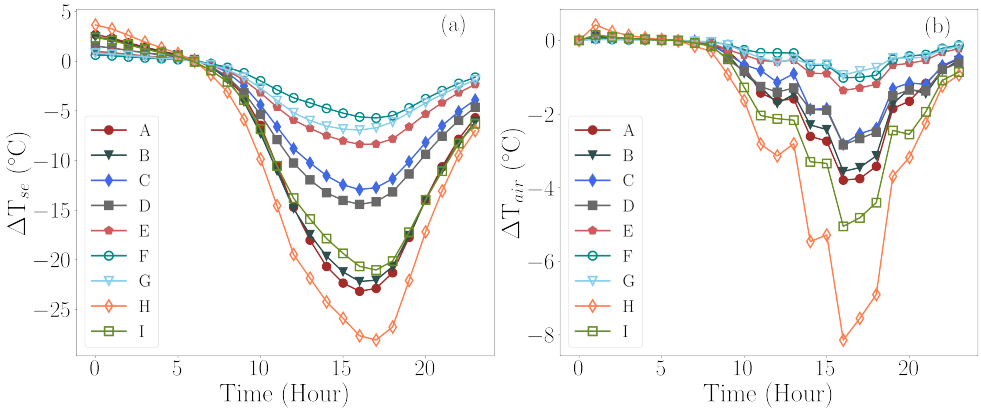

Figure 5.11: Diurnal variation of change in temperatures observed after adding green roofs to the archetypes (a) Surface temperature (b)Air temperature

It is worth noting here that, ΔT_{se} has a smooth variation in figure 5.11 (a) because it is dominantly influenced by the radiation than by turbulence. However, ΔT_{air} is influenced more by the near-surface turbulence modelling which has nonlinear and complex effect compared to the ΔT_{se} calculation with the radiation model of Solene-microclimat. Therefore, a smooth variation in ΔT_{air} is not possible, as it directly depends on resolving near surface turbulence.

Reduction in surface temperature:

Delving into the reduction in surface temperature (ΔT_{se}) for all the horizontal surfaces in archetypes during the heatwave (values averaged from 12:00 to 18:00), the ΔT_{se} for all surfaces ranges from 5°C to 28°C for all the archetypes. The reduction we observe here is coherent with other studies in similar temperate zones [320–322]. Maximum ΔT_{se} occurs at the roof level ranging from 14°C to 43°C (Figure 5.12 (b)). However, the ΔT_{se} at ground level is lesser than roof level and ranges from 0.2°C to 1.4°C (Figure 5.12 (c)). Figure 5.13 shows the spatial variation in ΔT_{se} in all archetypes, which shows that ΔT_{se} is generally higher at roof level. This suggests that green roofs, in general, have a lesser impact at ground level T_{se}, which is logical.

Comparing the ΔT_{se} of the archetypes, from figure 5.14 (a), we observe that the ΔT_{se} ranges from 0-50°C for compact/semi-compact high-rise/mid-rise archetypes (A and B) and large low-rise archetypes (H and I). we observe that the compact archetype with a large building (area-wise) (H) has the highest ΔT_{se} for all surfaces because the roof of larger building is greened (Figure 5.6). Similar archetypes which

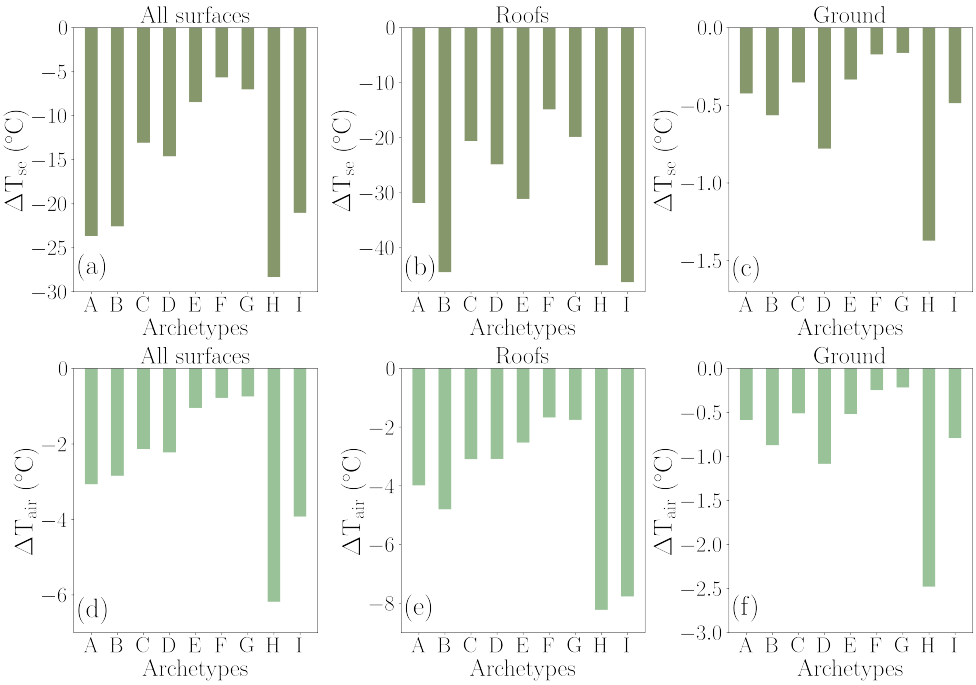

Figure 5.12: Average difference in temperatures during mid-day (12:00-18:00) for ((a) T_{se}-all surfaces (b) T_{se}-roof level (c) T_{se}-Ground (d) T_{air}-all surfaces (e) T_{air}-Roof level (f) T_{air}-ground level

are compact and semi-compact with no green space like A, B and I have lower ΔT_{se} compared to archetype H with similar ΔT_{se} values. The differences in ΔT_{se} for these archetypes occur at roof level, where compact high-rise archetype (A) has lower ΔT_{se} compared to semi-compact mid-rise archetype (B). This is because of the lower percentage of roof greening in archetype A. Apart from this, large low-rise archetype I has comparable ΔT_{se} with semi-compact mid-rise archetype B.

Low-rise archetypes like D, C, E, G and F have lower ΔT_{se} compared to the compact and impervious archetypes (H, A, B, and I). ΔT_{se} for the compact low-rise archetypes (C and D) ranges mostly from 0-30°C (Figure 5.14(a)). Compact mid-rise/low-rise archetype (D) has a higher ΔT_{se} than compact low-rise archetype (C) as the greened roof in archetype D is large in size and also low-rise. Open low-rise archetypes like E, G and F have comparable ΔT_{se} but the differences in ΔT_{se} are stark at roof and ground level. This can also be seen in the figure 5.13 which shows the spatial variation of ΔT_{se}. Although the built-up percentage is the lowest in elongated

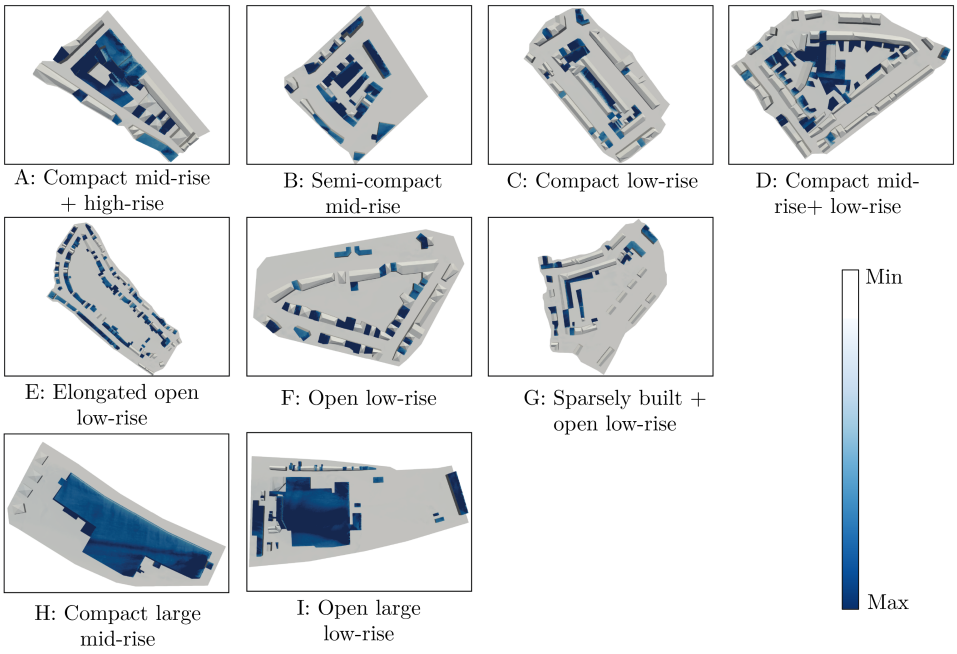

Figure 5.13: Spatial variation of ΔT_{se} in each archetype

open low-rise archetype (E), it has higher ΔT_{se} because of higher percentage of realistic roof greening in the archetype (Figure 5.5). Largely, the ΔT_{se} depends upon the percentage of potential roof greening in archetypes.

Reduction in air temperature:

The reduction in air temperature (ΔT_{air}) for all horizontal surfaces in archetypes ranges from 1°C to 6°C (Figure 5.12 (d)). At roof level, the ΔT_{air} ranges from 1.5°C to 8°C (Figure 5.12 (b)), whereas it ranges from 0.2°C to 2.4°C at ground level (Figure 5.12 (c)). The results of T_{air} at ground level are in the range observed in previous studies [278, 321]. Except, for the large mid-rise archetype (H), where the building with green roof is 10 m tall. Here, the difference in Tair is 1.3 °C due to a lower height [323, 324]. In terms of ΔT_{air} also, green roofs impact is lesser on ground as compared to roofs. Figure 5.15 indicating the spatial variation of ΔT_{air} that confirms this. However, the impact on ground level in terms of T_{air} is higher than T_{se} because of the vertical turbulent mixing of colder air from above after adding green roofs, especially in compact high-rise (A), semi-compact high-rise(B) and compact low-rise

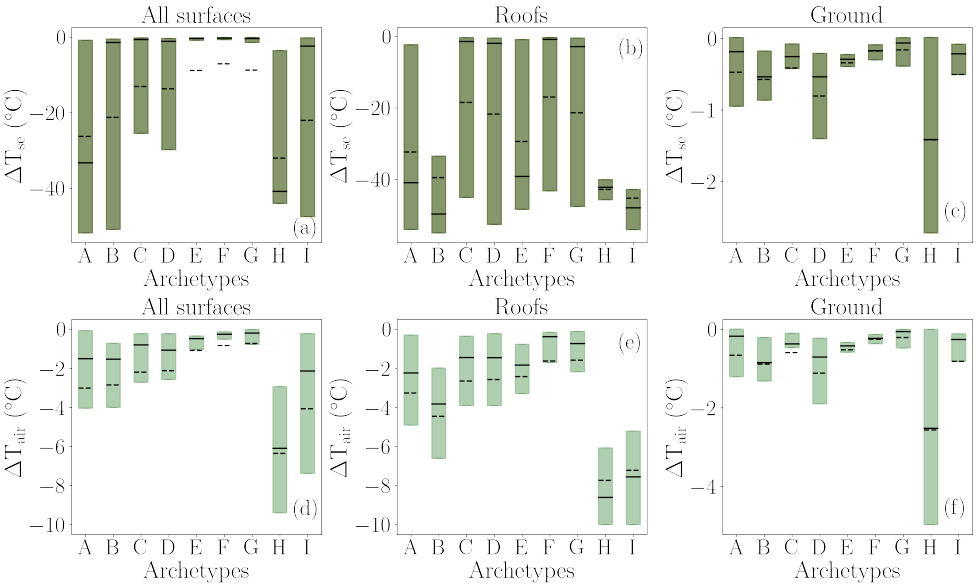

Figure 5.14: Variation in temperatures averaged during mid-day (12:00-18:00) for (a) T_{se}-all surfaces (b) T_{se}-roof level (c) T_{se}-Ground (d) T_{air}-all surfaces (e) T_{air}-Roof level (f) T_{air}-ground level (Note: Variation only shows the values within interquartile range (25th percentile to 75th percentile), dotted line represents the average and solid line represents the median value)

archetypes (D) and large low-rise archetypes (H and I).

Comparing the ΔT_{air} of archetypes, we observe that large compact mid-rise archetype (H) has the highest ΔT_{air} at all levels with 4-9°C variation in ΔT_{air} within the archetype (Figure 5.13(d)). Similar archetype with large building, large low-rise archetype (I) has a significant ΔT_{air}, which is 2°C less than archetype H (Figure 5.12 (a)). The ΔT_{air} of this archetype is lesser than archetype H because the ΔT_{air} values in this archetype vary from 0-8°C, with almost 50% grids having ΔT_{air} less than 2°C (Figure 5.14(d)). These two archetypes with a large mid-rise/low-rise building have higher ΔT_{air} due to the significant greening owing to the large building with flat roof. However, it is important to note that large low-rise archetype I has a lower ΔT_{air} at ground level as compared to large compact mid-rise archetype H. This is because of the large impervious ground area in archetype I, which contributes to heating.

Compact (A) and semi-compact (B) high-rise archetypes have comparable ΔT_{air}, which is less than the archetypes with large buildings (H and I), with a variation of 0.5 to 4.5°C within the archetype (Figure 5.14(d)). Subsequent archetypes in terms

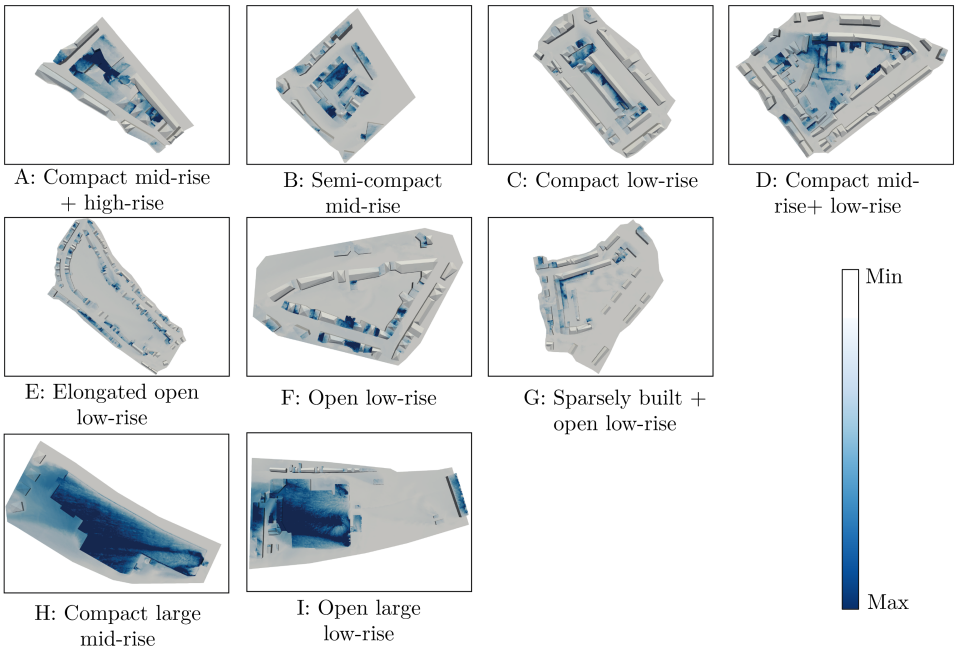

Figure 5.15: Spatial variation of ΔT_{air} in each archetype

of ΔT_{air} are the compact mid-rise/low-rise archetypes (D and C), with a variation of 0 – 3°C (Figure 5.14(d)). For the open low-rise archetypes with small sized buildings (area-wise) (E, F and G), the ΔT_{air} remains comparable. Similar to ΔT_{se}, the ΔT_{air} also mainly varies based on the percentage of potential roof greening in the archetypes except for elongated open low-rise archetype E. This is because, archetype E has existing green space and the existing Tair of the base scenario of this archetype is low. Apart from this, it is important to note that compact low-rise archetype (D) and large compact mid-rise archetype (H) have ΔT_{air} which is greater than 1°C. This is because of the large low-rise building in the archetype which is greened.

Summarising, based on the realistic green roof potential, the highest ΔT_{se} and ΔT_{air} are observed in the most compact high-rise/mid-rise archetypes (H, I, A, and B). The impact of green roofs on other low-rise archetypes (C, D, E, F, and G), which have green spaces other than green roofs, is lower. Moreover, only two archetypes (D and H) show greater than 1°C reduction in T_{air} at ground level, indicating the influence of large low-rise buildings in these archetypes. In this study, we focus on average values of ΔT_{se} and ΔT_{air}. However, spatial variation in ΔT_{se} and ΔT_{air} exists due to the difference in convective coefficient over the surfaces based on local turbulence

and velocities. Hence, there are areas with higher and lower ΔT_{se} or ΔT_{air} in an archetype, which also should be considered. For instance, some values have ΔT_{air} at ground level greater than the average (Figure 5.14(f)).

Apart from this, it is important to note that the ΔT_{se} and ΔT_{air} are the highest on the roofs where green roofs are introduced. Additionally, the ΔT_{se} and ΔT_{air} also depend on the position of the roof and morphology of built-up surrounding the roof as it varies in different places (Figure 5.15). Furthermore, the ΔT_{se} and ΔT_{air} largely vary based on the percentage of roof greening in the archetype. Therefore, to understand the importance of morphological archetypes in mitigating the heat, we formulate a cooling index, which is discussed in the next section.

Impact of Archetypes on cooling index

The clustering of the urban blocks into archetypes was done based on the exhaustive list of urban morphological parameters [289]. However, green roof potential was not one of the parameters. So, even though realistic, the percentage of the green roof area in each archetype influences their impact on ΔT_{se} and ΔT_{air}. This makes the comparison of different archetypes difficult as they have different percentage of roof greening. Therefore, to compare the impact of greening in the archetypes, we define cooling index (CI) values of archetypes to normalise the influence of percentage of green roof area on T_{se} and T_{air}. A high CI indicates a higher temperature reduction per percentage of roof greening, a lower CI indicates that green roofs are less effective in temperature reduction. We also note here that CI can be used to make a first estimation of the potential effects of greening roofs at the city scale by multiplying percentage of green roofs with CI. Still the non-linear nature of the physical processes should be taken into consideration before any attempt to generalise our results.

In Figure 5.16 we present the normalised temperature reduction due to roof greening ΔT_{se} and ΔT_{air} per percentage of roof greening. In the previous section, we observed that the compact large mid-rise archetype with a large building area with maximum greening potential (H) showed maximum temperature reduction. However, when normalised, the densely packed compact high-rise archetype A has the highest ΔT_{se} per percentage of green roof area (CI_{se}) for all surfaces. This is evidently due to the maximum building density in this archetype with a higher possibility of roof greening. Since these archetypes are also one of the hottest archetypes (see section 3.2), greening these archetypes would be useful in reducing the heat stress.

Compact archetypes A, D, C and H have percentages of built-up greater than 60% (Figure 5.4 and 5.17). After highly compact high-rise archetype A, archetypes C, D and H have comparable CI_{se} for all surfaces. However, compact mid/low-rise archetype D has the highest CI_{se} at ground level (Figure 5.16(c), followed by archetype H. This is

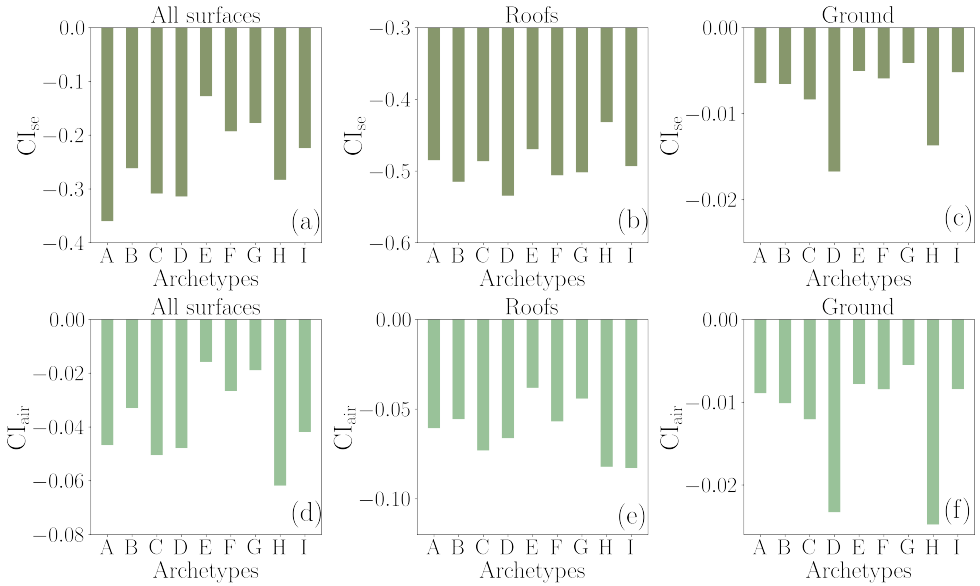

Figure 5.16: Average cooling index (CI) during mid-day (12:00-18:00) for (a) T_{se}-all surfaces (b) T_{se}-roof level (c) T_{se}-Ground (d) T_{air}-all surfaces (e) T_{air}-Roof level (f) T_{air}-ground level

primarily due to the lower height of the buildings with larger building areas (Figure 5.3). Semi-compact mid-rise archetype B is the subsequent archetype in terms of CI_{se} of all surfaces, followed by large low-rise archetype I. The CI_{se} in archetype B is higher than archetype I because of the larger built-up percentage in the archetype. Archetypes E, F and G are open low-rise, and the CI_{se} decreases with a decrease in built-up percentage (Figure 5.17).

The variation of CI_{air} is not similar to the CI_{se}. Large compact mid-rise archetype (H) has the highest CI_{air} due to the large low-rise buildings with green roof in the archetype. Other compact low-rise archetypes (D and C), high-rise archetype (A) and large low-rise archetype (I) have comparable CI_{air}. However, these archetypes have variation in CI_{air} at ground level. Compact low-rise archetype D has almost similar CI_{air} as compact mid-rise archetype H at ground level. Moreover, low-rise archetype C although is less than archetype D, has higher CI_{air} at ground level compared to archetypes A and I. Compact high-rise archetype A and large low-rise archetype I has similar CI_{air} at ground level. Therefore, we observe that mid-rise/low-rise archetypes like H, D and C have a better influence on ΔT_{air} and CI_{air} compared to others. Large low-rise archetype I is an exception to this because of the existing impervious open

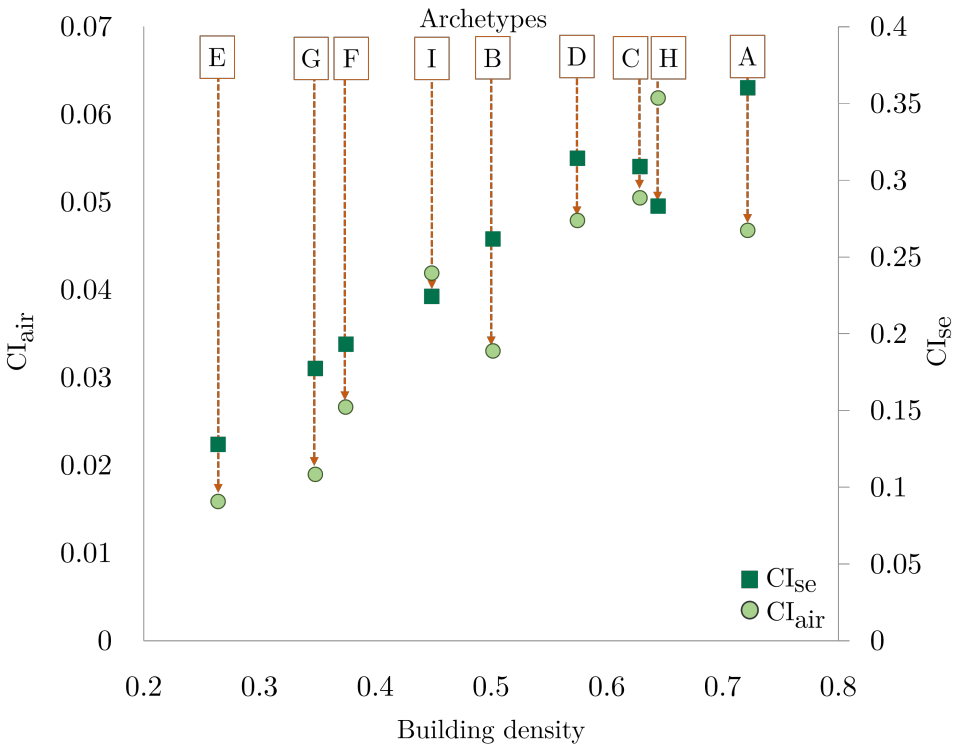

Figure 5.17: Correlation between building density and cooling intensity (CI) for archetypes (A-Compact mid-rise+high-rise, B-Semi-compact mid-rise, C-Compact low-rise, D-Compact mid-rise+low-rise, E-Elongated open low-rise, F-Open low-rise, H-Compact large mid-rise, I-Open low-rise)

surface in the archetype which contributes to the heat. Greening the open impervious area in this archetype could be beneficial but is out of scope of this paper.

Semi-compact archetype (B) and open low-rise archetypes (F, G, and E) are the subsequent archetypes with lower CI_{air} compared to compact and large low-rise archetypes. The CI_{air} value reduces with reduction in built-up area in these archetypes. Although semi-compact high/mid-rise archetype (B) has taller buildings and no green open space, roof greening in this archetype is not as effective for reducing the air temperature as it is for surface temperature. Open low-rise archetypes F, G and E have a limited impact on CI_{air} overall and at ground level, but there is a better impact at roof level in these archetypes.

Altogether, we observe that the CI values for archetypes are different from one

another either at the roof or ground level, indicating an influence of morphologies on CI in terms of surface and air temperature. Additionally, introducing green roofs in compact archetypes with taller buildings can be useful for mitigating surface temperatures. However, the impact of green roofs on air temperature in these archetypes could be limited at ground level. The impact of green roofs on air temperature is significant in terms of compact low-rise archetypes (H, D and C). Additionally, it is important to note that higher impact in terms of air temperature is observed at roof level for every archetype with variations depending upon the morphological characteristics.

5.4 Summary and Discussion

In this paper, we analyse the impact of green roofs on surface and near-surface air temperatures during a heatwave day in realistic urban morphological archetypes. Firstly, we obtain nine realistic morphological archetypes unique to the city of Liège, Belgium based on Joshi et al. (2022). According to LCZ classification in Europe, Liège city has five LCZ classes. However, as noted by Steward and Oke (2012) LCZs are a broad classification, where sub-classes within each LCZs are possible for different cities. Therefore, in this study, we use the method of Joshi et al. (2022) which provides the archetypes more specific to the city as they are obtained using a data-driven approach. We carry out an exploratory study of the impact of green roofs on the surface and air temperatures using the Solene-microclimat model which is a thermo-radiative model code coupled with CFD.

Based on the results, we observe that the archetypes obtained from the data-driven clustering approach are very distinct in terms of surface and air temperature. The differences between the extremely different archetypes like open low-rise and compact high-rise/mid-rise are higher, however, the differences between archetypes like compact high-rise and compact low-rise are reduced but still present, which is similar to the LCZ description in Stewart and Oke (2010). These nine archetypes capture the microclimatic situation of Liège appropriately. As the microclimate of the archetypes is distinct, we hypothesised that the relative impact of green roofs on surface and air temperatures in them, could also be different.

After introducing green roofs to the potential buildings in these archetypes, our results show that green roofs influence the surface energy balance at the roof level, resulting in lower roof temperatures and lower air temperatures near the roof. This indicates that green roofs can also be useful for reducing building energy requirement, especially cooling loads in commercial/office buildings Furthermore, we observe a significant drop in surface temperature for all archetypes with realistic roof green-

ing, with the lowest reduction for elongated open low-rise (archetype E) and highest reduction for compact large mid-rise (archetype H). The higher value is observed for the compact archetypes suggesting that green roofs are an effective solution for reducing the surface temperatures especially in the dense built-up areas of the city centre where deploying trees or ground green spaces is challenging. The impact of realistic roof greening on air temperature is significant for compact archetypes and large low-rise archetypes. It should also be noted that the impact of green roofs at ground level is significant for large compact mid-rise archetype (H) and compact mid-rise and low-rise archetype (D). This suggests that green roofs are most effective in terms of reducing the air temperature for archetypes with low-rise buildings with a larger area which can have green roofs. For compact high-rise or mid-rise archetypes, the reduction in air temperature is primarily at roof level.

As each archetype has a different percentage of realistic roof greening, it influences the reduction in surface or air temperature. Thus, to aid a logical comparison between archetypes and to analyse the influence of archetypes on reduction in air and surface temperature after roof greening, we formulated a cooling index (CI). CI is the reduction of air or surface temperature per percentage of greening in the archetype. We observe that the CI reduces with a decrease in built-up percentage in the archetype in terms of surface temperature (Figure 5.17). However, in terms of air temperature, the other morphological differences in archetypes also contribute to the CI. For instance, low-rise archetypes witness a reduction in Tair higher than the one of high-rise archetypes. Moreover, larger building area also influences the CI values. Additionally, availability of open space, which is impervious results in heating of the archetype, thus reducing the effects of green roofs.

Although CI has enabled a better comparison of archetypes in terms of reduction in surface and air temperature, it is important to acknowledge the existing flat roofs in an archetype. For instance, low-rise archetypes (C, D) are largely residential, with more buildings having sloped roofs. Therefore, although placing green roofs on low-rise buildings is favourable, green roofs are not an effective option in residential archetypes to regulate the local microclimate. Large mid-rise/low-rise archetypes (H, I) are largely industrial or commercial archetype, and have higher CI in terms of both air and surface temperature. Moreover, while implementing green roofs on commercial or industrial building is easier, their installation on residential buildings would require government interventions (Claus and Rousseau, 2012; Mullen et al., 2013). Implementing green roofs in compact large mid-rise and large low-rise archetypes could be useful as there are a significant number of H- and I-type blocks in Liège city (Joshi et al., 2022). Apart from this, archetypes like compact high-rise/mid-rise and semi-compact mid-rise which contribute to the UHI effect the most have higher

potential for green roofs. However, roof greening in these archetypes can only be effective to mitigate surface temperatures.

5.5 Conclusions

In this paper, we carry out an exploratory study of the role of roof greening on the local microclimate in Liège city using Solene-microclimat model. For the first time in the studies assessing UHI mitigation strategies, this paper analyses the impact of roof greening in all the realistic morphological archetypes in a city during a heatwave. We explore the impact of realistic roof greening by considering only the flat roofs suitable for roof greening. Additionally, we also discuss the impact of equal proportion of roof greening in each archetype based on a metric called as cooling index (CI).

Our main conclusions from this paper are:

- The archetypes obtained from a systematic data-driven approach by Joshi et al. (2022) for Liège city have distinctive microclimates.
- Because of the distinct morphologies and microclimates, the impact of roof greening on these archetypes is significantly different from one another.
- In compact high-rise and semi-compact high-rise archetypes, the green roofs can reduce surface temperatures effectively, whereas air temperature reduction from green roofs is limited.
- In compact low-rise archetypes, green roofs can be very useful in reducing surface and air temperatures, which is an important contribution as deploying trees and green areas in compact urban areas is not straightforward.
- Two low-rise residential archetypes have less percentage of flat roofs which can be greened which reduces the potential impact of roof greening.
- Compact large low-rise and large low-rise archetypes which are predominantly industrial or commercial can be usefully retrofitted with green roofs considering the large potential of roof greening and the effect of greening roofs on the surrounding of these blocks.

Proposed buildings can include roof greening if the buildings are large and low-rise. Moreover, the city master plan can integrate roof greening in the expansion of the city, if the urban blocks are dense and predominantly mid-rise or low-rise, as often observed in contemporary urban extensions. Additionally, as the obtained archetypes are distinct, future studies can assess other UHI mitigation strategies using this approach.

Apart from this, Solene-microclimat software enabled us to simulate the sloped

roofs, which is rarely found in the current literature. As the software can be modified by the user and is not a black box software, we could make use of high-performance computing (HPC) and make this analysis possible for 18 scenarios. Further studies can improve the results by increasing the mesh resolution to 1m. Additionally, Solene-microclimat uses RANS model which is good enough to obtain average air flows around buildings but it does not completely resolve turbulence. For higher fidelity, further studies can explore large eddy simulation (LES) models.

Apart from this, in this study, we assign evapotranspiration constant and albedo for green roofs considering the green roof in this study, to be extensive type. Further studies can explore different types of green roofs and experiment with various evapotranspiration constants and albedos by doing a sensitivity analysis of relative weights of different parameters. Moreover, future studies can incorporate hydrological models to model green roofs to improve the analysis.

Our novel approach of analysing influence of roof greening on all urban morphological archetypes holistically provides evidence on how realistic morphologies can influence green roof's role in regulating local microclimate during heatwave. This paper broadly provides an insight into the interplay between urban morphology, realistic roof greening potential, and UHI effect.

5.6 Key contributions

- Microclimate within the nine archetypes is distinct, leading to variations in the effectiveness of green roofs across these archetypes.
- Green roofs effectively reduce surface temperatures in compact high-rise and semi-compact high-rise archetypes, but their impact on air temperatures is limited.
- In compact low-rise archetypes, green roofs play a vital role in lowering both surface and air temperatures, addressing the challenge of deploying trees and green spaces in compact urban areas.
- Some low-rise residential archetypes, with a lower percentage of flat roofs suitable for greening, may experience a reduced potential impact of roof greening. Conversely, large low-rise archetypes, particularly industrial or commercial areas, offer substantial potential for green roof retrofitting and can positively influence their surroundings.
- This study advances the WRF-based analysis of green roofs' impact on UHI in various LCZs by offering an implementable scale for planners and higher resolution.
- Unlike the LCZs used in the WRF-based analysis, the archetype presents de-

tailed morphologies, providing better-captured variations in microclimate.

- Study provides an insight into the interplay between urban morphology, realistic roof greening and UHI effect.

6

Predicting Urban Heat Island Mitigation with Random Forest Regression in Belgian Cities. [1]

An abundance of impervious surfaces like building roofs in densely populated cities make green roofs a suitable solution for urban heat island (UHI) mitigation. Therefore, we employ random forest (RF) regression to predict the impact of green roofs on the surface UHI (SUHI) in Liege, Belgium. While there have been several studies identifying the impact of green roofs on UHI, fewer studies utilize a remote-sensing-based approach to measure impact on Land Surface Temperatures (LST) that are used to estimate SUHI. Moreover, the RF algorithm, can provide useful insights. In this study, we use LST obtained from Landsat-8 imagery and relate it to 2D and 3D morphological parameters that influence LST and UHI effects. Additionally, we utilise parameters that influence wind (e.g., frontal area index). We simulate the green roofs by assigning suitable values of normalised difference-vegetation index and built-up index to the buildings with flat roofs. Results suggest that green roofs decrease the average LST.

[1] Published as: **M.Y.Joshi**, D.G.Aliaga and J.Teller, *Predicting Urban Heat Island Mitigation with Random Forest Regression In: Goodspeed, R., Sengupta, R., Kyttä, M., Pettit, C. (eds) Intelligence for Future Cities. CUPUM 2023. The Urban Book Series. Springer, Cham.* doi:10.1007/978-3-031-31746-0_16

6.1 Introduction

Unprecedented urban growth has led to increased building densities resulting in limited green spaces in cities, exacerbating the impacts of climate change [141, 325]. Consequently, urban areas are experiencing higher temperatures as compared to rural regions, which is known as the urban heat island (UHI) effect [162, 200]. Negative impacts of UHI effect include increased energy consumption, carbon emissions, decreased comfort levels, and global warming [326]. Thus, to circumvent these impacts, identifying solutions to mitigate the UHI effect is crucial.

The UHI phenomenon is primarily caused by a high density of built-up areas, as well as low albedo of urban surfaces, resulting in absorption of excess solar radiation [295]. In this scenario, green roofs are highly relevant owing to the abundance of building rooftops made of impervious surfaces in cities [52, 327]. Green roofs prevent the absorption of short-wave radiation and act as thermal insulators [295]. Green roofs also prevent heat from entering the structures in summer, reducing energy consumption [328]. Moreover, green roofs also increase evapotranspiration and natural ventilation within built-up areas [153]. Along with this, green roofs also have other benefits in terms of biodiversity and runoff retention. Thus, considering their multifold benefits, green roofs are a suitable strategy for UHI mitigation [329].

Researchers have analyzed green roofs and their impact using numerous methods. Most of the studies use numerical modelling, simulations and statistical analysis to analyze greening scenarios [330]. However, micro-scale urban canopy models (UCM) and microclimate simulation models like ENVImet cannot be employed for entire city due to computational demands [331, 332]. While mesoscale models like weather research and forecasting (WRF) coupled with UCM aid in conducting research at a regional scale, running these models at high resolution requires significant computational resources. Therefore, most of the WRF studies are carried out at a resolution of 1 km (Yang and Bou-Zeid 2019; Wang et al. 2022). Moreover, analyzing and processing these models are generally challenging for most urban planners [332]. Therefore, remote sensing approach can be advantageous as finer resolution datasets are increasingly available. Furthermore, the analysis using remote sensing can be straightforward with existing geographic information system (GIS) softwares like QGIS and ArcGIS for urban practitioners [330, 332].In this study, we employ a remote sensing-based approach for analyzing the impact of green roofs on UHI.

Traditionally, UHI effect is classified into surface and air UHI, referring to the surface and air temperature respectively [201, 202, 333]. The impact of Green roofs on air temperature is debatable, however, their impact on surface temperature is significant [38, 327]. Thus, we focus mainly on the impact of green roofs on surface

temperature. This estimate, referred to as Land Surface Temperature (LST) is obtained using satellite images. UHI effect is the outcome of dynamic interactions between the macroclimate and urban morphology [205]. Thus, along with greening, several other morphological parameters influence LST. The relationship of LST with several morphological parameters has been investigated using satellite data [334]. For example, the Normalised difference vegetation index (NDVI) has a strong to moderate negative correlation with LST, whereas normalized difference built-up index (NDBI) has a positive correlation [335, 336]. Parameters such as building densities also influence LST. 3D data was also strongly influencing LST in some studies [251]. Moreover, detailed 3D parameters such as frontal area index (FAI) and sky view factor (SVF), can be now computed in a raster format for facilitating a better analysis [337]. Subsequently, 3D parameters can represent the contribution of shadows, solar radiation and orientation.

The relationship between LST and related parameters have been previously analyzed using ordinary least square (OLS) regression and graphically weighted regression [338]. Recent studies also have used machine learning in predicting changes in LST [339, 340]. For example, Asadi et al. [337] use Artificial neural network (ANN) to predict changes in LST after implementing green roofs in Austin, Texas. Their study showed that LST decreased by 1.96 degree Celsius on an average after greening 3.2% of the roofs. The study used 2D and 3D urban morphological parameters in their analysis. Although the parameters are comprehensive for the task, parameters influencing wind flow, such as frontal area index (FAI) could have enhanced the analysis [243]. Moreover, random forest (RF) regression has proven to be robust in predicting several scenarios [339, 340]. Along with this, RF regression prediction is regarded as being unaffected by the multicollinearity and distribution of data [341, 342]. Thus, in this study, we explore the performance of RF regression in predicting changes in LST caused by green roofs.

6.2 Methodology

Figure 6.1 represents the broad methodology used in this study.

6.2.1 Study area and dataset

In this study, we analyze the Brussels capital region and the city of Liege in Belgium. Brussels is the capital of Belgium and has an area of 161.4 km^2 with around 1,222,637 inhabitants [343]. As it is the national capital, it is highly dense and compact with limited space for developing green infrastructure within the city. Liege, on the other

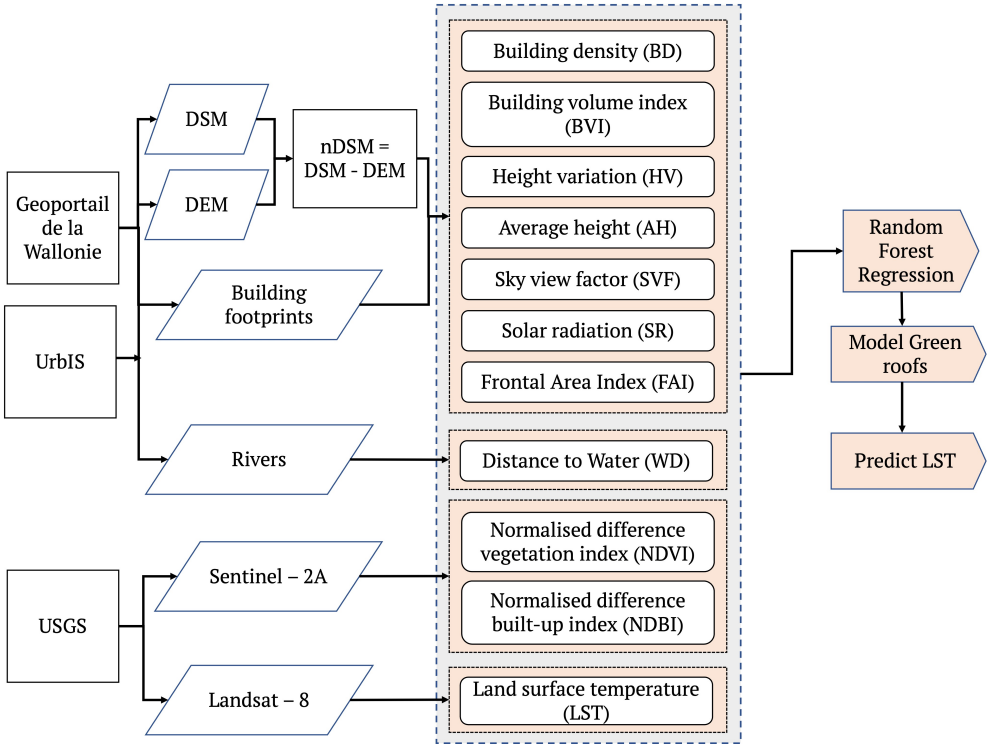

Figure 6.1: Methodology

hand, is located in the Wallonia region of Belgium. The city is the third largest city in terms of population in the country, with an area of 69 km^2 and 196,296 inhabitants. The city is highly compact with significant building density in the center and open residential areas in the outskirts [289]. Thus, roof greening is a suitable UHI mitigation strategy for both cities. We use four datasets mainly for computing the parameters influencing LST. Table 6.1 presents the dataset used and respective sources for Liege and Brussels. We processed all the rasters to 30 m resolution as it is the resolution of LST obtained from Landsat-8.

6.2.2 Parameters influencing LST

Building density

To obtain building density (BD), we first transform the building footprints to a raster with 1m resolution. Thereafter, we aggregate the raster by summing the building

Table 6.1: Datasets used for analysis with their respective sources for Liege and Brussels

Datasets	Liege	Brussels
Building footprints	PICC (Projet Informatique de Cartographie Continue) dataset, with an accuracy of less than 25 cm	the footprints are obtained from UrbIS online (data platform for Brussels capital region)
Building heights	digital surface model (DSM) and the digital elevation model (DEM)	3D model of Brussels from UrbIS
LST	Landsat-8 level 1 image captured on July 18, 2021	
NDVI and NDBI	Sentinel-2 multispectral image obtained on 21st July 2021.	

pixels to a raster with 30 m resolution, representing the building density. Thus, building density is computed as:

$$BD = \sum_{i=1}^{n} a_i, \tag{6.1}$$

where a_i is the 1 by 1 m pixel covered by building and n is the total number of 1 m pixels in 30 m pixel.

Building volume index

Building volume index (BVI) is the building volume in a pixel and it is calculated as follows:

$$BVI = \sum_{i=1}^{n} a_i \times h_i \tag{6.2}$$

where a_i is the 1 m pixel covered by building, hi is the height of the building in the 1 m pixel and n is the total number of 1 m pixels in 30 m pixel.

Sky view factor

Sky view factor (SVF) is the ratio of proportion of sky visible from the ground at a given position, to the proportion of sky not obstructed by the surrounding built-up [204]. We calculate it with the Relief Visualisation Toolbox of QGIS 3 [248, 249].

We use the DSM and the building footprint dataset to generate the raster with

building height information. We consider the open spaces and roads along with the bottom of the buildings at 0 m. We consider a search radius of 100 m and the number of directions as 16 for SVF calculation [246]. We compute SVF at a resolution of 1m and later resample it at 30 m resolution.

Solar radiation

The amount of solar radiation (SR) received by the surfaces in the city influences the LST [337, 344]. Therefore, we compute the SR using the solar radiation tool in ArcGIS Pro 2.9.1. This represents the global radiation, which is the total incoming solar radiation and is calculated for each pixel of DSM. The value of SR was calculated on July 18, 2021 to match the date of acquisition for Landsat-8 image.

Normalized Difference Vegetation Index (NDVI)

NDVI is used to detect bare soil and vegetation [254, 255]. In a way, it represents the pervious regions in the city. We calculate the NDVI using the Sentinel-2A satellite imagery captured on July 21, 2021, from the United States geological survey (USGS) (https://earthexplorer.usgs.gov/). We chose the image on this date as July and August experience higher temperatures. Moreover, among the images available for this time frame, the selected image had the lowest and most acceptable cloud coverage of less than one per cent. Sentinel-2A image is of 10 m spatial resolution and thus the obtained NDVI obtained is also at 10m. We calculate the NDVI using the near infrared (NIR) and red (R) bands of the image as follows:

$$NDVI = \frac{NIR - R}{NIR + R} \tag{6.3}$$

Normalized Difference Built-Up Index (NDBI)

Zha et al. [251] defined the NDBI to determine urban and built-up areas. It is used to express the intensity of urbanization [252]. Although, we use building density, we consider NDBI as one of the parameters as it will helps highlight other urban areas that are not buildings. Moreover, it also explains the development intensity by indicating the impervious surfaces. We calculate NDBI using the Sentinel-2A image used for obtaining NDVI. To compute NDBI, we need short wave infrared (SWIR) band, which has a resolution of 20 m and NIR with a resolution of 10 m. Therefore, the SWIR band was resampled to 10 m resolution for the calculation. NDBI is thus

calculated as follows:

$$NDBI = \frac{SWIR - NIR}{SWIR + NIR} \tag{6.4}$$

Frontal Area Index (FAI)

FAI influences the wind flow, thus influencing the UHI and LST. It is defined as the area of building walls facing the wind flow in a particular direction (Wong et al. 2010). We compute FAI using the methodology of H. Li et al. (2021) in this paper. The method involves rasterization of the building height and area and computing the FAI at 30 m resolution. The FAI is only calculated for northerly/easterly winds.

Height variation (HV)

Height Variation (HV) is the variation observed in building heights (1 m pixel) in 30 m pixel. For computing HV, we first transform, building heights to a 1 m raster. Then, we aggregate the raster to 30 m with standard deviation of heights in a 30 m pixel using geopandas package in python 3.

Average height (AH)

Similar to HV, we compute average height (AH) for the pixels by aggregating 1 m height pixels to 30 m, by averaging the heights of 1 m pixels.

Distance to water

Liege city is situated on the banks of river Meuse. The river divides the city into two parts. Similarly, Brussels has the river Senne that flows through the region. As water bodies have a significant impact on surface temperature [345], we consider this parameter in our analysis. We obtained the river shapefiles for Liege and Brussels from geoportail of Wallonia and UrBIS respectively. We calculate this parameter using Euclidean distance tool to the river shapefiles obtained from geoportail of Wallonia at 30 m resolution.

Land surface temperature (LST)

We calculate the LST using the Landsat-8 level 1 image captured on 18th July 2021. We chose the image on this date since July and August experience higher temperatures. Moreover, the image on this date had the lowest and most acceptable cloud coverage

of less than one per cent. We use the thermal band 10 to compute the LST (in Kelvin (K)) using the following equations (USGS 2019):

$$L_\lambda = M_L Q_{cal} + A_L, \tag{6.5}$$

Where L_λ = TOA (Top of Atmosphere) spectral radiance (Watts/(m^2 * srad * μm)), M_L = Band-Specific multiplicative rescaling factor from the metadata, A_L = Band-specific additive rescaling factor from the metadata, Q_{cal} = Quantized and calibrated standard product pixel values (DN)

$$T = \frac{K_2}{lnln\left(\frac{K_1}{L_\lambda} + 1\right)} \tag{6.6}$$

Where T = TOA brightness temperature (K), K_1 = Band-specific thermal conversion constant from the metadata, K_2 = Band-specific thermal conversion constant from the metadata. We further convert the LST values to degrees Celsius (°C).

6.2.3 Data Processing

We first generate random points in ArcGIS Pro 2.9.1 over the Brussels capital region and Liege city with 100 m spacing between the points to avoid spatial autocorrelation. We consider 100 m as minimum distance as spatial variability of urban temperatures is around 100 m [258,346,347]. We then use the "extract values to point" tool, to extract values of all the parameters mentioned above to the randomly generated points. We obtain 7500 points in Brussels and 4000 points in Liege, giving us a total of 11,500 points to for training and testing the RF regression model.

6.2.4 RF regression

RF is a supervised machine-learning algorithm proposed by [97]. The RF regression algorithm combines a large set of regression trees, where the dataset is broken down into smaller subsets to predict a response variable by learning decision rules [98]. The trees are combined using bootstrap aggregation or bagging, such that each set is run independently, and the outputs are merged to achieve an accurate prediction [99].

The regression begins by selecting n samples of k random observations from a training dataset. Then, individual decision trees are built for each sample. These n trees are run parallellyin parallel, and separate outputs are generated. The mean of these outputs results in the final prediction. The random selection in RF regression prevents overfitting [348].

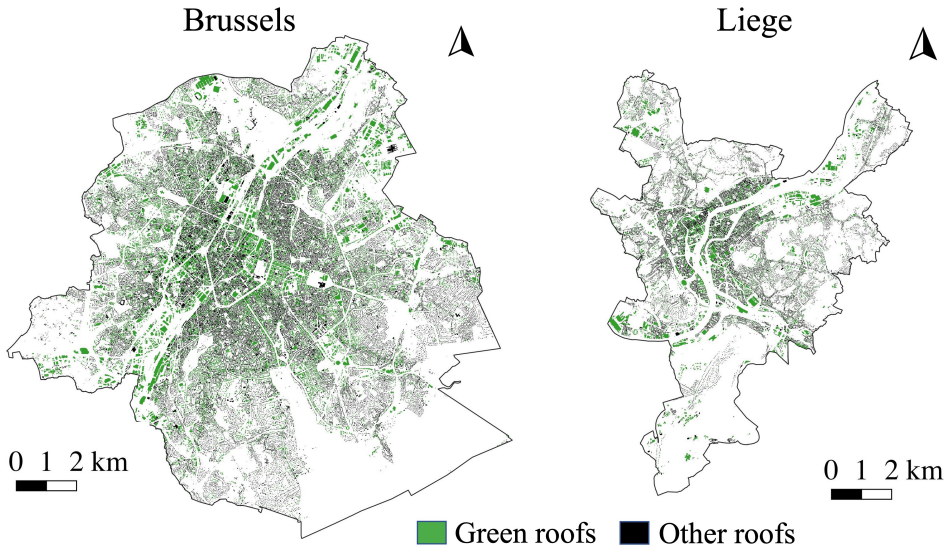

Figure 6.2: Potential roofs for greening in both the cities

In this study, RF regression is implemented in python through the scikit-learn package. The package includes several parameters that can be tuned for an improved performance. We focus on tuning the number of trees (ntree) and number of features randomly sampled at each split (mtry). RF regression is a supervised and straightforward method, which is fast and robust to the noise in the data [100, 101]. We train the RF regressor model using 80% of the data points and test it over the remaining 20% of the data points. We validate the RF regression model with k-fold cross-validation, with k as set at five. Additionally, we identify the suitable mtry and ntree based on the lowest value of RMSE (root mean squared error). We also analyse the R-squared value of the relation between observed and predicted LST for both cities to understand the goodness of fit.

6.2.5 Simulating green roofs

We simulate the green roofs similar to the method proposed by Asadi et al. [337]. Liege has around 20% of flat roofs as computed in the study by Joshi et al. [88]. For Brussels, we identify flat roofs using the 3D model of the region available at UrbIS online. As it will be unrealistic to simulate green roofs on all of these buildings, we consider buildings with areas larger than 100 m^2 to be suitable for greening in this

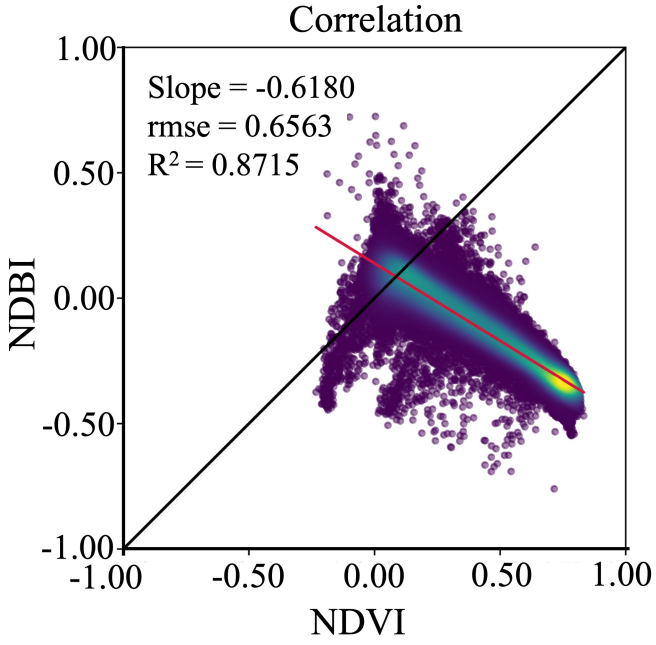

Figure 6.3: Correlation between NDVI and NDBI values

study. Figure 6.2 shows the potential roofs in Belgium Brussels and Liege. Around 92,333 roofs (out of 256484) in Brussels are flat, whereas 23,326 roofs (out of 136,170) are flat in Liege.

Green roofs are of mainly of two types: extensive and intensive green roofs. The third type of green roof is a green roof somewhere in between the two main types. Extensive green roofs have relatively thinner substrate vegetation compared to intensive ones. Intensive green roofs have a thick substrate layer and dense vegetation, such as rooftop gardens and agriculture [52]. We simulate green roofs by changing the value of NDVI and NDBI for the potential roofs in both cities.

The NDVI values for green surfaces vary from 0.3 to 1 depending upon the intensity of greening. However, for green roofs, NDVI values range from 0.3 to 0.8, considering the range from extensive to intensive green roofs. Further, changing NDBI values also becomes mandatory due to the change in NDVI. We change NDBI values according to the relationship derived between original NDVI and NDBI values obtained from Sentinel-2 for Brussels and Liege. Figure 6.3 represents this correlation.

The relation between NDBI and NDVI is significant, given that the R-squared

Table 6.2: Values of NDBI corresponding to NDVI values of green roofs

NDVI (x)	NDBI(y)
0.3	-0.054
0.4	-0.11
0.5	-0.17
0.6	-0.24
0.7	-0.30
0.8	-0.36

value is 0.87 and pearson correlation co-efficient is less than 0.05. Based on this relation, Table 6.2 provides the corresponding values of NDBI for each NDVI from 0.3 to 0.8.

Wherever there is a potential roof with 100 m^2, we convert the pixels to NDVI values indicated in the table. We do this by first resampling the 10 m NDVI to 1 m spatial resolution. Thereafter, we change the values of NDVI at the pixels corresponding to building footprints of potential roofs. Later, we aggregate the NDVI with green roofs to 30 m spatial resolution by calculating the average value. Similarly, we convert the NDBI values of potential green roofs to the values in Table 6.2 corresponding to the respective NDVI values. Thus, we generate predictions for six scenarios for six values of NDVI and NDBI in table 6.2. As only the roof is converted to a "green roof", we keep other building related parameters unchanged. We run the trained model on the newly built NDVI and NDBI along with other variables and predict changes in LST.

6.3 Results

6.3.1 Model results and accuracy

Figure 6.4 shows the results of RF hyperparameters (mtry and ntree). We did the optimization based on RMSE. Results indicate that RF hyperparameters affect prediction accuracy only by 0.02 °C. The optimal results are observed at ntree = 6000 and mtry = 3, with lowest RMSE (1.65 °C).

6.3.2 Variable importance at optimal ntree and mtry

Figure 6.5 shows feature importance in an optimized RF regression model. We observe that NDBI and NDVI are the most important parameters, followed by BVI, FAI, AH,

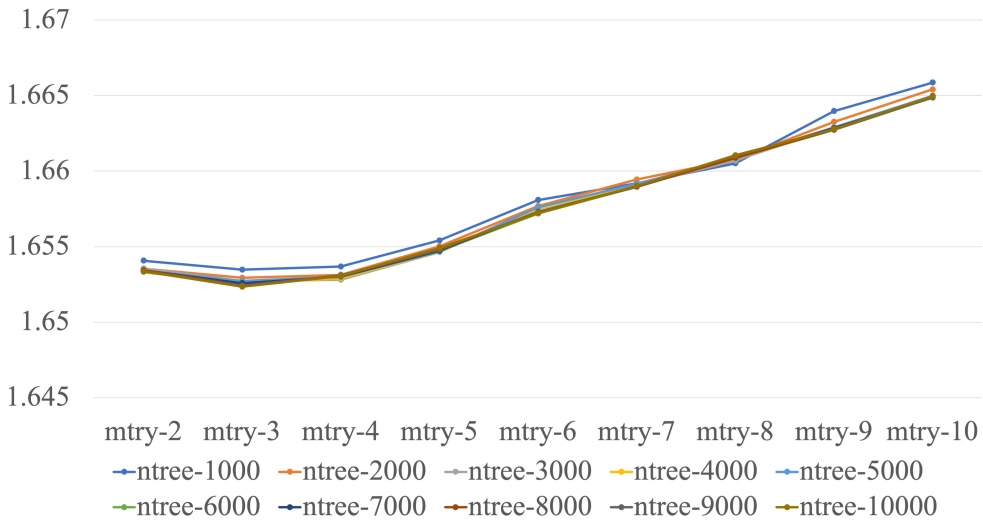

Figure 6.4: Optimisation of hyperparameters ntree and mtry

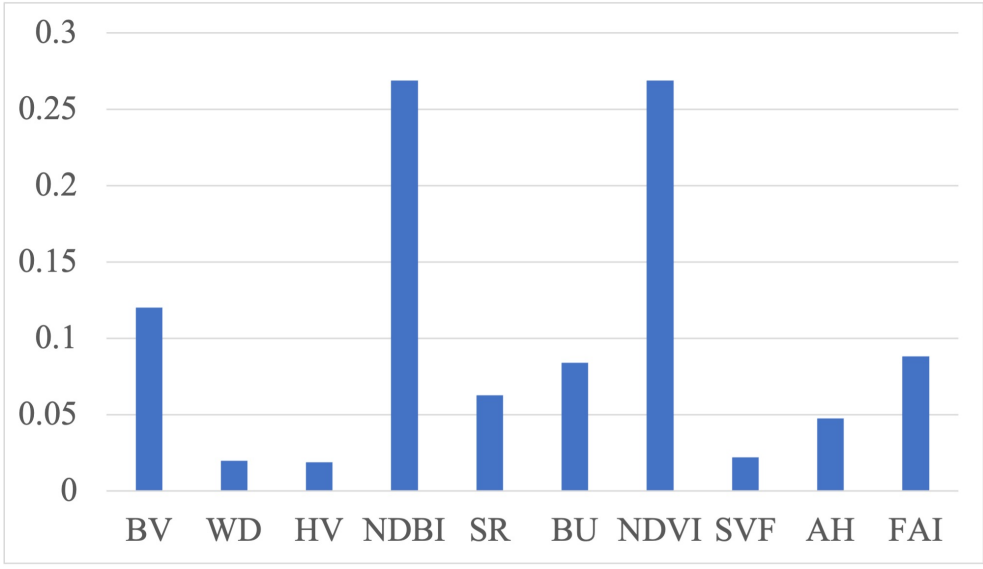

Figure 6.5: Feature importance of the optimised model

SVF, HV and WD. The model is mainly driven by NDBI, NDVI, BVI and FAI values, which decide the value of LST.

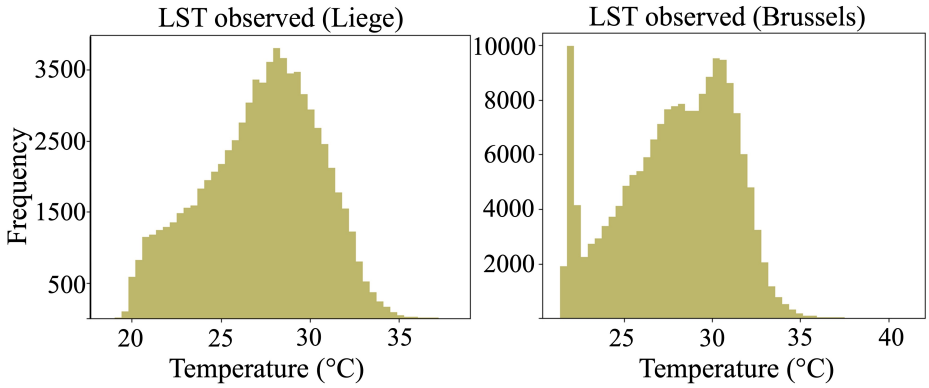

Figure 6.6: Distribution of observed LST values for Liege and Brussels

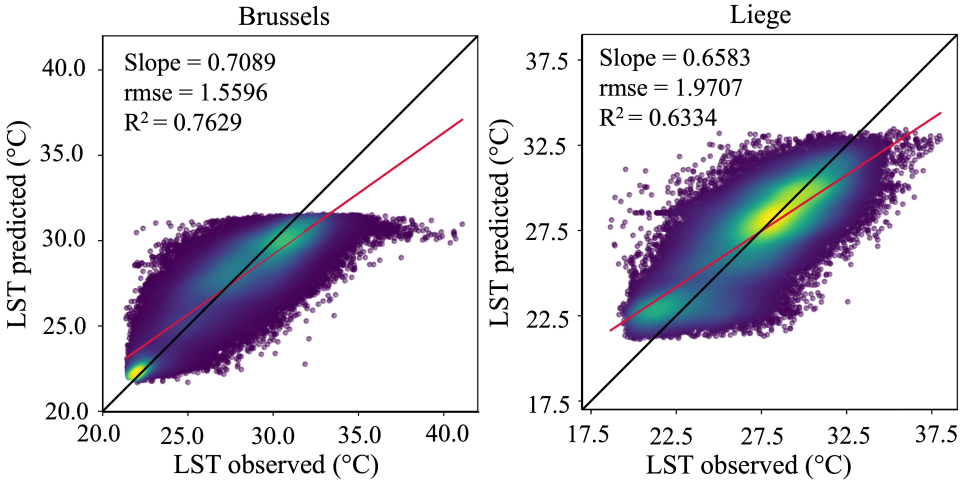

Figure 6.7: Comparison of predicted vs observed values of LST for Brussels and Liege

6.3.3 Comparing predicted and observed values of LST

Here, we compare the predicted values of LST with the observed values of LST from Landsat-8 for both the cities. The city of Brussels has observed values of LST ranging from 21 – 42 °C, whereas the city of Liege has the values of LST ranging from 18 – 38 °C (Figure 6.6). The predicted values for both the cities, however, fall between 21 – 33 °C (Figure 6.7).

We observe that the trained model's R-squared value is 0.76 with an RMSE of

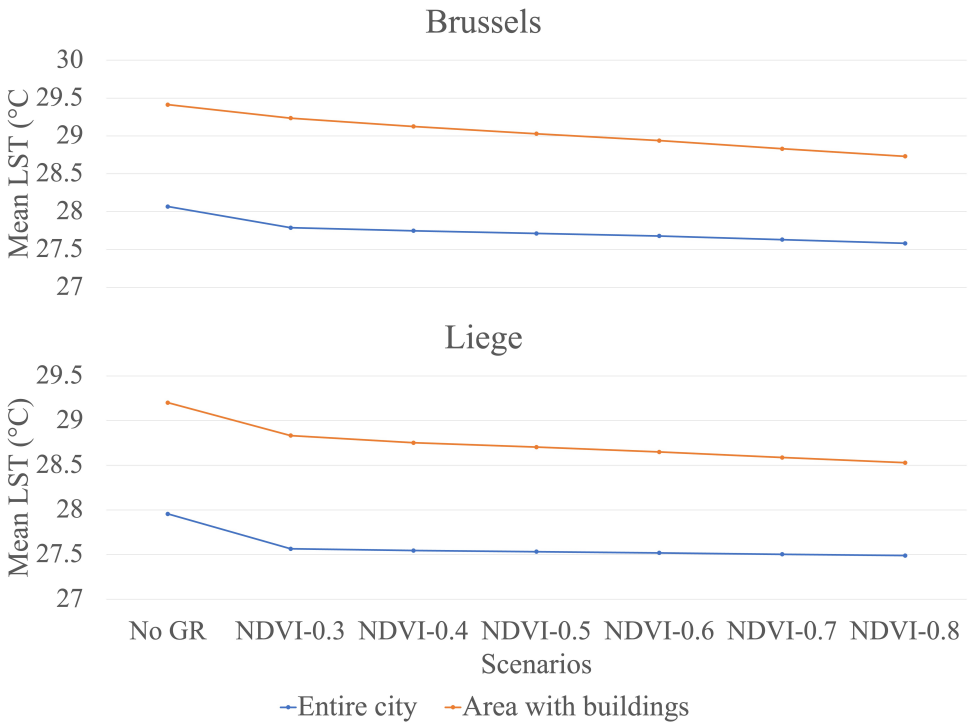

Figure 6.8: Mean of predicted LST in Liege and Brussels for different scenarios

1.55 °C for Brussels. For Liege, the R-squared value is 0.633 with an RMSE of 1.97 °C (Figure 6.7). We observe that the values between 21-33 °C are predicted more accurately compared to the values outside of this range (Figure 6.7). The reason could be the distribution of data which ranges from 19 – 38 °C, with 80% of the points in the range between 21-33 °C. As the model tends to underpredict LST slightly, we compare the effect of green roofs on LST with the predicted LST of our model, to understand the actual impact green roofs can have on LST.

6.3.4 Prediction after green roofs

Based on the model, after adding intensive green roofs (NDVI = 0.8) to potential buildings, average LST is shown to be reduced by 0.67 °C and 0.46 °C in Liege, whereas average LST is shown to be reduced by 0.68 and 0.48 °C in the Brussels capital region in building area and entire city respectively. On the other hand, when extensive green roofs (NDVI = 0.3) are added to potential buildings, the average LST can reduce by

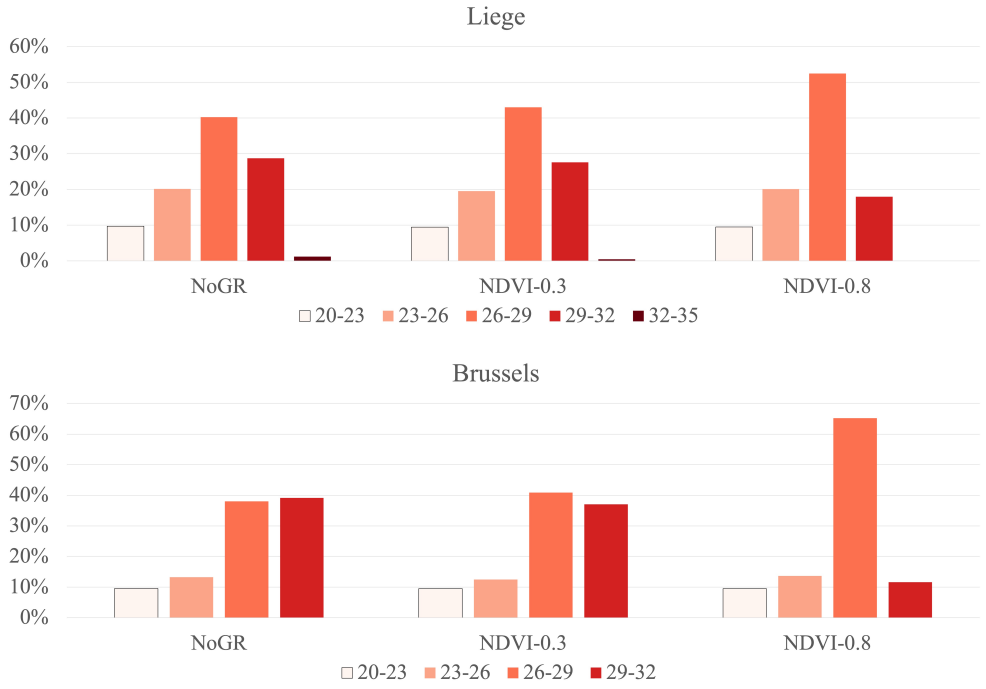

Figure 6.9: Distribution of proportion of pixels in LST ranges

0.32 °C and 0.36 °C in Liege, and the average LST can reduce by 0.22 and 0.26 °C in the Brussels capital region in building area and entire city respectively. Figure 6.8 shows the predicted LST for each green roof scenario ranging from NDVI of 0.3 to 0.8.

Figure 6.9 depicts the distribution of pixels in each class of LST. With increase in NDVI value corresponding to green roofs, there is a decrease in pixels within the range of 32 – 35 °C for Liege as well as Brussels.

Similarly, Figure 6.10 depicts the spatial variation in LST with adding intensive and extensive green roofs. As observed in figure 6.8, with increase in NDVI values of green roofs, we observe a reduction in pixels with temperature ranges between 29-35 °C.

6.4 Discussion and Conclusions

In this study, we explore the RF regressor model for predicting impact of green roofs on LST. When comparing the observed LST with predicted LST, the model shows a

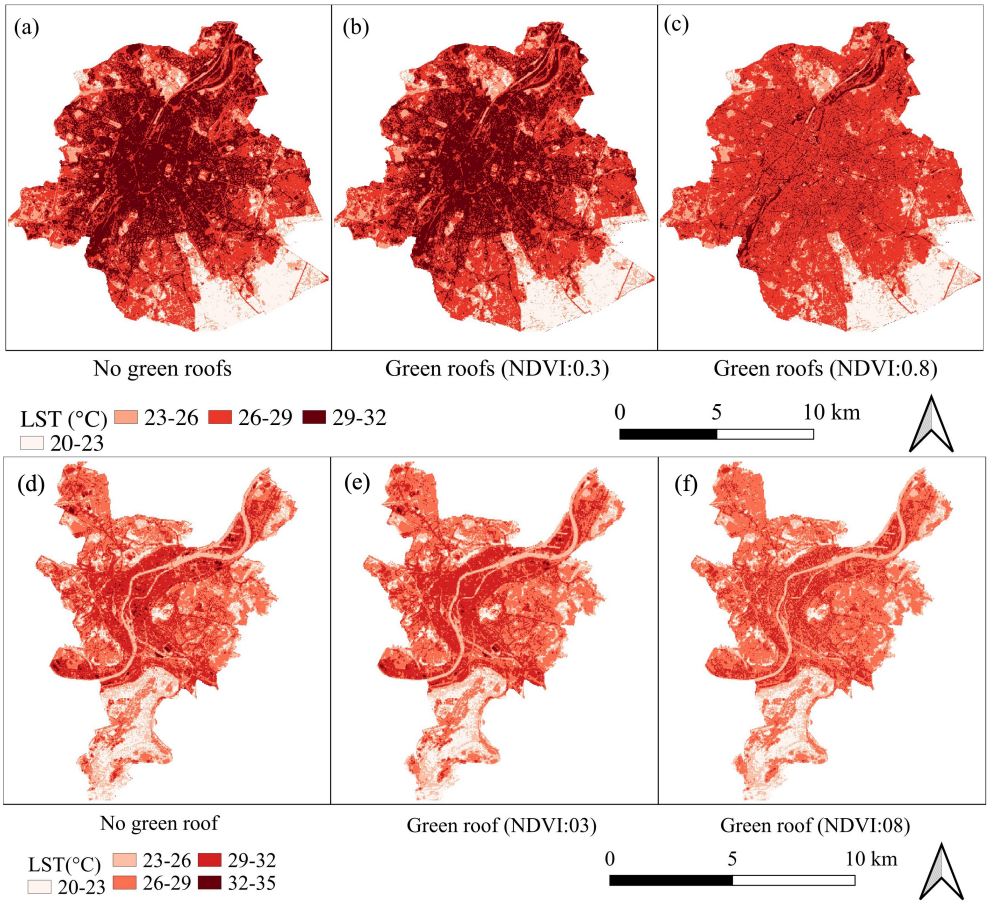

Figure 6.10: Differences in LST in Brussels and Liege city for different greening scenarios

significant goodness of fit. The RF model suggests that green roofs have potential to reduce LST. The benefit of green roofs is higher with intensive green roofs as compared to extensive green roofs.

Although the impact of green roofs on LST on an average seems to be smaller, it is significant in terms of number of pixels where we observe the reduction of temperature (Figure 6.9). However, small changes in LST may also indicate that when green roofs are placed on existing potential roofs, the impact may not be very significant (at least in case of extensive type of green roofs).

The prediction of LST depends on the training of the RF regressor model. Therefore,

we include the data from two major cities in Belgium namely, Brussels and Liege, in order to have sufficient data points for training. However, we observe that the model does not perform well to predict extreme temperatures. To overcome this issue, adding more cities to the dataset can improve prediction accuracy.

Apart from this, the parameter importance of the model implies that NDVI, NDBI and BV govern the predictions. Importance of other parameters such as SVF, WD and HV are relatively low, yet theyare known to be important predictors of the UHI effect [204]. A reason could be multi-collinearity within the variables. As multi-collinearity does not affect predictions, we consider all the variables to capture maximum variance in the model. For understanding the feature importance, it is important to drop the variables causing multi-collinearity. Further research can combine RF regressor with principal component analysis (PCA) to enhance this analysis. In this study, we include data points all over the city. However, splitting the training samples into built-up area and non-built up with added cities can improve the prediction accuracy of the model. Additionally, further research can also focus just on analyzing only the built-up area of several cities.

Current model only considers changes in NDVI and NDBI to simulate green roofs. As greening can influence neighborhood areas as well, addition of a neighborhood effect in the model can also increase the prediction accuracy of the model. Lastly, use of RF regression in prediction of changes in LST after introducing green roofs in a city is a novel and a promising approach, given the proven robustness of RF algorithm in several studies. The model successfully indicates the potential of greening the roofs for reducing the LST in cities. Asadi et al. [337] performed a similar study using ANN model for Austin, Texas. However, in this study, we introduced two additional parameters influencing wind flow, FAI and HV. We see that FAI influences the model, however, HV has the lowest impact.

6.5 Key contributions

- This approach, relying on open-source datasets, offers a large-scale, less data-intensive, and multi-city analysis. Thus, it holds potential for broader use in Global South cities.
- This approach facilitates the analysis of green roofs' impact on surface temperature, indicating a reduction in the average Land Surface Temperature (LST).
- However, the approach is only useful for analysing the impact on surface temperatures.
- The trained RF regression model does not predict extreme temperatures accurately.

- Other machine learning models or additional training data for the RF model are needed to improve the predictions.
- Combining this model with predictive urban growth models based on CA can also improve the predictions and enhance the results.

Part III

Green roofs' role in ecological connectivity

7

Effectiveness of Green Roofs in Strengthening Ecological Network.[1]

Improving biodiversity in urban areas is widely recognised as part of sustainable smart cities development framework. Due to unprecedented urbanisation, there is a lack of adequate green spaces which has in turn affected the urban biodiversity. Green roofs are argued to enhance and support the biodiversity by systematic inclusion into the urban ecological network. However, its connection to the existing natural ecological areas and connectivity are not discussed at a city scale. Thus, in this study, we aim at identifying the connectivity of potential areas for developing green roofs in strengthening the biodiversity and ecological network in cities. Altogether, we observe that the potential roofs are in the near proximity of these zones. The zones with dry lawns and meadows like environment are quite limited and spatially far from each other. Thus, developing green roofs can help in connecting these spaces. In this paper, we mainly focused on bees as they play an important role in pollination and are also declining in the urban areas. Further research can incorporate more detailed analysis on foraging distances of other species. A methodology can be developed to select which zones can be targeted for specific species.

[1] Published as: **M.Y.Joshi**, and J.Teller, *Effectiveness of Green Roofs in Strengthening Ecological Network*. (2021). The International Archives of the Photogrammetry, Remote Sensing and Spatial Information Sciences. **46**, 51-54doi:/10.5194/isprs-archives-XLVI-4-W1-2021-51-2021, 2021.

7.1 Introduction

Improving biodiversity in urban areas is now widely recognised as part of sustainable smart cities development framework [349]. Due to unprecedented urbanisation, there is a lack of adequate green spaces which has in turn affected the urban biodiversity. Urban green infrastructure is often suggested as a solution to improve biodiversity. However, its connection to the existing natural ecological areas and connectivity are not discussed at a city scale. In this study, we focus particularly on green roofs.

Extensive green roofs have a relatively thin layer of a lightweight substrate, which needs little or no additional structural support [38]. The species planted on EGR are mostly dry grass, succulents, herbs and mosses [31]. In dense urban areas, biodiversity is more fragmented and isolated. It is essential to plan ecological corridors to facilitate the dispersal of species between environments [56].

Ecological network is usually studied in order to plan the ecological corridors in urban areas. Ecological network can be defined as "A coherent system of natural and/or semi-natural landscape elements that is configured and managed with the objective of maintaining or restoring ecological functions as a means to conserve biodiversity while also providing appropriate opportunities for the sustainable use of natural resources" [6]. The ecological network is divided into a coherent system of areal components as shown in the figure 7.1. Core areas are the areas where preservation of biodiversity is of prime importance. The corridors are to maintain the vital ecological or environmental connections. The buffer zone is to protect the network from potentially damaging external damages. Sustainable use areas are the areas where there is enough opportunity for both exploitation of natural resources and maintenance of ecosystem functions [6, 350].

Green roofs are argued to enhance and support the biodiversity, and they can be highly effective if they are included in an ecological network [55]. Green roofs provide habitats and food to many species [28, 351]. They are often inaccessible, thus offering an undisturbed habitat. Various species such as birds, spiders, bees and arthropods are observed on green roofs [64, 352, 353]. However, their richness and abundance are dependent on various factors such as plant diversity, proximity of green roofs to other green roofs or green spaces, height and area of the roof [56]. Research has shown that green roof arthropod diversity is observed to increase with better connectivity between the green spaces [53]. Green roofs located in close proximity to each other and near the existing green biodiversity-rich areas can improve the abundance of species in urban areas.

Currently, the population of bees, arthropods and collembolas are observed to reduce in the urban areas. Utilizing green roofs to regulate their presence can strengthen

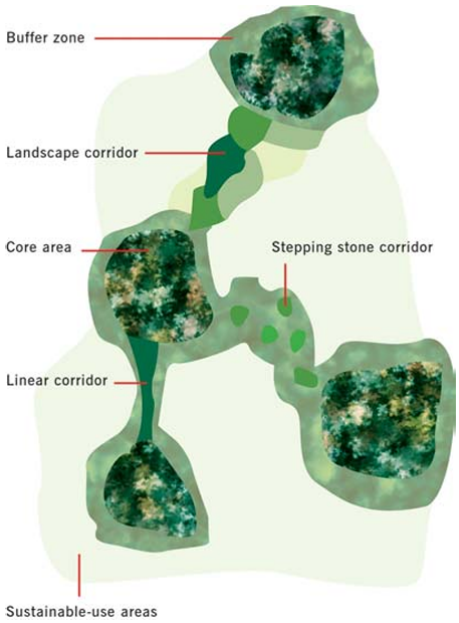

Figure 7.1: Components of ecological network [6]

the ecological network and also integrate the dense urban areas with nature. However, understanding the potential areas for green roofs along with the ecological network is an essential prelude to utilizing green roofs in biodiversity enhancement. Therefore, in this study, we aim at identifying the connectivity of potential areas for developing green roofs in strengthening the biodiversity and ecological network in cities.

7.2 Methodology

7.2.1 Study Area

Liege, a city in Wallonia region of Belgium, is the third-most populous city of Belgium with a total of 195,965 inhabitants and area around 69 km^2. There are 136,170 buildings in the city, with a total area of building roofs about 10 km^2, which represents around 14% of the city area.

7.2.2 Computing potential of green roofs

Green roof potential was estimated based on the methodology explained by Joshi et al. [88] for the city of Liege. We mainly consider flat roofs more suitable for green roof development. Apart from this, the reserved structural capacity of buildings was considered based on the height of the building where taller buildings were concrete (more strength) and shorter buildings were steel-based. The steel structure buildings were then classified based on the year of construction. The structure of the buildings was indeed corresponding to the norms that were in place during the period of construction. The buildings built before 1977 have more strength than required as they were built according to old standards, which were more conservative due to lower accuracy and precision. The Eurocode was proposed in the year 1977 after which the buildings were built with exact strength and capacity due to advancement in the technology. It is not possible to develop green roofs on these recent buildings without major structural changes. Therefore, we consider buildings with steel structure that are constructed before 1977 for implementing green roofs [88].

7.2.3 Analysing ecological networks

Public Service of Wallonia (SPW) launched a program called plan for development of nature in cities/ Plan communal de Développement de la Nature (PCDN) in 1995 for municiplaities in Wallonia region. Amongst the cities in Wallonia selected for PCDN, Liege is the most urbanised and populated city, which therefore requires a very particular approach for nature conservation. In the PCDN, which was drafted in 2016 [89], a detailed ecological network of city of Liege is developed by the Biodiversity and Landscape unit of Gembloux Agro-Bio Tech (ULg), in collaboration with the ICEDD (Institute for Consulting and Studies in Sustainable Development) and the collective Ipé (Interface for study projects) for urban planning aspects. The ecological network of Liege is mainly divided into four parts, namely, central zone (ZC), central zone restorable (ZCr), development zone (ZD), and development zone in urban area (ZD_Urb). These zones are further divided into open environments characterizing different habitats such as moors, meadows, dry lawns, agricultural areas, forests and water bodies.

The central zone is of great biological interest where everything should be in favour of nature conservation. The restorable zone is identified as interesting for certain target species that require restoration. The development zone is the area with less biological interest but has a significance. This zone is mainly with urban components such as cemeteries, storm basins and golf courses which have potential in terms of biodiversity. The development zones in urban areas are the artificial habitats such as

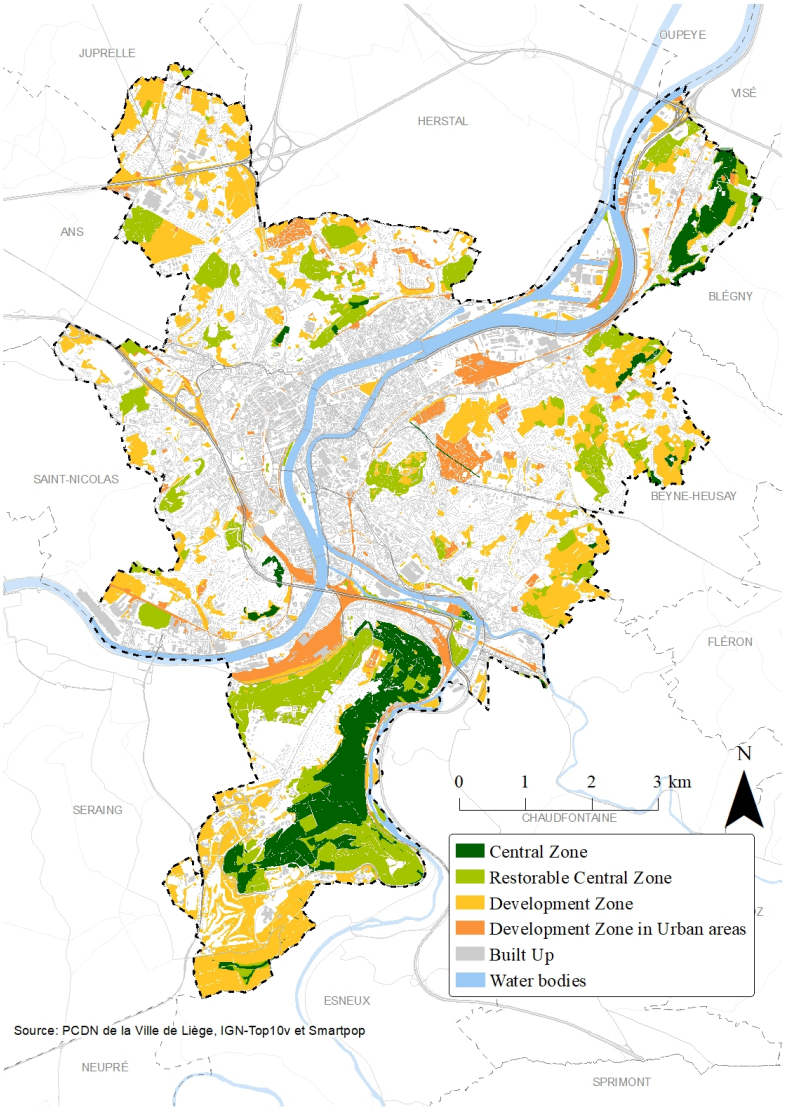

Figure 7.2: Zones in ecological network of Liege along with built-up (Source - ecological network: PCDN de la Ville de Liège, IGN-Top10v et Smartpop)

small green growth on railway tracks, which are similar to natural or semi-natural habitats. Figure 7.2 indicates the map with all the zones along with existing built-up of Liege.

As green roofs are observed to have ecosystems similar to dry lawns and meadows (not frequently), we consider only these two environments in our analysis. We also consider potential roofs with greater than 100 square meter area. We calculate the distance between the potential green roofs and the distance between ecological network zones (dry lawns and meadows environment) and potential green roofs. This was done using near distance tool in ArcGIS Pro 2.7. We consider bees in particular in this study as they play an important role in pollination and they are also declining in the urban areas. Foraging range of small bees is around 100-200 m and large bees is around 1000m [354]. Although reported foraging distance of bees is 1000m, we consider 1500 m threshold in this analysis. Height of the buildings is also observed to impact the abundance and richness of these species, we report and discuss the statistics of height of potential roofs.

7.3 Results and Discussion

There are a total of 6521 buildings (346 hectares) with potential for green roofs with an area greater than 100 square meters in the city of Liege. The distance between the potential green roofs located within 1500 m of each other is on an average around 930 m, ranging from 567 m to 1281 m. The minimum distance between the potential roofs is 2 m with a maximum of 355 m. This suggests that the potential green roofs are closer to each other if the target is to increase the spotting of bees. The closeness of potential roofs is also visible in figure 7.3.

The central zone has total 6 sites with dry lawns and meadows. Each site has around 176 to 1520 potential roofs (average: 959) in the proximity of 1500 m. The average distance between potential roofs to the dry lawns and meadows in central zone is 1044 m, with a minimum of 949 and maximum of 1080 m. The minimum distance between potential roofs and dry lawns and meadows in the central zone is around 54 m on an average with a minimum of 6 m and maximum of 159m.

There is total 389 sites in the restorable central zone. Each site has around 448 (6 to 1664) potential roofs within a distance of 1500 m. The average distance between potential roofs to the dry lawns and meadows in restorable central zone is 1004 m, with minimum distance of 567 m and a maximum of 1302 m. The minimum distance between green roofs and central zones with dry lawns and meadows is around 104 m on an average, with a maximum of 710 m. Also, the central zone sites are quite far from each other. Thus, the potential roofs near to these sites can be designed with species that are specific to the central zone to enhance biodiversity.

A total of 627 sites are observed in the development zone with dry lawns and

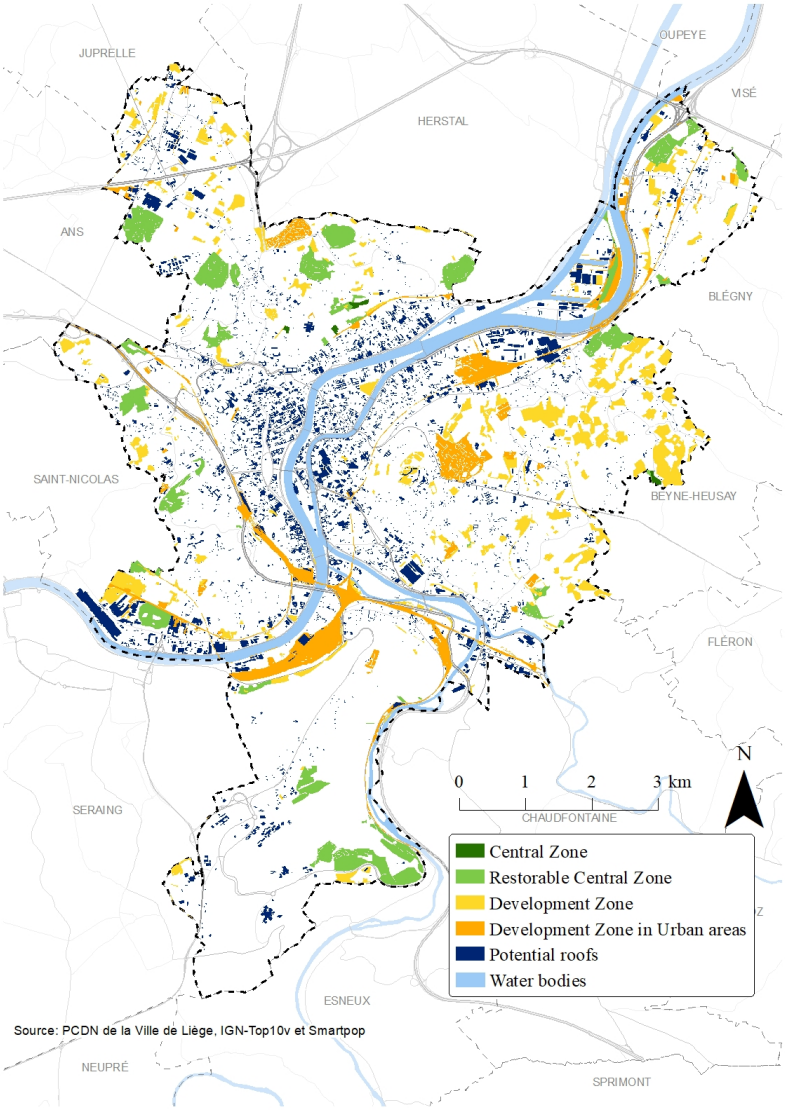

Figure 7.3: Ecological network zones with dry lawns and meadows environment along with potential roofs (Source - ecological network: PCDN de la Ville de Liège, IGN-Top10v et Smartpop)

meadows environment. Each site has around 23 to 2242 potential roofs, 516 on an average in the proximity of 1500 m. The average distance from sites with dry lawns and

meadows in development zone to potential roofs is around 980 m, with a minimum of 540 m and maximum of 1290 m. The average minimum distance between these sites and potential roofs is around 65 m with a maximum of 940 m.

There is a total of 1306 sites in the development zone of urban area with dry lawns. There are no sites with meadows environment as this region is quite disconnected with the central zone. Around 8 to 2211 potential roofs (average:779) are within 1500 m of these sites. The average distance between these sites to the potential roofs nearby is 974 m, with a minimum of 524 m and maximum of 1276 m. The minimum distance between these sites and potential roofs nearby on an average is 58 m, with a maximum of 500m.

On an average, the height of the buildings where green roofs can be implemented is around 8 m, with a maximum of 80 m and a minimum of 3 m. Most of the buildings are with a height less than 20 m. Braaker et al. [53] observed no impact of height on the abundance of species, this was partly due to sample with height less than 18 m. However, some studies point out that with increase in height, there is a lower number of species observed [355, 356]. Around 703 buildings out of 6521 with potential of greening are with a height greater than 20 m. These buildings need to be studied further for implementing green roofs in order to enhance biodiversity. As most of the roofs are less than 20 m, they can be useful in strengthening the ecological network.

Altogether, we observe that the potential roofs are in the near proximity of these zones. The zones with dry lawns and meadows like environment are quite limited and spatially far from each other. Thus, developing green roofs can help in connecting these spaces. Moreover, the minimum distances between potential green roofs and ecological network zones along with distance within potential green roofs are less than 200 m. This means that the potential roofs can be favourable for both small and large bees.

Further research can incorporate a more detailed analysis of area and height of potential green roofs within a buffer zone of the ecological network sites. It can also include in depth study of specific characteristics of these zones to ensure a better selection of species on green roofs. More detailed analysis on foraging distances of other species also can be done. A methodology can be developed to select which zones can be targeted for specific species.

7.4 Key contributions

- Potential green roofs are within the proximity of existing dry grassland sites, showing their potential in improving the connectivity for dry grasslands, when planted with biodiverse flora.

- Green roofs may offer benefits to both small and large bee species due to shorter Euclidean distances from existing dry grassland sites. However, it is essential to note that this measure does not account for resistance in the landscape.
- Since factors such as landscape elevation and existing land use hinder the species' movements, detailed analysis is necessary.

8

Exploring the impact of prospective extensive analogous green roofs on the functional ecological connectivity of urban dry grassland habitat[1]

Creating analogous habitats on potential green roofs can restore the urban dry grasslands network crucial for pollinator species in temperate Europe. In this paper, we explore the role of potential extensive green roofs in the functional ecological connectivity of urban dry grasslands in Liège city, Belgium. Two key questions are explored: the impact on functional connectivity and the required green roof percentage for significant impact on connectivity. Using landscape graphs, we modelled the ecological network for different scenarios of roof greening percentages in Liège. We specifically use a highly categorized urban green spaces in the land cover and assign costs to them based on a combination of resistance to flying insect movement and resources available for the species. Results indicate increased global urban dry grassland connectivity with analogous green roofs, particularly benefiting high and moderate-mobility species, with limited impact on low-mobility species. Local connectivity analysis reveals that retrofitting 30-50% of the potential green roofs will improve connectivity for high and moderate-mobility

[1]Published as: **M.Y.Joshi**, L.Rivière, A.Bourdouxhe, T.Pollet, T.Coppée, G.Mahy and J.Teller *Exploring the impact of prospective extensive analogous green roofs on the functional ecological connectivity of urban dry grassland habitat. Landscape and Urban Planning. (Ready to submit). 2023*

species. However, almost all potential roofs must be greened to enhance connectivity for lower-mobility species. Moreover, local connectivity is better for green roof patches than ground patches, suggesting that introduced green roofs mainly create a compact network of dry grasslands in the center, with limited improvement in connectivity of the existing dry grasslands. Additionally, results suggest that building height and urban configuration, in general, influence the role of green roofs in improving the connectivity of dry grasslands. This approach aids in establishing practical expectations when retrofitting lower to higher proportions of green roofs throughout the city.

8.1 Introduction

Dry grasslands are important environmentally as they support a diverse range of flora and fauna with genetic diversity that can withstand harsh conditions, including temperature and water stress. However, dry grasslands are highly fragmented due to intensive agriculture, pasture grazing and urbanisation [66]. Although, urbanisation is one of the causes for fragmentation, urban environment presents an opportunity to create analogous habitats on hard surfaces like pavements, roofs and walls, which can boost the ecosystem services in dense urban areas. Creating analogous habitats on these surfaces, which are the sites hosting indigenous biodiversity due to their structural or functional resemblance to natural habitats [67], can help restore species-rich dry grasslands networks in urban areas of temperate Europe [64, 68].

Dry grasslands can create suitable habitats for diverse and endangered insect species [69, 70]. The alarming decline in insect population is affecting pollination and decomposition along with an increase in pests in urban areas [71, 72]. However, dry grasslands have become rare due to anthropogenic activities in temperate Europe [73, 74]. The fragmentation and the consequent isolation of dry grasslands reduce insect diversity and richness [75] and decrease their functional dispersal [76]. This further lowers the ability of species to respond effectively to environmental changes, reducing their ecological resilience [77]. Creating micro-habitats of dry grasslands between larger habitat surfaces [357] can help restore functional networks and improve the functional connectivity for insects in the city. Creating analogous habitats on impervious roofs can be one of the suitable options for improving the connectivity for insects, as it can restore the dry grassland network in the city [78].

Extensive green roofs are targeted to increase biodiversity support in urban areas due to their lower constraint on building as compared to intensive green roofs. However, extensive green roofs face constraints like shallow substrate depth, low water retention, high sensitivity to climate variations and limited space for root and aboveground biomass development [79]. Extensive green roofs, planted with native

flora, are proposed as habitats analogous to dry grasslands and rocky environments in temperate regions, given their shared environmental constraints [65, 80]. This hypothesis of green roofs being analogous habitats of dry grasslands is also proven in recent studies like Rivière et al. [65], Schröder and Kiehl [81], and Thuring and Dunnett [82]. Hence, existing suitable building roofs can be retrofitted with extensive analogous green roofs to generate micro-habitats of dry grasslands within the city. However, the characteristics of green roofs, such as their number, size, rooftop height and their location, can influence the biodiversity observed on them, which may impact their role in functional connectivity [53, 358]. Moreover, the resistances offered by the different habitats in an urban landscape for species mobility and dispersal may influence the role of green roofs in functional ecological connectivity.

Until now, only Louis-Lucas et al. [359] have directly analyzed the green roofs' role in functional connectivity with a focus on flying species with low to high mobility using graph theory. Another study by Dong et al. [325] focused more on identifying useful corridors for implementing green roofs to improve ecological connectivity for high-mobility species like birds. In both these studies, the type of green roof (extensive, intensive or semi-intensive) was not specified. The study by Louis-lucas et al. [359] also considers all urban green spaces to be beneficial for flying species such as bees, hoverflies and butterflies. However, urban habitats are diversified, and different habitats host different insect communities and demonstrate different resistance to dispersal for species. For example, intensively managed green spaces, urban forests and mineralized habitat may be hypothesized to be less attractive and pose resistance to dispersal for natural grassland species.

Recognizing the resistance posed by different habitats to the species movement is crucial for analyzing green roofs' ecological connectivity. Previous studies also overlooked the altitude differences within urban habitats, which is vital for assessing ecological networks. Considering vertical distribution is essential, as it can hamper the connectivity between patches [360]. Therefore, integrating various habitats and building heights in the analysis is necessary for a comprehensive understanding. Furthermore, installing green roofs on every potential building is unfeasible, highlighting the importance of exploring different proportions of potential green roofs within the study area. Summarizing, there are mainly four research gaps in the existing research on green roofs' role in ecological connectivity: (1) Extensive green roofs are cost effective and can host dry grassland habitats, but their role in functional ecological connectivity of urban dry grasslands has not been particularly analyzed. (2) Previous studies did not consider the different hosting capacity and resistance to organism dispersal of the different urban habitats . (3) The altitude of habitats and landscapes are not considered in the analysis. (4) There is no analysis on the quantity

of roof greening required to get the desired improvement in ecological network of dry grasslands.

Therefore, in this paper, we address the research gaps by answering the following research questions:

1. How does retrofitting existing suitable buildings with Extensive green roofs analogous to dry grasslands affect the functional connectivity of urban dry grasslands flying insect species?

2. How much percentage of roof greening with analogous green roofs is required to improve the ecological connectivity of flying insect species on urban dry grasslands?

We answer these questions by modelling the ecological networks of dry grasslands in a Belgian city (Liège) using graph theory. We also use detailed land cover with classified urban green and artificialized spaces to ensure comprehensive computation of resistances to dispersal in urban landscapes for flying insects. Furthermore, we incorporate elevation of the terrain along with building heights in ecological network analysis.

8.2 Methodology

We analyse the green roofs' role in ecological connectivity by modelling the ecological networks using graph theory, which is widely used in several studies to analyse the contribution of green spaces, land cover changes and urban dynamics to ecological networks [361–363].

8.2.1 Study area and land use map

We analyse the city of Liège in Belgium in this study (Figure 8.1 (A)). Liège, located in the Mosan Valley of Wallonia region in Belgium, is an interesting case study as one of the key habitats for biodiversity in the Mosan Valley is dry calcareous grasslands [89–91]. The urbanised area of Liège creates a strong gap in the connectivity of specialist species, particularly in dry grasslands. Consequently, dry grasslands have been identified as a high priority for development in the ecological network of the city of Liège by the government [89]. However, developing ground dry grasslands in the heart of Liège is difficult given the dense built-up. The city is around 69 km^2, with a population of 196,296 inhabitants. For this study, we analyse the area as given in

Figure 8.1 (A), which also includes the area surrounding the city. This area is around 150 km^2.

Lifewatch Wallonia-Bruxelles project has generated a database describing homogenous units of the landscape called as "ecotopes" for Belgium. Ecotopes represent the smallest and ecologically unique landscape features in a landscape classification and mapping system that provide information concerning biodiversity and environmental quality [364, 365]. Each ecotope is described by the percentages of land cover and a combination of topographic, contextual, climate and ecosystem dynamics variables, based on aerial and satellite images.

This database is primarily used to develop models for describing habitats and predicting the ranges of animal species. We extracted the land cover classes and habitats from the ecotope database of 2018 generated by Radoux et al. [364] for Wallonia. This dataset is at 2 m spatial resolution with 13 different classes. Although the trees can be classified into 4 different categories, we consider all the trees to simplify the analysis. Thus, we have 10 classes in total as shown in Figure 8.1(A).

Potential green roofs are the available flat roofs in Liège city. The flat roofs are identified with processing the LiDAR point cloud data using RANSAC (random sampling algorithm) as described in Joshi et al. [88]. We consider only flat roofs as potential roofs, as installation and maintenance costs for installing green roofs on sloped roofs is extremely high [43–45]. In this study, we considered the potential green roofs with area greater than 100 m2 since smaller green roofs do not support significant biodiversity [64]. Figure 1(B) shows the potential (flat) roofs in the city of Liège. There are total 8311 potential roofs with an area of 439 hectares.

8.2.2 Species groups

We focus mainly on the flying insect species with three dispersion capacities [359, 362]: of 200 m for low mobility species like solitary bees or *Carabidae* taxa species [366, 367], 500 m for medium mobility species like butterfly species: *Polyommatus Icarus* or *Pieris Rapae* [368] and 1000 m for highly mobile species like other wild bees or hoverflies [69, 354, 369]. Species mentioned here are just examples; the results cover the entire pollinator group of species found on grasslands.

8.2.3 Modelling ecological network

The ecological network for the three groups of flying insect species is modelled based on spatial graph theory using Graphab 2.8 software [102, 103]. A spatial graph is a network of nodes connected by links. In ecological network applications, nodes correspond to habitat patches, and links indicate flows of individual species between

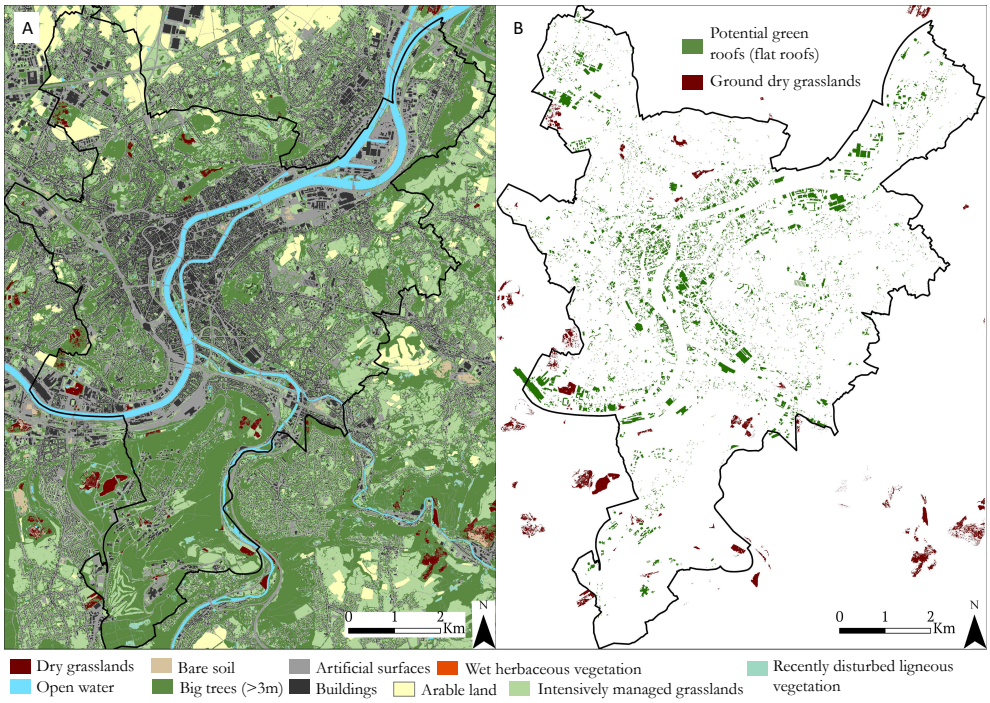

Figure 8.1: (A)Land use map (B)Potential green roofs

habitat patches. Spatial graphs have the advantage of being mathematic objects with network properties. It is, therefore, possible to calculate multiple metrics that help to evaluate the connectivity of the network and the importance of the different components of the network (nodes and links) for the overall connectivity [103, 104].

We assume that green roofs and ground dry grassland patches both offer habitats to the specialist species of dry grasslands. So, we define the habitat patches as a set of adjacent pixels of dry grasslands with biological value and potential GRs with at least an area of 100 m^2. We define the links that connect these habitat patches in planar topology where only neighbouring patches can be linked to the central patch instead of all patches in the landscape. The links were modelled using a least-cost path approach, i.e. the path between two patches with the least cumulated cost. Empirical data for the resistance value of land covers is not available. Therefore, we assign the resistance values to land covers based on two gradations for the three groups of specialist species on DGs (Table 8.1). The main assumption in both gradations is that the cost from habitat to non-habitat is high. The costs are estimated as a combination of resistance to insect movement (based on vegetation structure) and food and habitat resources

available for the insect species. For instance, although non-habitat open areas do not hinder species movement, they may provide resources for insects. Forests and buildings are the physical barriers for insect movement [370]. Gradation 1 accentuates the resistance effect with a logarithmic scale, and gradation 2 is a semi-linear scale with a lesser difference in costs attributed to land covers. For each group of species and gradation scenario, links with a higher cumulated cost than the dispersal capacity of the studied species are discarded. It is important to note that the resistance values can be species specific. But, for simplicity, we have generalised the resistance values for the three groups of species. We assume that the differences in these three groups is just their dispersal capacities and not the resistance faced by species on land covers.

Table 8.1: Gradations and costs given to the land uses

Land Use	**Justification for costs**	**G1**	**G2**
Extensively managed dry grasslands	These habitats have the highest species insect richness and host specialist grassland insect species. They also provide food resources. [371, 372]	1	1
Extensive green roofs	Vegetation developed on green roofs are analogous to dry grassland with biological interest. Thus, they provide food resources and habitat for generalist and specialist species of dry grasslands. However, the height of the green roofs maybe a barrier for movement. [67]	5	1
Wet herbaceous vegetation and Recently disturbed ligneous vegetation	No resistance for grassland insect movements; however, vegetation can provide limited food resources for specialist dry grassland insects. The habitat is more resistant for specialist grassland species due to lack of specific plant host. [372, 373]	10	5

Continued on next page

Table 8.1 – continued from previous page

Land Use	Justification for costs	G1	G2
Arable land and Intensively managed grasslands	No resistance for grassland insect movements; however, intensive croplands and otherwise managed lands are poor in food and habitat resources for generalist and specialist dry grassland insect species [374, 375].	100	10
Permanent bare soil	No resistance for grassland insect movements. It may sporadically present vegetation providing scattered food and habitat resources for generalist dry grassland insect species [376].	100	10
Open water (river, lakes)	No resistance for grassland insect movements. However, water habitat does not provide food and habitat resources for generalists and specialists dry grassland insect species [377].	500	20
Artificialised surfaces	No resistance for grassland insect movement. Artificialized habitats do not provide food and habitat resources for generalists and specialists dry grassland insect species [378].	500	20
Big trees	Forest habitat may hamper grassland insect movements due to vegetation height acting as a barrier. Forest habitat provides low resources for generalist grassland insects and no resources for specialist grassland species [368, 379].	1000	50
Buildings (without green roofs)	Buildings obstruct dry grassland insect movement due to height and lack of food and habitat resources significantly [359, 362].	10000	100

The species-specific maximal distance of dispersion is fixed to 200m, 500m and 1000m for low, medium and high mobility species. Those metric distances are converted to a maximum cost value using logarithmic regression between metric and

cost distance as follows:

$$Dist = e^{intercept + slope.log(DistM)} \tag{8.1}$$

In addition to the resistances assigned using the gradations, we also add building heights and elevation of natural terrain features using the digital surface model (DSM) of the study area. Graphab adds this additional cost with the following equation [380]:

$$r_{final} = r \times (1 + c.p)\,, \tag{8.2}$$

where r_{final} is the final value of the cost of the pixel, r is the cost assigned based on the gradation, and c is the parameter coefficient that can adjust the importance of the p, which is the slope in percentage rise computed using DSM. In this study, the value of c is 1.

With the resistance maps and dispersion distances, the links that connect the habitat patches are created, followed by the generation of landscape graphs.

8.2.4 Connectivity matrix and data analysis

8.2.5 Scenarios for Landscape graphs

Implementing green roofs on all the flat roofs is challenging and unrealistic as municipalities may find it difficult to convince all the building owners for the modifications. So, we generate different scenarios with varied percentages of green roofs. We generate 11 scenarios for each gradation, one without green roofs and 10 with increasing potential roof percentage (in terms of number of roofs) from 10 to 100% by 10. We randomly select the given percentage (based on scenarios) of flat roofs from all the available flat roofs with area greater than 100 m^2. Since random selection may give different selections at each run, we perform 1000 random selections on the potential roofs (10% to 90% roof greening) to test the robustness of the results obtained from random selections. Figure 8.2 shows the variation in total potential roof area for 1000 random selections in each scenario.

To understand whether the variation in total potential roof area in random selections influences the results, we select and analyse the scenarios closer to minimum, maximum and mean of the total area of green roofs of random samples (3 random samples in total for each green roof scenario). After the random selection of roofs, we convert the selected flat roofs to 2 m raster resolution and add it to the ecotope landuse map without green roof by replacing the flat roof building pixels with green roof using the raster calculator tool for each scenario.

We, then, use this newly generated land use map with green roofs for generating habitat patches, links and respective graphs to create ecological networks. We compute two link sets for gradation 1 and gradation 2 followed by three graphs for each gradation (for three species). In total, we analyse 29 scenarios: one without green roofs, one where all potential roofs are greened and 27 with different percentages of green roofs and corresponding random selections. For these 29 scenarios, we generate two link sets, each corresponding to two gradations with a threshold of 1000 m (which will include the links for moderate and low mobility species) followed by the generation of three graphs for three types of species as shown in figure 8.3.

Figure 8.4 shows the variation in green roof patch total area, mean area, standard deviation (std) and number of patches of green roofs for three random samples in each green roof scenario. It also shows the statistics of dry grassland (DG) patches. In terms of total area, there is not much variation. In terms of mean patch area and standard deviation, however, there is a significant variation between the three random samples of potential roofs in each scenario.

8.2.6 Green roofs' contribution to global connectivity

We compute the green roofs' contribution to the global connectivity of dry grasslands using the probability of connectivity (PC) metric. Global connectivity metrics describe the entire graph with one value. PC metric is calculated for all the scenarios and gradations. PC is the probability that two randomly placed habitat patches (potential green roofs and ground dry grasslands) in the landscape (study area) are interconnected [104]. It is computed as follows:

$$PC = \frac{1}{A^2} \sum_{i=1}^{n} \sum_{j=1}^{n} a_i a_j e^{-\alpha d_{ij}}, \tag{8.3}$$

where n is the total number of patches, a_i and a_j are the area of patches i and j, and A is the total area of the study area. $e^{-\alpha d_{ij}}$ is the probability that i and j are connected by a link. In this, d_{ij} is the least-cost path between patches i and j and α $(0 < \alpha < 1)$ represents the decrease in dispersion probabilities resulting from the exponential function. α is calculated as $\frac{-log(p)}{d}$, where p is the probability of movement between the patches and in this study, we assume it to be 0.5 and d is the dispersal distance (1000m, 500m, 200m). The PC metric calculation includes both habitat area and connections between the habitats. Therefore, this metric is sensitive to the area of the patch.

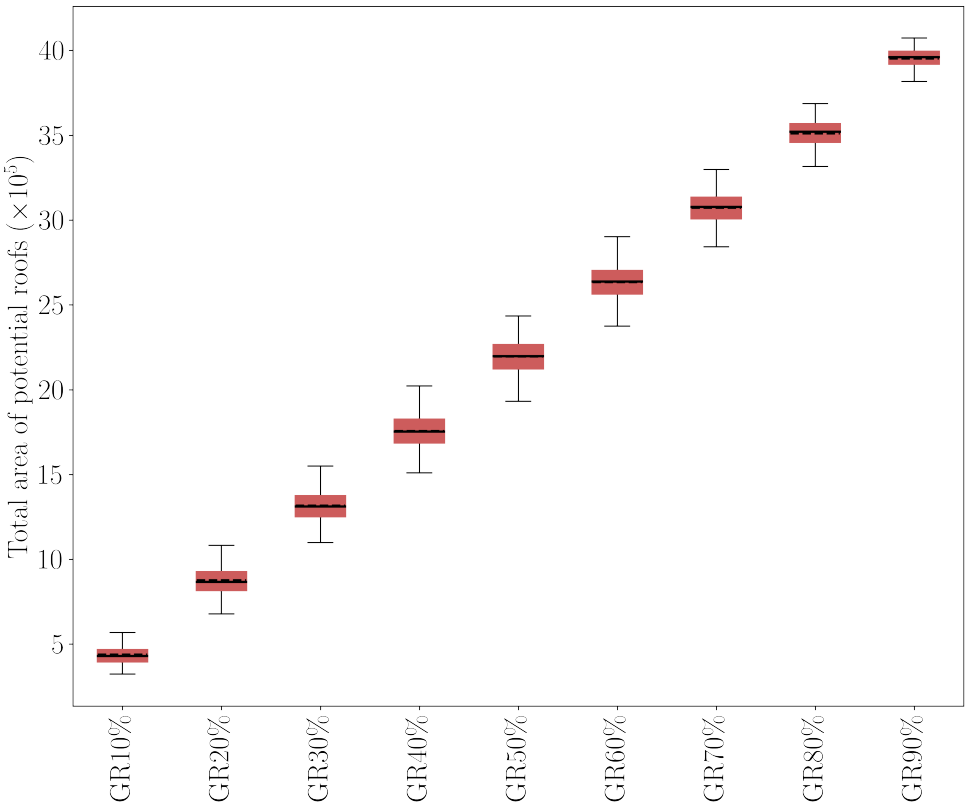

Figure 8.2: Variation in the total area of potential roofs in 1000 random samples of the percentages corresponding to the scenarios

8.2.7 Green roofs' contribution to local connectivity

We calculate two local metrics, namely, betweenness centrality (BC) and Flux. The BC metric highlights the patches with a strategic position in the network. It basically measures the number of times a patch lies on the shortest path between other patches [381]. It is computed as follows:

$$BC_i = \sum_j \sum_k a_j^\beta \times a_k^\beta \times e^{-\alpha d_{jk}} \tag{8.4}$$

The flux metric highlights the well-connected patches. The more connected a patch is to many other patches, the higher the value of the flux metric. This metric is the sum of the capacities of the patches connected to the central patch and weighed as per

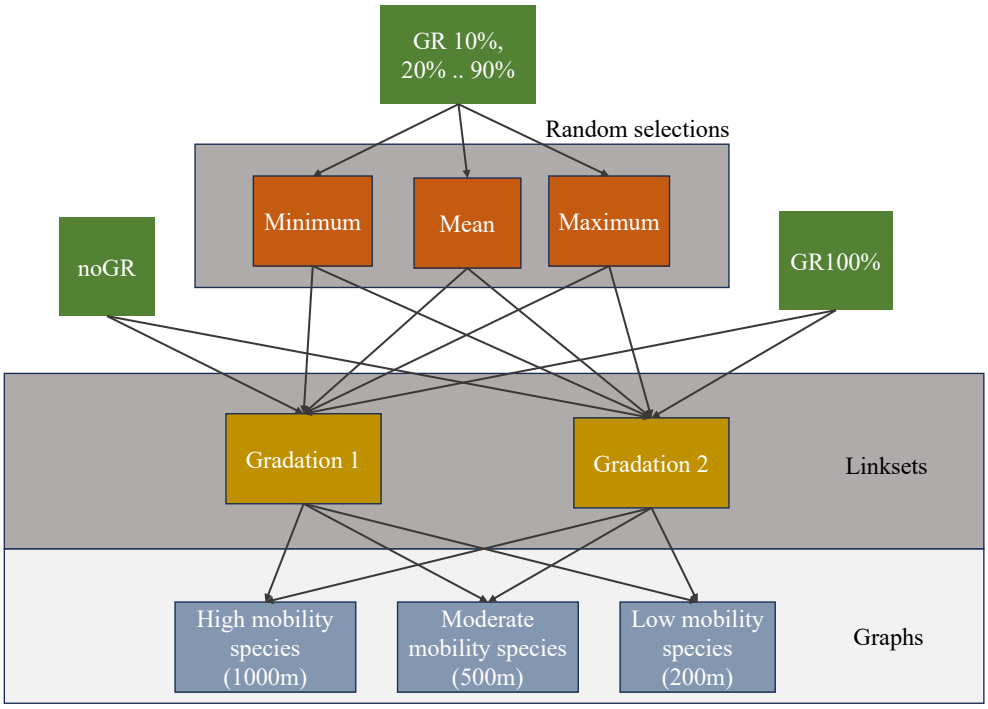

Figure 8.3: Scenarios run in the study

their minimum distance to this central patch in the graph. It is computed as follows:

$$F_i = \sum_{j=1}^{n} a_j^{\beta} \times e^{-\alpha d_{jk}} \tag{8.5}$$

In both the equations, a_j is the area of patch j and is weighted by the parameter β. Since mean area of green roofs is smaller than the area (Figure 4(b)) of dry grassland patches, the parameter β is set to 0 to remove the bias of differences in the area between the two categories. We compute these two matrices for green roofs and dry grassland patches and present a comparison between them in the results section. We compute these two metrics for green roofs and dry grassland patches and present a comparison between them in the results section.

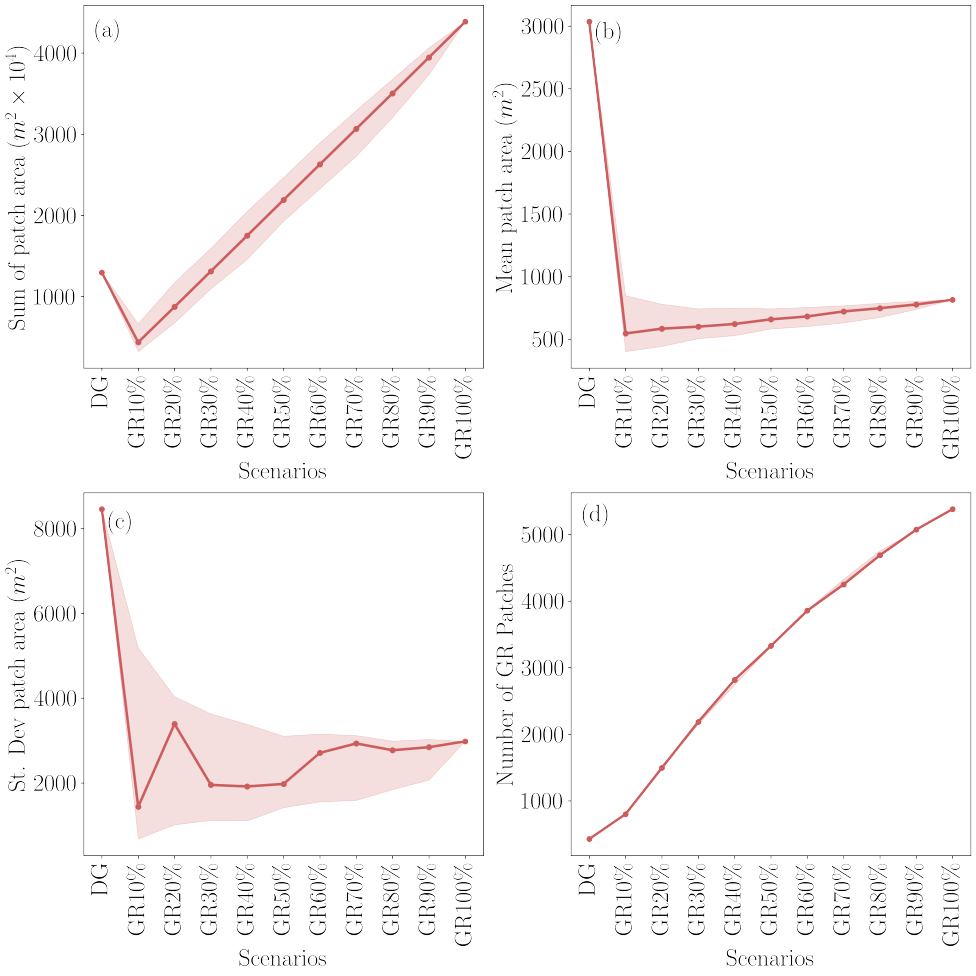

Figure 8.4: Statistics of the dry grassland and green roof patches for each scenario (Shaded areas show the variation in the randomly selected samples closer to minimum and maximum total area of potential roofs)

8.3 Results

8.3.1 Green roofs' contribution to global connectivity

Figure 8.5 shows the increase in PC of all the patches in the landscape for all the scenarios with two gradations used for computing the costs and the three groups of

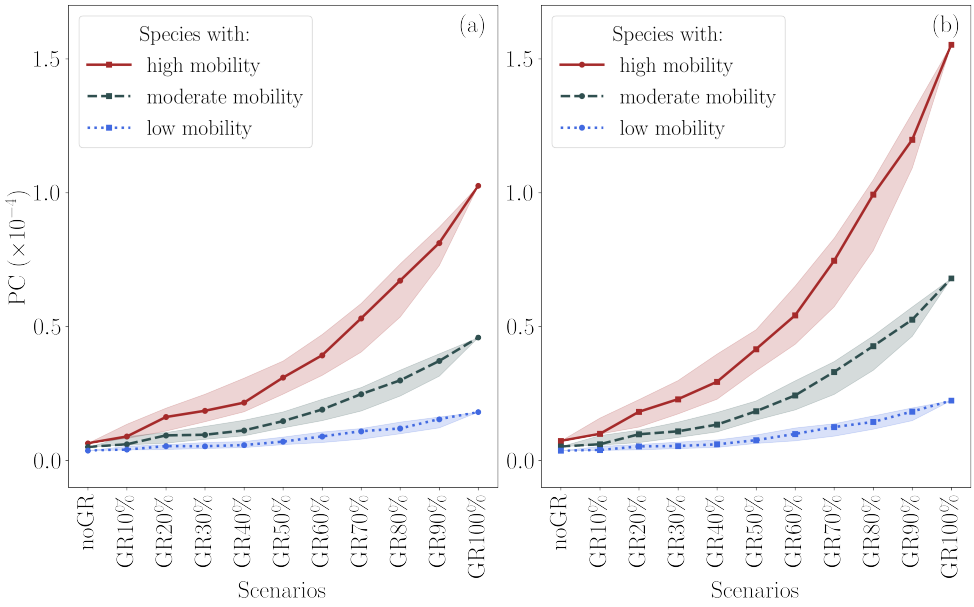

Figure 8.5: Probability of dry grassland connectivity (a)logarithmic gradation (b)semi-linear gradation

species with high, medium and low mobility. We observe that the increase in PC is lower with an increase in the percentage of green roofs with logarithmic gradation (Figure 5(a)) than with semi-linear gradation (Figure 5(b)). This is logical, given the lower resistance values for species with semi-linear gradation. The PC for the species with low mobility (200 m) is the lowest in all scenarios and gradations. Moreover, the rate of increase in PC, with increase in the percentage of green roofs, is also low for species with low mobility. The trend in increase in PC is similar to the trend of increase in mean patch size (Figure 5 (b)).

Comparing the three roof greening scenarios of random selections with the minimum, mean and maximum total area of potential roofs, we see that the PC values vary slightly for different random selections. The variation for high and moderate-mobility species is higher compared to lower-mobility species. At 20% roof greening scenario, there is a sudden increase in PC (in the mean random selection), because of a similar increase in mean patch area in this scenario. However, the increase in the PC is rather continuous and smooth. This means that random selection does not influence the trend of the PC in general. However, it may slightly influence the value of the PC.

In general, increasing green roof percentage improves the connectedness of the

dry grassland patches for high and moderate mobility species to an extent. However, for low mobility species, the increase in PC is low, suggesting that increasing the green roof percentage will barely improve the connectivity unless almost all the potential roofs are greened.

8.3.2 Green roofs' contribution to local connectivity

Influence of random selections on local connectivity

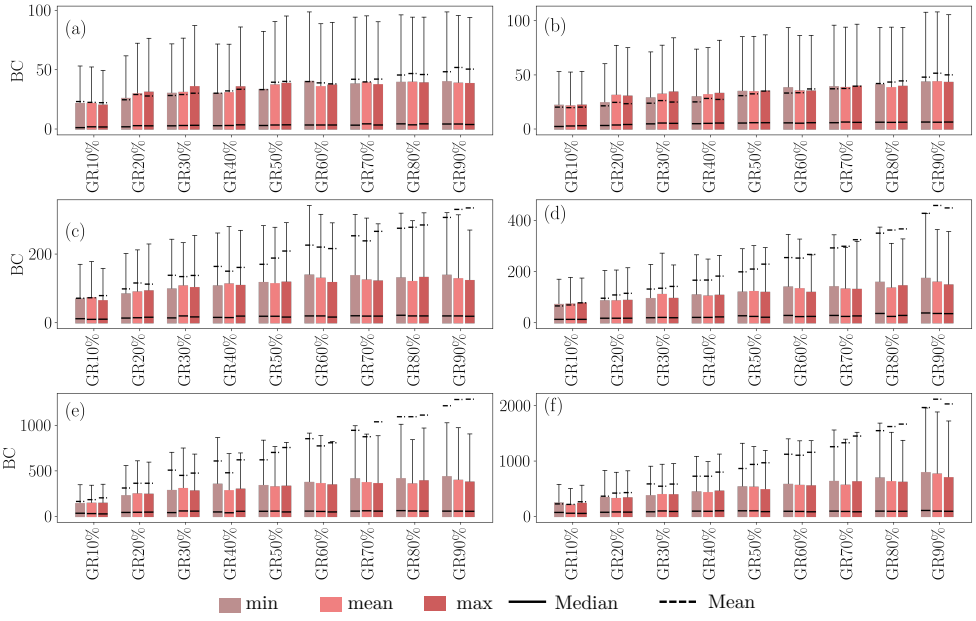

Figure 8.6: BC value of dry grassland patches for all scenarios with logarithmic gradation(a)200m, (c)500m, (e)1000m) and semi-linear gradation 2 (species with dispersal distances (b)200m, (d)500m, (f)1000m).

Figure 8.6 and 8.7 demonstrate the variation in the patch metrics BC, and Figure 8.8 and 8.9 demonstrate flux of potential green roofs and ground dry grassland patches respectively for the three random selections (closer to minimum, mean and maximum total patch area of 1000 random samples). The mean, median and minimum values of BC and flux of green roofs and dry grassland patches remain largely the same for the three random selections for each scenario, with slight variation in the maximum value for a few scenarios. Moreover, the trend of increase in mean

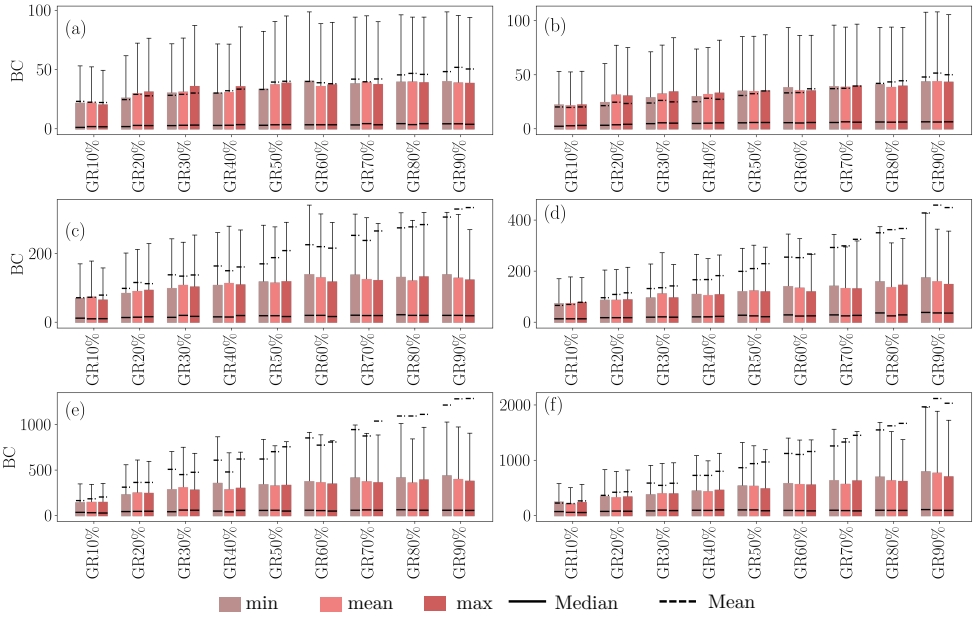

Figure 8.7: BC value of green roof patches for all scenarios with logarithmic gradation(a)200m, (c)500m, (e)1000m) and semi-linear gradation 2 (species with dispersal distances (b)200m, (d)500m, (f)1000m).

BC and flux value with an increase in potential green roofs is the same for all three random samples of each scenario. This means that the results obtained from the random selections are robust as they will deliver a similar trend every time. Therefore, we assume that the results obtained from random selection closer to the mean total patch area are largely robust and will be discussed in detail in the following sections.

Betweenness centrality

The distribution of local metric BC for all the potential green roofs and ground dry grassland patches are compared for all gradations and species in this section. Figure 8.10 demonstrates the variation of BC value of potential green roof and ground dry grassland patches for all the scenarios and species. We observe that the BC value for semi-linear gradation (Figure 8.10 (d,e,f)) is higher than the logarithmic gradation Figure 8.10 (a,b,c)). The BC value is the highest for the patches when high mobility species (Figure 8.10 (c and e)) are analysed, followed by moderate (Figure 8.10 (b and e)) and low mobility species (Figure 8.10 (a and d)). With the increase in green

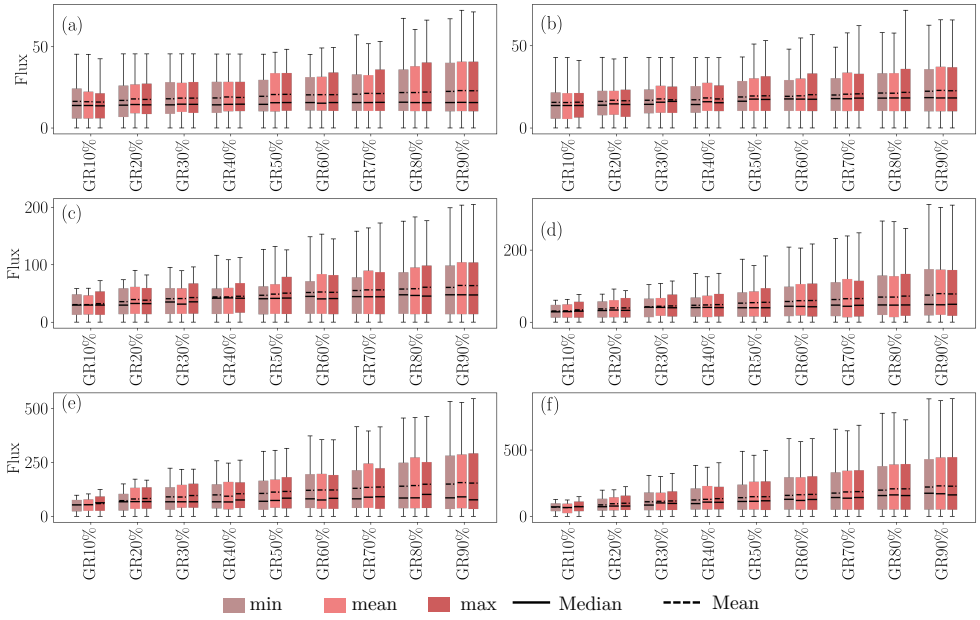

Figure 8.8: Flux value of dry grassland patches for all scenarios with logarithmic gradation(a)200m, (c)500m, (e)1000m) and semi-linear gradation 2 (species with dispersal distances (b)200m, (d)500m, (f)1000m).

roof percentage, the average BC value for green roof and dry grassland patches is increasing, with a larger increase in BC values of green roof patches than dry grassland patches. Moreover, this increase in BC of ground dry grassland patches is extremely low for lower mobility species. This is because the dry grassland patches are located on the outskirts of the city and green roof patches are centrally located. Therefore, the green roof patches lie more frequently between two random patches compared to existing dry grassland patches.

For higher mobility species (Figure 8.10 (c)), the mean BC value of green roofs is similar to ground dry grassland with logarithmic gradation for scenarios with 10% of green roofs. From 20% green roof scenario, mean value of BC of green roofs is higher than the dry grasslands. However, with semi-linear gradation (Figure 8.10 (f)), the mean BC value of green roof patches is always higher than the dry grassland patches.

For moderate mobility species (Figure 8.10 (b)), the mean BC value of green roof patches is almost similar to dry grassland patches for 10, 20 and 30% green roof scenario, with logarithmic gradation. But it is higher than dry grassland patches for scenarios with more than 40% potential green roof. With semi-linear gradation

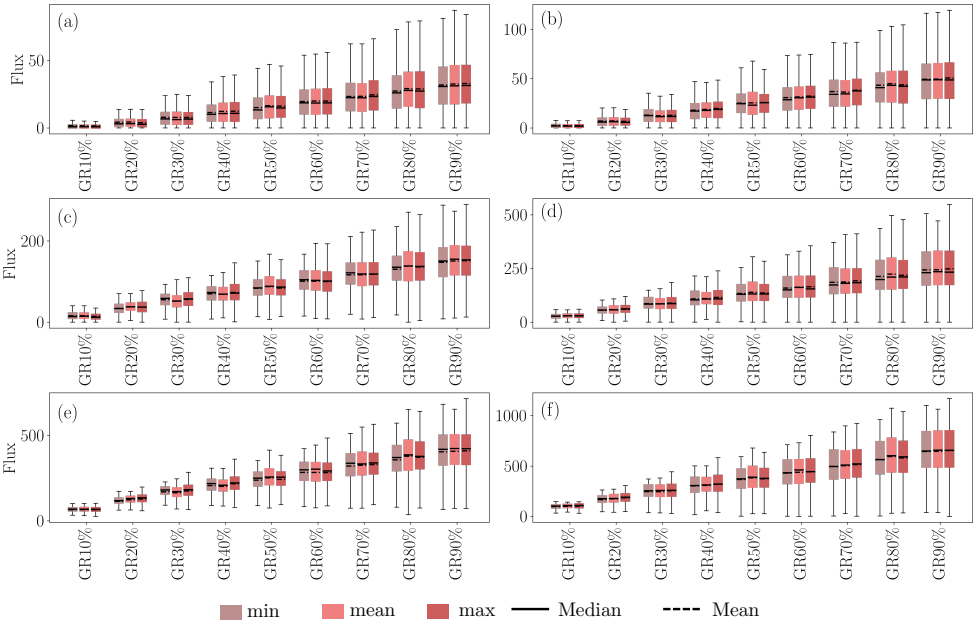

Figure 8.9: Flux value of green roof patches for all scenarios with logarithmic gradation(a)200m, (c)500m, (e)1000m) and semi-linear gradation 2 (species with dispersal distances (b)200m, (d)500m, (f)1000m).

(Figure 8.10 (e)), the mean BC value of green roof patches is higher than dry grassland patches for scenarios with more than 20% potential green roofs.

For species with low mobility, with logarithmic gradation (Figure 8.10 (a)), until 60% green roofing, the mean BC value of green roof patches is less than or equal to the dry grassland patches. Only after retrofitting 70% potential roofs, the mean BC value of green roofs is higher than the dry grassland patches. Similarly, with semi-linear gradation (Figure 8.10 (d)), after implementing green roofs on 40% of the potential buildings, the mean BC values of green roof patches are higher than the dry grassland patches.

BC mainly highlights the number of times a patch is in between other adjacent patches. It is evident that dry grassland patches on roof act more as connectors between other dry grassland patches compared to the ground dry grassland patches because of the spatial arrangement. Additionally, the results show that the green roof patches connect the two habitat patches effectively when more than 10%-20% (lower value is the threshold with semi-linear gradation, higher value is the threshold with logarithmic gradation), of the potential buildings are retrofitted with analogous green

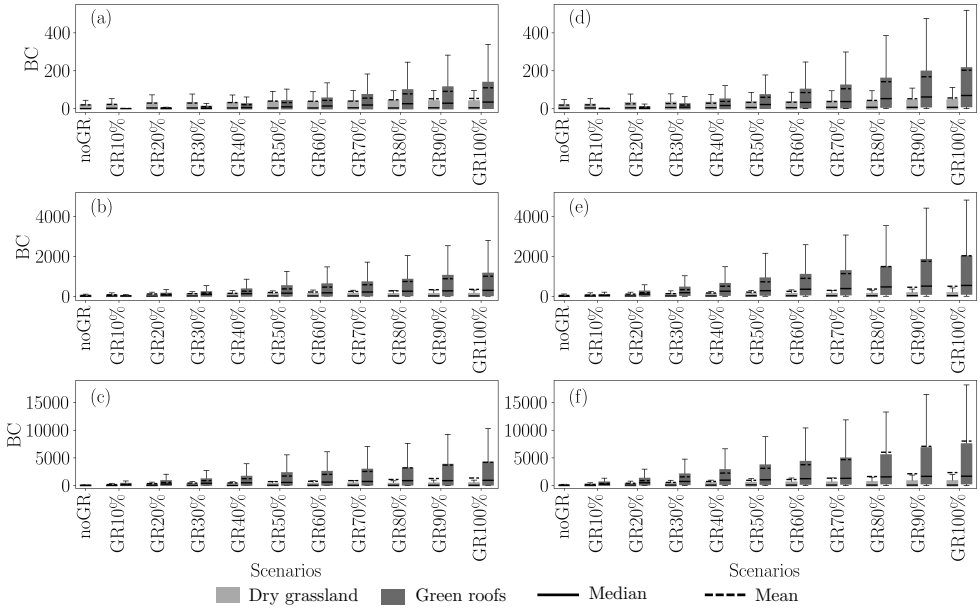

Figure 8.10: Betweenness centrality of green roof and dry grassland patches with non-linear gradation 1 (species with dispersal distances (a)200m, (b)500m, (c)1000m) and semi-linear gradation 2 (species with dispersal distances (d)200m, (e)500m, (f)1000m).

roofs for high mobility species. For moderate mobility species, more than 20-40% of the potential buildings must have green roofs so that green roofs can act as connectors between the existing dry grassland patches. For low mobility species, however, green roofs can act as connectors only after 40-70% of potential green roofing.

Apart from this, many green roof and ground dry grassland patches have zero BC values in all the scenarios (Figure 8.11 (a) and (b)). This means that these patches are not central to the network. With increase in proportion of green roofs, more green roof patches have become central to the network. However, less percentage of green roof are central to the network for low mobility species compared to moderate and high mobility species. This means that green roofs contribute to the centrality more for moderate and high mobility species compared to the low mobility species. On the other hand, introducing green roofs made minimal percentage of dry grassland patches central to the network for all species. Moreover, the percentage of zero valued dry grassland patches are almost similar for all green roof scenarios. This could be because of the location of the dry grassland patches which is in the outskirts, while

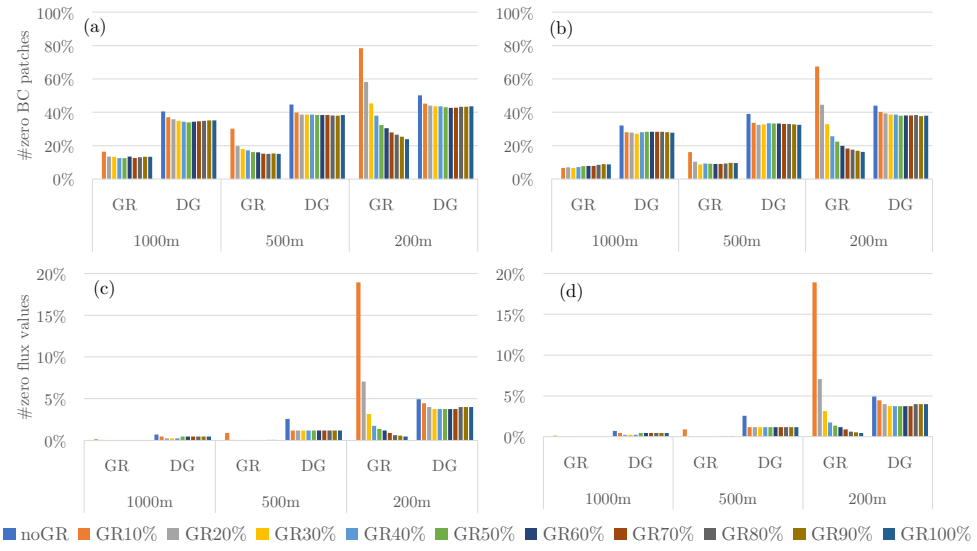

Figure 8.11: Percentage of green roof and dry grassland patches with zero values of BC ((a)logarithmic gradation and (b)semi-linear gradation) and flux (((c)logarithmic gradation and (d)semi-linear gradation)

green roof patches are located centrally in the study area.

Flux

Figure 8.12 compares the flux values of green roof and ground dry grassland patches across all the scenarios for all the species. The mean flux values increases with increase in green roof percentages for green roof and dry grassland patches. However, the increase in mean flux value is higher for green roof patches compared to the dry grassland patches. For the ground dry grassland patches, the mean flux value remains largely same for scenarios with more than 60% roof greening. However, flux value of a few patches of dry grasslands increases for moderate and high mobility species. This means that the dispersal probability of species on ground dry grassland patches is lower compared to the dry grassland patches on roofs. This could be associated to the spatial location of ground dry grassland patches, similar to BC values.

For high mobility species, with logarithmic gradation (Figure 8.12 (c)), the mean flux value of green roof patches is higher than the dry grassland patches for scenarios with more than 20% potential green roofs. However, with semi-linear gradation

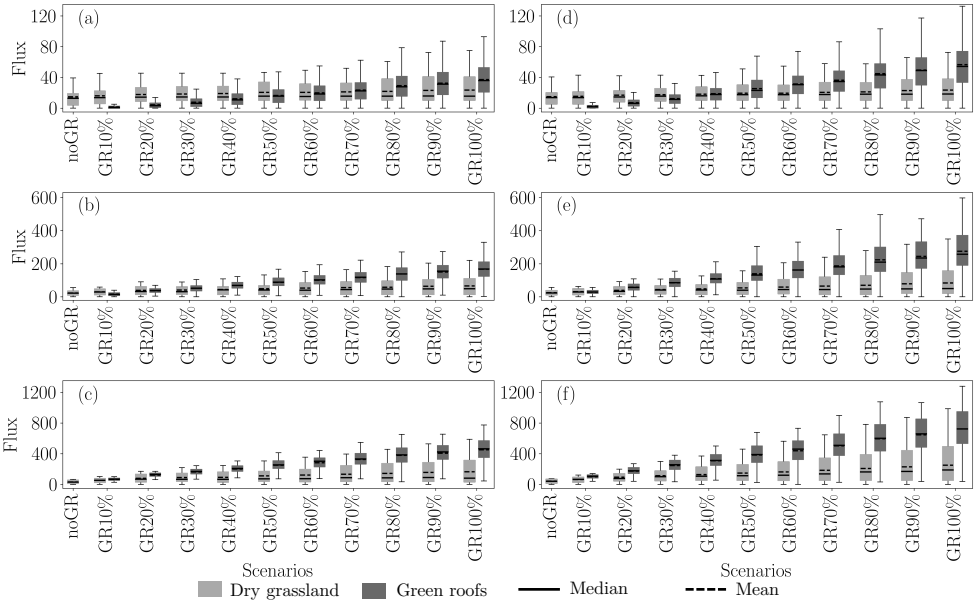

Figure 8.12: Flux values for green roof and dry grassland patches with logarithmic gradation 1 (species with dispersal distances (a)200m, (b)500m, (c)1000m) and semi-linear gradation 2 (species with dispersal distances (d)200m, (e)500m, (f)1000m).

(Figure 8.12 (f)), the mean flux value of green roof patches is always higher than the dry grassland patches. For moderate mobility species, with logarithmic gradation ((Figure 8.12 (b)), the mean flux value of green roof patches is higher than the dry grassland patches for scenarios with 40% or higher potential green roofs. With semi-linear gradation ((Figure 8.12 (e)), for scenarios with 20% or higher potential green roofs, the mean flux value of green roof patches is higher than the dry grassland patches.

For lower mobility scenario, with logarithmic gradation ((Figure 8.12 (a)), the flux value of green roofs is higher than dry grassland patches only after 80% of the potential roof greening, whereas, with semi-linear gradation (Figure 8.12 (d)), the flux value of green roof patches is higher after 50% of potential roof greening.

The flux value indicates the dispersal probability between a central patch and other patches in a landscape. Therefore, the results show that green roof patches help in dispersal flows of species in general. Green roofs aid in dispersal flow for high mobility species when 20% or more potential roofs are greened. While green roofs aid in dispersal flow for 30% or more potential roofs are greened for moderate mobility

species, they aid in the dispersal flow of species for low mobility species only after 50-80% of potential roof greening.

Apart from this, not many green roof patches have zero flux values (<1%) for high and moderate mobility species (Figure 8.11 (c) and (d)). However, the dry grassland patches had a few patches (1-5%) with zero flux values before introducing green roofs. Introducing green roofs has reduced the dry grassland patches with zero flux (1-2%). This means that introducing green roofs does not include more ground dry grassland patches in the network for dispersal. Moreover, there are more zero flux green roof patches for lower mobility species, indicating that the green roofs aid less in dispersal flows for low mobility species compared to moderate and high mobility species.

8.3.3 Effect of rooftop height on ecological network

Building height is a well-known parameter that influences green roofs' role in ecological connectivity. As Liège city has variation in the elevation throughout the city, instead of exact building heights, we analyse the correlation between the height of the rooftop and local metrics (BC and flux). Table 8.2 shows the Pearson's correlation coefficients (r) and highlights the significant correlations for the two gradations, 10 green roof scenarios and three types of species (120 pairs). In logarithmic gradation (60 pairs), the correlation between roof height and BC/flux is negative and statistically significant for 30 pairs. However, for 25 pairs the magnitude of statistically significant correlations is low (between -0.3 and 0, table 8.2). For other 12 pairs the statistically significant correlations are positive (less than 0.2). In 18 pairs, the correlation is insignificant.

In semi-linear gradation, however, the correlation between roof top height and local metrics is negative and statistically significant for all the scenarios. The magnitude of correlation between roof height and flux is low (<0.3). The difference in correlations between the two gradations is logical, given the higher costs for land uses in logarithmic gradation. The cost with slope of landscape (it is 0-100 for buildings and open areas and 150-500 for building and tree edges) is similar to the land use costs in semi-linear gradation (2-100), whereas it is lower than land use costs (1-10000) in logarithmic gradation.

Altogether, in scenarios with both gradations, the correlations are largely negative and statistically significant, suggesting that green roofs placed on buildings with lower heights can better aid in ecological connectivity. However, the correlations with lower magnitude and the statistically insignificant correlations suggest the possible influence of other factors in the role of green roofs in ecological connectivity.

Factors such as the urban configuration around the buildings can influence the role of green roofs in ecological connectivity [359]. For example, we present Figure

Table 8.2: Pearson's correlation coefficient of correlation between of green roof patches and height of buildings with green roofs.

Logarithmic gradation						
Scenarios	BC			Flux		
	1000m	500m	200m	1000m	500m	200m
GR10%	0.01	0.26**	0.17**	-0.02	0.10**	0.12**
GR20%	-0.17**	0.06	0.14**	-0.05	0	0.05
GR30%	-0.22**	0.05	0.20**	-0.05	0.01	0.14**
GR40%	-0.29**	0	0.18**	-0.09**	-0.03	0.11**
GR50%	-0.33**	-0.13**	0.11**	-0.09**	-0.06**	0.05**
GR60%	-0.28**	-0.08**	0.10**	-0.07**	-0.03	0.05**
GR70%	-0.39**	-0.21**	0.02	-0.11**	-0.08**	-0.01
GR80%	-0.42**	-0.26**	-0.02	-0.11**	-0.09**	-0.02
GR90%	-0.40**	-0.24**	-0.03	-0.11**	-0.09**	-0.02
GR100%	-0.42**	-0.27**	-0.08**	-0.11**	-0.09**	-0.04**
Semi-linear gradation						
Scenarios	BC			Flux		
	1000m	500m	200m	1000m	500m	200m
GR10%	-0.49**	-0.40**	-0.10**	-0.20**	-0.21**	-0.11**
GR20%	-0.50**	-0.49**	-0.32**	-0.19**	-0.22**	-0.20**
GR30%	-0.56**	-0.55**	-0.33**	-0.18**	-0.21**	-0.19**
GR40%	-0.53**	-0.52**	-0.31**	-0.17**	-0.19**	-0.15**
GR50%	-0.54**	-0.53**	-0.35**	-0.17**	-0.20**	-0.17**
GR60%	-0.52**	-0.50**	-0.37**	-0.16**	-0.18**	-0.16**
GR70%	-0.55**	-0.54**	-0.43**	-0.17**	-0.19**	-0.19**
GR80%	-0.56**	-0.55**	-0.41**	-0.16**	-0.17**	-0.16**
GR90%	-0.55**	-0.55**	-0.41**	-0.17**	-0.18**	-0.17**
GR100%	-0.56**	-0.55**	-0.42**	-0.16**	-0.18**	-0.17**
Values between -0.3 and 0 highlighted			Values between 0 and 0.3 highlighted in grey			
** - highlights significant correlations (p-value < 0.01)						

8.13 here which compares 10%, 50% and 100% GR scenario spatially for a small central part of Liège. We observe that the green roof on the building with lower height is surrounded by buildings without green roofs which are taller (Figure 8.13 (a)). Same building with 50% potential green roof scenario has a higher flux (Figure 8.13(b)). In the 100% GR scenario (Figure 8.13 (c)), all buildings in that urban block are greened,

and, in this situation, all the buildings have high flux value. This shows that when the short building with green roof is surrounded by taller buildings, the green roof does not contribute much to ecological connectivity. However, when the surrounding buildings also are implemented with green roofs, the same green roof can contribute to the ecological connectivity in a better way. Additionally, the flux value increases when all the tall buildings surrounding the shorter green roof patch are greened. This indicates that even if the building is taller, the green roof top on it can contribute to ecological connectivity if there are several other green roofs nearby.

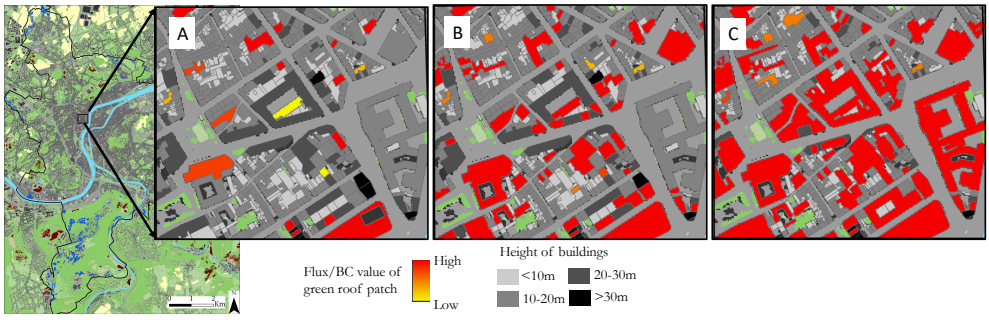

Figure 8.13: Central part of Liège (A) GR10% scenario (B)GR50% and (C)GR100%

8.4 Discussion

Urban dry grasslands, which are crucial for pollinator species, can be restored by creating analogous habitats on potential green roofs in the urban areas of temperate Europe [68–70, 73]. These urban dry grasslands are fragmented due to the exacerbated urbanisation, which has resulted in a reduction in pollinator diversity and resilience [76]. Creating micro-habitats like extensive analogous green roofs between these fragmented dry grasslands is hypothesized to help in improving the ecological connectivity of the dry grassland species [64, 65, 382]. However, no study has analysed the role of retrofitting existing roofs with analogous green roofs in the functional connectivity of urban dry grassland species. Therefore, in this paper we answer the following questions:

1. How does retrofitting existing potential buildings with extensive analogous green roofs affect the functional connectivity of urban dry grassland species?
2. How much percentage of roof greening with analogous green roofs is required to improve the ecological connectivity of species on urban dry grasslands?

We answer the questions by modelling ecological networks for different roof greening percentage scenarios using graph theory. The potential green roofs are the available flat roofs in Liège in this study. A further evaluation of buildings may be required to identify suitable buildings for green roof retrofitting, which might reduce the number of potential green roofs in the city. We incorporate this uncertainty by analysing 11 different scenarios, with one scenario without green roofs and ten scenarios with different potential green roof percentages (from 10 to 100%). We mainly generate landscape graphs, which are composed of dry grassland habitat patches on the ground (existing patches) and on roofs (potential green roofs). The links in the landscape graphs are constructed using the least cost distance computed with costs assigned to each land use with logarithmic and semi-linear gradation (Table 8.1). We also add the additional costs of altitude with DSM of the study area. Unlike previous studies, we use detailed land use (ecotope database) with classified urban green and artificialized spaces to ensure comprehensive computation of resistances in urban landscapes for pollinators. We also analyse the effect of random selections of potential roofs in each scenario from 10% to 90% to understand the robustness of the results.

We first analysed the global connectivity of the landscape in each scenario using PC metric, which shows how interconnected the habitats in the landscape. Our results suggest that introducing green roofs in the landscape increases the interconnectedness of the dry grassland patches in the study area. However, this probability varies for species with respect to their mobility. For instance, with an increase in green roofs, there is a larger increase in connectivity for high-mobility species, followed by moderate and then low-mobility species. For low-mobility species, the improvement in global connectivity with an increase in green roof percentage is limited. This result is similar to the results obtained in a few studies [119, 383], where habitat connectivity supported the community composition of high-mobility species more than low-mobility species. Low-mobility species were more impacted by the local environmental conditions.

Secondly, we analysed the local connectivity using patch metrics such as BC and flux. Generally, we observe that overall, the dry grassland (on roof and ground) patches have higher BC and flux values for scenarios with higher potential green roof percentages. This means that introducing green roofs generally aids in connecting the dry grassland patches and dispersal flows. Since we analyse two gradations, we obtain two threshold values for each species.

To enhance the role of green roofs as connectors between all dry grassland patches (roof and ground), more than 10-20% potential roofs for high mobility species, more than 20-40% potential roofs for the moderate mobility species and more than 40-70% potential roofs for the low mobility species, should be greened. On the other hand, to

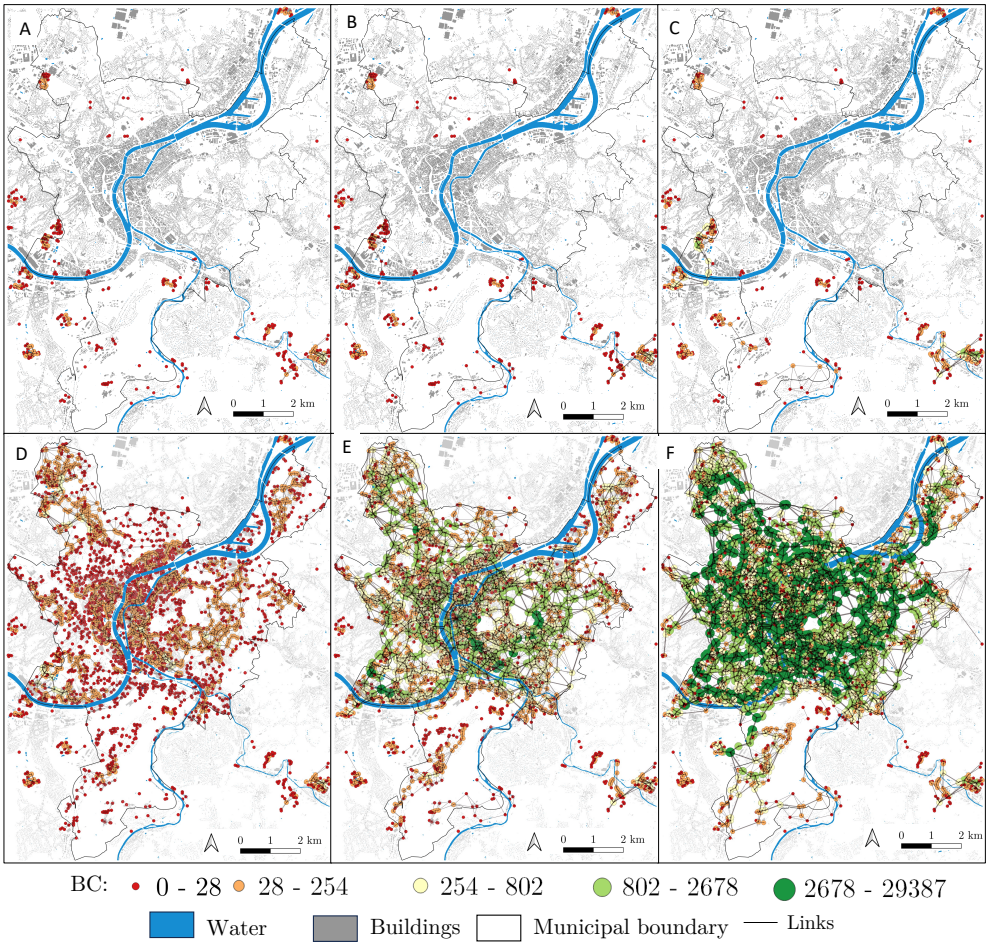

Figure 8.14: Spatial presentation of BC values for scenario with no green roofs ((a) low-mobility, (b) moderate mobility (c) high mobility species), for scenario with 50% green roofs ((d) low-mobility, (e) moderate mobility (f) high mobility species)

enhance the role of green roofs in dispersal flows, more than 20% potential roofs for high mobility species, more than 30% potential roofs for moderate mobility, and more than 50-80% potential roofs for low mobility species should be greened. For the low-mobility species, the value of BC and flux on ground dry grassland patches is higher with less than 50% roof greening. The reason could be the tendency of low-mobility species communities to stay connected to ground [119]. In addition to this, more green roofs have zero BC value, and very few green roof patches have zero flux value,

indicating green roofs' role is more prominent in dispersal flows than as connectors.

The local connectivity analysis also points out that the BC and flux values of dry grassland patches on the ground are lower than the patches on the roof. We can see this spatially in Figure 8.14 which shows a spatial comparison of BC values of patches between scenario without green roofs and scenario with 50% roofs greened. With 50% roof greening, there is not much difference in the BC values of existing ground grasslands. Moreover, the BC and flux values of ground dry grassland patches exhibit a slower increase with rising green roof percentage compared to green roof patches. This is mainly because of the spatial location of existing dry grassland patches in the periphery, while the roofs are in the centre, forming a more compact network (Figure 8.14 (D, E, and, F)). Therefore, an increase in green roofs primarily creates a network of highly connected dry grasslands on roofs but has limited impact on the connectivity of existing ground grasslands, especially for low-mobility species.

We also observed a statistically significant and negative correlation between the values of local metrics of green roof patches and roof height for most of the scenarios and species. These results match MacIvor [384] and Madre et al. [385], which advocate that buildings with low height are better for functional composition on green roofs. However, for a few scenarios in this study, the magnitude of statistically significant correlations was low or positive, and a few of them were also insignificant. This indicated a possibility of other factors influencing green roofs' role in ecological connectivity, like their surrounding urban configuration. It can explain why some studies [355, 383] did not find height as a significant parameter to indicate community composition.

8.5 Conclusions

Our main objective with this paper was to understand whether analogous green roofs can contribute to the ecological connectivity of dry grasslands in Liège, Belgium. We identified that analogous green roofs create a network of highly connected dry urban grassland habitats in the centre but have a limited impact on the connectivity of existing dry grasslands. Nevertheless, with an increase in analogous green roofs, the connectivity and dispersal of high and moderate-mobility species have increased, but there is no significant impact on the low-mobility species. We also found out that retrofitting half of the potential green roofs will improve the connectivity for high and moderate-mobility species specific to dry grasslands. However, almost all potential roofs need to be greened to improve the connectivity for lower mobility species. Along with this, the study, while confirming that rooftop height negatively influences connectivity, highlights the influence of other factors, such as urban configuration

and local environmental conditions, in improving the connectivity of dry grassland species [119,359]. Future studies should analyse the effect of green roofs' surroundings and height on their' contribution to ecological connectivity. In the study, we used two gradations to compute the resistance maps for the species. However, a combination of actual biological responses can help in assigning more realistic gradations for analysing ecological networks. This would require long-term monitoring of species mobility and green roofs with dry grasslands.

Our study is the first one to analyse extensive analogous green roof's role at a city scale in improving the connectivity of dry grasslands, which have become rare in the temperate European context. Moreover, habitats similar to dry grasslands on extensive green roofs can increase the occurrence of indigenous species and natural habitats for urban fauna. Although our approach is explorative, it certainly helps in providing realistic expectations with retrofitting lower to higher proportions of green roofs in the city. Since we use the detailed land use data for this analysis, our results are indicative of green roofs' usefulness in increasing the occurrence of dry grasslands along with increasing the connectivity of species such as bees, butterflies and other pollinator species. Additionally, the results of this study are specific to Liège City, however, the methodology can be utilised for other regions.

8.6 Key contributions

- This approach helps in providing realistic expectations with retrofitting lower to higher proportions of green roofs in the city.
- Analogous green roofs mainly create a network of highly connected dry urban grassland habitats in the centre but have a limited impact on the connectivity of existing dry grasslands.
- Greening approximately 50% of potential roofs with analogous habitats in Liège facilitates the movement of high and moderate-mobility flying species across dry grasslands.
- To support low-mobility flying species, greening around 80% of potential roofs is necessary. Although challenging to achieve in the short term, it proves more feasible than creating intensively managed urban parks, which do not attract a diverse variety of pollinators.
- Building heights and urban configurations can strongly influence the role of green roofs in ecological connectivity.

Part IV

Conclusions

9 General Conclusions

Green roofs, a sustainable alternative to conventional roofs, provide multiple ecosystem services. However, no study uses realistic fractions of green roofs to analyse their impact on UHI mitigation or ecological networks at a city scale. Moreover, given the limited research available at a city-scale, this study sought to assess the role of realistic roof greening in improving the urban climate and habitat. In this chapter, the PhD work is concluded by revisiting the research question and recommending possible further research in the area.

9.1 Revisiting research questions

Q1: What is the existing potential of green roofs in the city?

NBSs are recognized as important instruments in addressing urban environmental problems by providing ecosystem services. NBSs such as green roofs are gaining popularity owing to their multiple benefits and their ability to provide these benefits in compact cities. Chapter one showed that Liège has around 22% (486 hectares) of flat roof area, in which around 439 hectares are flat roofs with an area greater than 100 m^2. When further analysed for the structural strength of buildings in the city, Liège city offered a green roof potential area of about 350 hectares on 20% of the total number of buildings in the city. According to the analysis for priority zones,

we observed that the high-priority zone mainly comprises regions in the city centre near the river and some parts in the east, characterised by social deprivation and lack of green spaces. Based on the discussed benefits in the literature, developing green roofs in this zone can yield maximum benefits. We observed that the potential of green roofs in the high-priority zones, as compared to the moderate-priority zone, is low in terms of the number of roofs but is significant in terms of the area of roofs. Moreover, the high-priority zone of Liege, especially the region in the city's centre, has a significantly high built-up density, making green roof implementation extremely relevant. We targetted flat roofs with a roof area greater than 100 m^2 (8311 buildings, 436 ha) as the realistic potential to answer the rest of the questions in this PhD.

Q2: How will realistic roof greening impact the Urban heat island effect in different morphologies at the city scale?

This question was answered using three approaches. Chapter three identified the impact of realistic roof greening on the UHI effect using a high-resolution WRF study using BEP-BEM parameterization with LCZ as land-use classification. The resolution of this regional-scale study was 333m. Unlike most studies that solely focus on averages, this approach presents air and surface temperatures with spatial, temporal and typological variability. The study concluded that realistic roof greening may not significantly reduce the UHI effect, especially for air temperature. The decrease in air and surface temperature in each LCZ depends on the urban morphological characteristics of that LCZs and the roofs available for greening.

Although LCZs are widely used, they are generic and cannot capture the peculiarities of every urban area. Moreover, LCZs are raster-based, and urban planners and architects may find it challenging to utilise LCZs for policy-making as they predominantly use urban blocks as design and policy units. Therefore, a second approach was employed (chapters four and five) to analyse the local microclimate. In chapter four, nine distinct urban morphological clusters were determined using a systematic clustering approach on urban blocks with an exhaustive list of morphological parameters. Thereafter, nine distinct morphological archetypes representing the clusters were chosen by identifying the urban block nearest to the respective cluster centres.

Since the obtained nine archetypes represent the urban blocks of the city, analysing their microclimates can provide ideas for the initial implementation of green roofs in the clusters with the representative archetype that shows maximum reduction in air and surface temperature in the block. Therefore, the impact of realistic roof greening in the nine morphological archetypes on the local microclimate was assessed in Chapter Five. Chapter five concludes that the nine archetypes vary in terms

of air and surface temperature. Due to the variation in urban morphology in the archetypes, the impact of roof greening in these archetypes is also distinctive. The results obtained from the regional scale study and the block scale study are similar. For instance, realistic roof greening effectively reduces air and surface temperature in large low-rise archetypes/LCZs. Additionally, when all the roofs are greened, compact low-rise archetypes of LCZs are effective in reducing temperatures. However, the lesser availability of potential roofs for greening reduces the impact of green roofs there. The block scale study, however, advances the WRF-based analysis of green roofs' impact on UHI in various LCZs by offering an implementable scale for planners and higher resolution. The impact of green roofs is seen on both air and surface temperatures, especially in large low-rise archetypes where a large roof is greened. The impact on surface temperature is much higher compared to air temperature, especially at block scale. This could positively affect indoor temperature. This means that locally, green roofs impact significantly more than at city-scale.

The aforementioned two approaches to analyse the role of green roofs in mitigating urban climate use numerical modelling and simulations. However, models like Solene-microclimat cannot be employed for all the blocks in the city due to computational demands. While mesoscale models WRF coupled with UCM aid in conducting research at a regional scale, running these models at high resolution requires significant computational resources. Therefore, most of the WRF studies are carried out at a resolution of 1 km [141, 155]. Moreover, analysing and processing these models are generally challenging for most urban planners [332]. Therefore, remote sensing approaches can be useful as finer-resolution datasets are increasingly available with open data worldwide. Hence, in chapter six, the random forest (RF) regression model was applied to predict the impact of green roofs on surface UHI using the land surface temperature (LST) obtained from the Landsat-8 satellite image. Chapter six concludes that green roofs reduce the average LST in the cities. The reduction in LST is higher when the green roofs have higher NDVI (intensive greening). This approach successfully indicates the potential of green roofs for reducing LST in cities. However, the RF regression model does not predict extreme temperatures accurately. Therefore, other machine-learning models must be compared and explored.

All three approaches suggest that green roofs reduce the study area's air or surface temperatures. At regional or city scales, realistic roof greening may not be sufficient. However, both WRF-based and remote sensing approaches highlight that realistic roof greening may be effective in some parts of the city/region. At the block scale, realistic roof greening can be extremely beneficial in reducing the surface temperatures of the block. However, for a significant reduction in air temperature, the building height must be smaller, and the building area must be larger.

Policy recommendations: UHI mitigation

- Existing roofs in compact, large low-rise and large low-rise archetypes can be usefully retrofitted with green roofs.
- Proposed buildings can include green roofs if the buildings are low-rise.
- Green roofs can be integrated into the city master plans if the proposed expansion has dense and predominantly mid-rise or low-rise buildings.
- Lastly, green roofs must be accompanied by other mitigation solutions to obtain a significant impact on temperatures.

Limitations

There are a few limitations and considerations for the study. The impact of green roofs is modelled physically using energy and water balances, factoring in net radiation, precipitation, irrigation, vegetation evapotranspiration, atmospheric heat exchange, and soil energy and moisture diffusion in regional and block scale studies with WRF and Solene-microclimat model respectively. Both regional and block scale studies are conducted employing the WRF and Solene-microclimat models, respectively.

Within the WRF model, green roofs (Approx. 30 cm in width) are simulated as roofs with either grass or sedum, each characterized by distinct albedos (0.154 and 0.3, respectively). Currently, the type of green roof and irrigation are the adjustable parameters, with a focus on grass-covered roofs due to their biodiversity benefits. The Solene-microclimat model allows the users to categorise green roofs based on albedo, emissivity, and evapotranspiration rates. In this study, the established optimal settings for green roofs are adopted to delve into the interplay between urban morphology, green roofs, and temperature.

The impact of green roofs on air and surface temperatures is dependent upon the specific properties defined by the user. Consequently, alterations in the user-defined parameters may lead to varied outcomes in terms of green roof's effectiveness in regulating urban climate. Performing a sensitivity analysis was out of the scope of this dissertation. However, conducting a sensitivity analysis on parameters related to green roofs, such as albedo, emissivity, and irrigation, is crucial.

Apart from this, the remote-sensing approach at a city-scale models green roofs using NDVI values. As many green spaces may have similar NDVI values, utilising parameters such as albedo of the roofs can improve the analysis.

Lastly, we have simulated green roofs on all the flat roofs in Liège for regional

and block-scale studies. For the city-scale study, we simulated green roofs on flat roofs greater than 100 m^2. Although this assumption is realistic compared to an extreme scenario (100% greening), not all buildings that are flat can have the capacity to hold a green roof. The reduction in temperature obtained with the approaches in this dissertation may further reduce when the structural strength of the building is considered.

Q3: What is the role of green roofs in urban ecological connectivity?

The research on green roofs' role in ecological networks is fairly limited. While urban dry grasslands offer suitable habitats for endangered pollinator species [69, 70], they have become scarce in temperate Europe due to anthropogenic activities [73]. Creating analogous habitats, which are the sites that resemble natural habitats hosting indigenous biodiversity, is crucial for restoring species-rich dry grasslands in urban areas [68, 382]. Urban dry grasslands are often highly fragmented and isolated, declining the pollinator diversity and functional dispersion of insect species, diminishing their ecological resilience [66, 76]. Creating micro-habitats of dry grasslands in the form of analogous green roofs between existing ground grasslands in a city can help restore and improve functional connectivity for pollinators in the city. Chapters seven and eight investigate the role of extensive green roofs in the ecological network of dry grasslands.

Chapter seven used Euclidean distance to analyse the proximity of potential green roofs near existing dry grasslands. The results show that the green roofs are located near the existing dry grassland sites, i.e. within 200 and 1000m foraging distance. Thus, they could be beneficial in improving the connectivity for small and large bees. Since factors such as landscape elevation and land use hinder the species' movements, Chapter Eight analysed the role of green roofs in the ecological connectivity of dry grasslands in detail using graph theory. Additionally, we used the dry grassland sites from the ecological network established for the city in chapter seven, as the data was available at the time. However, since this ecological network does not provide all the possible sites of existing dry grasslands, we utilised the most recent ecotope database to enhance our analysis in chapter eight. Chapter eight shows that extensive analogous green roofs can strengthen the ecological networks of dry grasslands. Analogous green roofs mainly create a network of highly connected dry urban grassland habitats in the centre but have a limited impact on the connectivity of existing dry grasslands. Nevertheless, with an increase in analogous green roofs, the connectivity and dispersal of high and moderate-mobility species have increased, but there is no significant impact on the low-mobility species. Additionally, retrofitting half of the potential

green roofs will improve the connectivity for high and moderate-mobility species specific to dry grasslands. However, almost all potential roofs need to be greened to improve the connectivity for lower mobility species. Along with this, the study, while confirming that rooftop height negatively influences connectivity, highlights the influence of other factors, such as urban configuration and local environmental conditions, in improving the connectivity of dry grassland species.

Policy recommendations: Ecological connectivity

- Potential roofs for improving ecological connectivity of dry grasslands should not be surrounded by taller buildings without green roofs.
- Potential roofs that are on higher elevation, located between impervious areas or in the middle of forest regions, can be prioritised later for greening since they do not contribute much to the ecological networks
- For lower mobility species, other ground-level impervious areas in the city can be greened with analogous habitats in addition to the green roofs.
- For lower mobility species, it may be beneficial to add analogous green roofs in the neighbouring cities to increase connectivity at a regional scale.

Limitations

The dissertation prospectively analyses the green roof's role in ecological connectivity, and the approach used is explorative and theoretical. Therefore, some simplified assumptions to successfully perform the analysis were necessary, which were also limitations of the study.

Firstly, it was assumed that all the flat roofs could act as potential green roofs. Further investigation of the structural strength of buildings may reduce the number of potential green roofs in the city. To address this, we analyzed scenarios with different GR potentials. However, further research can include the evaluation of more realistic potential green roofs.

Secondly, green roofs were assumed as habitats similar to dry grassland also in terms of quality. Extensive green roofs can be created as analogous green roofs. However, the habitat quality may vary from the historic ground dry grassland habitat. To confirm our result based on this assumption, analogous green roofs need to be studied for habitat quality. This is important as habitat quality is more important for the specialist species [386].

Thirdly, we assume different resistance values based on gradations due to a lack of empirical data on actual resistances. Further research needs to be done to collect biological data to model ecological networks more realistically.

Apart from this, it is observed that the existing dry grasslands that are away from the city area remain isolated. This could be due to the potential roofs considered only within the Liège city boundary. If the study includes all the potential roofs even outside the Liège city (which is out of scope), the results would be different. Further research can analyse the role of extensive green roofs at a regional scale to test this.

9.2 Ease of Application: Proposed approaches

The approaches employed in this dissertation to assess the contributions of green roofs to urban climate regulation and biodiversity enhancement can be applied in other regions. These methodologies primarily rely on data-driven approaches. The physical models, such as Solene-microclimate and WRF, are well-documented and openly accessible, making them adaptable to various geographic locations. However, it's important to note that accurately estimating the potential green roofs requires access to LiDAR databases, which may not be universally available.

In particular, the Solene-microclimat model needs detailed 3D geometries to construct urban blocks. In our analysis, we focused on blocks specific to Liège, obtained through clustering of various urban morphological parameters. The feasibility of adopting this approach elsewhere is subject to the availability of 3D building datasets. Additionally, conducting Solene-microclimat simulations for larger or additional blocks may pose computational challenges and time constraints. The remote-sensing approach uses largely open-source data and due to the statistical modelling, the computational load of running physical models like WRF or Solene-microclimat is also reduced. However, the accuracy of this approach needs to be improved further.

Furthermore, in the analysis of green roofs' impact on ecological connectivity, the study relied on the ecotope database specific to the Walloon region of Belgium to identify significant dry grassland habitats within and around the city. To apply a similar approach in other regions, access to region-specific datasets or knowledge regarding habitats suitable for development on green roofs is essential.

Overall, while the approaches presented in this dissertation aid in the systematic analysis of green roofs' role in ecosystem services at city scale, their applicability in diverse geographic contexts is dependent on the availability of relevant data and resources tailored to each region.

9.3 Synergistic Urban Planning with Green Roofs

The dissertation comprehensively analyses the ecosystem service of urban heat island mitigation and enhancing biodiversity provided by realistic roof greening. Based

on the conclusions, realistic roof greening may not be beneficial in reducing air and surface temperatures at a city or regional scale. However, realistic roof greening can aid locally in regulating the microclimate in terms of air and surface temperatures in large low-rise archetypes. Additionally, realistic roof greening with analogous green roofs can increase the network of dry grasslands within the city and improve the ecological connectivity for high and medium-mobility species. For lower-mobility species, a regional network of analogous green roofs can be helpful.

With the focus on two ecosystem services, optimal conditions in which green roofs can be useful to provide each ecosystem service efficiently were obtained. For instance, retrofitting green roofs on large low-rise buildings can regulate the local microclimate and can contribute to the functional connectivity of flying insects in the cities. However, for improving the connectivity of flying insect specialist dry grassland species, retrofitting green roofs in just a few blocks, may not be sufficient.

In addition to this, realistic roof greening may not be sufficient to regulate the UHI effect at city- or regional scale. However, when combined with other mitigation strategies, such as cool roofs or solar photovoltaics, green roofs can contribute to a noticeable reduction in air temperatures at a city scale while simultaneously enhancing biodiversity. Moreover, Riviére [387] and Kazemi [388] highlight the benefits of green roofs in stormwater management. Therefore, while green roofs may not singularly address all urban environmental challenges, their integration into broader urban planning strategies can yield substantial benefits across multiple ecosystem services.

9.4 Recommendations for future research

Several directions and recommendations for future research can be drawn from this work. I have worked with several approaches and at different scales in this thesis. Every approach in itself is a vast field of research with several possibilities. With progress in this PhD, I came across several research ideas and directions for the future.

1 Green roof potential may not be very high for a single ecosystem but more effective when a combination of ecosystem services is considered. Therefore, other ecosystem services also should be analysed in the future.
2 This study provided suitable areas where installing green roofs can be beneficial for regulating climate and habitat. Future studies need to focus more on prioritising the implementation zones and interactions and collaborations with stakeholders in living lab experiments.
3 In the WRF-based approach, we utilised the existing LCZ dataset for Europe for this study. Although the analysis provided us with useful insights, LCZs

specifically curated for the study area can be used for such a study. Future research can be done to integrate the urban morphological clusters and WRF simulations, increasing the accuracy of the results.

4 We identified nine urban morphological archetypes using a systematic clustering approach in Liège. This approach can be used for a group of cities in Wallonia or the entire region to obtain morphological archetypes specific to the region for comparison studies in future.

5 We analysed the impact of green roofs on local microclimate using Solene-microclimat. Here, we assigned evapotranspiration constant and albedo for green roofs, considering an extensive type of green roof. Further studies can explore different types of green roofs and experiment with different evaporation constants and albedos by doing a sensitivity analysis of the model. Future studies can also incorporate hydrological models to model green roofs to improve accuracy.

6 In this PhD, two physical models (WRF and Solene) and one inference model (machine learning) were used for analysing green roofs' impact on the UHI effect. Running physical models is challenging as they are data-demanding and require high computational resources [155]. Inference models using openly available remote-sensing datasets can be helpful, however, the accuracy of these models depends on various factors. Therefore, there is a need to combine the physical models with inference models. Further research can explore the training of machine learning models using the results from physical models.

7 Here, we compared urban blocks (chapter five) and two cities (chapter six). More comparative studies on green roofs impact on UHI, for instance, for peri-urban and urban area, small and large cities or multiple cities in a region can enhance our understanding on the subject.

8 Unlike UHI mitigation, city-scale studies on green roofs' role in urban biodiversity are limited (just 2). More such studies are needed. Additionally, an integration of experimental studies analysing actual biological responses and modelling studies is necessary for analysing realistic costs of species movements. This would require long-term monitoring of species mobility and green roofs with dry grasslands.

9 Here we consider flat roofs to be suitable for greening. However, other roof-based mitigation strategies such as cool roofs and solar PVs are also helpful for UHI mitigation [120, 157]. In central European countries solar PV modules are highly subsidized for rooftops, whereas little attention has been paid to subsidizing green roofs [389], because of this green roofs always appear in competition with other strategies. Photovoltaic-green roofs [390], although recent,

offer environmental and economic benefits [391]. Future studies can analyse a combination of these solutions and photovoltaic-green roofs at various scales.

9.5 List of publications

9.5.1 Peer-reviewed journal/conference articles/book chapters

1 Joshi, M. Y., & Teller, J. (2021). Urban Integration of Green Roofs: Current Challenges and Perspectives. Sustainability, 13 (22), 33. doi:10.3390/su132212378 (Journal article)

2 Joshi, M.Y., Selmi, W., Binard, M., Nys, G.-A., & Teller, J. (2020). Potential for urban greening with green roofs: A way towards smart cities. ISPRS Annals of the Photogrammetry, Remote Sensing and Spatial Information Sciences, VI-4 (W2-2020), 87–94. doi:10.5194/isprs-annals-VI-4-W2-2020-87-2020 (Conference paper)

3 Joshi, M. Y., & Teller, J. (2023). Employing a highly resolved WRF-LCZ model to identify the influence of a realistic potential of green roofs in mitigating heatwave. Science of Total Environment. (Under review) (Journal article)

4 Joshi, M., Rodler, A., Musy, M., Guernouti, S., Cools, M., & Teller, J. (2022). Identifying urban morphological archetypes for microclimate studies using a clustering approach. Building and Environment. doi:10.1016/j.buildenv.2022.109574 (Journal article)

5 Joshi, M., Rodler, A., Musy, M., Guernouti, S., Cools, M., & Teller, J. (2023). Influence of urban morphology on the potential of green roofs in regulating local microclimate: A case study of Liège, Belgium. Urban Climate. (under review) (Journal article)

6 Joshi, M., Aliaga, D. G., & Teller, J. (2023). Predicting Urban Heat Island Mitigation with Random Forest Regression in Belgian Cities. In Urban Book Series. Springer Science and Business Media Deutschland GmbH. doi:10.1007/978-3-031-31746-0_16 (book chapter)

7 Joshi, M., Rivière, L., Mahy, G., & Teller, J. (2021). Effectiveness of green roofs in strengthening ecological networks. International Archives of the Photogrammetry, Remote Sensing and Spatial Information Sciences, XLVI-4/W1-2021, 51-54. doi:10.5194/isprs-archives-xlvi-4-w1-2021-51-2021 (Conference paper)

8 Joshi, M., Rivière, L., Bourdouxhe, A., Pollet, T., Coppée, T., Mahy, G., & Teller, J. (2024) Exploring the impact of prospective extensive analogous green roofs on the functional ecological connectivity of urban dry grassland species. Landscape and Urban Planning. (Ready to submit) (Journal article)

9.5.2 Conference presentation and posters

9. Joshi, M. Y., Rohon, S., Nys, G.-A., & Teller, J. (30 March 2021). Potential of green roofs in the East bank of Liege, Belgium. Paper presented at EARSeL Joint Workshop 2021, Liege, Belgium, Belgium.

10. Joshi, M., & Teller, J. (09 June 2021). Identifying urban typologies to analyze impact of green roofs on microclimate regulation. Paper presented at The 17th International Conference on CUPUM - Computational Urban Planning and Urban Management, Helsinki, Finland.

11. Joshi, M., Rivière, L., Mahy, G., & Teller, J. (28 June 2023). Contribution of green roofs to urban ecological network at a city scale. [Paper presentation] World Green Infrastructure Congress 2023, Berlin, Germany.

12. Joshi, M., & Teller, J. (28 August 2023). Green roof's role in mitigating heatwave in Liege, Belgium: A highly resolved WRF-based study with LCZ. [Paper presentation] International Conference on Urban Climate (ICUC), Sydney, Australia.

13. Rivière, L., Kazemi, M., Joshi, M., Mahy, G., Courard, L., & Teller, J. (04 May 2022). CityRoof -Analogous green roofs for cities in Wallonia. Poster session presented at DS²BE, Ghent, Belgium.

14. Joshi, M., & Teller, J. (October 2021). Analogous green roofs for cities and citizens. [Poster presentation] UEE Day, Liege, Belgium.

15. Joshi, M., & Teller, J. (November 2022). Impact of green roofs on surface urban heat island using random forest regression: A case study in Liege, Belgium. [Poster presentation] session presented at Urban Transitions, Sitges, Spain.

9.5.3 Other publications not included in PhD

16. Amaripadath, D., Joshi, M., Hamdy, M., Petersen, S., Stone Jr., B., & Attia, S. (2023). Thermal resilience in a renovated nearly zero-energy dwelling during intense heat waves. Journal of Building Performance Simulation, 1-20. doi:10.1080/19401493.2023.2253460

17. Schelings, C., Barcelloni Corte, M., Privot, J., Bianchet, B., Joshi, M., & Teller, J. (2023). Vulnérabilité et chemin de dépendance : quelle est notre marge d'adaptation au changement climatique ? Paper presented at 24èmes rencontres internationales en urbanisme de l'APERAU, Lausanne, Switzerland.

18. Joshi, M., Flacke, J., & Schwarz, N. (2020). Do microfinance institutes help slum-dwellers in coping with frequent disasters? An agent-based modelling study. International Journal of Disaster Risk Reduction, 49. doi:10.1016/j.ijdrr.2020.101627.

References

[1] T. R. Oke, "City size and the urban heat island", Atmospheric Environment (1967) **7**, 769–779 (1973).

[2] T. R. Oke, *Boundary layer Climates* (Routledge) (1987).

[3] G. Ouzeau, J.-M. Soubeyroux, M. Schneider, R. Vautard, and S. Planton, "Heat waves analysis over france in present and future climate: Application of a new method on the euro-cordex ensemble", Climate Services **4**, 1–12 (2016).

[4] M. Joshi, D. Amaripadath, A. Machard, and S. Attia, "Heatwaves identification classification and visualisation with python", (2022).

[5] A. Machard, "Amachard/assembling-future-weather-files-including-heatwaves: V1. 0.0", (2022).

[6] G. Bennett, *Integrating biodiversity conservation and sustainable use: lessons learned from ecological networks* (IUCN) (2004).

[7] S. E. Bibri and J. Krogstie, "Smart sustainable cities of the future: An extensive interdisciplinary literature review", Sustainable cities and society **31**, 183–212 (2017).

[8] U. Habitat, *State of the world's cities 2012/2013: Prosperity of cities* (Routledge) (2013).

[9] E. Gómez-Baggethun and D. N. Barton, "Classifying and valuing ecosystem services for urban planning", Ecological economics **86**, 235–245 (2013).

[10] K. Oh, D. Lee, and C. Park, "Urban ecological network planning for sustainable landscape management", Journal of Urban Technology **18**, 39–59 (2011).

[11] E. Cuce, "Thermal regulation impact of green walls: An experimental and numerical investigation", Applied Energy **194**, 247–254 (2017).

[12] B. Stone Jr, "Urban sprawl and air quality in large us cities", Journal of environmental management **86**, 688–698 (2008).

[13] S. S. Herrera-Gomez, A. Quevedo-Nolasco, and L. Pérez-Urrestarazu, "The role of green roofs in climate change mitigation. a case study in seville (spain)", Building and Environment **123**, 575–584 (2017).

[14] H. Akbari, S. Menon, and A. Rosenfeld, "Global cooling: increasing world-wide urban albedos to offset co2", Climatic change **94**, 275–286 (2009).

[15] J. B. Almenar, T. Elliot, B. Rugani, B. Philippe, T. N. Gutierrez, G. Sonnemann, and D. Geneletti, "Nexus between nature-based solutions, ecosystem services and urban challenges", Land use policy **100**, 104898 (2021).

[16] N. Bauduceau, P. Berry, C. Cecchi, T. Elmqvist, M. Fernandez, T. Hartig, W. Krull, E. Mayerhofer, N. Sandra, L. Noring, *et al.*, *Towards an EU research and innovation policy agenda for nature-based solutions & re-naturing cities: Final report of the horizon 2020 expert group on'nature-based solutions and re-naturing cities'* (Publications Office of the European Union) (2015).

[17] C. Cortinovis, P. Olsson, N. Boke-Olén, and K. Hedlund, "Scaling up nature-based solutions for climate-change adaptation: Potential and benefits in three european cities", Urban Forestry & Urban Greening **67**, 127450 (2022).

[18] N. Kabisch, H. Korn, J. Stadler, and A. Bonn, "Nature-based solutions to climate change adaptation in urban areas; theory and practice of urban sustainability transitions", (2017).

[19] D. E. Pataki, M. Alberti, M. L. Cadenasso, A. J. Felson, M. J. McDonnell, S. Pincetl, R. V. Pouyat, H. Setälä, and T. H. Whitlow, "The benefits and limits of urban tree planting for environmental and human health", Frontiers in Ecology and Evolution **9**, 603757 (2021).

[20] M. Grace, M. Balzan, M. Collier, D. Geneletti, J. Tomaskinova, R. Abela, D. Borg, G. Buhagiar, L. Camilleri, M. Cardona, *et al.*, "Priority knowledge needs for implementing nature-based solutions in the mediterranean islands", Environmental Science & Policy **116**, 56–68 (2021).

[21] Y. R. Jabareen, "Sustainable urban forms: Their typologies, models, and concepts", Journal of planning education and research **26**, 38–52 (2006).

[22] M. Jenks and C. Jones, *Dimensions of the sustainable city* (Springer Science & Business Media) (2009).

[23] W. Liu, W. Wei, W. Chen, R. C. Deo, J. Si, H. Xi, B. Li, and Q. Feng, "The impacts of substrate and vegetation on stormwater runoff quality from extensive green roofs", Journal of hydrology **576**, 575–582 (2019).

[24] T. Sangkakool, K. Techato, R. Zaman, and T. Brudermann, "Prospects of green roofs in urban thailand–a multi-criteria decision analysis", Journal of cleaner production **196**, 400–410 (2018).

[25] M. Shafique, R. Kim, and M. Rafiq, "Green roof benefits, opportunities and challenges–a review", Renewable and Sustainable Energy Reviews **90**, 757–773 (2018).

[26] X. Zhang, L. Shen, V. W. Tam, and W. W. Y. Lee, "Barriers to implement extensive green roof systems: A hong kong study", Renewable and sustainable energy reviews **16**, 314–319 (2012).

[27] A. Mahdiyar, S. Tabatabaee, A. Abdullah, and A. Marto, "Identifying and assessing the critical criteria affecting decision-making for green roof type selection", Sustainable cities and society **39**, 772–783 (2018).

[28] E. Oberndorfer, J. Lundholm, B. Bass, R. R. Coffman, H. Doshi, N. Dunnett, S. Gaffin, M. Köhler, K. K. Liu, and B. Rowe, "Green roofs as urban ecosystems: ecological structures, functions, and services", BioScience **57**, 823–833 (2007).

[29] A. Bonoli, A. Conte, M. Maglionico, and I. Stojkov, "Green roofs for sustainable water management in urban areas extended abstract", Environ. Eng. Manag. J **12**, 153–156 (2013).

[30] G. Tsantopoulos, G. Varras, E. Chiotelli, K. Fotia, and M. Batou, "Public perceptions and attitudes toward green infrastructure on buildings: The case of the metropolitan area of athens, greece", Urban Forestry & Urban Greening **34**, 181–195 (2018).

[31] K. L. Getter and D. B. Rowe, "The role of extensive green roofs in sustainable development", HortScience **41**, 1276–1285 (2006).

[32] G. Peri, M. Traverso, M. Finkbeiner, and G. Rizzo, "The cost of green roofs disposal in a life cycle perspective: Covering the gap", Energy **48**, 406–414 (2012).

[33] N. S. Williams, J. P. Rayner, and K. J. Raynor, "Green roofs for a wide brown land: Opportunities and barriers for rooftop greening in australia", Urban forestry & urban greening **9**, 245–251 (2010).

[34] L. L. Peng and C. Y. Jim, "Economic evaluation of green-roof environmental benefits in the context of climate change: The case of hong kong", Urban forestry & urban greening **14**, 554–561 (2015).

[35] L. Kosareo and R. Ries, "Comparative environmental life cycle assessment of green roofs", Building and environment **42**, 2606–2613 (2007).

[36] R. Jasionkowski and A. Lewandowska-Czarnecka, "The potential of urban agriculture for sustainability of cities in poland", Ecological Questions **24**, 59–64 (2016).

[37] A. Nardini, S. Andri, and M. Crasso, "Influence of substrate depth and vegetation type on temperature and water runoff mitigation by extensive green roofs: shrubs versus herbaceous plants", Urban Ecosystems **15**, 697–708 (2012).

[38] U. Berardi, A. GhaffarianHoseini, and A. GhaffarianHoseini, "State-of-the-art analysis of the environmental benefits of green roofs", Applied energy **115**, 411–428 (2014).

[39] C. Gargari, C. Bibbiani, F. Fantozzi, and C. A. Campiotti, "Environmental impact of green roofing: the contribute of a green roof to the sustainable use of natural resources in a life cycle approach", Agriculture and Agricultural Science Procedia **8**, 646–656 (2016).

[40] K. Claus and S. Rousseau, "Public versus private incentives to invest in green roofs: A cost benefit analysis for flanders", Urban forestry & urban greening **11**, 417–425 (2012).

[41] T. Carter and L. Fowler, "Establishing green roof infrastructure through environmental policy instruments", Environmental management **42**, 151–164 (2008).

[42] J. Langemeyer, D. Wedgwood, T. McPhearson, F. Baró, A. L. Madsen, and D. N. Barton, "Creating urban green infrastructure where it is needed–a spatial ecosystem service-based decision analysis of green roofs in barcelona", Science of the total environment **707**, 135487 (2020).

[43] L. Grunwald, J. Heusinger, and S. Weber, "A gis-based mapping methodology of urban green roof ecosystem services applied to a central european city", Urban Forestry & Urban Greening **22**, 54–63 (2017).

[44] M. Karteris, I. Theodoridou, G. Mallinis, E. Tsiros, and A. Karteris, "Towards a green sustainable strategy for mediterranean cities: Assessing the benefits of large-scale green roofs implementation in thessaloniki, northern greece, using environmental modelling, gis and very high spatial resolution remote sensing data", Renewable and Sustainable Energy Reviews **58**, 510–525 (2016).

[45] T. Santos, J. A. Tenedório, and J. A. Gonçalves, "Quantifying the city's green area potential gain using remote sensing data", Sustainability **8**, 1247 (2016).

[46] F. Meijer, L. Itard, and M. Sunikka-Blank, "Comparing european residential building stocks: performance, renovation and policy opportunities", Building Research & Information **37**, 533–551 (2009).

[47] J. Da Silva and R. Vicente, "Pathology and defects of building façades and roofs: A state-of-the-art report on building pathology", Building pathology 123–131 (2013).

[48] C. Ferreira, A. Silva, J. d. Brito, I. S. Dias, and I. Flores-Colen, "Maintenance modelling of ceramic claddings in pitched roofs based on the evaluation of their in situ degradation condition", Infrastructures **5**, 77 (2020).

[49] A. Marvuglia, R. Koppelaar, and B. Rugani, "The effect of green roofs on the reduction of mortality due to heatwaves: Results from the application of a spatial microsimulation model to four european cities", Ecological Modelling **438**, 109351 (2020).

[50] M. Blackhurst, C. Hendrickson, and H. S. Matthews, "Cost-effectiveness of green roofs", Journal of Architectural Engineering **16**, 136–143 (2010).

[51] H. F. Castleton, V. Stovin, S. B. Beck, and J. B. Davison, "Green roofs; building energy savings and the potential for retrofit", Energy and buildings **42**, 1582–1591 (2010).

[52] M. Y. Joshi and J. Teller, "Urban integration of green roofs: Current challenges and perspectives", Sustainability **13**, 12378 (2021).

[53] S. Braaker, M. K. Obrist, J. Ghazoul, and M. Moretti, "Habitat connectivity and local conditions shape taxonomic and functional diversity of arthropods on green roofs", Journal of Animal Ecology **86**, 521–531 (2017).

[54] J. W. Wang, C. H. Poh, C. Y. T. Tan, V. N. Lee, A. Jain, and E. L. Webb, "Building biodiversity: drivers of bird and butterfly diversity on tropical urban roof gardens", Ecosphere **8**, e01905 (2017).

[55] S. Joimel, B. Grard, A. Auclerc, M. Hedde, N. Le Doaré, S. Salmon, and C. Chenu, "Are collembola "flying" onto green roofs?", Ecological Engineering **111**, 117–124 (2018).

[56] F. Mayrand and P. Clergeau, "Green roofs and green walls for biodiversity conservation: a contribution to urban connectivity?", Sustainability **10**, 985 (2018).

[57] G. K. Wong and C. Y. Jim, "Do vegetated rooftops attract more mosquitoes? monitoring disease vector abundance on urban green roofs", Science of the Total Environment **573**, 222–232 (2016).

[58] M. Taleghani, L. Kleerekoper, M. Tenpierik, and A. Van Den Dobbelsteen, "Outdoor thermal comfort within five different urban forms in the netherlands", Building and environment **83**, 65–78 (2015).

[59] A. Speak, J. Rothwell, S. Lindley, and C. Smith, "Urban particulate pollution reduction by four species of green roof vegetation in a uk city", Atmospheric Environment **61**, 283–293 (2012).

[60] Z. Tong, T. H. Whitlow, A. Landers, and B. Flanner, "A case study of air quality above an urban roof top vegetable farm", Environmental Pollution **208**, 256–260 (2016).

[61] M. Moghbel and R. E. Salim, "Environmental benefits of green roofs on microclimate of tehran with specific focus on air temperature, humidity and co2 content", Urban Climate **20**, 46–58 (2017).

[62] D. Haase, S. Kabisch, A. Haase, E. Andersson, E. Banzhaf, F. Baró, M. Brenck, L. K. Fischer, N. Frantzeskaki, N. Kabisch, *et al.*, "Greening cities–to be socially inclusive? about the alleged paradox of society and ecology in cities", Habitat international **64**, 41–48 (2017).

[63] J. Song and Z.-H. Wang, "Diurnal changes in urban boundary layer environment induced by urban greening", Environmental Research Letters **11**, 114018 (2016).

[64] N. S. Williams, J. Lundholm, and J. Scott MacIvor, "Do green roofs help urban biodiversity conservation?", Journal of applied ecology **51**, 1643–1649 (2014).

[65] L. Rivière, A. Delruelle, J. Reniers, S. Boisson, and G. Mahy, "Disentangling dynamics of green roof vegetation analogue to dry grassland over 3 years: Plant and substrate response to microenvironmental variations", Journal of living architecture **9**, 1–17 (2022).

[66] J. Hejkal, T. K. Buttschardt, and V. H. Klaus, "Connectivity of public urban grasslands: implications for grassland conservation and restoration in cities", Urban ecosystems **20**, 511–519 (2017).

[67] J. Lundholm, J. S. MacIvor, Z. MacDougall, and M. Ranalli, "Plant species and functional group combinations affect green roof ecosystem functions", PLoS ONE **5**, e9677 (2010), URL https://journals.plos.org/plosone/article?id=10.1371/journal.pone.0009677https://dx.plos.org/10.1371/journal.pone.0009677.

[68] C. Thuring and G. Grant, "The biodiversity of temperate extensive green roofs–a review of research and practice", Israel Journal of Ecology & Evolution **62**, 44–57 (2016).

[69] Łukasz Dylewski, Łukasz Maćkowiak, and W. Banaszak-Cibicka, "Are all urban green spaces a favourable habitat for pollinator communities? bees, butterflies and hoverflies in different urban green areas", Ecological Entomology **44**, 678–689 (2019).

[70] A. J. Grossmann, J. Herrmann, S. Buchholz, and A. K. Gathof, "Dry grassland within the urban matrix acts as favourable habitat for different pollinators including endangered species", Insect Conserv. Divers (2022).

[71] M. R. Hunter and M. D. Hunter, "Designing for conservation of insects in the built environment", Insect Conservation and diversity **1**, 189–196 (2008).

[72] S. G. Potts, J. C. Biesmeijer, C. Kremen, P. Neumann, O. Schweiger, and W. E. Kunin, "Global pollinator declines: trends, impacts and drivers", Trends in ecology & evolution **25**, 345–353 (2010).

[73] C. Duprè, C. J. Stevens, T. Ranke, A. Bleeker, C. Peppler-Lisbach, D. J. Gowing, N. B. Dise, E. Dorland, R. Bobbink, and M. Diekmann, "Changes in species richness and composition in european acidic grasslands over the past 70 years: the contribution of cumulative atmospheric nitrogen deposition", Global Change Biology **16**, 344–357 (2010), URL https://onlinelibrary.wiley.com/doi/full/10.1111/j.1365-2486.2009.01982.xhttps://onlinelibrary.wiley.com/doi/abs/10.1111/j.1365-2486.2009.01982.xhttps://onlinelibrary.wiley.com/doi/10.1111/j.1365-2486.2009.01982.x.

[74] K. Kiehl, D. Jeschke, and R. Schröder, "Roof greening with native plant species of dry sandy grasslands in northwestern germany", Urban Services to Ecosystems: Green Infrastructure Benefits from the Landscape to the Urban Scale 115–129 (2021).

[75] F. S. Sivakoff, S. P. Prajzner, and M. M. Gardiner, "Unique bee communities within vacant lots and urban farms result from variation in surrounding urbanization intensity", Sustainability **10**, 1926 (2018).

[76] S. Buchholz, A. K. Gathof, A. J. Grossmann, I. Kowarik, and L. K. Fischer, "Wild bees in urban grasslands: Urbanisation, functional diversity and species traits", Landscape and Urban Planning **196**, 103731 (2020).

[77] M. Liebergesell, B. Reu, U. Stahl, M. Freiberg, E. Welk, J. Kattge, J. H. C. Cornelissen, J. Peñuelas, and C. Wirth, "Functional resilience against climate-driven extinctions–comparing the functional diversity of european and north american tree floras", PLoS One **11**, e0148607 (2016).

[78] C. Y. Jim, "Sustainable urban greening strategies for compact cities in developing and developed economies", Urban Ecosystems **16**, 741–761 (2013), URL https://link.springer.com/article/10.1007/s11252-012-0268-x.

[79] A. Nagase and N. Dunnett, "The relationship between percentage of organic matter in substrate and plant growth in extensive green roofs", Landscape and Urban Planning **103**, 230–236 (2011).

[80] J. T. Lundholm, N. S. G. Williams, and N. S. G. Williams, "Effects of vegetation on green roof ecosystem services", 211–232 (2015), URL https://link.springer.com/chapter/10.1007/978-3-319-14983-7_9.

[81] R. Schröder and K. Kiehl, "Extensive roof greening with native sandy dry grassland species: Effects of different greening methods on vegetation development over four years", Ecological Engineering **145**, 105728 (2020).

[82] C. E. Thuring and N. Dunnett, "Vegetation composition of old extensive green roofs (from 1980s germany)", Ecological Processes **3**, 1–11 (2014), URL https://ecologicalprocesses.springeropen.com/articles/10.1186/2192-1709-3-4.

[83] Statbel, "Population by statistical sector", (2021), URL https://statbel.fgov.be/nl/open-data/bevolking-statistische-sector-9.

[84] C. Breuer, J.-M. Halleux, and J. Teller, "Urban governance adaptation in an old industrial city: Liège (belgium)", 978-88-6026-197-7 (2014).

[85] M. Van den Berg and D. Chevalier, "Of "city lounges" "bans on gathering" and macho policies-gender, class and race in productions of space for rotterdam's post-industrial future", Cities **76**, 36–42 (2018).

[86] J.-M. Halleux, "Improve the dynamism and quality of the city through an ambitious urban policy to strengthen its role as an economic engine (dynamic horizon 2022: Mobilization of the territory, territorial communities and their organization)", (2012).

[87] S. Doutreloup, X. Fettweis, R. Rahif, E. Elnagar, M. S. Pourkiaei, D. Amaripadath, and S. Attia, "Historical and future weather data for dynamic building simulations in belgium using the regional climate model mar: typical and extreme meteorological year and heatwaves", Earth System Science Data **14**, 3039–3051 (2022), URL https://essd.copernicus.org/articles/14/3039/2022/.

[88] M. Joshi, W. Selmi, M. Binard, G.-A. Nys, and J. Teller, "Potential for urban greening with green roofs: A way towards smart cities", ISPRS Annals of the Photogrammetry, Remote Sensing and Spatial Information Sciences **6**, 87–94 (2020).

[89] J. Lebeau, M. Séleck, and G. Mahy, "Report relating to the updating of the study and mapping of the ecological network of the entity's territory of the municipal nature development plan of the city of liège tranche i: Updating the inventory of the municipal development plan", Liege, Belgium: Ville de Liege/PCDN (2016).

[90] E. BRANQUART, C. DEBRUYNE, L.-M. DELESCAILLE, and P. GOFFART, "Biodiversity in wallonia", Biodiversity in (2003).

[91] J. Piqueray, E. Bisteau, G. Bottin, and G. Mahy, "Plant communities and species richness of the calcareous grasslands in southeast belgium", Belgian Journal of Botany 157–173 (2007).

[92] I. Ribeiro, A. Martilli, M. Falls, A. Zonato, and G. Villalba, "Highly resolved wrf-bep/bem simulations over barcelona urban area with lcz", Atmospheric Research **248**, 105220 (2021).

[93] M. Musy, L. Malys, B. Morille, and C. Inard, "The use of solene-microclimat model to assess adaptation strategies at the district scale", Urban Climate **14**, 213–223 (2015).

[94] M. Musy, M.-H. Azam, S. Guernouti, B. Morille, and A. Rodler, "The solene-microclimat model: Potentiality for comfort and energy studies", Urban Microclimate Modelling for Comfort and Energy Studies 265–291 (2021), URL https://link.springer.com/chapter/10.1007/978-3-030-65421-4_13.

[95] L. Malys, M. Musy, and C. Inard, "Direct and indirect impacts of vegetation on building comfort: A comparative study of lawns, green walls and green roofs", Energies 2016, Vol. 9, Page 32 **9**, 32 (2016), URL https://www.mdpi.com/1996-1073/9/1/32/htmhttps://www.mdpi.com/1996-1073/9/1/32.

[96] M. Musy, L. Malys, and C. Inard, "Assessment of direct and indirect impacts of vegetation on building comfort: A comparative study of lawns, green walls and green roofs", Procedia Environmental Sciences **38**, 603–610 (2017).

[97] L. Breiman, "Random forests", Machine Learning 2001 45:1 **45**, 5–32 (2001), URL https://link.springer.com/article/10.1023/A:1010933404324.

[98] L. Breiman, J. H. Friedman, R. A. Olshen, and C. J. Stone, *Classification and regression trees* (CRC Press) (1984), URL https://www.taylorfrancis.com/books/mono/10.1201/9781315139470/classification-regression-trees-leo-breiman.

[99] L. Breiman, "Bagging predictors", Machine Learning 1996 24:2 **24**, 123–140 (1996), URL https://link.springer.com/article/10.1007/BF00058655.

[100] P. Kontschieder, S. R. Bulò, H. Bischof, and M. Pelillo, "Structured class-labels in random forests for semantic image labelling", Proceedings of the IEEE International Conference on Computer Vision 2190–2197 (2011).

[101] E. Izquierdo-Verdiguier and R. Zurita-Milla, "An evaluation of guided regularized random forest for classification and regression tasks in remote sensing", International Journal of Applied Earth Observation and Geoinformation **88**, 102051 (2020).

[102] J. C. Foltête, C. Clauzel, and G. Vuidel, "A software tool dedicated to the modelling of landscape networks", Environmental Modelling & Software **38**, 316–327 (2012).

[103] J. C. Foltête, G. Vuidel, P. Savary, C. Clauzel, Y. Sahraoui, X. Girardet, and M. Bourgeois, "Graphab: An application for modeling and managing ecological habitat networks", Software Impacts **8**, 100065 (2021).

[104] S. Saura and L. Rubio, "A common currency for the different ways in which patches and links can contribute to habitat availability and connectivity in the landscape", Ecography **33**, 523–537 (2010), URL https://onlinelibrary.wiley.com/doi/full/10.1111/j.1600-0587.2009.05760.xhttps://onlinelibrary.wiley.com/doi/abs/10.1111/j.1600-0587.2009.05760.xhttps://onlinelibrary.wiley.com/doi/10.1111/j.1600-0587.2009.05760.x.

[105] A. K. Jha, R. Bloch, and J. Lamond, *Cities and flooding: a guide to integrated urban flood risk management for the 21st century* (World Bank Publications) (2012).

[106] N. Stephenne, B. Beaumont, E. Hallot, E. Wolff, L. Poelmans, and C. Baltus, "Sustainable and smart city planning using spatial data in wallonia", ISPRS Annals of the Photogrammetry, Remote Sensing and Spatial Information Sciences **4**, 3–10 (2016).

[107] D. Dizdaroglu, T. Yigitcanlar, and L. Dawes, "A micro-level indexing model for assessing urban ecosystem sustainability", Smart and Sustainable Built Environment **1**, 291–315 (2012).

[108] Y. Wu, W. Zhang, J. Shen, Z. Mo, and Y. Peng, "Smart city with chinese characteristics against the background of big data: Idea, action and risk", Journal of Cleaner Production **173**, 60–66 (2018).

[109] A. Sodiq, A. A. Baloch, S. A. Khan, N. Sezer, S. Mahmoud, M. Jama, and A. Abdelaal, "Towards modern sustainable cities: Review of sustainability principles and trends", Journal of Cleaner Production **227**, 972–1001 (2019).

[110] J. Rice and N. Martin, "Smart infrastructure technologies: Crowdsourcing future development and benefits for australian communities", Technological forecasting and social change **153**, 119256 (2020).

[111] T. Yigitcanlar, M. Kamruzzaman, M. Foth, J. Sabatini-Marques, E. Da Costa, and G. Ioppolo, "Can cities become smart without being sustainable? a systematic review of the literature", Sustainable cities and society **45**, 348–365 (2019).

[112] I. Bouzguenda, C. Alalouch, and N. Fava, "Towards smart sustainable cities: A review of the role digital citizen participation could play in advancing social sustainability", Sustainable Cities and Society **50**, 101627 (2019).

[113] T. Yigitcanlar, J. Sabatini-Marques, C. Lorenzi, N. Bernardinetti, T. Schreiner, A. Fachinelli, and T. Wittmann, "Towards smart florianópolis: what does it take to transform a tourist island into an innovation capital?", Energies **11**, 3265 (2018).

[114] H. Dorst, A. Van der Jagt, R. Raven, and H. Runhaar, "Urban greening through nature-based solutions–key characteristics of an emerging concept", Sustainable Cities and Society **49**, 101620 (2019).

[115] A. Sharma, S. Woodruff, M. Budhathoki, A. F. Hamlet, F. Chen, and H. J. Fernando, "Role of green roofs in reducing heat stress in vulnerable urban communities—a multidisciplinary approach", Environmental Research Letters **13**, 094011 (2018), URL https://iopscience.iop.org/article/10.1088/1748-9326/aad93chttps://iopscience.iop.org/article/10.1088/1748-9326/aad93c/meta.

[116] S. Guzman-Sanchez, D. Jato-Espino, I. Lombillo, and J. M. Diaz-Sarachaga, "Assessment of the contributions of different flat roof types to achieving sustainable development", Building and Environment **141**, 182–192 (2018).

[117] M. Mesimäki, K. Hauru, D. J. Kotze, and S. Lehvävirta, "Neo-spaces for urban livability? urbanites' versatile mental images of green roofs in the helsinki metropolitan area, finland", Land Use Policy **61**, 587–600 (2017).

[118] K. Specht, T. Weith, K. Swoboda, and R. Siebert, "Socially acceptable urban agriculture businesses", Agronomy for sustainable development **36**, 1–14 (2016).

[119] S. Braaker, J. Ghazoul, M. K. Obrist, and M. Moretti, "Habitat connectivity shapes urban arthropod communities: the key role of green roofs", Ecology **95**, 1010–1021 (2014).

[120] A. Sharma, P. Conry, H. J. S. Fernando, A. F. Hamlet, J. J. Hellmann, and F. Chen, "Green and cool roofs to mitigate urban heat island effects in the chicago metropolitan area: evaluation with a regional climate model", Environmental Research Letters **11**, 064004 (2016), URL https://dx.doi.org/10.1088/1748-9326/11/6/064004.

[121] U. Habitat, "The state of european cities in transition 2013. taking stock after 20 years of reform", (2013).

[122] R. T. Berhe, J. Martinez, and J. Verplanke, "Adaptation and dissonance in quality of life: A case study in mekelle, ethiopia", Social Indicators Research **118**, 535–554 (2014).

[123] G. Mallinis, M. Karteris, I. Theodoridou, V. Tsioukas, and M. Karteris, "Development of a nationwide approach for large scale estimation of green roof retrofitting areas and roof-top solar energy potential using vhr natural colour orthoimagery and dsm data over thessaloniki, greece", Remote sensing letters **5**, 548–557 (2014).

[124] Y. Tian and C. Y. Jim, "Development potential of sky gardens in the compact city of hong kong", Urban forestry & urban greening **11**, 223–233 (2012).

[125] S. J. Wilkinson and R. Reed, "Green roof retrofit potential in the central business district", Property management **27**, 284–301 (2009).

[126] C. M. Silva, I. Flores-Colen, and M. Antunes, "Step-by-step approach to ranking green roof retrofit potential in urban areas: A case study of lisbon, portugal", Urban Forestry & Urban Greening **25**, 120–129 (2017).

[127] R. Cao, Y. Zhang, X. Liu, and Z. Zhao, "3d building roof reconstruction from airborne lidar point clouds: A framework based on a spatial database", International Journal of Geographical Information Science **31**, 1359–1380 (2017).

[128] R. Schnabel, R. Wahl, and R. Klein, "Efficient ransac for point-cloud shape detection", in *Computer graphics forum*, volume 26, 214–226 (Wiley Online Library) (2007).

[129] D. Ballard, "Generalizing the hough transform to detect arbitrary shapes. readings in computer vision", (1987).

[130] F. Tarsha-Kurdi, T. Landes, and P. Grussenmeyer, "Hough-transform and extended ransac algorithms for automatic detection of 3d building roof planes from lidar data", in *ISPRS Workshop on Laser Scanning 2007 and SilviLaser 2007*, volume 36, 407–412 (2007).

[131] B. Xu, W. Jiang, J. Shan, J. Zhang, and L. Li, "Investigation on the weighted ransac approaches for building roof plane segmentation from lidar point clouds", Remote Sensing **8**, 5 (2015).

[132] F. Rottensteiner, G. Sohn, M. Gerke, J. D. Wegner, U. Breitkopf, and J. Jung, "Results of the isprs benchmark on urban object detection and 3d building reconstruction", ISPRS journal of photogrammetry and remote sensing **93**, 256–271 (2014).

[133] S. Rohon *et al.*, "Energy renovation: Potential for revegetation of roofs on the east bank of liè ge", (2017).

[134] W. Su, C. Gu, and G. Yang, "Assessing the impact of land use/land cover on urban heat island pattern in nanjing city, china", Journal of Urban Planning and Development **136**, 365–372 (2010).

[135] F. Yuan and M. E. Bauer, "Comparison of impervious surface area and normalized difference vegetation index as indicators of surface urban heat island effects in landsat imagery", Remote Sensing of environment **106**, 375–386 (2007).

[136] B. Bianchet, J. Descamps, C. Ruelle, P.-F. Wilmotte, F. Bastin, C. Mercenier, and D. Claeys, "Localisations prioritaires en matière de dynamisation et de rénovation des quartiers urbains existants", (2016).

[137] F. Biljecki and Y. Dehbi, "Raise the roof: Towards generating lod2 models without aerial surveys using machine learning", ISPRS Annals of the Photogrammetry, Remote Sensing and Spatial Information Sciences **4**, 27–34 (2019).

[138] M. K. Singh, S. Mahapatra, and J. Teller, "An analysis on energy efficiency initiatives in the building stock of liege, belgium", Energy policy **62**, 729–741 (2013).

[139] I. Teotónio, C. M. Silva, and C. O. Cruz, "Eco-solutions for urban environments regeneration: The economic value of green roofs", Journal of Cleaner Production **199**, 121–135 (2018).

[140] J. Oehrlein, B. Niedermann, and J.-H. Haunert, "Analyzing the supply and detecting spatial patterns of urban green spaces via optimization", PFG–Journal of Photogrammetry, Remote Sensing and Geoinformation Science **87**, 137–158 (2019).

[141] X. Wang, H. Li, and S. Sodoudi, "The effectiveness of cool and green roofs in mitigating urban heat island and improving human thermal comfort", Building and Environment **217**, 109082 (2022).

[142] J. A. Patz, D. Campbell-Lendrum, T. Holloway, and J. A. Foley, "Impact of regional climate change on human health", Nature 2005 438:7066 **438**, 310–317 (2005).

[143] K. M. Gabriel and W. R. Endlicher, "Urban and rural mortality rates during heat waves in berlin and brandenburg, germany", Environmental Pollution **159**, 2044–2050 (2011), selected papers from the conference Urban Environmental Pollution: Overcoming Obstacles to Sustainability and Quality of Life (UEP2010), 20-23 June 2010, Boston, USA.

[144] D. Li and E. Bou-Zeid, "Synergistic interactions between urban heat islands and heat waves: The impact in cities is larger than the sum of its parts", Journal of Applied Meteorology and Climatology **52**, 2051 – 2064 (2013), URL https://www.scopus.com/inward/record.uri?eid=2-s2.0-84884236202&doi=10.1175%2fJAMC-D-13-02.1&partnerID=40&md5=c7e4b2f384f98dc780336b2736623358, cited by: 535; All Open Access, Bronze Open Access.

[145] L. W. Chew, X. Liu, X.-X. Li, and L. K. Norford, "Interaction between heat wave and urban heat island: A case study in a tropical coastal city, singapore", Atmospheric Research **247**, 105134 (2021), URL https://www.sciencedirect.com/science/article/pii/S016980952031070X.

[146] D. Li, T. Sun, M. Liu, L. Yang, L. Wang, and Z. Gao, "Contrasting responses of urban and rural surface energy budgets to heat waves explain synergies between urban heat islands and heat waves", Environmental Research Letters **10** (2015), URL https://www.scopus.com/inward/record.uri?eid=2-s2.0-84930216539&doi=10.1088%2f1748-9326%2f10%2f5%2f054009&partnerID=40&md5=7301481d9c1ef0d60e6de044be871a08, cited by: 150; All Open Access, Gold Open Access, Green Open Access.

[147] D. Li, T. Sun, M. Liu, L. Wang, and Z. Gao, "Changes in wind speed under heat waves enhance urban heat islands in the beijing metropolitan area", Journal of Applied Meteorology and Climatology **55**, 2369 – 2375 (2016), URL https://www.scopus.com/inward/record.uri?eid=2-s2.0-84998849962&doi=10.1175%2fJAMC-D-16-0102.1&partnerID=40&md5=bce9b20d09b3f010205e0bdc44392157, cited by: 52; All Open Access, Bronze Open Access, Green Open Access.

[148] K. Gunawardena, M. Wells, and T. Kershaw, "Utilising green and bluespace to mitigate urban heat island intensity", Science of the Total Environment **584-585**, 1040 – 1055 (2017), cited by: 526; All Open Access, Green Open Access, Hybrid Gold Open Access.

[149] M. Santamouris, S. Haddad, M. Saliari, K. Vasilakopoulou, A. Synnefa, R. Paolini, G. Ulpiani, S. Garshasbi, and F. Fiorito, "On the energy impact of urban heat island in sydney: Climate and energy potential of mitigation technologies", Energy and Buildings **166**, 154–164 (2018), URL https://www.sciencedirect.com/science/article/pii/S0378778817338021.

[150] X.-X. Li and X. Liu, "Effect of tree evapotranspiration and hydrological processes on urban microclimate in a tropical city: A wrf/slucm study", Urban Climate **40**, 101009 (2021).

[151] M. Santamouris, A. Synnefa, and T. Karlessi, "Using advanced cool materials in the urban built environment to mitigate heat islands and improve thermal comfort conditions", Solar Energy **85**, 3085 – 3102 (2011), cited by: 665.

[152] X. Liu, G. Tian, J. Feng, H. Hou, and B. Ma, "Adaptation strategies for urban warming: Assessing the impacts of heat waves on cooling capabilities in chongqing, china", Urban Climate **45**, 101269 (2022), URL https://www.sciencedirect.com/science/article/pii/S2212095522001870.

[153] D. Li, E. Bou-Zeid, and M. Oppenheimer, "The effectiveness of cool and green roofs as urban heat island mitigation strategies", Environmental Research Letters **9** (2014).

[154] C. He, L. He, Y. Zhang, P. L. Kinney, and W. Ma, "Potential impacts of cool and green roofs on temperature-related mortality in the greater boston region", Environmental Research Letters **15**, 094042 (2020), URL https://dx.doi.org/10.1088/1748-9326/aba4c9.

[155] J. Yang and E. Bou-Zeid, "Scale dependence of the benefits and efficiency of green and cool roofs", Landscape and urban planning **185**, 127–140 (2019).

[156] E. Bou-Zeid, M. B. Parlange, and C. Meneveau, "On the parameterization of surface roughness at regional scales", Journal of the atmospheric sciences **64**, 216–227 (2007).

[157] H. Tan, R. Kotamarthi, J. Wang, Y. Qian, and T. Chakraborty, "Impact of different roofing mitigation strategies on near-surface temperature and energy consumption over the chicago metropolitan area during a heatwave event", Science of The Total Environment **860**, 160508 (2023).

[158] A. Synnefa, A. Dandou, M. Santamouris, M. Tombrou, and N. Soulakellis, "On the use of cool materials as a heat island mitigation strategy", Journal of Applied Meteorology and Climatology **47**, 2846–2856 (2008).

[159] X.-X. Li and L. K. Norford, "Evaluation of cool roof and vegetations in mitigating urban heat island in a tropical city, singapore", Urban Climate **16**, 59–74 (2016).

[160] T. Sun, C. Grimmond, and G.-H. Ni, "How do green roofs mitigate urban thermal stress under heat waves?", Journal of Geophysical Research: Atmospheres **121**, 5320–5335 (2016).

[161] E. Morini, A. G. Touchaei, F. Rossi, F. Cotana, and H. Akbari, "Evaluation of albedo enhancement to mitigate impacts of urban heat island in rome (italy) using wrf meteorological model", Urban Climate **24**, 551–566 (2018).

[162] I. D. Stewart and T. R. Oke, "Local climate zones for urban temperature studies", Bulletin of the American Meteorological Society **93**, 1879–1900 (2012).

[163] M. Tewari, J. Yang, H. Kusaka, F. Salamanca, C. Watson, and L. Treinish, "Interaction of urban heat islands and heat waves under current and future climate conditions and their mitigation using green and cool roofs in new york city and phoenix, arizona", Environmental Research Letters **14**, 034002 (2019), URL https://dx.doi.org/10.1088/1748-9326/aaf431.

[164] J. Gilabert, S. Ventura, R. Segura, A. Martilli, A. Badia, C. Llasat, J. Corbera, and G. Villalba, "Abating heat waves in a coastal mediterranean city: What can cool roofs and vegetation contribute?", Urban climate **37**, 100863 (2021).

[165] N. Liu and L. Morawska, "Modeling the urban heat island mitigation effect of cool coatings in realistic urban morphology", Journal of cleaner production **264**, 121560 (2020).

[166] M. Mughal, X.-X. Li, and L. K. Norford, "Urban heat island mitigation in singapore: Evaluation using wrf/multilayer urban canopy model and local climate zones", Urban Climate **34**, 100714 (2020).

[167] F. Salamanca and A. Martilli, "A new building energy model coupled with an urban canopy parameterization for urban climate simulations—part ii. validation with one dimension off-line simulations", Theoretical and Applied Climatology **99**, 345–356 (2010).

[168] R. Segura, A. Badia, S. Ventura, J. Gilabert, A. Martilli, and G. Villalba, "Sensitivity study of pbl schemes and soil initialization using the wrf-bep-bem model over a mediterranean coastal city", Urban climate **39**, 100982 (2021).

[169] M. Demuzere, B. Bechtel, A. Middel, and G. Mills, "Mapping europe into local climate zones", PloS one **14**, e0214474 (2019).

[170] M. Demuzere, B. Bechtel, A. Middel, and G. Mills, "European lcz map (version2).figshare.", (2019).

[171] C. de Munck, G. Pigeon, V. Masson, F. Meunier, P. Bousquet, B. Tréméac, M. Merchat, P. Poeuf, and C. Marchadier, "How much can air conditioning increase air temperatures for a city like paris, france?", International Journal of Climatology **33**, 210–227 (2013).

[172] E. Gutierrez, "Quantification of environmental impacts of heat fluxes from built environments", Ph.D. thesis, The City College of New York (2016).

[173] A. Zonato, A. Martilli, E. Gutierrez, F. Chen, C. He, M. Barlage, D. Zardi, and L. Giovannini, "Exploring the effects of rooftop mitigation strategies on urban temperatures and energy consumption", Journal of Geophysical Research: Atmospheres **126**, e2021JD035002 (2021).

[174] J.-F. Louis, "A parametric model of vertical eddy fluxes in the atmosphere", Boundary-Layer Meteorology **17**, 187–202 (1979).

[175] B. Jacquemin and J. Noilhan, "Sensitivity study and validation of a land surface parameterization using the hapex-mobilhy data set", Boundary-Layer Meteorology **52**, 93–134 (1990).

[176] M. Demuzere, D. Argüeso, A. Zonato, and J. Kittner, "W2w: A python package that injects wudapt's local climate zone information in wrf", Journal of Open Source Software **7**, 4432 (2022).

[177] A. Kumar, F. Chen, M. Barlage, M. B. Ek, and D. Niyogi, "Assessing impacts of integrating modis vegetation data in the weather research and forecasting (wrf) model coupled to two different canopy-resistance approaches", Journal of Applied Meteorology and Climatology **53**, 1362–1380 (2014).

[178] A. M. Broadbent, E. S. Krayenhoff, and M. Georgescu, "Efficacy of cool roofs at reducing pedestrian-level air temperature during projected 21st century heatwaves in atlanta, detroit, and phoenix (usa)", Environmental Research Letters **15**, 084007 (2020).

[179] H. Hersbach, B. Bell, P. Berrisford, S. Hirahara, A. Horányi, J. Muñoz-Sabater, J. Nicolas, C. Peubey, R. Radu, D. Schepers, *et al.*, "The era5 global reanalysis", Quarterly Journal of the Royal Meteorological Society **146**, 1999–2049 (2020).

[180] M. Ek, K. Mitchell, Y. Lin, E. Rogers, P. Grunmann, V. Koren, G. Gayno, and J. Tarpley, "Implementation of noah land surface model advances in the national centers for environmental prediction operational mesoscale eta model", Journal of Geophysical Research: Atmospheres **108** (2003).

[181] F. Chen and J. Dudhia, "Coupling an advanced land surface–hydrology model with the penn state–ncar mm5 modeling system. part i: Model implementation and sensitivity", Monthly weather review **129**, 569–585 (2001).

[182] Z. Janjic, "Nonsingular implementation of the mellor-yamada level 2.5 scheme in the ncep meso model, ncep off", Note **437**, 61 (2002).

[183] G. Thompson and T. Eidhammer, "A study of aerosol impacts on clouds and precipitation development in a large winter cyclone", Journal of the atmospheric sciences **71**, 3636–3658 (2014).

[184] M. J. Iacono, J. S. Delamere, E. J. Mlawer, M. W. Shephard, S. A. Clough, and W. D. Collins, "Radiative forcing by long-lived greenhouse gases: Calculations with the aer radiative transfer models", Journal of Geophysical Research: Atmospheres **113** (2008).

[185] M. Tiedtke, "A comprehensive mass flux scheme for cumulus parameterization in large-scale models", Monthly weather review **117**, 1779–1800 (1989).

[186] D. Jacob, J. Petersen, B. Eggert, A. Alias, O. Bøssing Christensen, L. Bouwer, A. Braun, A. Colette, M. Déqué, G. Georgievski, *et al.*, "Eurocordex: New high-resolution climate change projections for european impact research, regional environmental changes, 14, 563–578", (2013).

[187] S. Chen, N. H. Wong, M. Ignatius, W. Zhang, Y. He, Z. Yu, and D. J. C. Hii, "Atlas: Software for analysing the relationship between urban microclimate and urban morphology in a tropical city", Building and Environment **208**, 108591 (2022).

[188] H. Li, Y. Zhou, X. Wang, X. Zhou, H. Zhang, and S. Sodoudi, "Quantifying urban heat island intensity and its physical mechanism using wrf/ucm", Science of the Total Environment **650**, 3110–3119 (2019).

[189] W. Liao, X. Liu, D. Li, M. Luo, D. Wang, S. Wang, J. Baldwin, L. Lin, X. Li, K. Feng, *et al.*, "Stronger contributions of urbanization to heat wave trends in wet climates", Geophysical Research Letters **45**, 11–310 (2018).

[190] R. G. Steadman, "The assessment of sultriness. part i: A temperature-humidity index based on human physiology and clothing science", Journal of Applied Meteorology and Climatology **18**, 861–873 (1979).

[191] L. P. Rothfusz and N. S. R. Headquarters, "The heat index equation (or, more than you ever wanted to know about heat index)", Fort Worth, Texas: National Oceanic and Atmospheric Administration, National Weather Service, Office of Meteorology **9023**, 640 (1990).

[192] S.-H. Lee, S.-W. Kim, W. Angevine, L. Bianco, S. McKeen, C. Senff, M. Trainer, S. Tucker, and R. Zamora, "Evaluation of urban surface parameterizations in the wrf model using measurements during the texas air quality study 2006 field campaign", Atmospheric Chemistry and Physics **11**, 2127–2143 (2011).

[193] Y. Kim, K. Sartelet, J.-C. Raut, and P. Chazette, "Evaluation of the weather research and forecast/urban model over greater paris", Boundary-layer meteorology **149**, 105–132 (2013).

[194] L. Giovannini, D. Zardi, M. De Franceschi, and F. Chen, "Numerical simulations of boundary-layer processes and urban-induced alterations in an alpine valley", International Journal of Climatology **34**, 1111–1131 (2014).

[195] B. Jänicke, F. Meier, D. Fenner, U. Fehrenbach, A. Holtmann, and D. Scherer, "Urban–rural differences in near-surface air temperature as resolved by the central europe refined analysis (cer): sensitivity to planetary boundary layer schemes and urban canopy models", International Journal of Climatology **37**, 2063–2079 (2017).

[196] X. Wang, H. Li, and S. Sodoudi, "The effectiveness of cool and green roofs in mitigating urban heat island and improving human thermal comfort", Building and Environment **217**, 109082 (2022).

[197] S. N. Gadde, A. Stieren, and R. J. Stevens, "Large-eddy simulations of stratified atmospheric boundary layers: Comparison of different subgrid models", Boundary-Layer Meteorology **178**, 363–382 (2021).

[198] M. Georgescu, P. E. Morefield, B. G. Bierwagen, and C. P. Weaver, "Urban adaptation can roll back warming of emerging megapolitan regions", Proceedings of the National Academy of Sciences **111**, 2909–2914 (2014).

[199] Y. Toparlar, B. Blocken, B. Maiheu, and G. J. van Heijst, "A review on the cfd analysis of urban microclimate", Renewable and Sustainable Energy Reviews **80**, 1613–1640 (2017).

[200] M. Santamouris, "The energy impact of the urban environment", in *Energy and Climate in the Urban Built Environment*, 97–109 (Routledge) (2013).

[201] S. W. Kim and R. D. Brown, "Urban heat island (uhi) variations within a city boundary: A systematic literature review", Renewable and Sustainable Energy Reviews **148**, 111256 (2021), URL https://linkinghub.elsevier.com/retrieve/pii/S1364032121005438.

[202] L. Kleerekoper, M. van Esch, and T. B. Salcedo, "How to make a city climate-proof, addressing the urban heat island effect", Resources, Conservation and Recycling **64**, 30–38 (2012), URL https://linkinghub.elsevier.com/retrieve/pii/S0921344911001303.

[203] V. Masson, W. Heldens, E. Bocher, M. Bonhomme, B. Bucher, C. Burmeister, C. de Munck, T. Esch, J. Hidalgo, F. Kanani-Sühring, Y.-T. Kwok, A. Lemonsu, J.-P. Lévy, B. Maronga, D. Pavlik, G. Petit, L. See, R. Schoetter, N. Tornay, A. Votsis, and J. Zeidler, "City-descriptive input data for urban climate models: Model requirements, data sources and challenges", Urban Climate **31**, 100536 (2020), URL https://linkinghub.elsevier.com/retrieve/pii/S2212095518303663.

[204] A. Rodler and T. Leduc, "Local climate zone approach on local and micro scales: Dividing the urban open space", Urban Climate **28**, 100457 (2019), URL https://linkinghub.elsevier.com/retrieve/pii/S2212095518303353.

[205] A. Boccalatte, M. Fossa, L. Gaillard, and C. Menezo, "Microclimate and urban morphology effects on building energy demand in different european cities", Energy and Buildings **224**, 110129 (2020).

[206] D. Xu, D. Zhou, Y. Wang, W. Xu, and Y. Yang, "Field measurement study on the impacts of urban spatial indicators on urban climate in a chinese basin and static-wind city", Building and Environment **147**, 482–494 (2019).

[207] A. Kamal, S. M. H. Abidi, A. Mahfouz, S. Kadam, A. Rahman, I. G. Hassan, and L. L. Wang, "Impact of urban morphology on urban microclimate and building energy loads", Energy and Buildings **253**, 111499 (2021), URL https://linkinghub.elsevier.com/retrieve/pii/S0378778821007830.

[208] K. K. L. Lau, Z. Tan, T. E. Morakinyo, and C. Ren, "Urban greening strategies for enhancing outdoor thermal comfort", SpringerBriefs in Architectural Design and Technology 85–100 (2022), URL https://link.springer.com/chapter/10.1007/978-981-16-5245-5_6.

[209] Y. Gao, J. Zhao, and L. Han, "Exploring the spatial heterogeneity of urban heat island effect and its relationship to block morphology with the geographically weighted regression model", Sustainable Cities and Society **76**, 103431 (2022), URL https://linkinghub.elsevier.com/retrieve/pii/S2210670721007046.

[210] S. Shareef and B. Abu-Hijleh, "The effect of building height diversity on outdoor microclimate conditions in hot climate. a case study of dubai-uae", Urban Climate **32**, 100611 (2020), URL https://linkinghub.elsevier.com/retrieve/pii/S2212095519301890.

[211] A. Bernabé, J. Bernard, M. Musy, H. Andrieu, E. Bocher, I. Calmet, P. Kéravec, and J. M. Rosant, "Radiative and heat storage properties of the urban fabric derived from analysis of surface forms", Urban Climate **12**, 205–218 (2015).

[212] C. Yuan and L. Chen, "Mitigating urban heat island effects in high-density cities based on sky view factor and urban morphological understanding: a study of hong kong", http://dx.doi.org/10.1080/00038628.2011.613644 **54**, 305–315 (2011), URL https://www.tandfonline.com/doi/abs/10.1080/00038628.2011.613644.

[213] O. Palusci, P. Monti, C. Cecere, H. Montazeri, and B. Blocken, "Impact of morphological parameters on urban ventilation in compact cities: The case of the tuscolano-don bosco district in rome", Science of The Total Environment **807**, 150490 (2022).

[214] C. Apreda, A. Reder, and P. Mercogliano, "Urban morphology parameterization for assessing the effects of housing blocks layouts on air temperature in the euro-mediterranean context", Energy and Buildings **223**, 110171 (2020), URL https://linkinghub.elsevier.com/retrieve/pii/S0378778820302838.

[215] R. Ma, X. Li, and J. Chen, "An elastic urban morpho-blocks (eum) modeling method for urban building morphological analysis and feature clustering", Building and Environment **192**, 107646 (2021).

[216] A. Meek, N. Jayasuriya, . E. Horan, and R. Adams, "Environmental benefits of retrofitting green roofs to a city block", Journal of Hydrologic Engineering **20**, 05014020 (2014), URL https://ascelibrary.org/doi/abs/10.1061/%28ASCE%29HE.1943-5584.0001048https://ascelibrary.org/doi/full/10.1061/%28ASCE%29HE.1943-5584.0001048.

[217] H. A. S. Othman and A. A. Alshboul, "The role of urban morphology on outdoor thermal comfort: The case of al-sharq city – az zarqa", Urban Climate **34**, 100706 (2020).

[218] M. H. Kristensen, R. E. Hedegaard, and S. Petersen, "Hierarchical calibration of archetypes for urban building energy modeling", Energy and Buildings **175**, 219–234 (2018).

[219] J. Sokol, C. C. Davila, and C. F. Reinhart, "Validation of a bayesian-based method for defining residential archetypes in urban building energy models", Energy and Buildings **134**, 11–24 (2017).

[220] J. Geletič and M. Lehnert, "Gis-based delineation of local climate zones: The case of medium-sized central european cities", Moravian Geographical Reports **24**, 2–12 (2016), URL https://www.sciendo.com/article/10.1515/mgr-2016-0012.

[221] R. Kotharkar and A. Bagade, "Local climate zone classification for indian cities: A case study of nagpur", Urban Climate **24**, 369–392 (2018).

[222] C. Zhao, J. Jensen, Q. Weng, N. Currit, and R. Weaver, "Application of airborne remote sensing data on mapping local climate zones: Cases of three metropolitan areas of texas, u.s.", Computers, Environment and Urban Systems **74**, 175–193 (2019), URL https://linkinghub.elsevier.com/retrieve/pii/S0198971518301212.

[223] C. M. Hsieh and H. C. Huang, "Mitigating urban heat islands: A method to identify potential wind corridor for cooling and ventilation", Computers, Environment and Urban Systems **57**, 130–143 (2016).

[224] M. Taleghani, M. Tenpierik, A. V. D. Dobbelsteen, and R. D. Dear, "Energy use impact of and thermal comfort in different urban block types in the netherlands", Energy and Buildings **67**, 166–175 (2013).

[225] H. López-Moreno, M. Núñez-Peiró, C. Sánchez-Guevara, and J. Neila, "On the identification of homogeneous urban zones for the residential buildings' energy evaluation", Building and Environment **207**, 108451 (2022), URL https://linkinghub.elsevier.com/retrieve/pii/S0360132321008477.

[226] G. Meinel, R. Hecht, and H. Herold, "Analyzing building stock using topographic maps and gis", Building Research & Information **37**, 468–482 (2009), URL https://www.tandfonline.com/doi/abs/10.1080/

09613210903159833https://www.tandfonline.com/doi/full/10.1080/09613210903159833.

[227] S. Vanderhaegen and F. Canters, "Mapping urban form and function at city block level using spatial metrics", Landscape and Urban Planning **167**, 399–409 (2017).

[228] J. Gil, J. Beirão, N. Montenegro, and J. Duarte, "On the discovery of urban typologies: Data mining the many dimensions of urban form", Urban Morphology **16**, 27–40 (2012).

[229] P. M. Schirmer and K. W. Axhausen, "A multiscale classification of urban morphology", Journal of Transport and Land Use **9**, 101–130 (2016), URL http://www.jstor.org/stable/26203210.

[230] P. M. Schirmer and K. W. Axhausen, "A multiscale clustering of the urban morphology for use in quantitative models", Modeling and Simulation in Science, Engineering and Technology 355–382 (2019), URL https://link.springer.com/chapter/10.1007/978-3-030-12381-9_16.

[231] G. Tardioli, R. Kerrigan, M. Oates, J. O'Donnell, and D. P. Finn, "Identification of representative buildings and building groups in urban datasets using a novel pre-processing, classification, clustering and predictive modelling approach", Building and Environment **140**, 90–106 (2018).

[232] G. W. Milligan and M. C. Cooper, "Methodology review: Clustering methods", Applied Psychological Measurement **11**, 329–354 (1987), URL https://journals.sagepub.com/doi/10.1177/014662168701100401http://journals.sagepub.com/doi/10.1177/014662168701100401.

[233] D. Godoy-Shimizu, P. Steadman, and S. Evans, "Density and morphology: from the building scale to the city scale", Buildings and Cities **2**, 92–113 (2021), URL http://journal-buildingscities.org/articles/10.5334/bc.83/.

[234] I. D. Dwiputra, I. W. K. Mt, and H. Winarso, "Impact of urban block typology on microclimate performance in a hot-humid high-density city", IOP Conference Series: Earth and Environmental Science **738**, 012067 (2021), URL https://iopscience.iop.org/article/10.1088/1755-1315/738/1/012067https://iopscience.iop.org/article/10.1088/1755-1315/738/1/012067/meta.

[235] X. Zhou and H. Chen, "Experimental analysis of the influence of urban morphological indices on the urban thermal environment of zhengzhou, china", Atmosphere 2021, Vol. 12, Page 1058 **12**, 1058 (2021), URL https://www.mdpi.com/2073-4433/12/8/1058/htmhttps://www.mdpi.com/2073-4433/12/8/1058.

[236] J. Yang, Y. Yang, D. Sun, C. Jin, and X. Xiao, "Influence of urban morphological characteristics on thermal environment", Sustainable Cities and Society **72**, 103045 (2021).

[237] M. B. Pont and P. Haupt, "The spacemate: Density and the typomorphology of the urban fabric", Nordisk Arkitekturforskning **18**, 55–68 (2005).

[238] J. Allegrini and J. Carmeliet, "Simulations of local heat islands in zürich with coupled cfd and building energy models", Urban Climate **24**, 340–359 (2018).

[239] A. A. Razak, A. Hagishima, N. Ikegaya, and J. Tanimoto, "Analysis of airflow over building arrays for assessment of urban wind environment", Building and Environment **59**, 56–65 (2013), URL https://linkinghub.elsevier.com/retrieve/pii/S0360132312002090.

[240] M. P. Heris, A. Middel, and B. Muller, "Impacts of form and design policies on urban microclimate: Assessment of zoning and design guideline choices in urban redevelopment projects", Landscape and Urban Planning **202**, 103870 (2020).

[241] R. Louf and M. Barthelemy, "A typology of street patterns", Journal of The Royal Society Interface **11** (2014), URL https://royalsocietypublishing.org/doi/abs/10.1098/rsif.2014.0924.

[242] E. Ng, C. Yuan, L. Chen, C. Ren, and J. C. Fung, "Improving the wind environment in high-density cities by understanding urban morphology and surface roughness: A study in hong kong", Landscape and Urban Planning **101**, 59–74 (2011).

[243] B. Wang, S. Geoffroy, and M. Bonhomme, "Urban form study for wind potential development:", https://doi.org/10.1177/2399808321994449 **49**, 76–91 (2021), URL https://journals.sagepub.com/doi/full/10.1177/2399808321994449.

[244] M. S. Wong, J. E. Nichol, P. H. To, and J. Wang, "A simple method for designation of urban ventilation corridors and its application to urban heat island analysis",

Building and Environment **45**, 1880–1889 (2010), URL https://linkinghub.elsevier.com/retrieve/pii/S0360132310000776.

[245] J. Bernard, E. Bocher, G. Petit, and S. Palominos, "Sky view factor calculation in urban context: Computational performance and accuracy analysis of two open and free gis tools", Climate 2018, Vol. 6, Page 60 **6**, 60 (2018), URL https://www.mdpi.com/2225-1154/6/3/60/htmhttps://www.mdpi.com/2225-1154/6/3/60.

[246] M. Dirksen, R. J. Ronda, N. E. Theeuwes, and G. A. Pagani, "Sky view factor calculations and its application in urban heat island studies", Urban Climate **30**, 100498 (2019).

[247] J. Teller and S. Azar, "Townscope ii - a computer systems to support solar access decision-making", Solar Energy **70**, 187–200 (2001).

[248] Žiga Kokalj and M. Somrak, "Why not a single image? combining visualizations to facilitate fieldwork and on-screen mapping", Remote Sensing 2019, Vol. 11, Page 747 **11**, 747 (2019), URL https://www.mdpi.com/2072-4292/11/7/747/htmhttps://www.mdpi.com/2072-4292/11/7/747.

[249] K. Zakšek, K. Oštir, and Žiga Kokalj, "Sky-view factor as a relief visualization technique", Remote Sensing 2011, Vol. 3, Pages 398-415 **3**, 398–415 (2011), URL https://www.mdpi.com/2072-4292/3/2/398/htmhttps://www.mdpi.com/2072-4292/3/2/398.

[250] M. Bruwier, A. Mustafa, D. Aliaga, P. Archambeau, S. Erpicum, G. Nishida, X. Zhang, M. Pirotton, J. Teller, and B. Dewals, "Influence of urban pattern on inundation flow in floodplains of lowland rivers", Science of The Total Environment **622-623**, 446–458 (2018), URL https://linkinghub.elsevier.com/retrieve/pii/S0048969717333831.

[251] Y. Zha, J. Gao, and S. Ni, "Use of normalized difference built-up index in automatically mapping urban areas from tm imagery", https://doi.org/10.1080/01431160304987 **24**, 583–594 (2010), URL https://www.tandfonline.com/doi/abs/10.1080/01431160304987.

[252] X.-L. Chen, H.-M. Zhao, P.-X. Li, and Z.-Y. Yin, "Remote sensing image-based analysis of the relationship between urban heat island and land use/cover changes", Remote Sensing of Environment **104**, 133–146 (2006), URL https://linkinghub.elsevier.com/retrieve/pii/S0034425706001787.

[253] P. Macarof and F. Statescu, "Comparasion of ndbi and ndvi as indicators of surface urban heat island effect in landsat 8 imagery: a case study of iasi", Present Environment and Sustainable Development **2**, 141–150 (2017), URL https://ibn.idsi.md/vizualizare_articol/105363.

[254] L. S. Ferreira and D. H. S. Duarte, "Exploring the relationship between urban form, land surface temperature and vegetation indices in a subtropical megacity", Urban Climate **27**, 105–123 (2019), URL https://linkinghub.elsevier.com/retrieve/pii/S2212095518303389.

[255] L. Montandon and E. Small, "The impact of soil reflectance on the quantification of the green vegetation fraction from ndvi", Remote Sensing of Environment **112**, 1835–1845 (2008), URL https://linkinghub.elsevier.com/retrieve/pii/S0034425707004245.

[256] A. Martilli, E. S. Krayenhoff, and N. Nazarian, "Is the urban heat island intensity relevant for heat mitigation studies?", Urban Climate **31**, 100541 (2020).

[257] E. Bocher, J. Bernard, E. Wiederhold, F. Leconte, G. Petit, S. Palominos, and C. Noûs, "Geoclimate: a geospatial processing toolbox for environmental and climate studies", Journal of Open Source Software **6**, 3541 (2021), URL https://joss.theoj.org/papers/10.21105/joss.03541.

[258] H. Li, Y. Liu, H. Zhang, B. Xue, and W. Li, "Urban morphology in china: Dataset development and spatial pattern characterization", Sustainable Cities and Society **71**, 102981 (2021), URL https://linkinghub.elsevier.com/retrieve/pii/S2210670721002675.

[259] R. Burghardt, "Development of an arcgis extension to model urban climate factors", Ph.D. thesis, University of Kassel (2015).

[260] P. Berkhin, "A survey of clustering data mining techniques", Grouping Multidimensional Data: Recent Advances in Clustering 25–71 (2006), URL https://link.springer.com/chapter/10.1007/3-540-28349-8_2.

[261] C. Ding and X. He, "K-means clustering via principal component analysis", in *Proceedings of the twenty-first international conference on Machine learning*, 29 (2004).

[262] H. F. Kaiser, "The varimax criterion for analytic rotation in factor analysis", Psychometrika 1958 23:3 **23**, 187–200 (1958), URL https://link.springer.com/article/10.1007/BF02289233.

[263] A. K. Jain, "Data clustering: 50 years beyond k-means", Pattern Recognition Letters **31**, 651–666 (2010), URL https://linkinghub.elsevier.com/retrieve/pii/S0167865509002323.

[264] D. Arthur and S. Vassilvitskii, "K-means++ the advantages of careful seeding", in *Proceedings of the eighteenth annual ACM-SIAM symposium on Discrete algorithms*, 1027–1035 (2007).

[265] J. Rhee, J. Im, G. J. Carbone, and J. R. Jensen, "Delineation of climate regions using in-situ and remotely-sensed data for the carolinas", Remote Sensing of Environment **112**, 3099–3111 (2008), URL https://linkinghub.elsevier.com/retrieve/pii/S0034425708000862.

[266] X. Wang, Z. Zou, and H. Zou, "Using discriminant analysis to assess polycyclic aromatic hydrocarbons contamination in yongding new river", Environmental Monitoring and Assessment **185**, 8547–8555 (2013), URL https://link.springer.com/article/10.1007/s10661-013-3194-3.

[267] W. S. Sarle, *Cubic clustering criterion* (SAS Institute) (1983).

[268] G. W. Milligan and M. C. Cooper, "An examination of procedures for determining the number of clusters in a data set", Psychometrika 1985 50:2 **50**, 159–179 (1985), URL https://link.springer.com/article/10.1007/BF02294245.

[269] T. Caliński and J. Harabasz, "A dendrite method for cluster analysis", Communications in Statistics **3**, 1–27 (1974).

[270] D. Maroni, G. T. Cardoso, A. Neckel, L. S. Maculan, M. L. Oliveira, E. T. Bodah, B. W. Bodah, and M. Santosh, "Land surface temperature and vegetation index as a proxy to microclimate", Journal of Environmental Chemical Engineering **9**, 105796 (2021).

[271] R. Borge, J. Lumbreras, S. Vardoulakis, P. Kassomenos, and E. Rodríguez, "Analysis of long-range transport influences on urban pm10 using two-stage atmospheric trajectory clusters", Atmospheric Environment **41**, 4434–4450 (2007).

[272] K. jae Kim and H. Ahn, "A recommender system using ga k-means clustering in an online shopping market", Expert Systems with Applications **34**, 1200–1209 (2008).

[273] L. A. Kort-Butler and K. A. Tyler, "A cluster analysis of service utilization and incarceration among homeless youth", Social Science Research **41**, 612–623 (2012).

[274] U. G. S. (USGS), "Landsat 8 (l8) data users handbook", (2019).

[275] M. Lehnert, S. Savić, D. Milošević, J. Dunjić, and J. Geletič, "Mapping local climate zones and their applications in european urban environments: A systematic literature review and future development trends", ISPRS International Journal of Geo-Information **10**, 260 (2021), URL https://www.mdpi.com/2220-9964/10/4/260/htmhttps://www.mdpi.com/2220-9964/10/4/260.

[276] E. Bocher, G. Petit, J. Bernard, and S. Palominos, "A geoprocessing framework to compute urban indicators: The mapuce tools chain", Urban Climate **24**, 153–174 (2018), URL https://linkinghub.elsevier.com/retrieve/pii/S2212095518300117.

[277] N. Mohajeri, G. Upadhyay, A. Gudmundsson, D. Assouline, J. Kämpf, and J. L. Scartezzini, "Effects of urban compactness on solar energy potential", Renewable Energy **93**, 469–482 (2016).

[278] A. Solcerova, F. van de Ven, M. Wang, M. Rijsdijk, and N. van de Giesen, "Do green roofs cool the air?", Building and Environment **111**, 249–255 (2017).

[279] J. Tan, Y. Zheng, G. Song, L. S. Kalkstein, A. J. Kalkstein, and X. Tang, "Heat wave impacts on mortality in shanghai, 1998 and 2003", International Journal of Biometeorology **51**, 193–200 (2007).

[280] S. E. Perkins, L. V. Alexander, and J. R. Nairn, "Increasing frequency, intensity and duration of observed global heatwaves and warm spells", Geophysical Research Letters **39**, 20714 (2012), URL https://onlinelibrary.wiley.com/doi/full/10.1029/2012GL053361https://onlinelibrary.wiley.com/doi/abs/10.1029/2012GL053361https://agupubs.onlinelibrary.wiley.com/doi/10.1029/2012GL053361.

[281] K. Degirmenci, K. C. Desouza, W. Fieuw, R. T. Watson, and T. Yigitcanlar, "Understanding policy and technology responses in mitigating urban heat islands: A literature review and directions for future research", Sustainable Cities and Society **70**, 102873 (2021).

[282] P. Herath, M. Thatcher, H. Jin, and X. Bai, "Effectiveness of urban surface characteristics as mitigation strategies for the excessive summer heat in cities", Sustainable Cities and Society **72**, 103072 (2021).

[283] H. M. Imran, J. Kala, A. W. Ng, and S. Muthukumaran, "Effectiveness of vegetated patches as green infrastructure in mitigating urban heat island effects during a heatwave event in the city of melbourne", Weather and Climate Extremes **25**, 100217 (2019).

[284] H. L. Macintyre and C. Heaviside, "Potential benefits of cool roofs in reducing heat-related mortality during heatwaves in a european city", Environment International **127**, 430–441 (2019).

[285] M. Santamouris, "Cooling the cities – a review of reflective and green roof mitigation technologies to fight heat island and improve comfort in urban environments", Solar Energy **103**, 682–703 (2014).

[286] J. Yang, D. llamathy Mohan Kumar, A. Pyrgou, A. Chong, M. Santamouris, D. Kolokotsa, and S. E. Lee, "Green and cool roofs' urban heat island mitigation potential in tropical climate", Solar Energy **173**, 597–609 (2018).

[287] I. Teotónio, C. M. Silva, and C. O. Cruz, "Economics of green roofs and green walls: A literature review", Sustainable Cities and Society **69**, 102781 (2021).

[288] X. Zhou and H. Chen, "Impact of urbanization-related land use land cover changes and urban morphology changes on the urban heat island phenomenon", Science of The Total Environment **635**, 1467–1476 (2018).

[289] M. Y. Joshi, A. Rodler, M. Musy, S. Guernouti, M. Cools, and J. Teller, "Identifying urban morphological archetypes for microclimate studies using a clustering approach", Building and Environment **224**, 109574 (2022).

[290] A. Meek, N. Jayasuriya, E. Horan, and R. Adams, "Environmental benefits of retrofitting green roofs to a city block", Journal of Hydrologic Engineering **20**, 05014020 (2015), URL https://ascelibrary.org/doi/abs/10.1061/%28ASCE%29HE.1943-5584.0001048https://ascelibrary.org/doi/10.1061/%28ASCE%29HE.1943-5584.0001048.

[291] S. S. Alcazar, F. Olivieri, and J. Neila, "Green roofs: Experimental and analytical study of its potential for urban microclimate regulation in mediterranean–continental climates", Urban Climate **17**, 304–317 (2016).

[292] U. Berardi and Y. Wang, "The effect of a denser city over the urban microclimate: The case of toronto", Sustainability **8**, 822 (2016), URL https://www.mdpi.com/2071-1050/8/8/822/htmhttps://www.mdpi.com/2071-1050/8/8/822http://www.mdpi.com/2071-1050/8/8/822.

[293] A. Cortes, A. J. Rejuso, J. A. Santos, and A. Blanco, "Evaluating mitigation strategies for urban heat island in mandaue city using envi-met", Journal of Urban Management **11**, 97–106 (2022).

[294] Y. Feng, J. Wang, W. Zhou, X. Li, and X. Yu, "Evaluating the cooling performance of green roofs under extreme heat conditions", Frontiers in Environmental Science **10**, 874614 (2022).

[295] M. Razzaghmanesh, S. Beecham, and T. Salemi, "The role of green roofs in mitigating urban heat island effects in the metropolitan area of adelaide, south australia", Urban Forestry & Urban Greening **15**, 89–102 (2016).

[296] Y. Chen, B. Zheng, and Y. Hu, "Numerical simulation of local climate zone cooling achieved through modification of trees, albedo and green roofs—a case study of changsha, china", Sustainability 2020, Vol. 12, Page 2752 **12**, 2752 (2020), URL https://www.mdpi.com/2071-1050/12/7/2752/htmhttps://www.mdpi.com/2071-1050/12/7/2752.

[297] L. Schibuola and C. Tambani, "A monthly performance comparison of green infrastructures enhancing urban outdoor thermal comfort", Energy and Buildings **273**, 112368 (2022).

[298] C. Jin, X. Bai, T. Luo, and M. Zou, "Effects of green roofs' variations on the regional thermal environment using measurements and simulations in chongqing, china", Urban Forestry & Urban Greening **29**, 223–237 (2018).

[299] J. Kim, S. Y. Lee, and J. Kang, "Temperature reduction effects of rooftop garden arrangements: A case study of seoul national university", Sustainability 2020, Vol. 12, Page 6032 **12**, 6032 (2020), URL https://www.mdpi.com/2071-1050/12/15/6032/htmhttps://www.mdpi.com/2071-1050/12/15/6032.

[300] G. Zhang, B. J. He, Z. Zhu, and B. J. Dewancker, "Impact of morphological characteristics of green roofs on pedestrian cooling in subtropical climates", International Journal of Environmental Research and Public Health 2019, Vol. 16, Page 179 **16**, 179 (2019), URL https://www.mdpi.com/1660-4601/16/2/179/htmhttps://www.mdpi.com/1660-4601/16/2/179.

[301] J. Vinet, M. Antoine, F. Raymond, and C. Inard, "Modelling the impact of urban vegetation to analyse urban microclimate and outdoor thermal comfort", in *15th International Congress of Biometeorology1 International Conference on Urban Climatology*, na (1999).

[302] M. Robitu, M. Musy, C. Inard, and D. Groleau, "Modeling the influence of vegetation and water pond on urban microclimate", Solar Energy **80**, 435–447 (2006).

[303] L. Malys, "Évaluation des impacts directs et indirects des façades et des toitures végétales sur le comportement thermique des bâtiments", Ph.D. thesis, Ecole Centrale de Nantes (2012).

[304] J. Bouyer, "Modélisation et simulation des microclimats urbains-etude de l'impact de l'aménagement urbain sur les consommations énergétiques des bâtiments", Ph.D. thesis, Université de Nantes (2009).

[305] T. Robineau, A. Rodler, B. Morille, D. Ramier, J. Sage, M. Musy, V. Graffin, and E. Berthier, "Coupling hydrological and microclimate models to simulate evapotranspiration from urban green areas and air temperature at the district scale", Urban Climate **44**, 101179 (2022).

[306] R. Allen, L. Pereira, D. Raes, and M. Smith, "Crop evapotranspiration-guidelines for computing crop water requirements-fao irrigation and drainage paper 56", (1998).

[307] L. Malys, M. Musy, and C. Inard, "A hydrothermal model to assess the impact of green walls on urban microclimate and building energy consumption", Building and Environment **73**, 187–197 (2014).

[308] S. E. Ouldboukhitine, R. Belarbi, I. Jaffal, and A. Trabelsi, "Assessment of green roof thermal behavior: A coupled heat and mass transfer model", Building and Environment **46**, 2624–2631 (2011).

[309] K. Athamena, "Modélisation et simulation des microclimats urbains: Etude de l'impact de la morphologie urbaine sur le confort dans les espaces extérieurs. cas des éco-quartiers", Ph.D. thesis, Ecole Centrale de Nantes (ECN) (2012).

[310] P. G. Mestayer, J.-M. Rosant, F. Rodriguez, and J.-M. Rouaud, "La campagne expérimentale fluxsap 2010 - mesures de climatologie en zone urbaine hétérogène", La Météorologie **2011**, 34–44 (2011), URL https://lameteorologie.fr/issues/2011/73/meteo_2011_73_34.

[311] A. Rodler, S. Guernouti, M. Musy, and J. Bouyer, "Thermal behaviour of a building in its environment: Modelling, experimentation, and comparison", Energy and Buildings **168**, 19–34 (2018).

[312] M. H. Azam, B. Morille, J. Bernard, M. Musy, and F. Rodriguez, "A new urban soil model for solene-microclimat: Review, sensitivity analysis and validation on a car park", Urban Climate **24**, 728–746 (2018).

[313] D. Jacob, J. Petersen, B. Eggert, A. Alias, O. B. Christensen, L. M. Bouwer, A. Braun, A. Colette, M. Déqué, G. Georgievski, E. Georgopoulou, A. Gobiet, L. Menut, G. Nikulin, A. Haensler, N. Hempelmann, C. Jones, K. Keuler, S. Kovats, N. Kröner, S. Kotlarski, A. Kriegsmann, E. Martin, E. van Meijgaard, C. Moseley, S. Pfeifer, S. Preuschmann, C. Radermacher, K. Radtke, D. Rechid, M. Rounsevell, P. Samuelsson, S. Somot, J. F. Soussana, C. Teichmann, R. Valentini, R. Vautard, B. Weber, and P. Yiou, "Euro-cordex: New high-resolution climate change projections for european impact research", Regional Environmental Change **14**, 563–578 (2014), URL https://link.springer.com/article/10.1007/s10113-013-0499-2.

[314] B. Morille and M. Musy, "Comparison of the impact of three climate adaptation strategies on summer thermal comfort – cases study in lyon, france", Procedia Environmental Sciences **38**, 619–626 (2017).

[315] H. Lee and H. Mayer, "Thermal comfort of pedestrians in an urban street canyon is affected by increasing albedo of building walls", International Journal of Biometeorology **62**, 1199–1209 (2018), URL https://link.springer.com/article/10.1007/s00484-018-1523-5.

[316] D. J. Sailor and H. Fan, "Modeling the diurnal variability of effective albedo for cities", Atmospheric Environment **36**, 713–725 (2002).

[317] J. A. Palyvos, "A survey of wind convection coefficient correlations for building envelope energy systems' modeling", Applied Thermal Engineering **28**, 801–808 (2008).

[318] S. Peng, S. Piao, P. Ciais, P. Friedlingstein, C. Ottle, F. M. Bréon, H. Nan, L. Zhou, and R. B. Myneni, "Surface urban heat island across 419 global big cities", Environmental Science and Technology **46**, 696–703 (2012), URL https://pubs.acs.org/doi/full/10.1021/es2030438.

[319] K. Ward, S. Lauf, B. Kleinschmit, and W. Endlicher, "Heat waves and urban heat islands in europe: A review of relevant drivers", Science of The Total Environment **569-570**, 527–539 (2016).

[320] I. Jaffal, S. E. Ouldboukhitine, and R. Belarbi, "A comprehensive study of the impact of green roofs on building energy performance", Renewable Energy **43**, 157–164 (2012).

[321] M. Knaus and D. Haase, "Green roof effects on daytime heat in a prefabricated residential neighbourhood in berlin, germany", Urban Forestry & Urban Greening **53**, 126738 (2020).

[322] M. V. Monteiro, T. Blanuša, A. Verhoef, M. Richardson, P. Hadley, and R. W. Cameron, "Functional green roofs: Importance of plant choice in maximising summertime environmental cooling and substrate insulation potential", Energy and Buildings **141**, 56–68 (2017).

[323] Y. Hirano, T. Ihara, K. Gomi, and T. Fujita, "Simulation-based evaluation of the effect of green roofs in office building districts on mitigating the urban heat island effect and reducing co2 emissions", Sustainability 2019, Vol. 11, Page 2055 **11**, 2055 (2019), URL https://www.mdpi.com/2071-1050/11/7/2055/htmhttps://www.mdpi.com/2071-1050/11/7/2055.

[324] N. Müller, W. Kuttler, and A. B. Barlag, "Counteracting urban climate change: Adaptation measures and their effect on thermal comfort", Theoretical and Applied Climatology **115**, 243–257 (2014), URL https://link.springer.com/article/10.1007/s00704-013-0890-4.

[325] J. Dong, M. Lin, J. Zuo, T. Lin, J. Liu, C. Sun, and J. Luo, "Quantitative study on the cooling effect of green roofs in a high-density urban area—a case study of xiamen, china", Journal of Cleaner Production **255**, 120152 (2020).

[326] D. E. Bowler, L. Buyung-Ali, T. M. Knight, and A. S. Pullin, "Urban greening to cool towns and cities: A systematic review of the empirical evidence", Landscape and Urban Planning **97**, 147–155 (2010).

[327] L. F. M. Francis and M. B. Jensen, "Benefits of green roofs: A systematic review of the evidence for three ecosystem services", Urban forestry & urban greening **28**, 167–176 (2017).

[328] E. D. Giuseppe and M. D'Orazio, "Assessment of the effectiveness of cool and green roofs for the mitigation of the heat island effect and for the improvement of thermal comfort in nearly zero energy building", http://dx.doi.org/10.1080/00038628.2014.966050 **58**, 134–143 (2014), URL https://www.tandfonline.com/doi/abs/10.1080/00038628.2014.966050.

[329] E. Jamei, H. W. Chau, M. Seyedmahmoudian, and A. Stojcevski, "Review on the cooling potential of green roofs in different climates", Science of The Total Environment **791**, 148407 (2021).

[330] C. B. Koc, P. Osmond, and A. Peters, "Evaluating the cooling effects of green infrastructure: A systematic review of methods, indicators and data sources", Solar Energy **166**, 486–508 (2018).

[331] P. A. Mirzaei, "Recent challenges in modeling of urban heat island", Sustainable Cities and Society **19**, 200–206 (2015).

[332] M. Lin, J. Dong, L. Jones, J. Liu, T. Lin, J. Zuo, H. Ye, G. Zhang, and T. Zhou, "Modeling green roofs' cooling effect in high-density urban areas based on law of diminishing marginal utility of the cooling efficiency: A case study of xiamen island, china", Journal of Cleaner Production **316**, 128277 (2021).

[333] M. ROTH, T. R. OKE, and W. J. EMERY, "Satellite-derived urban heat islands from three coastal cities and the utilization of such data in urban climatology", International Journal of Remote Sensing **10**, 1699–1720 (1989).

[334] A. M. El-Zeiny and H. A. Effat, "Environmental monitoring of spatiotemporal change in land use/land cover and its impact on land surface temperature in el-fayoum governorate, egypt", Remote Sensing Applications: Society and Environment **8**, 266–277 (2017).

[335] O. E. Adeyeri, A. A. Akinsanola, and K. A. Ishola, "Investigating surface urban heat island characteristics over abuja, nigeria: Relationship between land surface temperature and multiple vegetation indices", Remote Sensing Applications: Society and Environment **7**, 57–68 (2017).

[336] H. Govil, S. Guha, P. Diwan, N. Gill, and A. Dey, "Analyzing linear relationships of lst with ndvi and mndisi using various resolution levels of landsat 8 oli and tirs data", Advances in Intelligent Systems and Computing **1042**, 171–184 (2020), URL https://link.springer.com/chapter/10.1007/978-981-32-9949-8_13.

[337] A. Asadi, H. Arefi, and H. Fathipoor, "Simulation of green roofs and their potential mitigating effects on the urban heat island using an artificial neural network: A case study in austin, texas", Advances in Space Research **66**, 1846–1862 (2020).

[338] K. Deilami, M. Kamruzzaman, and Y. Liu, "Urban heat island effect: A systematic review of spatio-temporal factors, data, methods, and mitigation measures", International Journal of Applied Earth Observation and Geoinformation **67**, 30–42 (2018).

[339] D. Jato-Espino, C. Manchado, A. Roldán-Valcarce, and V. Moscardó, "Arcuhi: A gis add-in for automated modelling of the urban heat island effect through machine learning", Urban Climate **44**, 101203 (2022).

[340] F. Lyu, S. Wang, S. Y. Han, C. Catlett, and S. Wang, "An integrated cybergis and machine learning framework for fine-scale prediction of urban heat island using satellite remote sensing and urban sensor network data", Urban Informatics 2022 1:1 **1**, 1–15 (2022), URL https://link.springer.com/article/10.1007/s44212-022-00002-4.

[341] K. Matsuki, V. Kuperman, and J. A. V. Dyke, "The random forests statistical technique: An examination of its value for the study of reading", Scientific Studies of Reading **20**, 20–33 (2016), URL https://www.tandfonline.com/doi/abs/10.1080/10888438.2015.1107073.

[342] S. Busato, M. Gordon, M. Chaudhari, I. Jensen, T. Akyol, S. Andersen, and C. Williams, "Compositionality, sparsity, spurious heterogeneity, and other data-driven challenges for machine learning algorithms within plant microbiome studies", Current Opinion in Plant Biology **71**, 102326 (2023).

[343] M. Christis, A. Athanassiadis, and A. Vercalsteren, "Implementation at a city level of circular economy strategies and climate change mitigation – the case of brussels", Journal of Cleaner Production **218**, 511–520 (2019).

[344] K. L. Bristow and G. S. Campbell, "On the relationship between incoming solar radiation and daily maximum and minimum temperature", Agricultural and Forest Meteorology **31**, 159–166 (1984).

[345] Z. Wu and Y. Zhang, "Spatial variation of urban thermal environment and its relation to green space patterns: Implication to sustainable landscape planning", Sustainability 2018, Vol. 10, Page 2249 **10**, 2249 (2018), URL https://www.mdpi.com/2071-1050/10/7/2249/htmhttps://www.mdpi.com/2071-1050/10/7/2249.

[346] B. Bechtel, P. J. Alexander, J. Böhner, J. Ching, O. Conrad, J. Feddema, G. Mills, L. See, and I. Stewart, "Mapping local climate zones for a

worldwide database of the form and function of cities", ISPRS International Journal of Geo-Information 2015, Vol. 4, Pages 199-219 **4**, 199–219 (2015), URL https://www.mdpi.com/2220-9964/4/1/199/htmhttps://www.mdpi.com/2220-9964/4/1/199.

[347] M. Hereher, R. Eissa, A. Alqasemi, and A. M. E. Kenawy, "Assessment of air pollution at greater cairo in relation to the spatial variability of surface urban heat island", Environmental Science and Pollution Research **29**, 21412–21425 (2022), URL https://link.springer.com/article/10.1007/s11356-021-17383-9.

[348] V. A. Huynh-Thu and P. Geurts, "Unsupervised gene network inference with decision trees and random forests", Methods in Molecular Biology **1883**, 195–215 (2019), URL https://link.springer.com/protocol/10.1007/978-1-4939-8882-2_8.

[349] S. Benvenuti, "Wildflower green roofs for urban landscaping, ecological sustainability and biodiversity", Landscape and urban planning **124**, 151–161 (2014).

[350] C. Froment, "Arthropods communities on green roofs in brussels: Influence of roof vegetation and landscape context", (2017).

[351] B. Y. Schindler, A. B. Griffith, and K. N. Jones, "Factors influencing arthropod diversity on green roofs", Cities and the Environment (CATE) **4**, 5 (2011).

[352] R. Fernández Cañero, P. González Redondo, *et al.*, "Green roofs as a habitat for birds: a review", Journal of Animal and Veterinary Advances, 9 (15), 2041-2052. (2010).

[353] K. Parkins and J. A. Clark, "Green roofs provide habitat for urban bats", Global Ecology and Conservation **4**, 349–357 (2015).

[354] A. Zurbuchen, L. Landert, J. Klaiber, A. Müller, S. Hein, and S. Dorn, "Maximum foraging ranges in solitary bees: only few individuals have the capability to cover long foraging distances", Biological Conservation **143**, 669–676 (2010).

[355] K. Kyrö, S. Brenneisen, D. J. Kotze, A. Szallies, M. Gerner, and S. Lehvävirta, "Local habitat characteristics have a stronger effect than the surrounding urban landscape on beetle communities on green roofs", Urban Forestry & Urban Greening **29**, 122–130 (2018).

[356] F. Madre, A. Vergnes, N. Machon, and P. Clergeau, "A comparison of 3 types of green roof as habitats for arthropods", Ecological Engineering **57**, 109–117 (2013).

[357] J. Beninde, M. Veith, and A. Hochkirch, "Biodiversity in cities needs space: a meta-analysis of factors determining intra-urban biodiversity variation", Ecology Letters **18**, 581–592 (2015), URL https://onlinelibrary.wiley.com/doi/full/10.1111/ele.12427https://onlinelibrary.wiley.com/doi/abs/10.1111/ele.12427https://onlinelibrary.wiley.com/doi/10.1111/ele.12427.

[358] J. W. Wang, C. H. Poh, C. Y. T. Tan, V. N. Lee, A. Jain, E. L. Webb, C. H. Poh, C. Y. T. Tan, V. N. Lee, A. Jain, and E. L. Webb, "Building biodiversity: drivers of bird and butterfly diversity on tropical urban roof gardens", Ecosphere **8**, e01905 (2017).

[359] T. Louis-Lucas, C. Clauzel, F. Mayrand, P. Clergeau, and N. Machon, "Role of green roofs in urban connectivity, an exploratory approach using landscape graphs in the city of paris, france", Urban Forestry & Urban Greening **78**, 127765 (2022).

[360] S. Casalegno, K. Anderson, D. T. Cox, S. Hancock, and K. J. Gaston, "Ecological connectivity in the three-dimensional urban green volume using waveform airborne lidar", Scientific Reports 2017 7:1 **7**, 1–8 (2017), URL https://www.nature.com/articles/srep45571.

[361] Y. Sahraoui, J. C. Foltête, and C. Clauzel, "A multi-species approach for assessing the impact of land-cover changes on landscape connectivity", Landscape Ecology **32**, 1819–1835 (2017), URL https://link.springer.com/article/10.1007/s10980-017-0551-6.

[362] H. Serret, R. Raymond, J. C. Foltête, P. Clergeau, L. Simon, and N. Machon, "Potential contributions of green spaces at business sites to the ecological network in an urban agglomeration: The case of the ile-de-france region, france", Landscape and Urban Planning **131**, 27–35 (2014).

[363] S. Tarabon, C. Calvet, V. Delbar, T. Dutoit, and F. Isselin-Nondedeu, "Integrating a landscape connectivity approach into mitigation hierarchy planning by anticipating urban dynamics", Landscape and Urban Planning **202**, 103871 (2020).

[364] J. Radoux, A. Bourdouxhe, T. Coppée, M. D. Vroey, M. Dufrêne, and P. Defourny, "A consistent land cover map time series at 2 m spatial resolution—the lifewatch 2006-2015-2018-2019 dataset for wallonia", Data **8**, 13 (2022), URL https://www.mdpi.com/2306-5729/8/1/13/htmhttps://www.mdpi.com/2306-5729/8/1/13.

[365] J. C.-W. Chan and D. Paelinckx, "Evaluation of random forest and adaboost tree-based ensemble classification and spectral band selection for ecotope mapping using airborne hyperspectral imagery", Remote Sensing of Environment **112**, 2999–3011 (2008).

[366] M. M. Hofmann, A. Fleischmann, and S. S. Renner, "Foraging distances in six species of solitary bees with body lengths of 6 to 15 mm, inferred from individual tagging, suggest 150 m-rule-of-thumb for flower strip distances", Journal of Hymenoptera Research 77: 105-117 **77**, 105–117 (2020), URL https://jhr.pensoft.net/article/51182/.

[367] T. Sattler, P. Duelli, M. K. Obrist, R. Arlettaz, and M. Moretti, "Response of arthropod species richness and functional groups to urban habitat structure and management", Landscape Ecology **25**, 941–954 (2010), URL https://link.springer.com/article/10.1007/s10980-010-9473-2.

[368] E. Rochat, S. Manel, M. Deschamps-Cottin, I. Widmer, and S. Joost, "Persistence of butterfly populations in fragmented habitats along urban density gradients: motility helps", Heredity 2017 119:5 **119**, 328–338 (2017), URL https://www.nature.com/articles/hdy201740.

[369] L. Moquet, E. Laurent, R. Bacchetta, and A. L. Jacquemart, "Conservation of hoverflies (diptera, syrphidae) requires complementary resources at the landscape and local scales", Insect Conservation and Diversity **11**, 72 (2018), URL /pmc/articles/PMC7165621//pmc/articles/PMC7165621/?report=abstracthttps://www.ncbi.nlm.nih.gov/pmc/articles/PMC7165621/.

[370] B. Krämer, D. Poniatowski, and T. Fartmann, "Effects of landscape and habitat quality on butterfly communities in pre-alpine calcareous grasslands", Biological Conservation **152**, 253–261 (2012).

[371] S. L. Olsen, M. Evju, and A. Endrestøl, "Fragmentation in calcareous grasslands: species specialization matters", Biodiversity and Conservation **27**, 2329–2361 (2018).

[372] K. P. Zulka, M. Abensperg-Traun, N. Milasowszky, G. Bieringer, B.-A. Gereben-Krenn, W. Holzinger, G. Hölzler, W. Rabitsch, A. Reischütz, P. Querner, *et al.*, "Species richness in dry grassland patches of eastern austria: a multi-taxon study on the role of local, landscape and habitat quality variables", Agriculture, Ecosystems & Environment **182**, 25–36 (2014).

[373] J. Herrmann, S. Buchholz, and P. Theodorou, "The degree of urbanisation reduces wild bee and butterfly diversity and alters the patterns of flower-visitation in urban dry grasslands", Scientific Reports **13**, 2702 (2023).

[374] G. Aguilera, J. Ekroos, A. S. Persson, L. B. Pettersson, and E. Öckinger, "Intensive management reduces butterfly diversity over time in urban green spaces", Urban Ecosystems **22**, 335–344 (2019), URL https://link.springer.com/article/10.1007/s11252-018-0818-y.

[375] T. Tscharntke, A. M. Klein, A. Kruess, I. Steffan-Dewenter, and C. Thies, "Landscape perspectives on agricultural intensification and biodiversity–ecosystem service management", Ecology letters **8**, 857–874 (2005).

[376] B. A. Norton, L. J. Thomson, N. S. Williams, and M. J. McDonnell, "The effect of urban ground covers on arthropods: An experiment", Urban ecosystems **17**, 77–99 (2014).

[377] R. S. King and D. A. Wrubleski, "Spatial and diel availability of flying insects as potential duckling food in prairie wetlands", Wetlands **18**, 100–114 (1998).

[378] R. Duflot, H. Daniel, S. Aviron, A. Alignier, V. Beaujouan, F. Burel, A. Cochard, A. Ernoult, G. Pain, and J. A. Pithon, "Adjacent woodlands rather than habitat connectivity influence grassland plant, carabid and bird assemblages in farmland landscapes", Biodiversity and Conservation **27**, 1925–1942 (2018), URL https://link.springer.com/article/10.1007/s10531-018-1517-y.

[379] M. Balbi, S. Croci, E. J. Petit, A. Butet, R. Georges, L. Madec, J. P. Caudal, and A. Ernoult, "Least-cost path analysis for urban greenways planning: A test with moths and birds across two habitats and two cities", Journal of Applied Ecology **58**, 632–643 (2021), URL https://onlinelibrary.wiley.com/doi/full/10.1111/1365-2664.13800https://onlinelibrary.wiley.com/doi/abs/10.1111/1365-2664.13800https://besjournals.onlinelibrary.wiley.com/doi/10.1111/1365-2664.13800.

[380] C. Clauzel, D. Xiqing, W. Gongsheng, P. Giraudoux, and L. Li, "Assessing the impact of road developments on connectivity across multiple scales: Application to yunnan snub-nosed monkey conservation", Biological Conservation **192**, 207–217 (2015).

[381] Örjan Bodin and S. Saura, "Ranking individual habitat patches as connectivity providers: Integrating network analysis and patch removal experiments", Ecological Modelling **221**, 2393–2405 (2010).

[382] J. T. Lundholm and P. J. Richardson, "Mini-review: Habitat analogues for reconciliation ecology in urban and industrial environments", Journal of Applied Ecology **47**, 966–975 (2010).

[383] L. Blank, A. Vasl, B. Y. Schindler, G. J. Kadas, and L. Blaustein, "Horizontal and vertical island biogeography of arthropods on green roofs: a review", Urban Ecosystems **20**, 911–917 (2017), URL https://link.springer.com/article/10.1007/s11252-016-0639-9.

[384] J. S. MacIvor, "Building height matters: nesting activity of bees and wasps on vegetated roofs", Israel Journal of Ecology & Evolution **62**, 88–96 (2016).

[385] F. Madre, A. Vergnes, N. Machon, and P. Clergeau, "Green roofs as habitats for wild plant species in urban landscapes: First insights from a large-scale sampling", Landscape and urban Planning **122**, 100–107 (2014).

[386] D. Poniatowski, G. Stuhldreher, F. Löffler, and T. Fartmann, "Patch occupancy of grassland specialists: Habitat quality matters more than habitat connectivity", Biological Conservation **225**, 237–244 (2018).

[387] L. Rivière, "Concevoir des toitures vertes analogues aux pelouses sèches indigènes pour la biodiversité et l'hydrologie", Ph.D. thesis, University of Liège (2023).

[388] M. Kazemi, "Water transfer and insulation dynamic of green roofs with coarse recycled materials", Ph.D. thesis, ULg-Université de Liège [Faculty of Applied Sciences], Liege, Belgium (2023).

[389] T. Brudermann and T. Sangkakool, "Green roofs in temperate climate cities in europe–an analysis of key decision factors", Urban forestry & urban greening **21**, 224–234 (2017).

[390] D. Chemisana and C. Lamnatou, "Photovoltaic-green roofs: An experimental evaluation of system performance", Applied Energy **119**, 246–256 (2014).

[391] C. Lamnatou and D. Chemisana, "Photovoltaic-green roofs: a life cycle assessment approach with emphasis on warm months of mediterranean climate", Journal of cleaner production **72**, 57–75 (2014).